

**Climate and land use change impacts on water
resources in the Lusatian river catchments (Germany) -
Analysis and assessment considering modelling
uncertainties**

Von der Fakultät für Umweltwissenschaften und Verfahrenstechnik der
Brandenburgischen Technischen Universität Cottbus-Senftenberg zur Erlangung
des akademischen Grades eines Doktor-Ingenieurs (Dr.-Ing.) genehmigte
Dissertation

vorgelegt von

M.Sc. Anne Gädeke

aus

Berlin (Deutschland)

Gutachter: Prof. Dr. Uwe Grünewald

Gutachter: Prof. Dr. Markus Disse

Tag der mündlichen Prüfung: 18. September 2014

Abstract

In anthropogenically heavily impacted river catchments, such as the Lusatian river catchments Spree and Schwarze Elster in Germany, the robust assessment of potential impacts of climate change on the regional water resources is of high relevance for water resources management. Large uncertainties inherent in future scenarios may, however, reduce the willingness of regional stakeholders to develop and implement suitable adaptation strategies to climate change.

This thesis proposes the use of an integrated framework consisting of i) an ensemble-based modelling approach and ii) the incorporation of measured and simulated meteorological and hydrological trends to consider uncertainties in climate change impact assessments. In addition, land use, as the most responsive catchment characteristic to buffer potential climate change impacts, is considered as one suitable trigger for climate change adaptation.

The ensemble-based modelling approach consists of the meteorological output of four climate downscaling approaches (DAs): two dynamical and two statistical. These DAs drive different model configurations of the two conceptually different hydrological models WaSiM-ETH and HBV-light. The objective of incorporating measured meteorological trends into the analysis was twofold: trends in measured time series can i) be regarded as harbinger for future change and ii) serve as a mean to validate the results of the DAs. In order to evaluate the nature of the trends, both gradual (Mann-Kendall test) and step changes (Pettitt test) are considered as well as temporal and spatial correlations in the data. The suitability of land use change as an adaptation strategy to climate change is evaluated in the form of different land use change scenarios: i) extreme scenarios where the entire catchment is parameterised as coniferous forest and uncultivated land and ii) scenarios of changes in crop cultivation and ii) a combination of a change in crop cultivation and forest conversion. As study areas serve three almost natural subcatchments of the Spree and Schwarze Elster (Germany).

The results of the ensemble-based climate change impact analysis show that depending on the type (dynamical or statistical) of DA used, opposing trends in precipitation, actual evapotranspiration and discharge are simulated in the scenario period (2031-2060). While the statistical DAs simulate a decrease in future long term annual precipitation, the dynamical DAs simulate a tendency towards increasing precipitation. The trend analysis suggests that measured precipitation has not changed significantly during the period 1961-2006. Therefore, the strong decrease in precipitation simulated by the statistical DAs should be interpreted as a rather dry future scenario. The dynamical DAs, on the other hand, are too wet in the reference period and needed to be statistically bias corrected which destroys the physical consistency between the parameters. Concerning temperature,

measured and simulated trends agree on a positive trend. The uncertainty related to the hydrological model within the climate change modelling chain is comparably low when long term averages are considered but increases during low-flow events. The proposed framework of combining an ensemble-based modelling approach with trend analysis on measurements is a promising approach to gain more confidence into the final results of climate change impact assessments and to obtain an increased process understanding of the interrelation between climate and water resources.

In terms of climate change adaptation, land use alternatives can have a considerable impact on the water balance components as the analysis of the extreme scenarios revealed. The scenarios of changes in crop cultivation in combination with forest conversion show, however, that the impact on the long term annual water balance is comparably low. An intra-annual shift in the water balance components can be triggered which makes these scenarios suitable to reduce low-flow risks during the summer. Overall, land use change can serve as one part of an integrated climate change adaptation strategy. Such as strategy needs, depending on the severity of the climate change impact, to include other, especially technical measures of water resources management, such as additional water storage, different strategies to manage the existing and new reservoirs. It may also consider additional water transfers from neighbouring, more water rich, river catchments. Regional adaptation planning needs also to consider problems related to water quality which are a consequence of the long term mining activities in the Lusatian river catchments. Last but not least, adaptation strategies should not only consider climate but also other aspects of global change.

Zusammenfassung

In anthropogen stark überprägten Einzugsgebieten, wie den Lausitzer Flusseinzugsgebieten von Spree und Schwarzer Elster in Deutschland, ist die robuste Abschätzung von potentiellen Auswirkungen des Klimawandels auf die regionalen Wasserressourcen von hoher Relevanz für die Wasserbewirtschaftung. Unsicherheiten in solchen Abschätzungen können jedoch die Bereitschaft von regionalen Akteuren für die Entwicklung und Umsetzung von Anpassungsmaßnahmen an den Klimawandel mindern.

Um den Unsicherheiten in der Modellierung von Klimafolgen Rechnung zu tragen, wird ein Ansatz bestehend aus i) einem modellgestützten Ensemble und ii) die Integration von Trendanalysen an gemessenen und simulierten meteorologischen und hydrologischen Zeitreihen vorgeschlagen. Zusätzlich wird die Landnutzung, welche eine sensitive Einzugsgebietseigenschaft zur Pufferung von potentiellen Einflüssen des Klimawandels darstellt, als mögliche Anpassungsmaßnahme an den Klimawandel berücksichtigt.

Der modellgestützte Ensembleansatz besteht aus den meteorologischen Ausgaben von vier, zwei statistischen und zwei dynamischen, regionalen Klimamodellen, welche den Antrieb für unterschiedliche Modellkonfigurationen der konzeptionell unterschiedlichen hydrologischen Modelle WaSiM-ETH and HBV-light darstellen. Der Integration von Trendanalysen an meteorologischen und hydrologischen Zeitreihen liegen folgende Annahmen zu Grunde: Trends in den Messungen können i) als Vorboten für zukünftige Veränderungen interpretiert werden und ii) zur Validierung der simulierten meteorologischen Größen der regionalen Klimamodelle dienen. Um die Art der Trends zu beurteilen wurden graduelle (Mann-Kendall Test) und abrupte Trends (Pettitt Test) sowie zeitliche und räumliche Korrelationen in den Daten berücksichtigt.

Die Eignung von Landnutzungsänderungen als Anpassungsmaßnahme an den Klimawandel wurde in Form von unterschiedlichen Szenarien bewertet: i) extreme Szenarien, bei welchen das gesamte Einzugsgebiet als Nadelwald und Brache parametrisiert wird, ii) eine Verschiebung der Vegetationsperiode von Nutzpflanzen und iii) eine Kombination aus der Verschiebung der Vegetationsperiode von Nutzpflanzen und Waldumbau. Als Einzugsgebiete dienen drei anthropogen kaum beeinflusste Teileinzugsgebiete der Spree und Schwarzen Elster (Deutschland).

Die Ergebnisse des modellgestützten Ensembles zeigen, dass abhängig von der Wahl des regionalen Klimamodells (dynamisch oder statistisch), gegensätzliche Trends für Niederschlag, aktuelle Verdunstung und Abfluss in der Szenarioperiode (2031-2060) simuliert werden. Die statistischen regionalen Klimamodell berechnen eine Abnahme der langjährigen mittleren Niederschläge, die dynamischen hingegen eine Zunahme. Die Trendanalysen anhand der gemessenen Niederschlagszeitreihen zeigen, dass sich der

Niederschlag im Zeitraum 1961-2006 kaum verändert hat. Daraus folgend sollte die starke Niederschlagsabnahme, wie sie von den regionalen statistischen Klimamodellen berechnet wird, als trockenes Zukunftsszenarium interpretiert werden. Andererseits sind die dynamischen regionalen Klimamodelle in der Referenzperiode zu feucht und müssen statistisch Bias-korrigiert werden, was die physikalische Konsistenz zwischen den Parametern zerstört. Bezüglich der Lufttemperatur werden sowohl in den Messungen als auch in den Simulationen positive Trends berechnet. Die Unsicherheit bezüglich der Wahl des hydrologischen Modells im modellgestützten Ensemble ist vergleichsweise gering bei der Betrachtung von langjährigen mittleren Wasserhaushaltsgrößen, nimmt jedoch für Niedrigwässer stark zu. Es konnte gezeigt werden, dass der vorgeschlagene Ansatz bestehend aus Trendanalysen und modellgestütztem Ensemble vielversprechend ist, um mehr Vertrauen in die Ergebnisse von Klimafolgenabschätzungen und ein erhöhtes Prozessverständnis zwischen Klimaveränderungen und deren Auswirkungen auf regionale Wasserressourcen zu erlangen.

Landnutzungsänderungen können einen erheblichen Einfluss auf die Wasserbilanz eines Einzugsgebiets haben, wie die Analysen der Extremszenarios belegen. Gleichzeitig zeigen die Szenarien bezüglich einer Verschiebung der Vegetationsperiode von Nutzpflanzen, dass deren Einfluss auf die langjährigen Wasserhaushaltsgrößen gering ist. Eine Verschiebung der Vegetationsperiode eignet sich jedoch, um eine innerjährliche Umverteilung der Wasserhaushaltsgrößen zu bewirken und so das Risiko von Niedrigwässern während der Sommermonate zu reduzieren. Insgesamt können Landnutzungsänderungen einen Bestandteil einer integrierten Strategie zur Anpassung an den Klimawandel darstellen. Diese muss jedoch, in Abhängigkeit der Stärke der Klimaänderungen, auch andere, insbesondere technische Wasserbewirtschaftungsmaßnahmen, wie zusätzlicher Wasserspeicher, unterschiedliche Strategien zur Bewirtschaftung vorhandener und neuer Speicher enthalten. Diese Strategien können auch zusätzliche Wasserüberleitungen aus wasserreicheren Nachbareinzugsgebieten, berücksichtigen. Außerdem müssen Probleme bezüglich der Wasserbeschaffenheit, als eine Konsequenz der langjährigen Bergbauaktivitäten in den Lausitzer Flusseinzugsgebieten, in die regionale Planung zur Anpassung an den Klimawandel einbezogen werden. Schließlich sollten Anpassungsmaßnahmen nicht nur den Klimawandel, sondern auch andere Aspekte des globalen Wandels berücksichtigen.

Comment

Parts of the study are previously published as follows:

Gädeke, A., Hölzel, H., Koch, H., Pohle, I., Grünewald, U., 2014. Analysis of uncertainties in the hydrological response of a model-based climate change impact assessment in a subcatchment of the Spree River, Germany. *Hydrological Processes*, 28(12): 3978-3998.

Gädeke, A., Koch, H., Pohle, I., Grünewald, U., 2014. Möglichkeiten zur Berücksichtigung von Unsicherheiten in Klimawandelimpaktstudien. In: Cyffka, B. (Ed.), *Wasser - Landschaft – Mensch in Vergangenheit, Gegenwart und Zukunft. Beiträge zum Tag der Hydrologie am 20./21. März 2014* Katholische Universität Eichstätt-Ingolstadt, pp. 49-56.

Gädeke, A., Hölzel, H., Koch, H., Grünewald, U., 2012. Analysis of uncertainties related to regional climate and hydrological models on the water balance in a subcatchment of the Spree river, Germany. In: Hinkelmann, R., Nasermoaddeli, M.H., Liong, S.-Y., Savic, D., Fröhle, P., Daemrich, K.F. (Eds.), *HIC 2012 - 10th International Conference on Hydroinformatics: "Understanding Changing Climate and Environment and Finding Solutions"*, July 14.-18. 2012, Hamburg.

Gädeke, A., Pohle, I., Hölzel, H., Koch, H., Grünewald, U., 2012. Analyse zum Einfluss des Landschafts- und Klimawandels auf den Wasserhaushalt in einem Teileinzugsgebiet der Spree. In: Grünewald, U., Bens, O., Fischer, H., Hüttl, R.F., Kaiser, K., Knierim, A. (Eds.), *Wasserbezogene Anpassungsmaßnahmen an den Landschafts- und Klimawandel*. Schweizerbart, Stuttgart, pp. 81-94.

Table of contents

1	Introduction	1
1.1	Background and motivation	1
1.2	Objectives	2
1.3	Research approach	4
1.4	Outline of the thesis	5
2	State of the art of research	6
2.1	Trend analysis	6
2.1.1	Trend detection and attribution	6
2.1.2	Gradual trends	6
2.1.3	Change points	8
2.1.4	Field significance	8
2.1.5	Limitations of trend analysis	9
2.2	Hydrological climate change impact assessments	9
2.2.1	Climate scenarios for hydrological climate change impact assessments	9
2.2.2	Hydrological models for hydrological climate change impact assessments	12
2.2.3	Cascade of uncertainty and ensemble-based modelling	13
2.3	Climate change policy: mitigation and adaptation	14
2.4	Low-flow analysis	15
3	Data basis, data preparation and climate downscaling approaches	18
3.1	Data basis and data preparation	18
3.2	Climate downscaling approaches	19
3.2.1	Characteristics of downscaling approaches	19
3.2.2	STAR	20
3.2.3	WettReg	21
3.2.4	CCLM	22
3.2.5	REMO	22
3.3	Bias correction of REMO and CCLM	23
4	Study areas	24
4.1	Characterisation of selected Lusatian river catchments	24
4.1.1	Spree and Schwarze Elster river catchments	24
4.1.2	The Pulsnitz river catchment (Schwarze Elster river)	28
4.1.3	The Weißer Schöps river catchment (Spree river)	30
4.1.4	The Dahme river catchment (Spree river)	32

4.2	Comparison between land use and soil properties _____	34
4.3	Climatic and hydrological conditions _____	36
4.4	Detection of anthropogenic impact _____	39
5	Trend analysis for change detection _____	41
5.1	Materials and methods _____	41
5.2	Results _____	44
5.2.1	Autocorrelation _____	44
5.2.2	Trend detection in the Spree and Schwarze Elster river catchments _____	45
5.2.3	Trend detection in the subcatchments _____	57
5.2.4	Consistency of observed changes with climate change scenarios _____	58
5.3	Discussion _____	61
6	Hydrological modelling _____	64
6.1	Materials and methods _____	64
6.1.1	The hydrological simulation models WaSiM-ETH and HBV-light _____	64
6.1.2	Evaluation of hydrological model performance _____	70
6.2	Set up of specific hydrological models _____	71
6.2.1	Parameterisation of site specific WaSiM-ETH models _____	71
6.2.2	Parameterisation of site specific HBV-light models _____	74
6.2.3	Calibration and validation _____	75
6.3	Results _____	78
6.3.1	Mean discharge analysis _____	78
6.3.2	Low-flow analysis _____	83
6.4	Discussion _____	85
7	Hydrological climate change impact assessments _____	88
7.1	Materials and methods _____	88
7.2	Results _____	91
7.2.1	Evaluation of uncertainties of downscaling approaches during reference period _____	91
7.2.2	Simulations for the reference period and climate change impact during the scenario period _____	93
7.2.3	Low-flow analysis under climate change impact _____	101
7.2.4	Climate change impact analysis on spatial patterns of actual evapotranspiration and groundwater recharge _____	105
7.3	Discussion _____	108

8	Land use change analysis as a climate change adaptation strategy	112
8.1	Material and methods	112
8.2	Results	114
8.2.1	Extreme land use scenarios as boundary conditions	114
8.2.2	Change in crop cultivation	116
8.2.3	Combination of change in crop cultivation and forest conversion	118
8.3	Discussion	119
9	Summary and conclusion	122
10	Outlook	127
11	References	130
	Acknowledgements	155
	Appendix	157

List of figures

Figure 1-1:	Research approach considering modelling uncertainties	4
Figure 2-1:	The uncertainty cascade of climate change impact assessments.....	13
Figure 4-1:	Location and overview of study catchments.....	25
Figure 4-2:	Temporal development of mining drainage discharge in the catchments of Spree and Schwarze Elster rivers	26
Figure 4-3:	The Pulsnitz river catchment with position of climate and precipitation stations as well as discharge gauges and elevation	29
Figure 4-4:	Distribution of land use, soil type, hydraulic conductivity [m/s] and aquifer type in the Pulsnitz river catchment	30
Figure 4-5:	The Weißer Schöps river catchment with position of climate and precipitation stations as well as discharge gauges and elevation.....	31
Figure 4-6:	Distribution of land use, soil type, hydraulic conductivity [m/s] and aquifer type in the Weißer Schöps river catchment	32
Figure 4-7:	The Dahme river catchment with position of precipitation stations as well as discharge gauges and elevation.....	33
Figure 4-8:	Distribution of land use, soil type, hydraulic conductivity [m/s] and aquifer type in the Dahme river catchment	34
Figure 4-9:	Comparison of the land use proportions between the different study catchments	35
Figure 4-10:	Comparison of the soil types proportions between the different study catchments	35
Figure 4-11:	Long term (1963-2006) monthly sums of corrected precipitation (P) after SEVRUK (1986), potential evapotranspiration (ETP) calculated after WENDLING et al. (1991), climatic water balance (CWB) and mean temperature (T)	37
Figure 4-12:	Long term mean, minimum and maximum discharge	38
Figure 4-13:	Temporal development of the annual cumulative precipitation (uncorrected), runoff and runoff coefficient.....	39
Figure 4-14:	Temporal development of the decadal monthly mean discharge at the gauge Prierow in the Dahme river catchment	40
Figure 5-1:	Approach for analysing monthly significant and non-significant positive (a) and negative (b) trends, (c) number of significant trends and field significance	41
Figure 5-2:	Location of meteorological stations.	42

Figure 5-3:	Approach to evaluate field significance of spatially correlated time series.....	44
Figure 5-4:	Mean temperature (interpolated annual values, 1951-2006) in the Spree and Schwarze Elster river catchments and trend interpretation.....	45
Figure 5-5:	Mean temperature (1951-2006): number of stations with significant and non-significant (a) positive and (b) negative trends, (c) number of significant trends and field significance for change points and gradual trends in the Spree (left) and Schwarze Elster (right) river catchments.....	47
Figure 5-6:	Mean temperature (1951-2006): spatial distribution of significant and non-significant gradual trends as well as gradient in trend magnitude in May.....	48
Figure 5-7:	Mean temperature (1951-2006): spatial distribution of change points in the month of January.....	49
Figure 5-8:	Mean air temperature in January: representative example (station Seelow, Spree river catchment) with significant mean temperature change point, but non-significant gradual trend.....	50
Figure 5-9:	Potential evapotranspiration (interpolated annual values, 1951-2006) in the Spree and Schwarze Elster river catchments and trend interpretation.....	51
Figure 5-10:	Potential evapotranspiration (1951-2006): number of stations with significant and non-significant (a) positive and (b) negative trends, (c) number of significant trends and field significance for change points and gradual trends in the Spree (left) and Schwarze Elster (right) river catchments.....	52
Figure 5-11:	Potential evapotranspiration (1951-2006): spatial distribution of significant and non-significant change points as well as gradient in trend magnitude.....	53
Figure 5-12:	Potential evapotranspiration (1951-2006): spatial distribution of significant and non-significant gradual trends as well as gradient in trend magnitude.....	54
Figure 5-13:	Precipitation (interpolated annual values, 1951-2006) in the Spree and Schwarze Elster river catchments and trend interpretation.....	55
Figure 5-14:	Precipitation (1951-2006): number of stations with significant and non-significant (a) positive and (b) negative trends, (c) number of significant trends and field significance for change points and gradual trends in the Spree (left) and Schwarze Elster (right) river catchments.....	56

Figure 5-15:	Mean temperature: Comparison of trend magnitude between measured and simulated temperature for the period 1961-2006 (top) and between simulations for the period 2015-2061 (bottom) in the Spree and Schwarze Elster river catchments	59
Figure 5-16:	Precipitation: Comparison of trend magnitude between measured and simulated temperature for the period 1961-2006 (top) and between simulations for the period 2015-2061 (bottom) in the Spree and Schwarze Elster river catchments.....	60
Figure 6-1:	Schematic structure of the WaSiM-ETH model.....	65
Figure 6-2:	Schematic illustration of the interaction between unsaturated and saturated zone in WaSiM-ETH	67
Figure 6-3:	Schematic structure of the HBV-light model.....	68
Figure 6-4:	Soil routine in HBV-light: Contribution from rainfall or snowmelt to soil moisture storage/groundwater recharge (left) and reduction of potential evaporation depending on soil moisture storage.....	69
Figure 6-5:	Runoff response routine in HBV-light.....	69
Figure 6-6:	Routing routine HBV-light: example of runoff transformation with MAXBAS = 5	70
Figure 6-7:	Sensitivity of baseflow as a function of saturated hydraulic conductivity in WaSiM-ETH (example Dahme river catchment); high represents the upper limit of the saturated hydraulic conductivity, low the lower limit and medium the average.....	74
Figure 6-8:	Calibration strategy for HBV-light and WaSiM-ETH	76
Figure 6-9:	Comparison between measured and simulated mean monthly runoff for the Pulsnitz (1988-2006), Weißer Schöps (1963-1992) and Dahme (1963-1992)	81
Figure 6-10:	Flow duration curve for measured and simulated discharge for the Pulsnitz, Weißer Schöps and Dahme river catchments for the period 1999-2006.....	84
Figure 6-11:	Comparison of measured and simulated MAM(7) for the low-flow years 1999-2005 for the Pulsnitz, Weißer Schöps and Dahme river catchments	85
Figure 7-1:	Model chain for hydrologic climate change impact assessments.....	88
Figure 7-2:	Approach for estimating the change in the return period of the 50-year AM(7) flow between reference and scenario period	90
Figure 7-3:	Measured and simulated precipitation and temperature distribution on a daily, monthly and annual basis during the reference period (1963-1992)	92

Figure 7-4:	Precipitation: Intra-annual variability of measurements and simulations as well as the absolute difference between both (upper left corner) for the Pulsnitz, Weißer Schöps and Dahme river catchments	94
Figure 7-5:	Mean temperature: Intra-annual variability of measurements and simulations as well as the absolute difference between both (upper left corner) for the Pulsnitz, Weißer Schöps and Dahme river catchment.....	95
Figure 7-6:	Intra-annual variability of simulated discharge of a) WaSiM-ETH and b) HBV-light driven by meteorological measurements, meteorological output from DAs for the reference period and scenario period.....	98
Figure 7-7:	Density function of discharge for a) WaSiM-ETH and b) HBV-light driven by the meteorological measurements (“Measured”), meteorological output from the DAs for the reference and scenario period	99
Figure 7-8:	Flow duration curve based on WaSiM-ETH and HBV-light driven by the DAs in the reference and the scenario period for Weißer Schöps river catchment.....	102
Figure 7-9:	Change in the return period of the 50-year AM(7) between reference and scenario period for the Weißer Schöps river catchment. The arrows in the Figure display the change in occurrence of the return period of the reference 50 year low-flow in the scenario period.....	103
Figure 7-10:	Difference in actual evapotranspiration (ETA) based on REMO (top left), CCLM (top right), STAR (bottom left) and WettReg (bottom right) between the scenario and reference period for the Pulsnitz river catchment. The average change is displayed in each figure.....	106
Figure 7-11:	Difference in groundwater recharge (GWR) based on REMO (top left), CCLM (top right), STAR (bottom left) and WettReg (bottom right) between the scenario and reference period for the Pulsnitz river catchment. The average change is displayed in each figure.....	107
Figure 8-1:	Long term potential evapotranspiration (ETP), actual evapotranspiration (ETA) and runoff (R) for extreme land use scenarios (all area coniferous forest or uncultivated land) as well as current land use under current climate conditions	115
Figure 8-2:	Potential (ETP), actual evapotranspiration (ETA) and discharge (Q) for current land use and changed agricultural parameterisation under current climate conditions (1963-1992) as well as the dry, moderate and wet climate realisation of STAR 2 K (2031-2060) in the Dahme river catchment	117

Figure 8-3: Difference in long term actual evapotranspiration (ETA, left) and groundwater recharge (GWR, right) between the simulations with and without land use change (forest and crop change) based on the moderate climate change scenario in the Pulsnitz (top) and Dahme (bottom) river catchments 118

List of tables

Table 2-1:	Comparison of the main strengths and weaknesses of statistical and dynamical DAs.....	11
Table 3-1:	Characteristics of the downscaling approaches	19
Table 4-1:	Comparison of land use distribution [%] in the Spree and Schwarze Elster catchments between 1990 and 2006	27
Table 4-2:	Long term (1963-2006) annual mean temperature (T [°C]), corrected precipitation (P_{cor} [mm/a]) after SEVRUK (1986), potential evapotranspiration (ETP [mm/a]) calculated after WENDLING et al. (1991) and climatic water balance (CWB [mm/a])	37
Table 5-1:	Months with autocorrelation of time series above field significance in the Spree and Schwarze Elster river catchments	45
Table 5-2:	Magnitude of significant mean (T_{mean}), minimum (T_{min}) and maximum (T_{max}) temperature [°C] increase averaged over all stations (1951-2006)	48
Table 6-1:	Discretisation of unsaturated zone in the study catchments.....	72
Table 6-2:	Spatial data input requirements and parameterisation basis for 2D groundwater model	73
Table 6-3:	WaSiM-ETH parameters chosen for hydrological model calibration and their ranges used for calibration	76
Table 6-4:	Characteristics of HBV-light parameters chosen for hydrological model calibration	77
Table 6-5:	Performance criteria of discharge calibration and validation based on *daily and ** long-term mean monthly time step	79
Table 6-6:	Water balance components: corrected precipitation (P_{cor} [mm/a]), actual evapotranspiration (ETA [mm/a]), runoff (R [mm/a]), change in storage (ΔS [mm/a]) for the calibration and validation periods	82
Table 7-1:	Mass Balance Error [%] between simulated long term mean discharge driven by the meteorological measurements and by the meteorological output of the DAs during the reference period (1963 1992) for WaSiM ETH and HBV light.....	97
Table 8-1:	Overview of land use change scenarios	112

List of abbreviations

AM(7)	annual minimum 7-day mean flow
ASTER	advanced spaceborne thermal emission and reflection radiometer
BGR	Federal Institute for Geosciences and Natural Resources (proper name: Bundesanstalt für Geowissenschaften und Rohstoffe)
BK	conceptual soil map (proper name: Bodenkzeptkarte)
BMBF	Federal Ministry for Education and Research (proper name: Bundesministerium für Bildung und Forschung)
BTU	Brandenburg Technical University
BÜK	general soil map (proper name: Bodenübersichtskarte)
DA	downscaling approach
DEM	digital elevation model
DIFGA	runoff component analysis technique
DJF	December, January, February (winter)
DWD	Germany meteorological service (proper name: Deutscher Wetterdienst)
ETP	potential evapotranspiration
ETA	actual evapotranspiration
FDC	flow duration curve
GCM	general circulation model
GWR	groundwater recharge
HBV-light	conceptual hydrological model based on HBV-6
HUM	air humidity
HZG	Helmholtz-Zentrum Geesthacht – Centre for Materials and Coastal Research
IDW	inverse distance weighting
JJA	June, July, August (summer)
LAI	leaf area index
LfULG	Saxon State Agency of Environment, Agriculture and Geology (proper name: Sächsisches Landesamt für Umwelt, Landwirtschaft und Geologie)
LUGV	Ministry of Environment, Health and Consumer Protection of the Federal State of Brandenburg (proper name: Landesamt für Umwelt, Gesundheit und Verbraucherschutz, Brandenburg)
LNSE	nash-sutcliffe-efficiency using logarithmic values
MAM	March, April, May (spring)
MARE	mean average relative error
MBE	mass balance error
MQ	mean Discharge

NAU	precipitation-runoff-difference atlas (proper name: Niederschlags-Abfluss-Unterschiedsatlas)
NSE	nash-sutcliffe-efficiency
P	precipitation
PIK	Potsdam Institute for Climate Impact Research
Q	discharge
Q95	flow that is exceeded in 95 % of the time
R	runoff
RAD	global radiation
RCM	regional climate model
RH	relative humidity
RMSE	root mean square error
r^2	coefficient of determination
SD	sunshine duration
SLZ	HBV-light, response function, storage in lower zone [mm]
SON	September, October, November (autumn)
SWIM	soil and water integrated tool
T	temperature
VCF	vegetation covered fraction
W	wind speed
WaSiM-ETH	water balance simulation model developed at the ETH-Zurich

List of nomenclatures and symbols

BETA	HBV-light model parameter: parameter that determines the relative contribution to runoff from rain or snowmelt [-]
CFMAX	HBV-light model parameter: degree-day factor [mm/°C · day]
c_p	specific heat capacity of dry air at constant pressure, $c_p = 1.005 \text{ kJ}/(\text{kg} \cdot \text{K})$
d_r	drainage density for interflow [1/m]
E	latent heat flux [mm/m ²]
e	observed actual vapour pressure [hPa]
e_s	saturation vapour pressure at temperature T [hPa]
FC	HBV-light model parameter: maximum value of soil moisture storage [mm]
G	soil heat flux, here $0.1 \cdot R_N$ [Wh/m ²]
k_{rec}	recession of the hydraulic conductivity with depth [-]
k_{sat}	saturated hydraulic conductivity [m/s]
K0	HBV-light model parameter: recession coefficient (upper box) [1/day]
K1	HBV-light model parameter: recession coefficient (upper box) [1/day]
K2	HBV-light model parameter: recession coefficient (lower box) [1/day]
LP	HBV-light model parameter: soil moisture value above which ETA reaches ETP [mm]
MAXBAS	HBV-light model parameter: length of triangular weighting function in routing routine [day]
PERC	HBV-light model parameter: maximum rate of recharge between the upper and lower groundwater boxes [mm/day]
Qi	HBV-light, response function, runoff component [mm d ⁻¹]
r_a	bulk-aerodynamic resistance [s/m]
R_N	net radiation [Wh/m ²]
r_s	bulk-surface resistance [s/m]
SFCF	HBV-light model parameter: snow correction factor [-]
SUZ	HBV-light, response function, storage in upper zone [mm]
TT	HBV-light model parameter: threshold temperature [°C]
UZL	HBV-light model parameter: threshold for Q ₀ flow [mm]
λ	latent vaporization heat $\lambda = (2500.8 - 2.372 \cdot T)$ [kJ/kg]
Δ	tangent of the saturated vapour pressure curve [hPa/K]
ρ	density of dry air [kg/m ³]
γ_p	psychrometric constant [hPa/K]
$\theta(\psi)$	actual relative soil water content at suction [-]
θ_m	water content in the actual layer m [-]

θ_{sat}	saturation water content of the soil [-]
θ_{pwp}	water content of the soil at permanent wilting point (=1.5 MPa \approx 150 m)
θ_{ψ_g}	soil water content at a given suction
ψ	actual suction (capillary pressure) [m]

1 Introduction

1.1 Background and motivation

In the scientific community, there is a broad consensus about human induced changes to the climate system which can be attributed to increased greenhouse gas emissions during the last century (IPCC, 2007). Since the 1970s, when the impact of increasing CO₂ concentrations on global climate became better understood and started to be discussed by different scientific communities, climate change impact assessments have increasingly been reported. First studies have for example investigated the impact of climate change on the cryosphere (PARKINSON and BINDSCHADLER, 1984; THOMAS, 1984), sea level (SCHNEIDER and CHEN, 1980), agricultural production (BACH, 1979; ROSENBERG, 1982) and regional hydrology (BEARD and MARISTANCY, 1979). The majority of these studies have used rather simple modelling approaches such as hypothetical climate change scenarios of temperature and precipitation as input data for regression based methods which related the change in climate to an impact variable of interest. Other studies have simply performed a qualitative analysis (SCHNEIDER and CHEN, 1980). Since that time, the understanding of the factors, mechanisms and processes related to climate change and the modelling thereof on the global as well as regional scale have been improved considerably due to extensive research (CHRISTENSEN et al., 2007; KOUTSOYIANNIS, 2003; VAN DER LINDEN and MITCHELL, 2009). According to BATES et al. (2008), climate change will significantly affect regional water availability in many parts of the world with societal consequences related to agricultural productivity, floods and droughts, energy use, domestic municipal and industrial water supply, fish and wildlife management (TEUTSCHBEIN and SEIBERT, 2010; XU, 1999a). Consequently, determining possible impacts of climate change on the water balance, which is one major challenge in recent hydrological research (ELFERT and BORMANN, 2010), should be included in a successful integrated river catchment planning and management as well as for developing suitable climate change adaptation strategies on the regional scale (BORMANN et al., 2012; FÜSSEL, 2007).

In fact, improved forecasts of the hydrological response to a changing environment have “long been recognized as a means of more effectively managing water resources” (HAMLET and LETTENMAIER, 2000). This is especially true for catchments with a high anthropogenic impact, such as the Lusatian river catchments of Spree and Schwarze Elster in Germany. Large-scale interventions in the landscape due to lignite mining activities in the past hundred years as well as the sudden abandonment of the majority of the mines in the early 1990s have caused severe impacts on the water and mass balance and resulted in manifold user conflicts. The impact of climate change may aggravate these conflicts (GRÜNEWALD, 2001b;

KOCH et al., 2005; SCHOENHEINZ et al., 2011). Consequently, the project “Innovation Network Climate Change Adaptation Brandenburg Berlin (INKA BB)” (INKA BB, 2009) was launched by the Federal Ministry for Education and Research (BMBF) into whose framework this thesis is integrated.

In Eastern Germany, climate change impact studies have so far mainly been conducted on the scale of the Elbe river catchment (148,000 km²). For example, HUANG et al. (2010) made a German-wide climate change impact analysis based on the STATistical Regional (STAR) model (ORLOWSKY et al., 2008) and the ecohydrological Soil and Water Integrated Model (SWIM, (KRYSANOVA et al., 1998)), which clearly showed a reduction in the long term average water availability in the Elbe catchment. Within the framework of the GLOWA-Elbe project (GLOWA ELBE, 2013), CONRADT et al. (2012) confirmed the results of HUANG et al. (2010) using the same models but concentrating only on the Elbe catchment, which allowed them to make a more detailed analysis. The hydrological analyses by HUANG et al. (2010) and CONRADT et al. (2012) are, however, not detailed enough for the Lusatian river catchments of Spree and Schwarze Elster. Moreover, since they are based on only one climate downscaling approach (DA) and one hydrological model, uncertainty estimation is not possible. However, uncertainties related to climate change impact assessment have to be properly addressed and quantified because they can have important implications for water resource management and for the development of adaptive water resources management plans (DESSAI et al., 2009; FÜSSEL, 2007; JUNG et al., 2012; PATRINOS and BAMZAI, 2005). Besides technical measures, land use change, can have a significant impact on the hydrological behaviour of a catchment (ELFERT and BORMANN, 2010; HÖRMANN et al., 2005). The evaluation of the suitability and effectiveness of land use change as a climate change adaptation strategy is of high interest for regional stakeholders in the Lusatian river catchments (SWOT, 2014).

1.2 Objectives

The main objective of this thesis is the robust assessment of climate change impacts on the regional water resources in subcatchments of the anthropogenically heavily impacted Lusatian river catchments of Spree and Schwarze Elster (Germany) considering modelling uncertainties. For this purpose an integrated approach consisting of i) an ensemble-based modelling approach and ii) the incorporation of measured and simulated meteorological trends is proposed. Moreover, the effectiveness of land use based adaptation strategies is evaluated. Due to the susceptibility of the study region towards decreasing water availability (DIETRICH et al., 2012; KOCH et al., 2012), this thesis focusses not only on changes in the long term mean water balance components and discharge but also on low-flows.

The following research questions are addressed:

- 1) **Change detection in the measurements:** *Which changes in the meteorological measurements can be detected? How have the observed changes in the measured meteorological variables affected the measured hydrological variables? Have these changes occurred gradually or step-wise?*
- 2) **Comparison between trends in measurements and DA output:** *Do the trends simulated by the climate DAs coincide with the trends in the meteorological measurements of temperature and precipitation during the period 1961-2006? Do the simulated temperature and precipitation trends based on the DAs for the period 2015-2060 agree with the direction of change if the measurements were extrapolated into the future?*
- 3) **Comparison of conceptually different hydrological models:** *Do the results simulated by conceptual and process-based models differ during hydrological model calibration and validation?*
- 4) **Climate change analysis:** *What is the uncertainty bandwidth of the simulated water balance components resulting from an ensemble-based climate change impact analysis? Which ensemble member, the climate DA or the hydrological model and its parameterisation, adds the largest share of uncertainty to the final results during mean and low-flow conditions? What does a large uncertainty bandwidth imply for the development of adaptation strategies? Is it possible to narrow the uncertainty bandwidth of the final results by for example the integration of the results of the trend analysis?*
- 5) **Land use based adaptation to climate change:** *Which catchment characteristic dominates how catchments buffer potential climate change impacts on the hydrological cycle? What is the impact of land use change on the water balance components? Can land use change possibly compensate the simulated climate change impacts and therefore serve as a suitable climate change adaptation strategy in the Lusatian river catchments?*

1.3 Research approach

An integrated approach consisting of four different steps was chosen (Figure 1-1):

- 1) Trend analysis
- 2) Climate change analysis
- 3) Land use change analysis
- 4) Hydrological impact assessment.

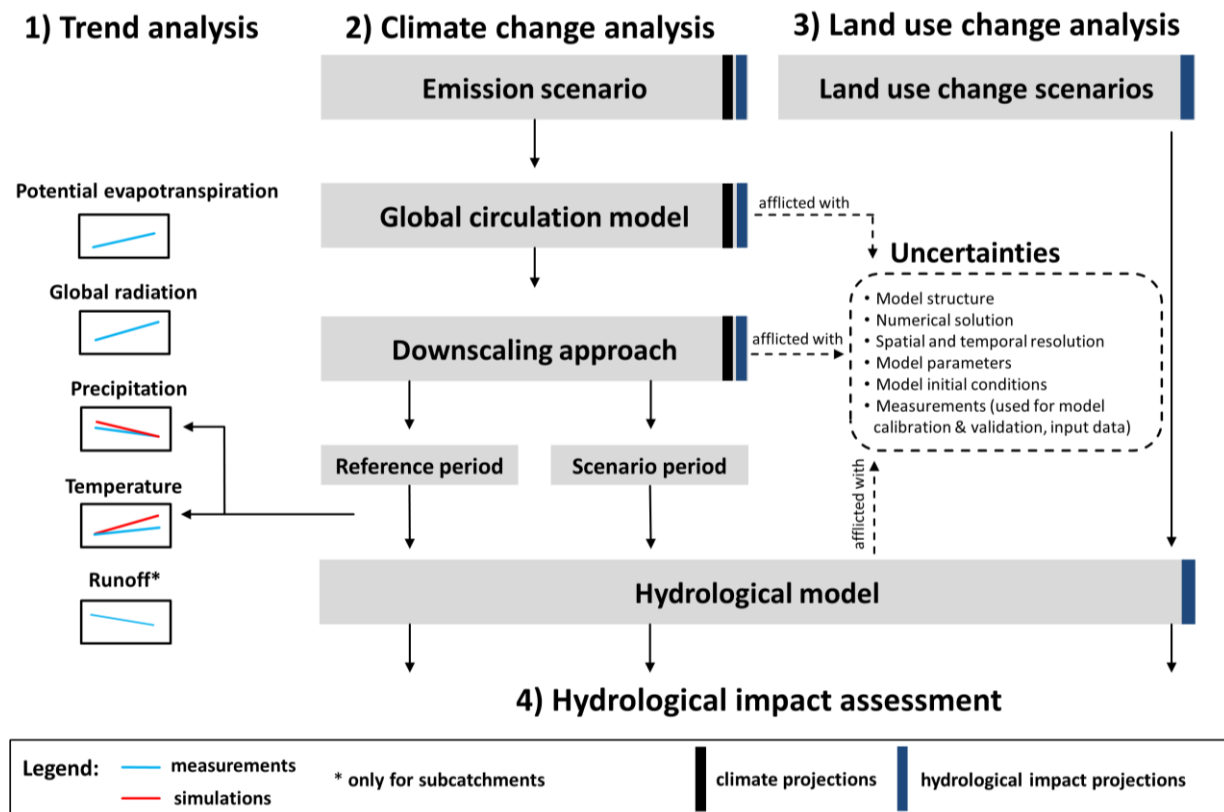


Figure 1-1: Research approach considering modelling uncertainties

In the first part, trend tests for gradual and step-wise change are performed on meteorological time series in the Spree and Schwarze Elster river catchments as well as in selected subcatchments. Trends in measured and simulated (by DAs) temperature and precipitation time series are also compared (Figure 1-1, Trend Analysis).

In the second part, a model based climate change impact assessment is performed for one subcatchment of the Schwarze Elster river and two subcatchments of the Spree river catchment. The subcatchments were chosen as study areas because it was postulated that their discharge has relatively low anthropogenic impact, facilitating hydrological model calibration and validation. At the same time, the subcatchments should be regarded as representatives for the entire catchment scale. For climate change impact assessments, a step-wise coupled modelling approach is used (Figure 1-1, Climate change analysis). The emission scenario, provided by the IPCC (IPCC, 2000), constitute the boundary conditions for

the Global Circulation Model (GCM). Since the spatial resolution of the currently available GCMs is too coarse for regional climate change impact studies, the GCM output needs to be downscaled. The downscaled meteorological time series serve as input for the hydrological model. This approach constitutes an explicit forward coupling in which no feedbacks are considered. The water balance components computed by the hydrological models are compared between the reference and scenario periods in order to analyse the change signal simulated by each DA for mean and low-flow conditions. Each item of the model chain is afflicted with considerable uncertainty (Figure 1-1, Uncertainties). In order to estimate the uncertainties related to the choice of the DA as well as to the hydrological model, an ensemble-based approach was chosen consisting of different DAs and conceptually different hydrological models.

In the third part of this thesis, the impact of land use change on the water balance components is analysed on the subcatchment scale. The aim of this analysis is to estimate the land use based adaptive capacity of the catchments to climate change as well as to evaluate the suitability of land use change as an adaptation strategy to climate change (Figure 1-1, Land use change analysis).

1.4 Outline of the thesis

This thesis is organised into ten chapters and is structured as follows: After the introductory chapter (Chapter 1), Chapter 2 presents the state of the art in the research areas of trend analysis for change detection, hydrological climate change impact assessments, climate change policy and low-flow analysis. Chapter 3 gives an overview of the data basis, data preparation and climate downscaling approaches before Chapter 4 introduces the study areas. Chapter 5, 6, 7 and 8 present the main results of this thesis. Chapter 5 focusses on the results of the trend analysis on the measurements and the meteorological output of the DAs. Chapter 6 describes the hydrological simulation tools, their set up, parameterisation and the results of model calibration and validation focussing both on mean and low-flows. Chapter 7 presents the climate change impact assessment focussing on the long term average water balance components, low-flows and spatial patterns of actual evapotranspiration and groundwater recharge considering modelling uncertainties. In Chapter 8 the potential of land use change as an adaptation strategy to climate change is assessed. The thesis closes with a summary and conclusion (Chapter 9) and an outlook (Chapter 10). It needs to be pointed out that the hierarchical structure of this scientific work does not reflect the development of this work at all times. Therefore, cross-referencing between different chapters was necessary.

2 State of the art of research

2.1 Trend analysis

2.1.1 Trend detection and attribution

According to the IPCC (2007), trend analysis can be differentiated between detection and attribution. Trend detection, on which emphasis is placed in this thesis, is the demonstration that an observed variable has changed in a statistical sense without necessarily knowing the reason for the change. Change in a time series can occur gradually, step-wise or in a more complex form affecting almost any aspect of the data, for example the mean, median, variance, etc. (KUNDZEWICZ and ROBSON, 2004). This is confirmed by MERZ et al. (2012) who pointed out that even opposing changes may occur simultaneously in the data structure. An example was given by DELGADO et al. (2010) in which the probability of an average flood decreased while the likelihood of extreme floods increased during the last half of the 20th century in the Mekong river catchment. For the evaluation of potential climate change, detecting trends in measured meteorological and hydrological time series has received increasing attention during the last decades (BIRSAN et al., 2005; KUNDZEWICZ and ROBSON, 2004; MERZ et al., 2012). In addition, the differentiation between gradual trends and change points has become a focus of many research studies for climate change analysis (GUERREIRO et al., 2014; MCCABE and WOLOCK, 2002; ROUGÉ et al., 2013; VILLARINI et al., 2009; VILLARINI and SMITH, 2010; VILLARINI et al., 2011; XIONG and GUO, 2004) and for designing future water resources projects (EHSANZADEH et al., 2011). Trend detection generally consists of two steps: determination of i) trend magnitude and ii) significance testing. Trend attribution, on the other hand, is the process of identifying the most likely causes for the detected change, which is, however, often difficult to achieve.

2.1.2 Gradual trends

A gradual trend, which can be defined as a regular change in data over time, can be expected to continue into the future and may therefore be interpreted as a harbinger of future change (BARKHORDARIAN et al., 2011). Therefore, gradual trends in measurements should be seen as an opportunity to validate the output from regional climate models, an approach, which has not yet been made use of in an integrated fashion in the majority of climate change impact studies.

The most common test used for assessing the significance of a trend in hydrological and meteorological time series is the non-parametric, rank-based Mann-Kendall test (KENDALL, 1975; MANN, 1945) which accepts or rejects the null hypothesis of randomness against the alternative of a monotonic trend. The test has been applied in numerous research studies

focussing on meteorological (GUERREIRO et al., 2014; TABARI et al., 2011), hydrological (ABDUL AZIZ and BURN, 2006; BURN, 1994; BURN and HAG ELNUR, 2002) and both meteorological and hydrological variables (BIRSAN et al., 2005; BURNS et al., 2007). The advantages of the Mann-Kendall test include that it can be applied to data sets containing outliers as well as non-linear trends. The main drawback of the Mann-Kendall test is that it is not robust against autocorrelation which was first noted by VON STORCH (1995) for positive autocorrelations. The stronger the data are positively autocorrelated, the higher the probability that the null hypothesis is rejected. This is referred to as error type I: false trend detected when none exists. In order to eliminate the influence of autocorrelation, VON STORCH (1995) suggests the “pre-whitening” approach. YUE et al. (2002b) extended the work of VON STORCH (1995) and found out that not only positive, but also negative autocorrelations affect the outcome of the Mann-Kendall test. For negative autocorrelations, the Mann-Kendall test rather tends to underestimate the probability of a trend which is denoted as error type II: failure to detect an existing trend. Furthermore, YUE et al. (2002b) notice that the “pre-whitening”, as proposed by VON STORCH (1995), affects the magnitude of a trend in a way that after “pre-whitening” the slope of the trend is reduced. Therefore, YUE et al. (2002b) propose the “trend-free-pre-whitening” procedure in which the trend of a time series is removed prior to the “pre-whitening”.

Other tests for evaluating the significance of a gradual trend include the Seasonal Kendall test (HIRSCH et al., 1982) which allows for seasonality in the data. The test has been applied in numerous trend analysis studies (ANGHILERI et al., 2014; MARCHETTO et al., 2013; SICARD et al., 2011; SKJELKVÅLE et al., 1999) and was extended by HIRSCH and SLACK (1984) to be robust against some autocorrelation in the data. The Spearman’s Rho (WOLFE, 2012) is another frequently applied statistical test (GELLENS, 2000; LETTENMAIER, 1976; LI et al., 2008; SHADMANI et al., 2012; YUE et al., 2002a) which is non-parametric and applicable for linear and non-linear trends. The test constitutes the rank-based version of the parametric Pearson correlation coefficient (KUNDZEWICZ and ROBSON, 2004). The most common tests for gradual trend detection is the linear regression test statistic, which is based on the regression gradient and assumes that data are normally distributed. Also other regression based methods have been developed and applied for trend analysis (BLOOMFIELD and STEIGER, 1983; ROUSSEUW and LEROY, 1987). The application of wavelets to hydrological and meteorological time series started to receive increasing attention during the last decades for trend analysis of floods (KALLACHE et al., 2005), streamflow data (ADAMOWSKI et al., 2009) as well as precipitation (PARTAL and KÜÇÜK, 2006) and temperature data (ALMASRI et al., 2008).

2.1.3 Change points

A change point is the point in time when the statistical properties of the time series change. Change points in time series must not necessarily be related to climate change but can also be related to changes in the measurement instrumentation, change in instrument location, and/or change in field procedure (CLARKE, 2010). Moreover, a change point can be interpreted as the beginning of a linear trend or the change of piecewise (linear) trends (RYBSKI and NEUMANN, 2011). Change points are often difficult to predict unless their cause is known.

KUNDZEWICZ and ROBSON (2004) characterise the non-parametric, rank-based Pettitt test (PETTITT, 1979) as a powerful test which is robust to changes in distributional form. The test accepts or rejects the null hypothesis of no change point against the alternative that a change point is present in the mean and has been applied in numerous research studies related to climate change detection (GEBREMICAEL et al., 2013; GUERREIRO et al., 2014; MA et al., 2008; ZHANG et al., 2008).

Another commonly used test is the distribution-free, non-parametric, rank-based CUSUM test (AFZAL et al., 2011; KAMPATA et al., 2008; KINAL and STONEMAN, 2012; WEBB et al., 2012). Using this test, successive observations are compared to the median of the series. The test statistic is the maximum cumulative sum (CUSUM) of the signs of the difference from the median starting from the beginning of the series (PAGE, 1954). Other statistical tests to identify the significance of change points in time series, but requiring the time of change to be known, are the student's t test (BONEAU, 1960) and the Wilcoxon-Mann-Whitney test (MANN and WHITNEY, 1947; WILCOXON, 1945). The student's t test is a standard parametric test assuming normally distributed data. The Wilcoxon-Mann-Whitney test is a rank-based test which looks for differences between two independent sample groups and due to its rank-based character does not require the data to be normally distributed.

2.1.4 Field significance

When a statistical test is performed on one single site, the significance of this individual test is the local significance α which is equal to the probability of falsely rejecting the null hypothesis (WILKS, 2006). When multiple tests are evaluated jointly at K gauges, a simultaneous evaluation of multiple hypothesis tests is performed and on average $K\alpha$ of them will be erroneously rejected (DOUGLAS et al., 2000; GUERREIRO et al., 2014). Therefore, the global significance level (field significance) needs to be considered. If the data which are evaluated simultaneously are independent, field significance can be determined using a binomial probability distribution (LETTENMAIER et al., 1994). Cross-correlation needs to be accounted for when the data are not independent because a spatial interdependence of the data reduces the effective number of degrees of freedom of the sample size. If for

example temperature measurements are spatially correlated and a trend is detected at one site, it is quite likely that a trend is also found at nearby sites. As a consequence, the null hypothesis will be rejected more often than it should. In addition, cross-correlation complicates the derivation of an exact probability distribution for the test statistic. Therefore, an approximate distribution must be developed (DOUGLAS et al., 2000). Bootstrapping is one suitable approach which preserves the cross-correlation among sites but removes any temporal correlation and possible trends (YUE et al., 2003). Based on this method, an empirical cumulative distribution function can be obtained to assess field significance of cross-correlated data.

2.1.5 Limitations of trend analysis

Independent of the choice of the statistical trend test used, trend analysis has several limitations. According to MERZ et al. (2012), trend detection is strongly dependent on the changes in the signal-noise-proportion as well as the structure and length of the measured time series. KUNDZEWICZ and ROBSON (2004) recommend to use at least 50 years of time series record in order to have confidence that climate variability does not obscure other changes. Detecting changes in the signal-noise-proportion implies the separation of anthropogenic signals and natural forcing factors by distinguishing between deterministic trends and stochastic variability. ASKEW (1987) argues that due to the complexity of the processes taking place in a river catchment and the climate system, a differentiation between natural variability and real trends is highly complex. This is in line with REFSGAARD (1987) and STAHL et al. (2010) who point out that the increasing human interaction with the natural environment needs to be considered because it aggravates the differentiation between natural trends and human interventions on the catchments scale. CHANDLER and SCOTT (2011) state that also the interconnection between different environmental variables needs to be considered during trend analysis as they may impact or mask each other. Due to these facts, BURN and HAG ELNUR (2002) argue that a rigorous, systematic procedure, including the consideration of different correlation structures of the data, is necessary.

2.2 Hydrological climate change impact assessments

2.2.1 Climate scenarios for hydrological climate change impact assessments

According to KEMFERT (2003), long term climate projections of future climate states require sophisticated modelling approaches. Today, at least three different approaches to generate climate projections for climate change impact assessments can be differentiated (BRONSTERT et al., 2007; XU, 1999b; XU et al., 2005): i) GCM climate output, ii) hypothetical climate scenarios and iii) downscaled GCM climate output, in the form of Regional Climate Models (RCMs) or statistical DAs.

While the use of GCM climate output (i) for climate change impact assessments is only applicable for macro-scale catchments, the focus of this thesis is on the other approaches (ii, iii) which can be used for catchments of any scale. Their purpose is to overcome the spatial mismatch between the resolution of the GCM (100-250 km) and the input data required for regional hydrological impact assessments.

1) Hypothetical scenarios as input to hydrological models

Hypothetical scenarios represent a simple alteration of the present climatic conditions by applying change factors to the measured meteorological variables of interest. This approach has initially been used in several climate change impact studies related to regional water resources (ARNELL, 1992; ENGELAND et al., 2001; JIANG et al., 2007; NASH and GLEICK, 1991; NĚMEC and SCHAAKE, 1982) due to the simplicity of the approach and the unavailability of regional climate models for many parts of the world. Even though, it is possible to analyse the sensitivity of hydrological variables to changes in the meteorological drivers using this approach, a changes in temporal and spatial variability, such as a shift in the temporal patterns of wet and dry days, is not considered (FOWLER et al., 2007; XU et al., 2005). Thus, hypothetical scenarios cannot be regarded as climate scenarios that are most likely to occur in the future (XU, 1999b).

2) Downscaled GCM climate output as input to hydrological models

To bridge the gap between the scale of the GCMs and the input data required for regional hydrological modelling, different DAs have been developed during the last years. Nowadays, the use of downscaled GCM climate data represents the state of the art approach, especially for regional applications. According to FOWLER et al. (2007), two fundamental approaches can be differentiated: dynamical and statistical DAs. Each of them have their strength and weaknesses (Table 2-1).

The use of dynamical DAs refers to the use of RCMs (FOWLER et al., 2007). RCMs simulate atmospheric processes at a resolution in the order of up to tens of kilometres over selected areas of interest. Due to the refined resolution (10-50 km) compared to GCMs (100-250 km), RCMs are able to simulate regional climate features such as orographic precipitation (FREI et al., 2003; RAGHAVAN et al., 2012) and extreme climate events (FOWLER et al., 2005; FREI et al., 2006) more precisely. Lately, the quality of RCMs to reproduce present-day climate has improved considerably (VARIS et al., 2004). Consequently, the number of impact studies using RCM output data has increased significantly over the last years (KÖPLIN et al., 2010; LEANDER et al., 2008; RÖSSLER et al., 2012; SENATORE et al., 2011; TEUTSCHBEIN and SEIBERT, 2010).

Table 2-1: Comparison of the main strengths and weaknesses of statistical and dynamical DAs (adapted from FOWLER et al. (2007), JIANG et al. (2007), KREIENKAMP et al. (2011), WILBY et al. (2002))

	Statistical DAs	Dynamical DAs
Strengths	<ul style="list-style-type: none"> - Can directly incorporate observation records of the region under investigation - Meteorological variables computed do not differ substantially from the measurements during the control period - Low computational demand, which facilitates the computation of a large number of realisations permitting the analysis of uncertainties related to the statistical approach - Based on standard and accepted statistical procedures - Easily transferable to other regions 	<ul style="list-style-type: none"> - Respond in a physically consistent way to their external forcing which also means that the statistical relationship between meteorological variables can be changed - Consistency with driving GCM - Produces finer resolution information from GCM-scale output (10-50 km resolution) - Resolve smaller scale atmospheric processes such as orographic precipitation
Weaknesses	<ul style="list-style-type: none"> - Require high quality input data, both temporally as well as spatially - Consideration of the predictor/predictand relationship as stationary - In case they depend on a driving GCM, they are affected by its bias - Climate system feedbacks are not included - When no changes in the statistical relation between the climate variables are assumed, the statistical DAs should only be used as long as the simulated climate does not diverge too strongly from the observed climate 	<ul style="list-style-type: none"> - Computationally intensive - therefore, only few realisations available - Due to their strong dependence on the driving GCM, RCMs are susceptible to systematic errors in the driving fields, for example in the boundary conditions - Lack of a two-way interaction between the GCM and RCM - Due to large deviations to measurements, a bias correction is necessary

TEUTSCHBEIN and SEIBERT (2012a) as well as HAMLET and LETTENMAIER (2000) point out that the output of dynamical RCMs is often afflicted with a considerable bias, a systematic deviation between measurements and simulations, as a result of “model errors caused by imperfect conceptualization, discretization and spatial averaging within grid cells” (TEUTSCHBEIN and SEIBERT, 2010). Consequently, before the meteorological output of RCMs can be used for climate change impact assessments, a bias correction is necessary.

Statistical DAs are based on the assumption that regional climate is a function of the large-scale atmospheric state. The relationship between the global and local climate can be expressed as a stochastic and/or deterministic function between predictors (large-scale atmospheric variables) and predictands (local or regional climate variables, (FOWLER et al., 2007)). Different statistical DAs have been developed including regression models, weather typing schemes and weather generators and applied in various research studies (BORMANN, 2009; CONRADT et al., 2012; HATTERMANN et al., 2011; HUANG et al., 2013a; HUANG et al., 2013b; HUANG et al., 2010; TEUTSCHBEIN et al., 2011).

2.2.2 Hydrological models for hydrological climate change impact assessments

Hydrological models simulate the hydrological response to changes in the meteorological drivers in climate change impact assessments. For this purpose, several conceptually different hydrological models are available, ranging from process-based fully distributed to process-oriented semi distributed and conceptual lumped hydrological models (SINGH, 1995).

Representatives for each hydrological model type include:

- Process-based fully distributed: WaSiM-ETH (SCHULLA and JASPER, 2012), CATFLOW (MAURER, 1997; ZEHE et al., 2001), MIKE-SHE (REFSGAARD and STORM, 1995)
- Process-oriented semi distributed: SWAT (ARNOLD et al., 1993; ARNOLD et al., 1998), SWIM (KRYSANOVA et al., 1998), TOPMODEL (BEVEN et al., 1995; BEVEN and KIRKBY, 1979)
- Lumped conceptual: HEC-HMS (FELDMANN, 2000), NAM (NIELSEN and HANSEN, 1973), WatBal (YATES, 1996)

The choice of a model depends, among others, on the study aim and required model outputs, available resources in terms of data, time and money, the hydrological modellers experience as well as the characteristics of the study area (CUNDERLIK, 2003). The existence of physically-based models is, according to ROSBJERG and MADSEN (2005), an illusion due to simplifications of the physics made in models and lack of complete knowledge of many processes in hydrology.

An advantage of process-based models is that their parameters generally have a physical basis and can therefore be based on measurements. Consequently, also the system dynamics should be maintained beyond calibration (ABBOTT et al., 1986; CULLMANN et al., 2011) which makes their application promising in climate change impact assessments. The parameters of conceptual models, on the other hand, are not measurable and must be calibrated (KAVETSKI et al., 2006; SEIBERT, 2000). As a result of that, the application of conceptual models is, as reported in many research studies, limited to the conditions represented by the data used for model calibration (CULLMANN et al., 2011); thus, if

changes in these conditions occur, as may be expected in the context of climate change, the validity of the calibrated parameters is questionable (MERZ et al., 2011). Two frequently used hydrological models in climate change impact assessments are the process-based, fully distributed hydrological model WaSiM-ETH (CALANCA et al., 2006; FUHRER et al., 2006; GRAHAM et al., 2007b; JASPER et al., 2006; NATKHIN et al., 2012; RÖSSLER et al., 2012) and the conceptual model HBV-light which can be used as a lumped and semi-distributed model (STEELE-DUNNE et al., 2008; TEUTSCHBEIN and SEIBERT, 2010; TEUTSCHBEIN and SEIBERT, 2012a; TEUTSCHBEIN and SEIBERT, 2012b; TEUTSCHBEIN et al., 2011).

2.2.3 Cascade of uncertainty and ensemble-based modelling

During the last decades, the number of research projects and publications dealing with the impacts of climate change, especially focussing on water, have increased considerably, even turning into a “fashionable indoor sport” (BEVEN, 2001). Due to these research efforts, the capabilities of modelling, analysing and assessing climate change impacts on water resources have significantly improved. Nevertheless, each item of the climate change model chain is subject to considerable uncertainty (MAURER, 2007; SURFLEET and TULLOS, 2013; WILBY and DESSAI, 2010; XU et al., 2005) which amplifies itself leading to a “cascade of uncertainty” (SCHNEIDER, 1983) or an “uncertainty explosion” (HENDERSON-SELLERS, 1993; Figure 2-1).

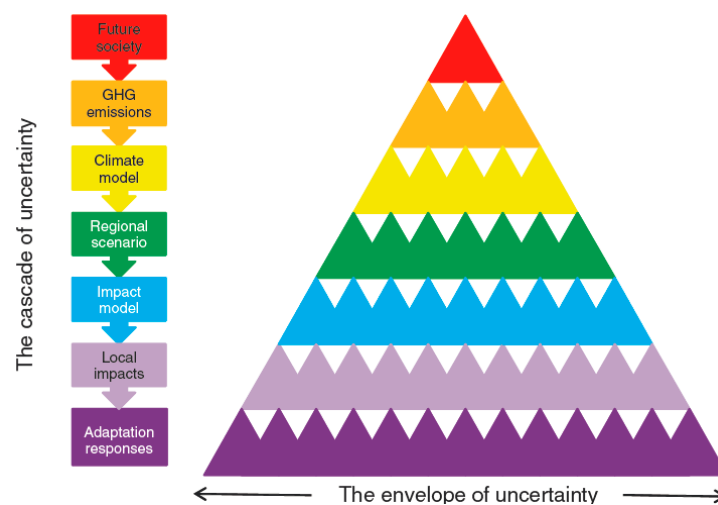


Figure 2-1: The uncertainty cascade of climate change impact assessments (WILBY and DESSAI, 2010)

WILBY and DESSAI (2010) call the total number of permutations at each step with the model chain the envelope of uncertainty. Due to the expansion of uncertainty at the regional impact level, BLÖSCHL and MONTANARI (2010) raise concerns about the reliability of the step-wise coupled model approach as well as the representativeness of the final results. Consequently, several studies have stressed the need for ensemble-based climate change impact studies (DÉQUÉ et al., 2007; LOPEZ et al., 2009; RÖSSLER et al., 2012; TEUTSCHBEIN and SEIBERT, 2010), where several representatives of each model chain item are included

allowing for an uncertainty estimation. Through that, it is hoped to gain more confidence in the final results which is a crucial criterion for decision makers (BORMANN et al., 2012). Currently, the majority of the ensemble-based climate change impact studies conducted in Europe use the dynamical RCMs from the ENSEMBLES project (VAN DER LINDEN and MITCHELL, 2009), without considering additional statistical approaches. Multiple dynamical climate models should rather be regarded as “a family of coexisting models” (KNUTTI, 2008) which cannot be regarded as independent (JUN et al., 2008) because they are calibrated on the “same (possibly biased) observations” (KNUTTI, 2008) and have not been developed for uncertainty exploration. Therefore, dynamical as well as statistical DAs should be included in order to get an adequate and representative sample of possible future conditions. However, *Fowler et al.* [2007] point out that yet only few studies have compared the relative performance of statistical and dynamical DAs in climate change impact assessments.

Also the uncertainty related to the hydrological models should not be underestimated within the climate change model chain. In fact, uncertainties related to hydrological models, including among others model structure, parameters and spatial and temporal model resolution, have long been regarded as an important factor in water resources decision making (WOOD, 1978).

Based on an ensemble-based modelling approach, a bandwidth of results is obtained and the uncertainties related to model based climate change impact study can be evaluated. If the bandwidth of the final results is not too large, it allows regional stakeholders to make informed decisions concerning an integrated sustainable water resources management and the development of suitable adaptation strategies.

2.3 Climate change policy: mitigation and adaptation

Climate change policy can be subdivided into two complementary strategies: mitigation and adaptation. The primary aim of climate change mitigation is to reduce greenhouse gas emissions, by for example reducing the burning of fossil fuels, and/or to increase greenhouse emission sinks, for example in the form of tree plantations. Adaptation, on the other hand, focusses on possible actions to moderate negative climate change impacts on a vulnerable system and if possible to exploit opportunities resulting from a changing climate (BORMANN et al., 2012; FÜSSEL, 2007; MCCARTHY et al., 2001; VON STORCH, 2009).

In contrast to climate change mitigation which is evaluated on the global scale, climate change adaptation has always been part of human development (REYER et al., 2011) and its scale of effect is regional to local (BORMANN et al., 2012; FÜSSEL, 2007; GRÜNEWALD, 2012b; KLEIN et al., 2005; VON STORCH, 2009). During the last decades, climate change mitigation has received significantly greater attention, both scientifically as well as from a policy perspective (FÜSSEL, 2007; PIELKE et al., 2007; VON STORCH, 2009). According to

FÜSSEL (2007), this is mainly due to the fact that the success of climate change mitigation is easier to monitor and measure. Moreover, all climate-sensitive systems benefit from mitigation action. The potential of many systems to adapt to climate change is, however, limited (ADGER and BARNETT, 2009). PIELKE et al. (2007) noted that adaptation to climate change was initially regarded as an important policy option during the early policy discussion in the 1980s. After that, however, climate change adaptation has been regarded as a way of accepting the failure of political action towards climate mitigation (PIELKE et al., 2007), and has therefore turned into a “secondary concern” (VON STORCH, 2009). The “taboo on adaptation” (PIELKE et al., 2007) was consolidated by several policy makers and scientists who have been arguing that the uncertainty related to climate change scenarios need first to be reduced before suitable adaptation strategies can be developed (COOPER, 1978; DESSAI et al., 2009; FÜSSEL, 2007; KELLY, 1979; MURPHY et al., 2004; PATRINOS and BAMZAI, 2005). However, climate change is only one stressor of global change (GRÜNEWALD, 2012b; REYER et al., 2011) and economical and societal changes are also hardly predictable. Recently, mainly driven by several climate related extreme events, public interest in climate change adaptation has risen (BORMANN et al., 2012; FÜSSEL, 2007; KRYSANOVA et al., 2010). These extreme events, including for example the hurricane Katrina in the United States in 2005 and the Elbe river flood in 2002 and 2013 in Germany, demonstrated the vulnerability of societies to current climatic conditions (VON STORCH, 2009). Additionally, it has become obvious that independent of the progress made in climate change mitigation during the next years, there is a clear mismatch between the effects of mitigation and climate change impacts due to the inertia of the climate system (PIELKE et al., 2007). Thus, adaptation to climate change is inevitable.

In fact, throughout history, water managers have always been balancing the diverse water needs of society with the greatly fluctuating, both spatially and temporally, natural water yield using different methodological and technological approaches (GRÜNEWALD, 2001a; GRÜNEWALD, 2012b). These approaches have so far been based on the stationarity assumption whose validity was questioned by MILLY et al. (2008) since climate change may not only affect the extremes but also the potential and stable water yield (GRÜNEWALD, 2012b).

2.4 Low-flow analysis

Low-flow can be defined as “flow of water in a stream during prolonged dry weather” (WMO, 1974). SMAKHTIN (2001) argued however, that this definition does not explicitly differentiate between low-flow and drought. Low-flow is a seasonal phenomenon and an integral component of a flow regime in any river. Drought, on the other hand, which can be differentiated into meteorological, atmospheric, agricultural, hydrological and water

management drought, is a natural event resulting from an extended period of time with precipitation less than normal. DINGMAN (2008) argue that to qualify as a drought, “dry periods must have a duration of at least a few months and be a significant departure from normal”. According to SMAKHTIN (2001), knowledge of the frequency as well as the magnitude of low-flows is important for water resources management purposes: water supply planning and design, reservoir storage design, maintenance of quantity and quality of water for irrigation. In addition to that, societal and ecological requirements are receiving increasing attention since low-flows impact recreation, wildlife and water-related flora and fauna conservation.

According to the WMO (2008), different ways of analysing a discharge time series exist to describe the low-flow regime of a river. Frequently used approaches include the base flow index, recession analysis, low-flow statistical indicators and frequency analysis of extreme low-flow events. The base flow index is derived by separating the hydrograph into a quick and a delayed component, assuming that the delayed component corresponds to the base flow. The base flow index is correlated with the hydrological properties of soil, geology and other storage related descriptors (GUSTARD, 1983; WMO, 2008). Recession analysis examines the falling limb of the hydrograph during discharge depletion. Again, the rate of recession and the shape of the recession curve reflect catchment characteristics (SMAKHTIN, 2001). Furthermore, different low-flow statistical indicators exist including the ninety-five percentile flow (Q95) and annual minimum flow for different durations (AM(n-day)). The Q95 is defined as the flow that is exceeded 95 % of the observed time period (WMO, 2008). In order to estimate the Q95, the Flow Duration Curve (FDC) has to be determined which is, according to SMAKHTIN (2001), “one of the most informative methods of displaying the complete range of river discharges from low-flows to flood events” describing the relationship between magnitude and frequency of discharge. The annual minimum 7-day mean flow (AM(7)) is referred to as the dry weather flow by HINDLEY (1973) and is commonly used for low-flow analysis (FEYEN and DANKERS, 2009; MAMUN et al., 2010; STAHL et al., 2010; SVENSSON et al., 2005). According to STAHL et al. (2010), the AM(7) provides a “true” low-flow value which is highly relevant for water resources management purposes. Choosing longer averaging windows, for example 30 days, can be rather interpreted as an indicator of extended-duration low-flow or even a drought, especially in smaller fast reacting catchments. By frequency analysis, estimates of the probability of occurrences of low-flow events from historical records can be derived (WMO, 2008). Even though low-flows are part of the natural variability of climate, due to climate change, changes in the occurrence and frequency in low-flows can be expected (ALLEN et al., 2010; DAI, 2013; KUNDZEWICZ et al., 2007; VROCHIDOU et al., 2013). To what extend low-flows

will change under climate change is currently one of the main research challenges, especially in areas which are, already under current climate conditions, prone to low-flows.

3 Data basis, data preparation and climate downscaling approaches

3.1 Data basis and data preparation

The data basis (Table A-1 in Appendix A) can be subdivided into three main categories:

- Climatic data: meteorological measurements (Table A-2 (Schwarze Elster) and Table A-3 (Spree) in Appendix A), meteorological output from DAs
- Hydrological data: measured discharge
- Spatial data sets: digital elevation model, soil, land use and hydrogeological maps.

The meteorological data were provided by the Potsdam Institute for Climate Impact Research (PIK). At the PIK, the measured meteorological time series were already pre-processed including:

- Interpolation of variables that are only measured at climate stations (temperature, global radiation, wind speed, sunshine duration and humidity) onto the precipitation stations
- Complementation of missing values
- Homogenizing of the data.

The discharge time series and spatial data set were provided by governmental authorities. Measured meteorological time series were used for i) time series trend analysis (chapter 5) and ii) as boundary condition for the hydrological modelling (chapter 6). The meteorological output of the DAs was used for i) comparison to trends in the measured meteorological time series (chapter 5) and ii) as a driver for the hydrological models in the climate and land use change impact assessments (chapter 7 and 8). Measured discharge was used for i) time series trend analysis and ii) hydrological model calibration and validation (chapter 5 and section 6.2.3). In addition, the data and information contained in the Precipitation-Runoff-Difference (NAU) atlas (IFWW, 1959) and the water balance information portal by the Saxon State Agency of Environment, Agriculture and Geology (“Wasserhaushaltsportal Sachsen” (LFULG, 2012)) were used to assist hydrological model parameterisation and calibration. The water balance information portal contains simulated water balance based on the runoff component analysis technique DIFGA for river catchments located in the Free State of Saxony (LFULG, 2012; SCHWARZE, 1991; SCHWARZE et al., 1989). The spatial data sets were used for catchment characterisation (chapter 4) and as input for the spatially distributed hydrological model WaSiM-ETH (section 6.2.1). The fact that the study catchments are located in different federal states (Pulsnitz: more than 95 % in Saxony, the rest in Brandenburg; Weißer Schöps: Saxony; Dahme: Brandenburg (Figure 4-1)) resulted in different data bases as well as data incompatibilities at the state borders which were adjusted during data pre-processing.

3.2 Climate downscaling approaches

3.2.1 Characteristics of downscaling approaches

The meteorological output of four different DAs was used in this thesis, whose characteristics are summarized in Table 3-1.

Table 3-1: Characteristics of the downscaling approaches

	REMO	CCLM	STAR	WettReg
Model type	Dynamical	Dynamical	Statistical	Statistical
Source	(JACOB, 2001)	(BÖHM et al., 2008)	(ORLOWSKY et al., 2008)	(SPEKAT et al., 2010)
Simulation period	1951-2100	1961-2100	2007-2060	1961-2100
Driving GCM	ECHAM5/ MPI-OM	ECHAM5/ MPI-OM	Not directly depending on a GCM, only driven by a linear temperature trend	ECHAM5/ MPI-OM
Emission scenario available	A1B, A2, B1	A1B, B1	No Emission scenario, but three different temperature trends (0K, + 2K and + 3K)	A1B, A2, B1
Spatial resolution	0.088° (10 x 10 km)	0.2° (18 x 18 km)	Station-based	Station-based
Number of realisations per emission scenario	1	2	100	10

The boundary conditions of the DAs are all based on the GCM ECHAM 5/MPI-OM (ROECKNER et al., 2003) driven by emission scenario A1B. Since the existing emission scenarios (A1B, A2, B1) do not differ considerably until the middle of the 21st century, to which this study is restricted by the STAR model (Table 3-1), the focus on only the A1B emission scenario was regarded as sufficient. This model basis, same emission scenario and GCM, guarantees that differences in the meteorological variables (Table 3-1) are predominantly related to the DA. The DAs differ, however, in the number of available realisations (Table 3-1) and the available output data. The two model realisations of CCLM are a result of using different years for initialising the driving GCM. Due to the fact that the RCMs are computationally demanding, only few realizations are available. For WettReg and STAR, which are computationally less demanding, the large number of realisations are a result of different combinations/variants of statistical time series construction (more details in section 3.2.2 and 3.2.3).

The spatial discretisation of the dynamical (uniform grid cells) and the statistical (meteorological stations) DAs leads to differences in the spatial output format of their meteorological variables. To avoid the introduction of uncertainties related to the difference in the availability of the spatial format of the data, the meteorological variables of four grid cells of the dynamical RCMs REMO and CCLM surrounding a meteorological station are interpolated onto the station using the inverse distance method. This approach guarantees that more grid cells are considered in the analysis and thereby reduces the bias a single RCM grid cell might introduce. So far, the DAs REMO, CCLM, STAR and WettReg have been used in several climate change impact studies in Germany (CONRADT et al., 2012; GRAHAM et al., 2007b; HATTERMANN et al., 2011; HUANG et al., 2010).

3.2.2 STAR

The STAtistical Regional model STAR represents a temporal analogue resampling technique developed by ORLOWSKY et al. (2008) at the PIK. Temporal analogue resampling techniques use past climate records as an analogue of a possible future climate (BUDYKO, 1989; SANTOSO et al., 2008; WARRICK, 1984). Consequently, the generation of future climate time series using the STAR approach fully relies on high quality measured data. The resampling is only driven by the prescribed temperature trend; all other variables (precipitation, radiation, etc.) are carried along. This implies that the consistency of the statistical relationship between meteorological variables, such as the variability and frequency distribution, is conserved.

In a first step, for each climate station, one year from the measured climate time series (1951-2006) is randomly chosen and appointed to a year in the scenario period (2007-2060). Doing so, warm years are preferably chosen in order to comply with the prescribed temperature trend. The same years cannot directly follow each other. Since this is a random, heuristic process and the recombination of years can generate different variants of projected time series which all follow an increasing temperature trend but differ in the other meteorological variables, many different variants (realisations) are produced. If after step one, the prescribed temperature trend of the newly designed time series is not met, in step two, blocks of 12 days are substituted in such a way that the time series shifts towards reaching the prescribed temperature trend. The choice of blocks of 12 days ensures that the future time series have realistic persistence features (HUANG, 2012).

The fact that STAR is driven only by a linear temperature trend implies that it is independent of the deficits and bias of a driving GCM. However, this also infers that the increase in temperature is only generated from the measurements from the past without considering physical effects such as the increase in radiative forcing as a result of rising greenhouse gas concentration in the atmosphere (WECHSUNG, 2013). In the study region, warmer winter

days are on average characterised by higher precipitation rates compared to colder winter days while warm summer days are generally dryer compared to cold summer days. Consequently, the results based on the STAR approach are not open-ended, because the probability that cold dry winter days are substituted by warm wet winter days and cold wet summer days by warm dry summer days is very likely. Therefore, STAR simulates a shift towards wetter winters and dryer summers in the study region which WECHSUNG (2013) called an energetic bias. Another drawback of the model is that it cannot generate extremes that exceed the already observed ones due to its analogues approach. In this study, 100 realisations of the STAR + 2K were used.

3.2.3 WettReg

The Weather-type Regionalisation method (WettReg) in the 2010 version was developed by the Climate & Environment Consulting Potsdam GmbH (CEC), Germany (SPEKAT et al., 2010). The model algorithm is based on measured meteorological variables from climate and precipitation stations operated by the DWD, reanalysis data and the output of the GCM ECHAM 5/MPI-OM. The model uses the statistical relationship between large scale atmospheric conditions by circulation pattern classification and local climate to compute future time series of meteorological variables (ENKE et al., 2005a; ENKE et al., 2005b). WettReg was developed based on the assumption that the GCM is able to produce climate patterns in a consistent way and that the large scale climate patterns can be utilized to derive climate information at the regional scale. This implies that changes in large scale atmospheric patterns initiate changes at the regional scale. Making use of this assumption, WettReg combines the advantages of dynamic models, in the form of a GCM, with the possibilities of a statistical weather generator.

The WettReg algorithm can be summarized as follows: At first, observed weather types are objectively classified into 10 classes for measured temperature and eight classes for measured precipitation for each season. Future time series are derived using a stochastic weather generator who rearranges episodes from the current climate into new synthesized time series which should reflect the (shifted) frequency of weather patterns simulated by the driving GCM. Furthermore, the synthesized time series are adjusted by means of regression to changes in the simulated physical properties of the atmosphere (KREIENKAMP et al., 2011). Thus, the algorithm generates meteorological station based time series which represent the shifts in climate derived from the driving GCM. The relationship between large-scale climate patterns and regional climate is, however, established for the control period. Consequently, the validity of this relationship for future time periods can be questioned (HUANG et al., 2013b).

One of the particularities of the 2010 version of WettReg is the consideration of so called “Trans Weather Patterns” (KREIENKAMP et al., 2011) which are weather patterns that are not yet characteristic for the current climate but may emerge in the future. An advantage of WettReg over STAR is the fact that extreme values exceeding the observed ones can be generated which makes the model applicable for analysing changes in extreme values, such as changes in flood or drought frequencies (HUANG et al., 2013a; HUANG et al., 2013b). In this study, 10 realisations of the A1B scenario of WettReg were used.

3.2.4 CCLM

The COSMO (Consortium for Small-scale Modelling) model in Climate Mode (CCLM) is a RCM developed by a consortium of three different research institutions: BTU Cottbus-Senftenberg, PIK and Helmholtz-Zentrum Geesthacht (HZG) (BÖHM et al., 2008; ROCKEL et al., 2008). CCLM is the climate version of the non-hydrostatic weather forecast model, the “Local Model” which was originally developed by the DWD.

CCLM is a limited-area atmospheric prediction model based on thermo-hydrodynamical equations which describe compressible flow in a moist atmosphere. The model equations are solved numerically on rotated geographical coordinates and a generalized terrain following height coordinates with a horizontal resolution of 18 x 18 km. The atmosphere is subdivided into 32 vertical atmospheric layers and 10 vertical soil layers. Processes such as turbulence, formation of clouds and precipitation and soil processes cannot be resolved at the modelling spatial scale and are parameterised based on the “Local Model”. In this study, two realisations of the A1B scenario of CCLM were used.

3.2.5 REMO

The REgional climate Model REMO was developed at the Max-Planck-Institute for meteorology (MPI-M) (JACOB, 2001; JACOB et al., 2001) based on the former numerical weather prediction model of the DWD, the “EUROPA-MODELL” (MAJEWSKI, 1991). It is a three dimensional hydrostatic climate model. As CCLM, REMO is based on the thermo-hydrodynamical equations solved on rotated geographical coordinates with a finer horizontal resolution of 10 x 10 km. Vertically, the atmosphere is discretised into 26 layers and into 5 soil layers. Processes occurring below the spatial grid scale are parameterised based on ECHAM, but adjusted to the finer spatial scale. In REMO the hydrostatic approximation replaces the vertical momentum equation. Therefore, vertical acceleration is negligible compared to vertical pressure gradients and vertical buoyancy forces. Different from the other DAs, time series of global radiation, which are necessary for calculating potential evapotranspiration using the Penman-Monteith approach, are not available for REMO. As an alternative, the approach of OESTERLE (2001) was used to reconstruct daily

global radiation time series based on simulated cloud cover and humidity time series which are simulated by REMO. In this study, one realisations of the A1B scenario was used.

3.3 Bias correction of REMO and CCLM

The linear scaling approach (LENDERINK et al., 2007) was used to correct the bias of the simulated meteorological variables temperature, precipitation and global radiation of REMO and CCLM. The linear scaling approach operates with monthly correction values based on the differences between measured and simulated values. Equation 3-1 was used to calculate the monthly correction value for temperature and Equation 3-2 for precipitation, global radiation, and wind speed. The calculation was based on the longest available time period (CCLM: 1961-2006; REMO: 1951-2006, Table 3-1). The correction terms were then applied to the daily simulated values.

$$T_{cor}(m) = T_{RCM}(m) + [\bar{T}_{ref}(m) - \bar{T}_{RCM_{ref}}(m)] \quad \text{Equation 3-1}$$

$$V_{cor}(m) = V_{RCM}(m) * \frac{\bar{V}_{ref}(m)}{\bar{V}_{RCM_{ref}}(m)} \quad \text{Equation 3-2}$$

with T temperature
 V precipitation, global radiation, wind speed
 \bar{T} mean temperature
 \bar{V} mean of precipitation, global radiation, wind speed
 cor bias corrected
 m month
 ref reference period

The main advantage of the linear scaling method is that it is relatively simple. The disadvantage of this method is that it only accounts for the bias in the mean, but differences in other statistical properties, such as the variance and frequencies, are not taken into account. In contrast to REMO, the air humidity simulated by CCLM, necessary for calculating potential evapotranspiration using the Penman-Monteith approach, also needed to be bias corrected due to large deviations from the measurements. Since the linear scaling approach proved to be insufficient for bias correcting air humidity, a distribution mapping approach was used (SENNIKOV and BETHERS, 2009). Defining and applying two linear transfer functions resulted in a good agreement between simulated and measured humidity values by CCLM. The statistical DAs were not bias corrected. According to KREIENKAMP et al. (2011), WettReg is not afflicted with a considerable bias within the period 1971-2000 and the analogue STAR method uses the measured meteorological time series from the past to generate future time series by a date-to-date mapping approach (ORLOWSKY et al., 2008). Consequently, no simulated meteorological STAR data are available for the past.

4 Study areas

4.1 Characterisation of selected Lusatian river catchments

4.1.1 Spree and Schwarze Elster river catchments

The second and first order Elbe river tributaries Spree and Schwarze Elster are located in eastern Germany (Figure 4-1). Due to the extensive lignite mining activities during the last century in this region, the groundwater and surface water resources are substantially impacted (GRÜNEWALD, 2001b).

The Spree river catchment ($A \approx 10,000 \text{ km}^2$, river length $\approx 376 \text{ km}$) extends from the Free State of Saxony, where the Spree river rises in the Lusatian Highlands, to Brandenburg and drains into the Havel river at the German capital Berlin (Figure 4-1). On its way, the Spree river passes through the Lower Lusatian lignite mining district, where five active lignite mines, several abandoned opencast mines and the UNESCO biosphere reserve Spreewald are located (Figure 4-1). Being a highly regulated wetland area, the Spreewald covers an area of around 320 km^2 with a running water system of $1,600 \text{ km}$ in length (DIETRICH et al., 2007; GROSSMANN and DIETRICH, 2012).

The Schwarze Elster river catchment ($A \approx 5,665 \text{ km}^2$, river length $\approx 169 \text{ km}$) also rises in the Lusatian Highlands in Saxony and flows through the state of Brandenburg before it drains into the Elbe river at the municipality Elster in Saxony-Anhalt. In the upper part of the catchment, many abandoned opencast lignite mines are located.

The abandoned opencast mines in the Schwarze Elster as well as in the Spree river catchment are successively converted to post mining lakes. After complete filling, these lakes are expected to cover an area of around $24,000$ hectares which corresponds to about $1/4^{\text{th}}$ of the lignite mining area utilised (DREBENSTEDT and MÖCKEL, 1998). Due to the large surface water area of the lakes, large evaporation losses, especially during warm summer months, are expected. The intended use of the “lake district” ranges from water reservoirs, fish farming lakes to recreational purposes. It is expected that the “lake district” will be of great relevance for the touristic development as an important economic sector in this region.

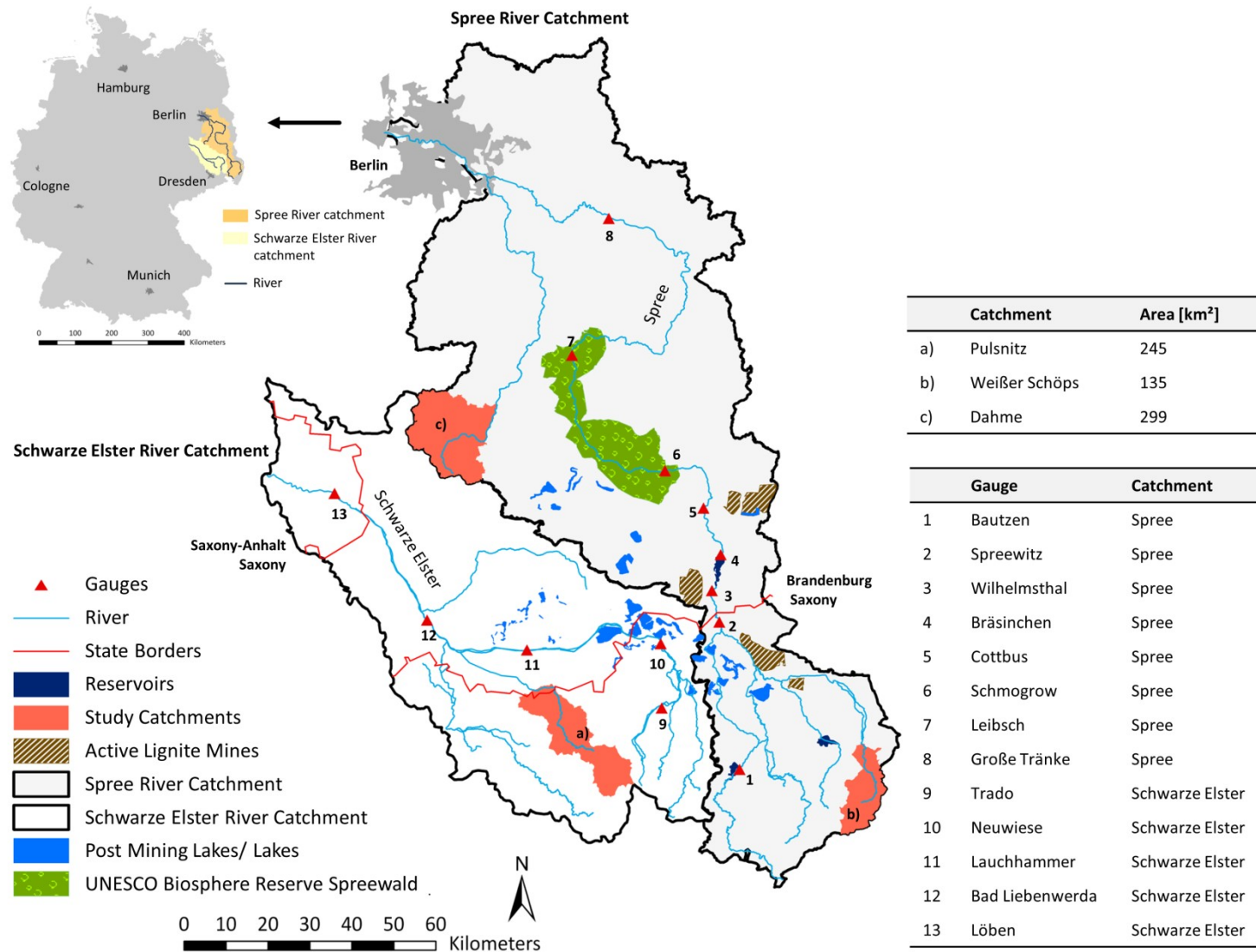


Figure 4-1: Location and overview of study catchments (data basis: LUGV (2013), LFULG (2013))

As a result of more than 100 years of excessive open cast lignite mining in Lower Lusatia, a significant groundwater depression with a deficit of approximately 13 billion m³ was present in the Lusatian river catchments in 1990 (GRÜNEWALD, 2001b). The groundwater pumped was partially drained into the river systems and has thereby artificially augmented the discharge for many years (Figure 4-2).

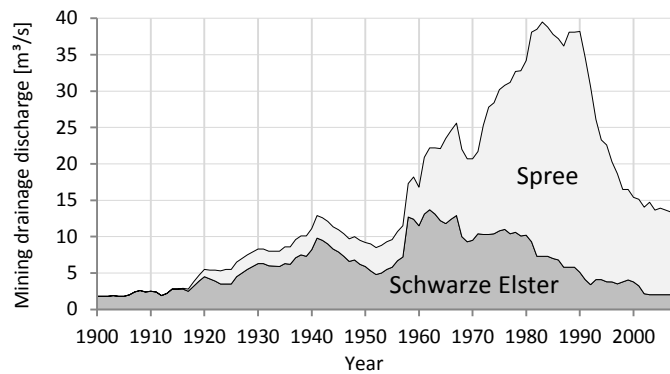


Figure 4-2: Temporal development of mining drainage discharge in the catchments of Spree and Schwarze Elster rivers (SCHOENHEINZ et al. (2011))

After 1989, 12 of 17 active lignite mines were closed. Consequently, the mining drainage water decreased significantly especially into the Spree river (GRÜNEWALD, 2001b; Figure 4-2). However, the water requirements of the various users in the catchment remained constant, including, amongst others, lignite-based power plants and numerous fish farms. In fact, fish farming is an important economic sector in Lusatia with around 1,000 fish ponds covering an area of 55 km² (SIMON et al., 2005). Moreover, the drinking water supply of the German capital Berlin, which is mostly realized by river bank filtration, heavily relies on the discharge of the Spree river. Besides the concerns about water quantity, significant water quality problems are arising in the post mining landscape due to oxidized pyrite being leached out during groundwater rise after active lignite mining. This acidic mining drainage water constitutes a threat to ecosystems and the various water users in the catchment (GRÜNEWALD, 2001b; UHLMANN et al., 2012). Therefore, flooding of the post mining lakes using surface water is the preferred option for filling up the post mining lakes in Lower Lusatia to mitigate water deficits and water quality problems (GRÜNEWALD, 2001b; KOCH et al., 2005). This option requires, however, the availability and the technical allocation of sufficient amounts of surface water for flooding which is already difficult to be realized under current climate conditions. These facts highlight the necessity of robust quantification of possible impacts of climate change on the water balance for a sustainable integrated water resources management in the Lusatian river catchments of Spree and Schwarze Elster.

In terms of land use, the study catchments are intensively used by agriculture (Table 4-1 and Figure B-1, B-2 in Appendix B). Forests, dominated by coniferous forest, make up the second largest proportion, followed by infrastructure and settlements as well as grassland. Cambisols make up the dominant soil type in both catchments (Figure B-1, B-2 in Appendix B). In the Spree river, 50 % of the forested areas are located on Cambisols while Gleysols and Luvisols, the second most common soil types, are mostly agriculturally used (50 %). In the Schwarze Elster river catchment, Alluvial soils make up the second largest portion of soil types followed by Luvisols and Podzols. Similar to the Spree river catchment, Cambisols are mostly used for forestry (43 %) while Luvisols, Alluvial soils and Gleysols are rather used agriculturally (56 %). Changes in land use resulting from lignite mining, such as increasing share of water bodies and open spaces as well as decreasing mining extraction sites, can be detected when comparing land cover data from the year 1990 with the year 2006 (Table 4-1). Moreover, societal developments such as increasing urbanisation (infrastructure and settlements) by 0.8 % in the Spree and by 0.9 % in the Schwarze Elster river catchment can be identified. Moreover, an increasing share of mixed and deciduous forest (0.1 %) can be detected.

Table 4-1: Comparison of land use distribution [%] in the Spree and Schwarze Elster catchments between 1990 and 2006 (data basis: CLC (1990) and CLC (2006))

	Schwarze Elster		Spree	
	1990	2006	1990	2006
Agriculture	50.0	48.0	41.0	38.0
Coniferous forest	28.0	28.0	34.0	34.0
Deciduous forest	1.0	1.1	2.0	2.1
Dump sites	0.05	0.04	0.05	0.04
Grassland	4.8	6.2	4.5	6.2
Infrastructure/settlements	5.3	6.2	9.4	10.2
Mineral extraction sites	2.1	1.5	2.8	1.3
Mixed forest	4.0	4.1	1.6	1.7
Water bodies	1.3	1.7	2.2	2.8
Wetlands	0.1	0.1	0.3	0.3
Woodland shrub	3.8	2.9	2.4	2.7
Open spaces	0.0	0.3	0.0	0.4

Due to the large anthropogenic impact on the Spree and Schwarze Elster river catchment, the traditional approach of hydrological model calibration and validation on measured discharge is not possible. Therefore, three subcatchments, namely of the rivers Pulsnitz,

Weißer Schöps and Dahme (Figure 4-1), have been chosen as study catchments for detailed investigations. These study catchments fulfil the following requirements:

- Anthropogenic impact on discharge is relatively low
- Good data base available
- Catchments possess different hydrological and physiographic characteristics while being based on their physiographic characteristics (land use, soil conditions) representative for the entire catchments, and hence permitting the transfer of the results obtained on the scale of the subcatchments to the entire catchment scale.

STAHL et al. (2010) suggest the choice of smaller subcatchments ($A < 300 \text{ km}^2$) for climate change impact assessments. In larger catchments, processes with opposing hydrological influences may act simultaneously and thus overlap each other possibly disguising the climate change impact. For example, an increase in temperature in early spring may lead to increasing snowmelt in catchment's mountain range headwaters. At the same time, higher evapotranspiration due to increasing temperatures in the lowland regions may counter this effect at the downstream gauge and no net change in river discharge can be detected. Hence, smaller catchments are useful for the identification of predominant climate and catchment processes that govern changes in regional hydrology.

4.1.2 The Pulsnitz river catchment (Schwarze Elster river)

The Pulsnitz river catchment is a subcatchment of the Schwarze Elster river catchment and covers an area of 245 km^2 up to gauge Ortrand and 92 km^2 up to the gauge Königsbrück (Figure 4-3). While the southern part up to gauge Königsbrück represents low-mountain range conditions with elevations reaching up to 436 m a.s.l., the part from gauge Königsbrück to Ortrand is representative for the plane landscape part of the Schwarze Elster river catchment with elevations down to 80 m a.s.l. The meteorological measurements of the climate station Pulsnitz, located in the southern part of the catchment, as well as measured precipitation from the stations, Ruhland, Hirschfeld and Radeburg located 7.4 km, 7 km and 7.5 km, respectively, outside the catchment area, are used to characterise the climatic conditions of the catchment.

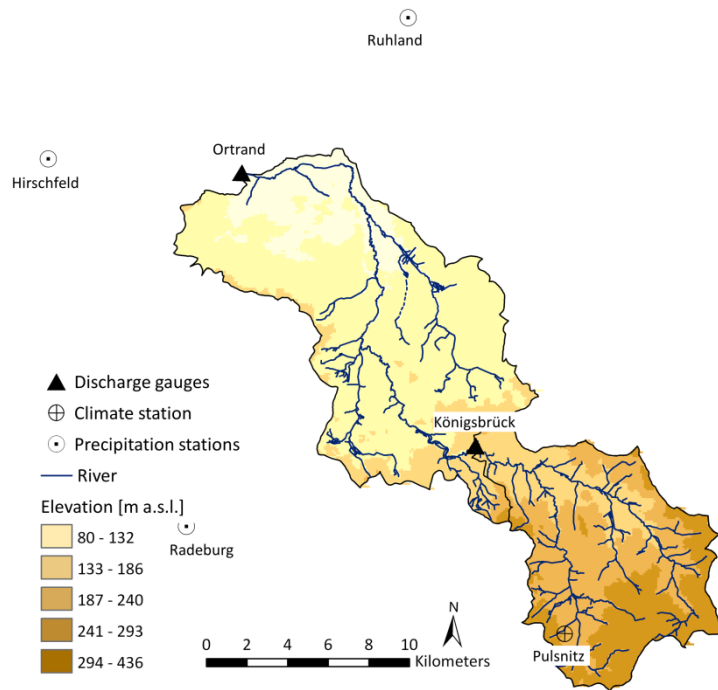


Figure 4-3: The Pulsnitz river catchment with position of climate and precipitation stations as well as discharge gauges and elevation (data basis: ASTER DEM (2009))

The Pulsnitz river catchment is intensively used for agriculture (52 %, Figure 4-4 upper left). According to the statistical state authority, root crops including sugar beets and potatoes as well as silage maize and winter crops (winter wheat and rye) are preferably cultivated (SLFS, 2012). Forests (32 %), which are dominated by coniferous forests, make up the second largest land use proportion. Other land uses include settlements and infrastructure (6 %), grassland (6 %) and moor- and heathlands (4 %). Based on the soil maps (BÜK 200, 2007; BÜK 300, 2007), the dominant soil types are Cambisols (53 %), followed by Luvisols (15 %), Gleysols (13 %) and Alluvial soils (10 %, Figure 4-4 upper right). In the southern part of the catchment, joint aquifers with saturated hydraulic conductivities $< 1 \cdot 10^{-5}$ m/s dominate while in the northern part porous aquifers characterized by saturated hydraulic conductivities $> 1 \cdot 10^{-5}$ m/s are located (Figure 4-4 lower left and right).

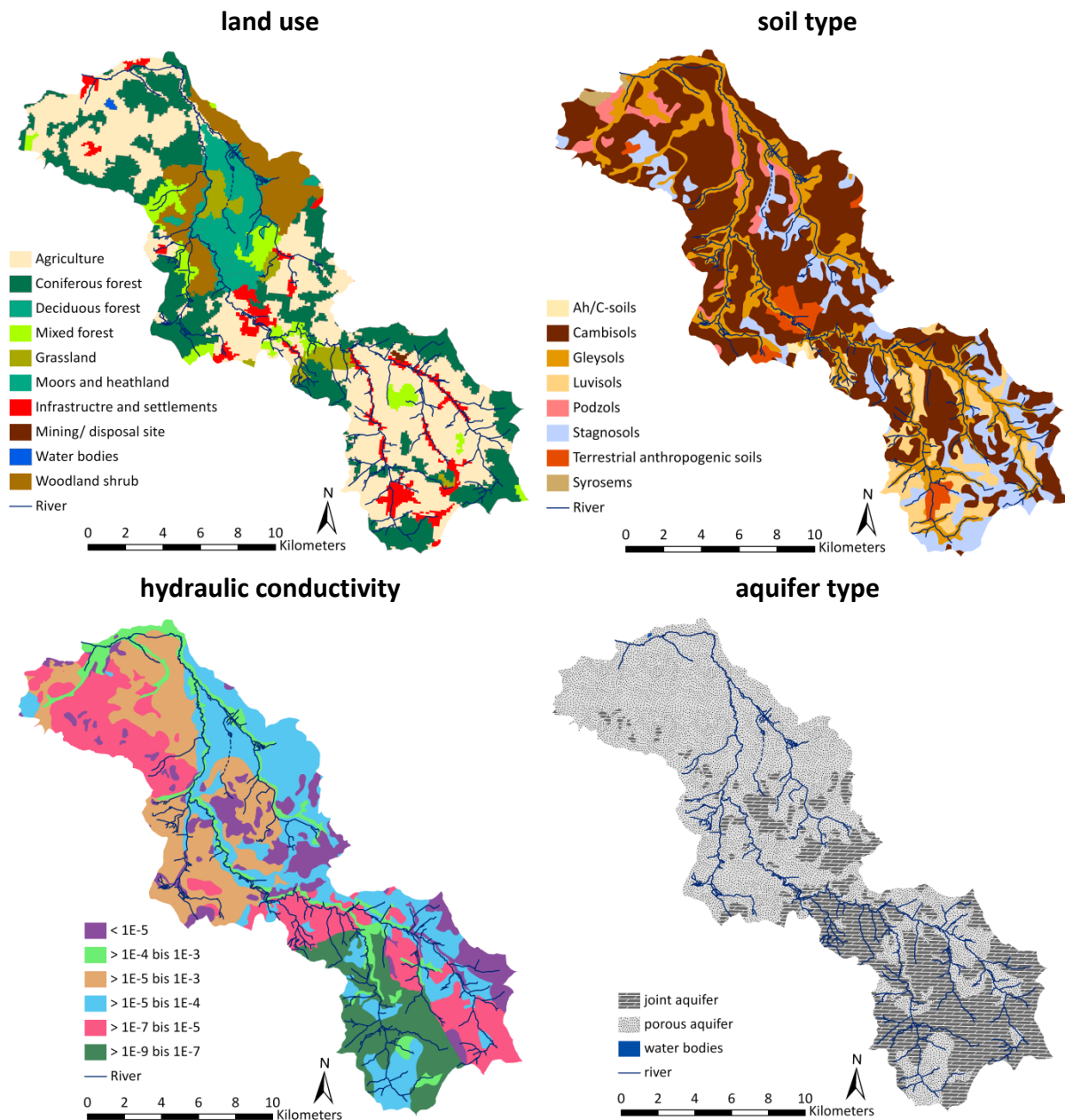


Figure 4-4: Distribution of land use, soil type, hydraulic conductivity [m/s] and aquifer type in the Pulsnitz river catchment (data basis: CLC (2006), BÜK 300 (2007), BÜK 200 (2007), HÜK 200 (2007))

4.1.3 The Weißer Schöps river catchment (Spree river)

The Weißer Schöps river catchment is a headwater subcatchment of the Spree river and representative for the conditions in the upper Spree. It covers an area of 135 km² up to the gauge Särichen, 54 km² up to gauge Holtendorf and 7.6 km² up to gauge Königshain. The Weißer Schöps river catchment is located in a low-mountain range with an elevation ranging from 165 m a.s.l. in the north to 407 m a.s.l. in the south (Figure 4-5). The study area is restricted up to gauge Särichen, because further north the influence of the opencast lignite mine Reichwalde commences. The meteorological measurements of the climate station

Görlitz as well as the measured precipitation of the stations Hähnichen, Hohendubrau-Gebelzig and Löbau, being located 11 km, 12.5 km and 10 km, respectively, outside of the catchment area, are used to characterise the climatic conditions of the catchment (Figure 4-5).

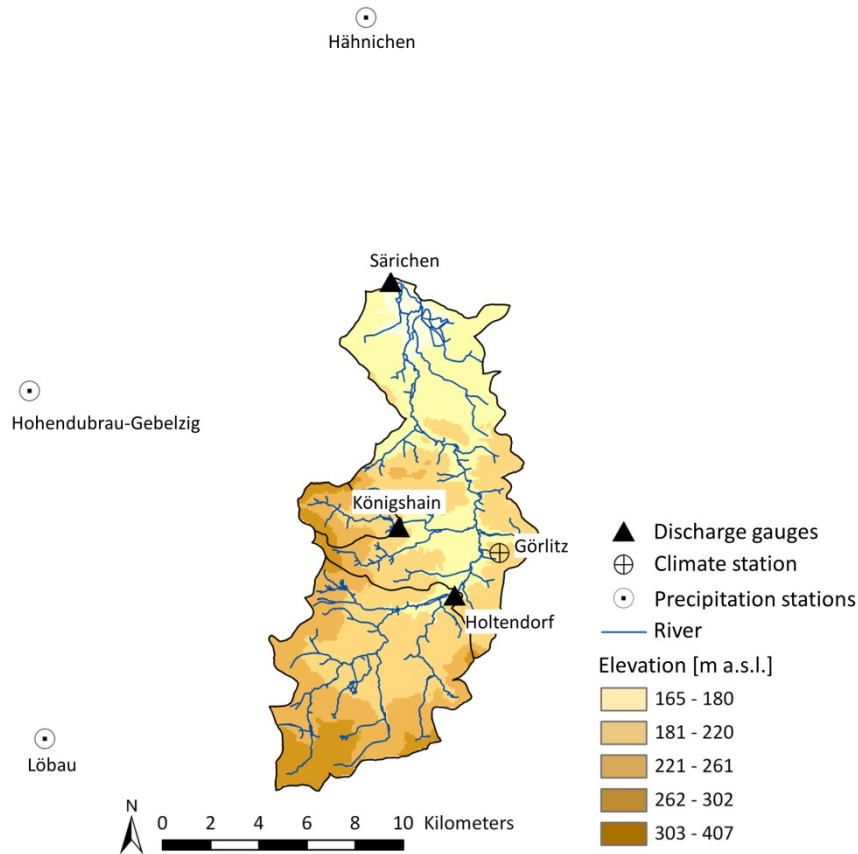


Figure 4-5: The Weißer Schöps river catchment with position of climate and precipitation stations as well as discharge gauges and elevation (data basis: ASTER DEM (2009))

Due to silty soils with a high water holding capacity, the Weißer Schöps river catchment is intensively used for agriculture (72 %, Figure 4-6 upper left). Similarly to the Pulsnitz river catchment, root crops including sugar beets and potatoes as well as silage maize and winter crops are preferably cultivated (SLFS, 2012). Forests (10 %), which are dominated by coniferous forests, make up the second largest land use proportion. Other land uses include settlements and infrastructure (9 %), grassland (8 %) and water bodies (1 %). Based on the Saxonian soil map BÜK200 (BÜK 200, 2007), the dominant soil types are Luvisols and Stagnosols followed by Gleysols and Cambisols (Figure 4-6 upper right). In almost 70 % of the catchment area, joint aquifers can be found. These are characterized by hydraulic conductivities $< 1 \cdot 10^{-5}$ m/s while porous aquifers are mostly located in the northern flatter part where hydraulic conductivities $> 1 \cdot 10^{-5}$ m/s can be encountered (Figure 4-6 lower left and right).

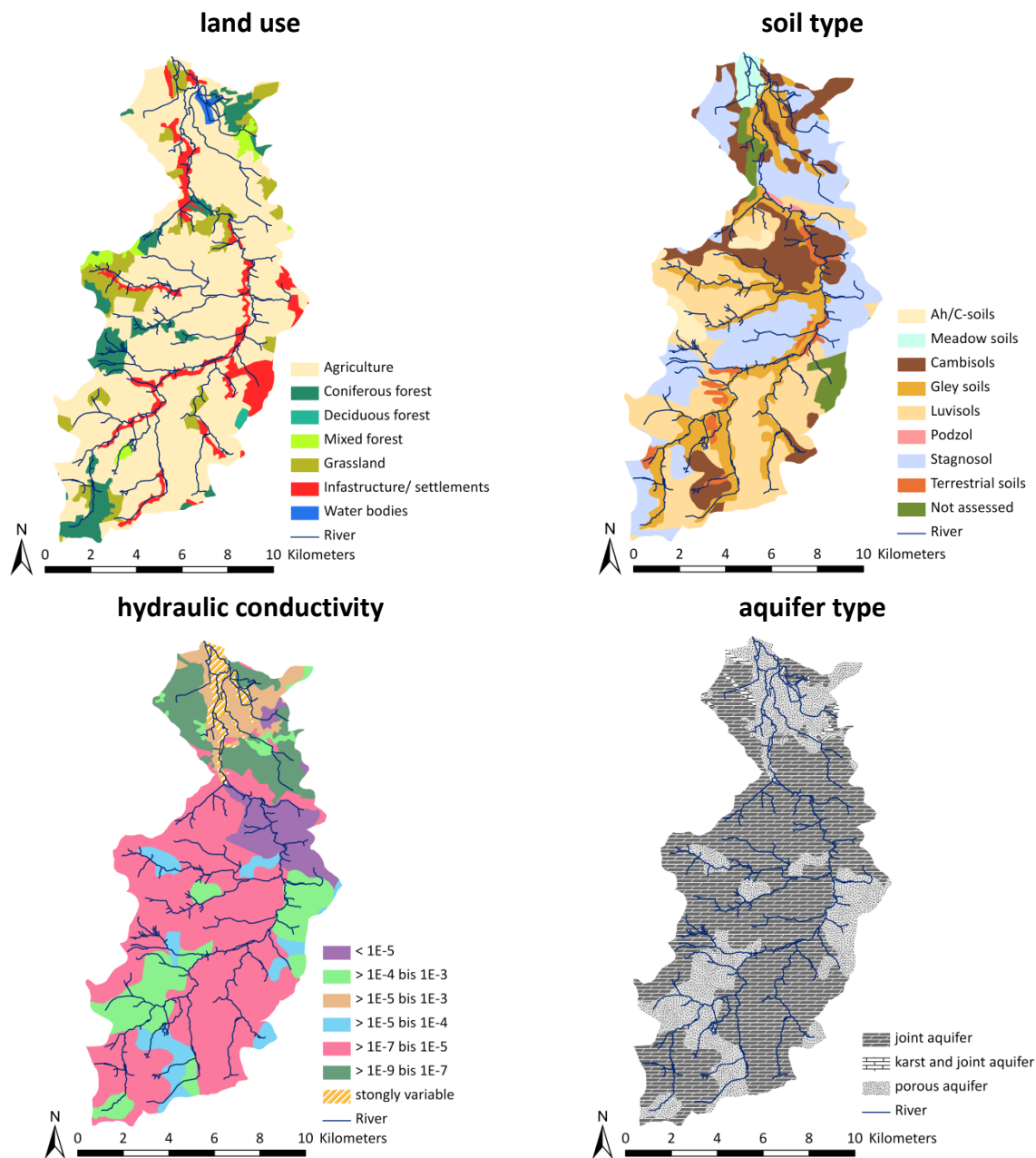


Figure 4-6: Distribution of land use, soil type, hydraulic conductivity [m/s] and aquifer type in the Weißer Schöps river catchment (data basis: CLC (2006), BÜK 200 (2007), HÜK 200 (2007))

4.1.4 The Dahme river catchment (Spree river)

The Dahme river catchment, being representative for the lower part of the Spree, covers an area of 299 km² up to gauge Prierow and 22 km² up to gauge Dahme Stadt. With elevations ranging from 50 m a.s.l. to 174 m a.s.l., the catchment is characteristic for lowland conditions with low gradients in land surface and can be regarded as highly complex from a hydrological viewpoint. Several studies have investigated the particularities of similar catchments in the Pleistocene landscape (CONRADT et al., 2012; GERMER et al., 2011;

LISCHEID and NATKHIN, 2011; MERZ and PEKDEGER, 2011; THOMAS et al., 2012). The main uncertainty when investigating such catchments arises from the fact that the surface and subsurface catchment boundaries do not necessarily coincide and are temporally not fixed, which makes closing the water balance difficult. The climate of the catchment was characterized using the precipitation stations of Petkus, Dahme and Kemnitz located within the catchment area (Figure 4-7) at which other meteorological variables (for example temperature, global radiation etc.) were also available (see section 3.1).

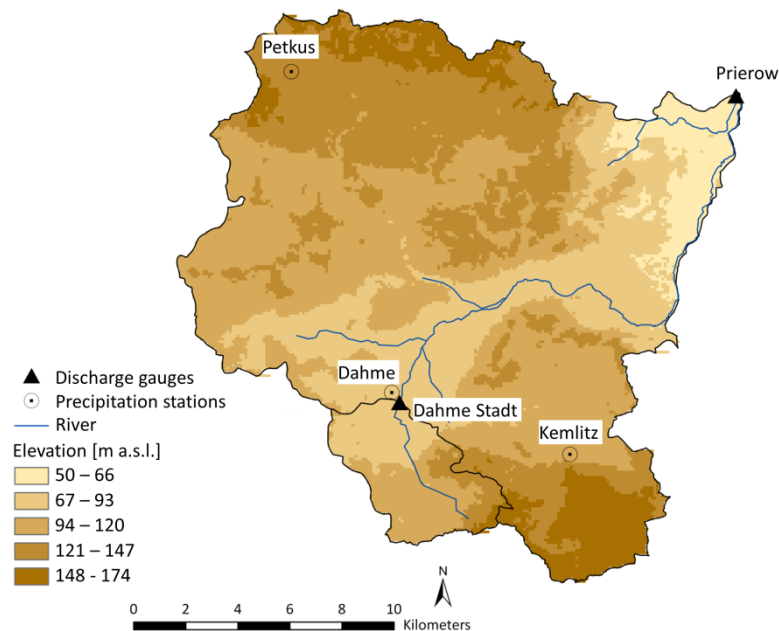


Figure 4-7: The Dahme river catchment with position of precipitation stations as well as discharge gauges and elevation (data basis: ASTER DEM (2009))

Even though sandy soils dominate the Dahme river catchment, the catchment is also intensively used for agriculture (53 %, Figure 4-8 upper left). Forests (41 %), also mainly composed of coniferous forest, make up the second largest land use proportion. Other land uses include grassland (4 %), settlements and infrastructure (2 %) and water bodies (0.1 %). Based on the Brandenburg soil map BÜK300 (BÜK 300, 2007), the main soil types are Luvisols and Cambisols. Stagnosols, Histosols, Gleysols and Podzols make up smaller proportions (Figure 4-8 upper right). Porous aquifers characterized by high hydraulic conductivities of $1 \cdot 10^{-3}$ m/s to $1 \cdot 10^{-5}$ m/s (Figure 4-8 lower left and right) dominate the catchment and are characteristics for the lowland catchments in the region (MERZ and PEKDEGER, 2011).

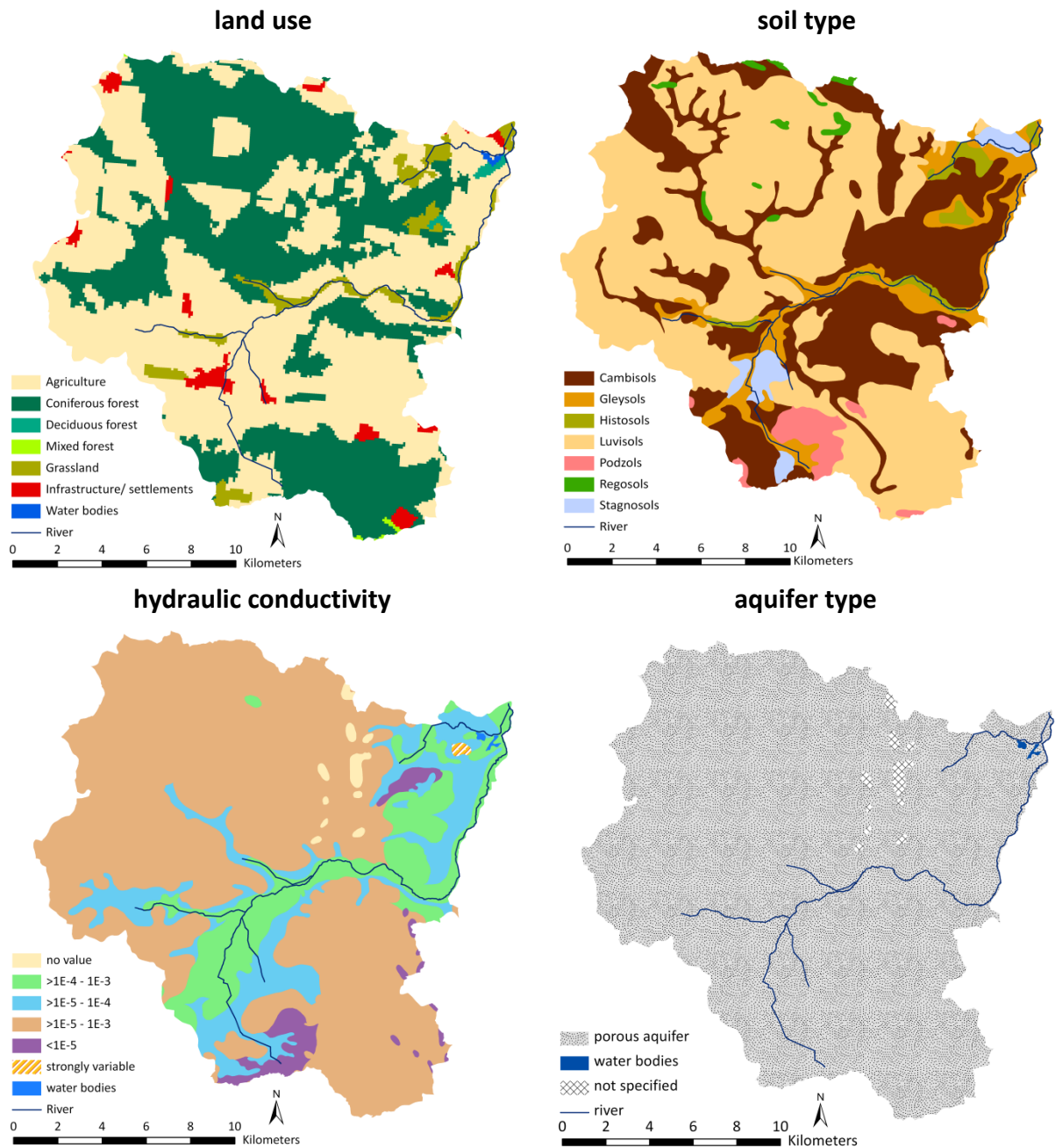


Figure 4-8: Distribution of land use, soil type, hydraulic conductivity [m/s] and aquifer type in the Dahme river catchment (data basis: CLC (2006), BÜK 300 (2007), HÜK 200 (2007))

4.2 Comparison between land use and soil properties

Comparing the land use distribution of the catchments of Spree and Schwarze Elster with their subcatchments consolidates the representativity of the subcatchments for the larger region (Figure 4-9). In fact, between the land use distribution of the Schwarze Elster river catchment and the Pulsnitz river catchment (Figure 4-9), only small differences can be identified: in the Pulsnitz river catchment, the proportion of agriculture is 4 % higher while

the share of forests and settlements is 2 % lower compared to the Schwarze Elster river catchment.

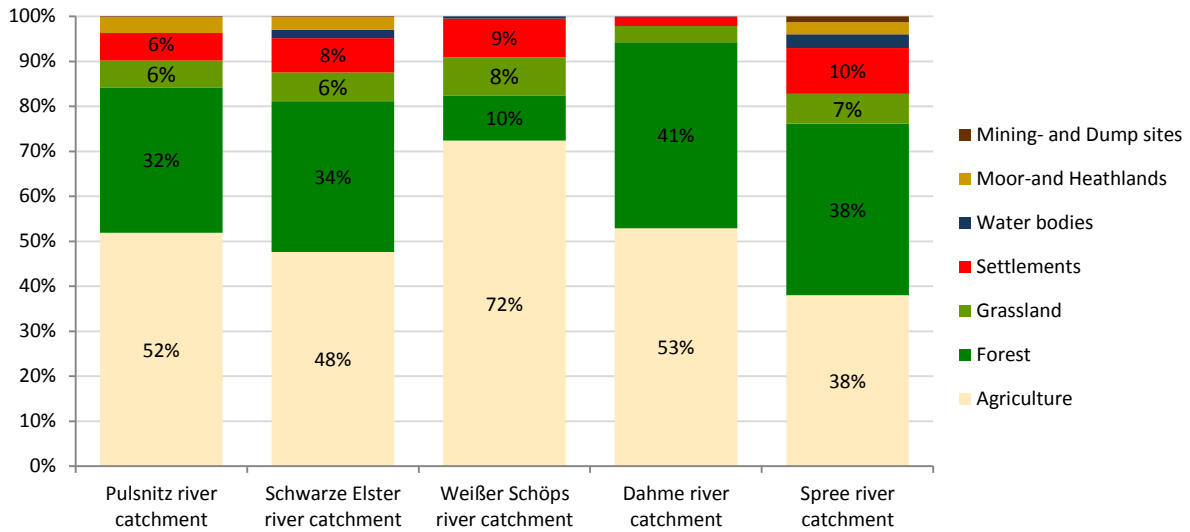


Figure 4-9: Comparison of the land use proportions between the different study catchments (percentages below 5 are not displayed, data basis: CLC (2006))

In terms of land use, the Dahme river catchment can be regarded as a good representative for the entire Spree river catchment with a larger share of agriculture (+ 15 %) and forest (+ 3 %) but less settlements and infrastructure. The Weißer Schöps river catchment is a good representative for the land use distribution in the upper Spree river catchment.

The comparison of the soil type distribution between the Spree and Schwarze Elster river catchments and their subcatchments reveals that differences exist (Figure 4-10).

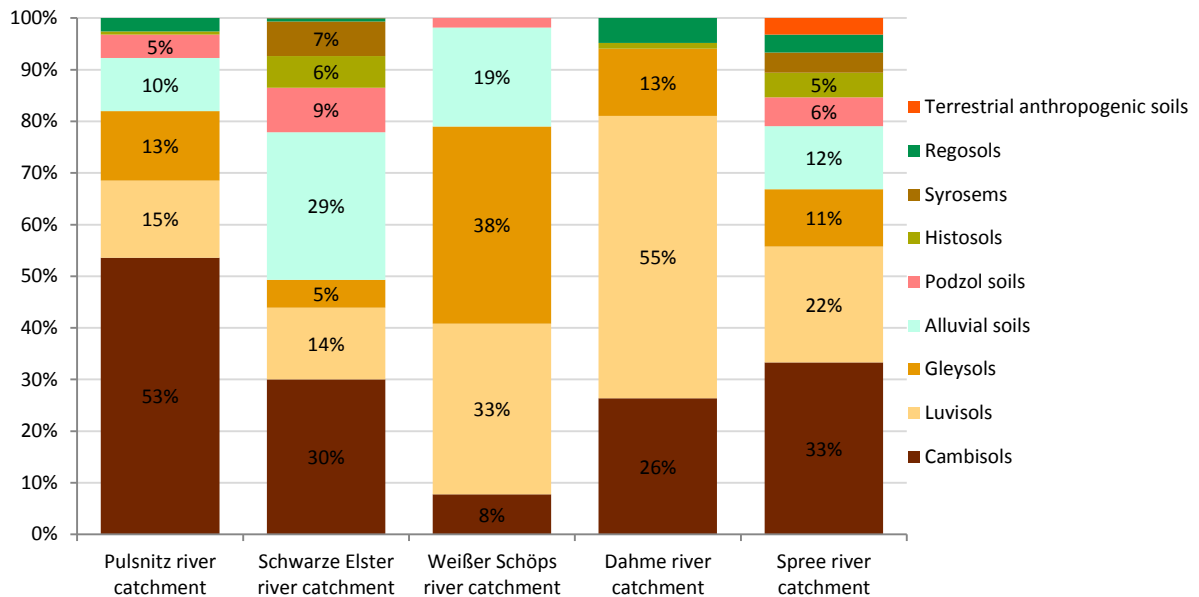


Figure 4-10: Comparison of the soil types proportions between the different study catchments (percentages below 5 are not displayed, data basis: BÜK 1000 (1998))

However, the dominant soil types are present in all catchments.

- Schwarze Elster river catchment and its subcatchment Pulsnitz: Cambisols make up the dominant soil type in both the Schwarze Elster (30 %) and the Pulsnitz river catchment (53 %). Alluvial, Gleysoils and Luvisols constitute the other major soil types with proportions above 10 %.
- Spree river catchment and its subcatchments Weißer Schöps and Dahme: The dominant soil types differ between the catchments (Spree: Cambisols (33 %), Weißer Schöps: Gleysols (38 %), Dahme: Luvisols (55 %)). Nevertheless, the Weißer Schöps and Dahme river catchments are regarded as good representatives for the upper and lower Spree, respectively.

4.3 Climatic and hydrological conditions

The study catchments are located within a transition zone between the continental eastern and the maritime western European climate conditions. Therefore, the Spree and Schwarze Elster river catchments are characterized by relatively low amounts of precipitation throughout the year (corrected precipitation ≈ 747 mm/a) ranging from 997 mm/a in the Pulsnitz to 713 mm/a in the Dahme river catchment (Table 4-2). Intra-annually, precipitation has its maximum during the summer months (up to 88 mm/month) except in the Pulsnitz river catchment (December: up to 100 mm/month, Figure B-3 in Appendix B). Precipitation has its minimum during October (down to 48 mm/month), except in the Weißer Schöps and Dahme river catchments (February: down to 45 mm/month).

Long term average temperature amounts to 8.8 °C in the study catchments with a comparatively large difference between summer (July up to 18 °C) and winter (January down to -1.1 °C, Table 4-2 and Figure 4-11).

Potential evapotranspiration reaches on average 685 mm/a ranging from 708 mm/a in the Pulsnitz and 665 mm/a in the Dahme river catchment. Intra-annually, potential evapotranspiration reaches its maximum in July (up to 117 mm/month) and its minimum in December (down to 10 mm/month).

The climatic water balance amounts to 78 mm/a in the Schwarze Elster catchment and 57 mm/a in the Spree catchment on the annual long term scale. Due to their location in a low-mountain range, the Pulsnitz and Weißer Schöps river catchments are characterised by higher precipitation and lower temperatures. Consequently their climatic water balance is more positive compared to the other river catchments.

Table 4-2: Long term (1963-2006) annual mean temperature (T [°C]), corrected precipitation (P_{cor} [mm/a]) after SEVRUK (1986), potential evapotranspiration (ETP [mm/a]) calculated after WENDLING et al. (1991) and climatic water balance (CWB [mm/a], data basis: PIK)

Catchment	T	P_{cor}	ETP	CWB
Schwarze Elster	8.9	751	673	78
Pulsnitz	8.7	997	708	289
Spree	9.0	742	685	57
Weißer Schöps	8.5	818	696	122
Dahme	8.8	713	665	48

Intra-annually, the climatic water balance is negative already under current climate conditions during the vegetation period from April to September in all catchments (Figure 4-11 and B-3 in Appendix B). During this period, potential evapotranspiration also exceeds precipitation.

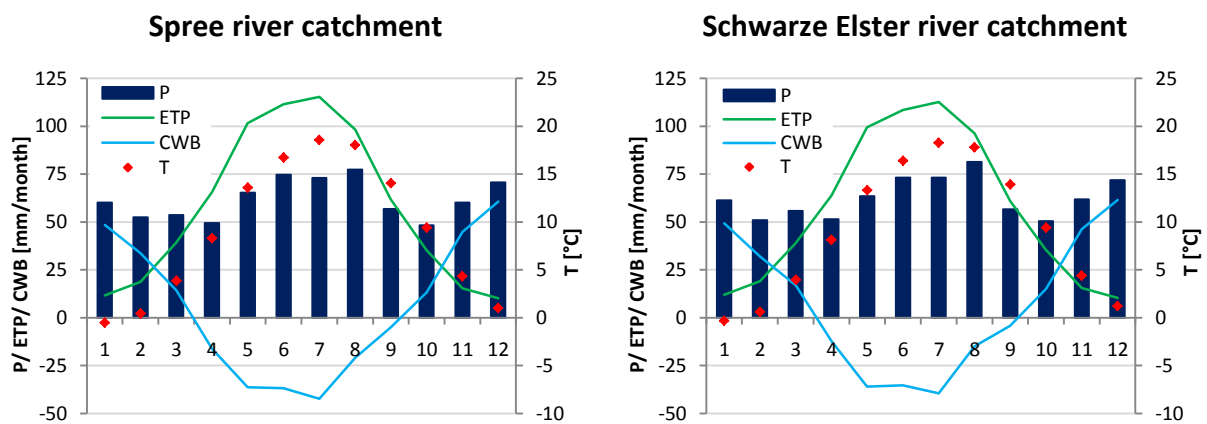


Figure 4-11: Long term (1963-2006) monthly sums of corrected precipitation (P) after SEVRUK (1986), potential evapotranspiration (ETP) calculated after WENDLING et al. (1991), climatic water balance (CWB) and mean temperature (T) (data basis: PIK)

The natural discharge regime, which can be characterised as pluvial, is mainly dominated by evapotranspiration in the study catchments. Even though more precipitation falls during the summer, the mean discharge is the lowest due to high evapotranspiration during this period (Figure 4-12).

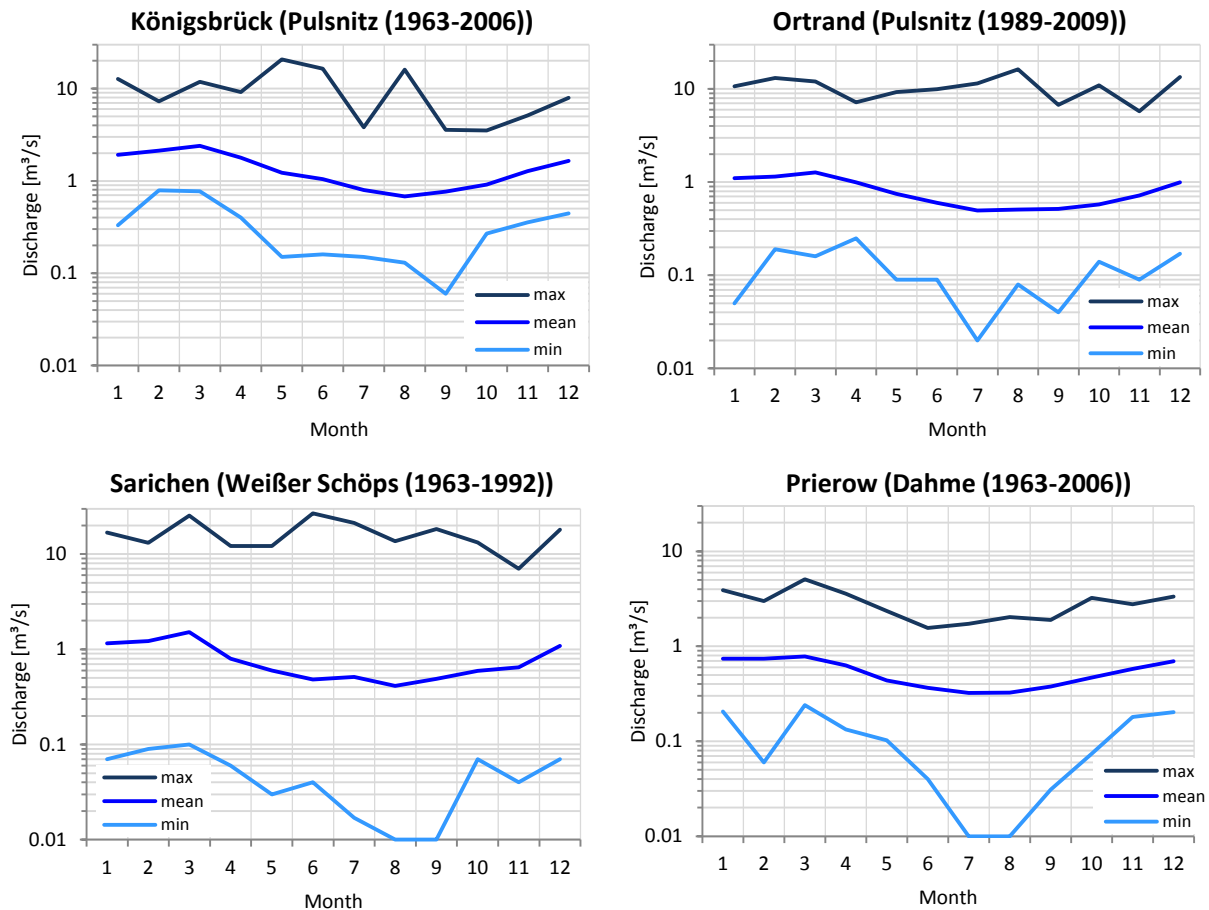


Figure 4-12: Long term mean, minimum and maximum discharge (data basis: LfLUG and LUGV)

As a consequence, there are no considerable differences in the discharge regime between the catchments, especially concerning the mean discharge which is characterised by a small peak in March as a result of snow melt and spring precipitation and lower discharge during the summer. In all study catchments, the lowest value of the minimum monthly discharge occurs during the period from July to September. In the Weißer Schöps and Dahme river catchments, the minimum flow reaches down to $0.01 \text{ m}^3/\text{s}$ which can be explained by the catchments physiographic characteristics. The Weißer Schöps river catchment is, as a headwater catchment, characterised by joint aquifers with comparably low water storage (see section 4.1.3). In the Dahme river catchment, mostly sandy aquifers are located whose storages quickly deplete when evapotranspiration rates are high during the summer months. The Pulsnitz river catchment, on the other hand, has a smaller proportion of joint aquifers and a larger proportion of porous aquifers where water storage is larger and rainfall variations can be buffered more effectively.

In the Dahme river catchment, the maximum discharge also has its minimum during the summer. In the low-mountain range catchments of the Pulsnitz and Weißer Schöps river, high discharges have also been observed during the summer months as a consequence of

high intensive convective summer and/or orographic precipitation events. The largest variability in the discharge regime can be observed in the Weißer Schöps river subcatchment ranging from 0.01 m³/s to 26.9 m³/s and the smallest in the Dahme river catchment ranging from 0.01 m³/s to 5 m³/s.

4.4 Detection of anthropogenic impact

The main reason why these catchments were initially chosen for the investigation was the fact that a low anthropogenic impact on the discharge was assumed. Analysing the discharge data of the Dahme river catchment and comparing it to the values of the NAU atlas showed that the runoff regime has changed considerably since the 1960s. In fact, the MQ decreased by 50 % from 1 m³/s during the period 1921-1940 (NAU) to 0.5 m³/s during 1981-2000. In the other study catchments, such a strong deviation was not observed.

Figure 4-13 compares the temporal development of the cumulative annual values of precipitation, runoff and the resulting runoff coefficient, defined as the ratio between runoff and precipitation.

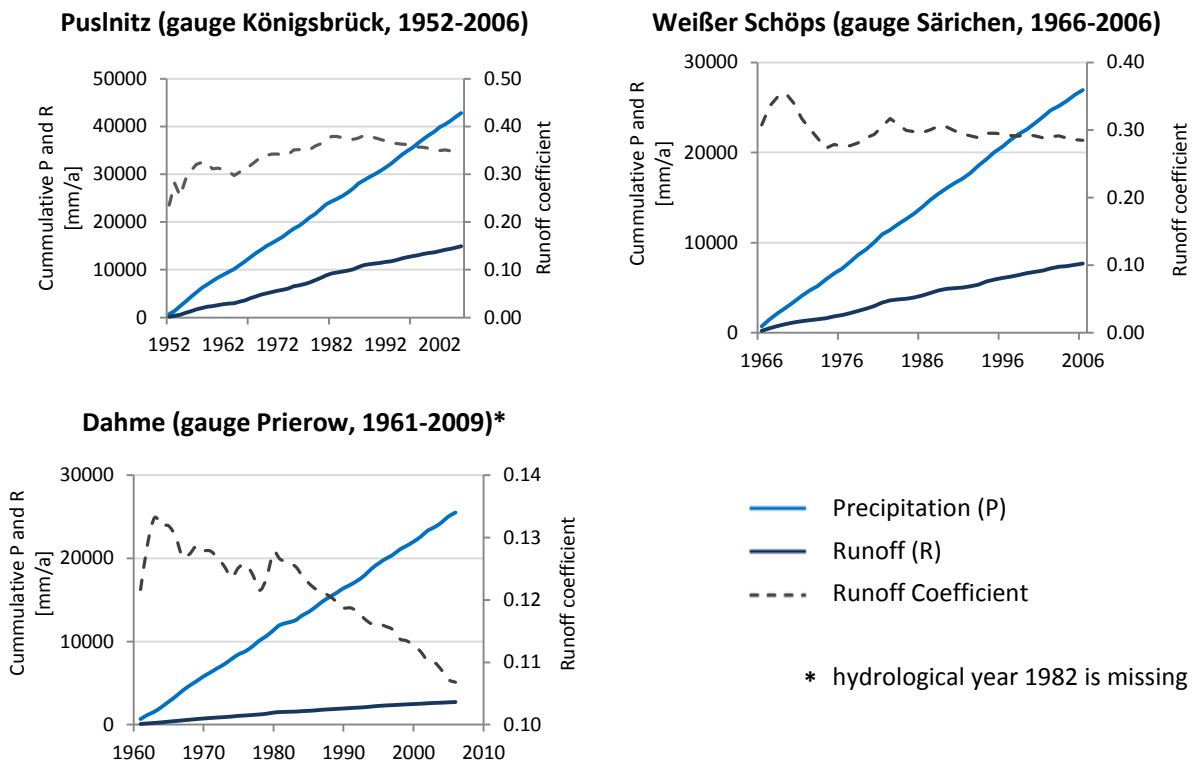


Figure 4-13: Temporal development of the annual cumulative precipitation (uncorrected), runoff and runoff coefficient (data basis: PIK, LfULG, LUGV)

The analysis reveals that runoff coefficient at gauge Prierow (Dahme) has decreased significantly since in the 1980s, even though considerable changes for precipitation could not be observed. In the Pusnitz and Weißer Schöps river catchments, such strong trend

behaviour, which may be an indication of anthropogenic impact on runoff, cannot be identified. An increase in the runoff coefficient can be detected in the Pulsnitz and fluctuations in the Weißer Schöps river catchment. However, stable conditions prevail during model calibration (1999-2001) and validation (2002-2006).

Analysing groundwater levels in the Dahme river catchment (Figure B-4 in Appendix B) also shows a significant decrease since the 1970s. An increase in water use for irrigational purposes during the summer months could be excluded since no intra-annual shifts in the MQ can be detected (Figure 4-14). In fact, between the decade of 1961-1970 and 1999-2008, the mean discharge has decreased on average by 44 %.

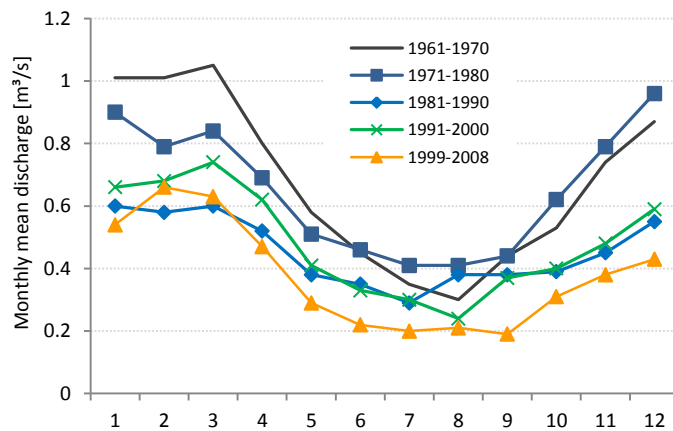


Figure 4-14: Temporal development of the decadal monthly mean discharge at the gauge Prierow in the Dahme river catchment (data basis: LUGV)

Therefore, a natural reason for this development can be excluded and anthropogenic impacts must be the cause for these changes, such as the numerous existing trenches and fisheries located within the catchment, especially around the city of Golßen. This is supported by GRÜNEWALD (2010) who states that the catchments in the lowland areas of Brandenburg have been subject to extensive water management and drainage practices for centuries. Furthermore, three water works are located within the catchment. Information on their pumping amounts as well as changes thereof were, however, not available. These facts complicate hydrological model calibration and validation for the Dahme river catchment.

5 Trend analysis for change detection

5.1 Materials and methods

The objective of incorporating trends analysis into this thesis framework was twofold: trends in measured time series can i) be regarded as harbinger for future change (1, 2) and ii) serve as a mean to validate the results of the DAs (3).

1) On the catchment scale of the Spree and Schwarze Elster rivers, trend analysis was carried out for minimum, mean, and maximum temperature, potential evapotranspiration, global radiation, and precipitation for the time period 1951-2006. Firstly, the analysis was conducted on interpolated time series (by Thiessen polygons) on an annual basis to analyse the temporal development and the type of potential change (gradual and step-wise). Secondly, the time series analysis was carried out station-wise on a monthly basis in order to detect intra-annual shifts for both gradual and step-wise changes under the consideration of different correlation structures, including auto- and cross-correlation. For visualising the outcome of the analysis, the number of stations with positive (Figure 5-1, a) and negative trends (Figure 5-1, b) were subdivided and compared to the total number of stations. Moreover, the numbers of significant (red) and non-significant (white) trends were distinguished by colour. The total number of significant trends was compared to the field significance (Figure 5-1, c).

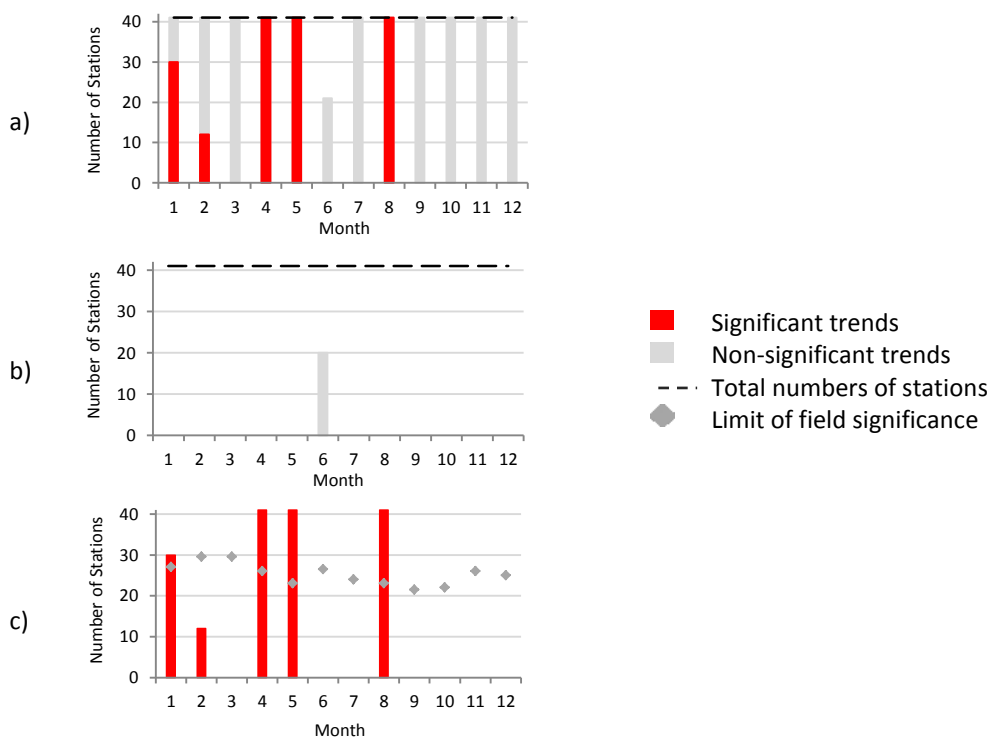


Figure 5-1: Approach for analysing monthly significant and non-significant positive (a) and negative (b) trends, (c) number of significant trends and field significance

In addition, a spatial analysis was carried out. For this purpose, stations with significant, above field significant, trends as well as gradients of trend magnitude were visualized in order to identify spatial patterns of change. Figure 5-2 displays the stations used for the analysis and their corresponding ID. Additional information on the stations is provided in Table A-2 (Schwarze Elster) and A-3 (Spree) in Appendix A.

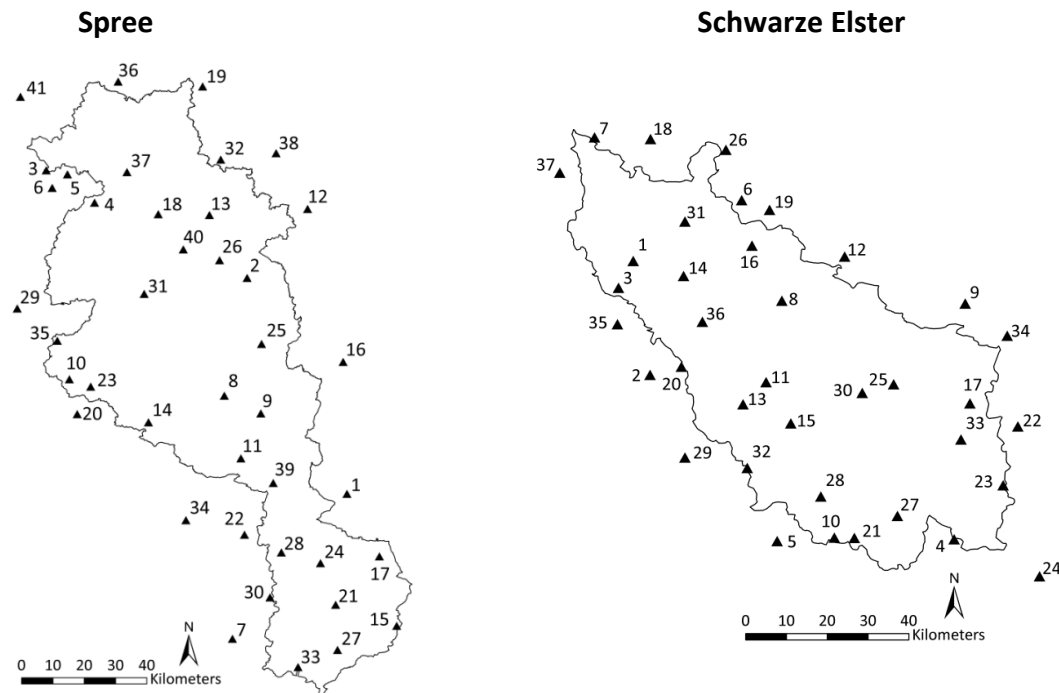


Figure 5-2: Location of meteorological stations. Station IDs are related to Table A-2 (Schwarze Elster) and A-3 (Spree) in Appendix A

- 2) On the subcatchment scale, due to the low anthropogenic influence, the impact of changes in the meteorological drivers on runoff, as an integrated catchment response, was analysed. Again, the trend analysis was carried out for both gradual and change points on the annual and seasonal basis. As a result of differences in data availability, which was determined by the time series lengths of measured discharge values (Table A-1 in Appendix A, Pulsnitz: 1951 – 2006, Weißer Schöps: 1963 – 2006, Dahme: 1961 – 2006), the results of the trend analyses are not directly comparable between the different catchments.
- 3) The ability of the DAs to reproduce measured mean temperature and precipitation trends was analysed for the longest overlapping time period (1961-2006). Furthermore, the mean temperature and precipitation trends of the DAs were compared for the period 2015-2060. Both periods, past and future, contain the same time series length (45 years) in order to guarantee the same statistical population. As a measure of comparison, the slope of the linear regression line (Equation C-1 in Appendix C) was used. The analyses were carried out on annual and seasonal basis.

The time series analyses computations were implemented into the software R for statistical computing (R, 2011). Potential evapotranspiration was calculated using the Turc-Wendling approach (WENDLING et al., 1991) which requires mean temperature and global radiation as input. For all analysis, except stated otherwise, a significance level of 0.05 was chosen. Trend magnitude was calculated based on the slope of the linear regression (Equation C-1 in Appendix C). Trend significance was evaluated using the Pettitt test for change points (PETTITT, 1979) and the Mann-Kendall test for gradual changes (KENDALL, 1975; MANN, 1945). The Pettitt test statistics can be found in Appendix C, page C-2. The Mann-Kendall test statistic is presented Appendix C, page C-3. Autocorrelation was removed, if necessary, using the “trend-free-pre-whitening” procedure which is also displayed in Appendix C, page C-3.

For a qualitative visual analysis of the temporal change of the investigated data, a LOcally WEighted Scatterplot Smoothing (LOWESS) procedure was applied (CLEVELAND, 1979; CLEVELAND and DEVLIN, 1988). LOWESS is a nonparametric regression model based on local polynomial fits describing the relationship between x and y without assuming linearity or normality of residuals. How many neighbouring data points influence the local polynomial fits is determined by a smoothing parameter which was chosen to be 0.45 in this study. This implies that 45 % of the data points influence the smooth at each value. The larger the values of the smoothing span, the smoother the fluctuation of the LOWESS function while choosing a too small smoothing factor comprises the risk of capturing random errors. Therefore, 45 % was regarded as a good compromise between capturing the overall data variability and the trend behaviour. The advantage of this method over simple linear regression is that natural variations inherent in climatological and hydrological time series are considered. More detailed information on the LOWESS procedure is presented in Appendix C, page C-6.

In order to evaluate if detected trends are truly significant on the catchment scale, a bootstrapping approach was used to assess field significance for cross-correlated meteorological time series (Figure 5-3). When bootstrapping a time series, it is resampled x times, with replacement, to generate x bootstrap samples. Using this approach, the spatial correlation is preserved but the temporal correlation and any possible trend is removed. In a first step, the time series were resampled randomly with replacement 10,000 times, thereby generating 10,000 bootstrap samples. The resulting 10,000 time series are of the same length as the original time series but with a different year order. For each bootstrap sample, the significance of the Mann-Kendall test, Pettitt test and autocorrelation is evaluated (Figure 5-3, step one). In a second step, for each bootstrap sample, the number of significant trends (significance level of 0.05) is counted (Figure 5-3, step two). In the third step, the empirical cumulative distribution function is computed based on the counts (Figure 5-3, step

three). In the fourth step, the field significance is evaluated at the 95th percentile (for 5 % field significance) of the empirical cumulative distribution function (Figure 5-3, step four).

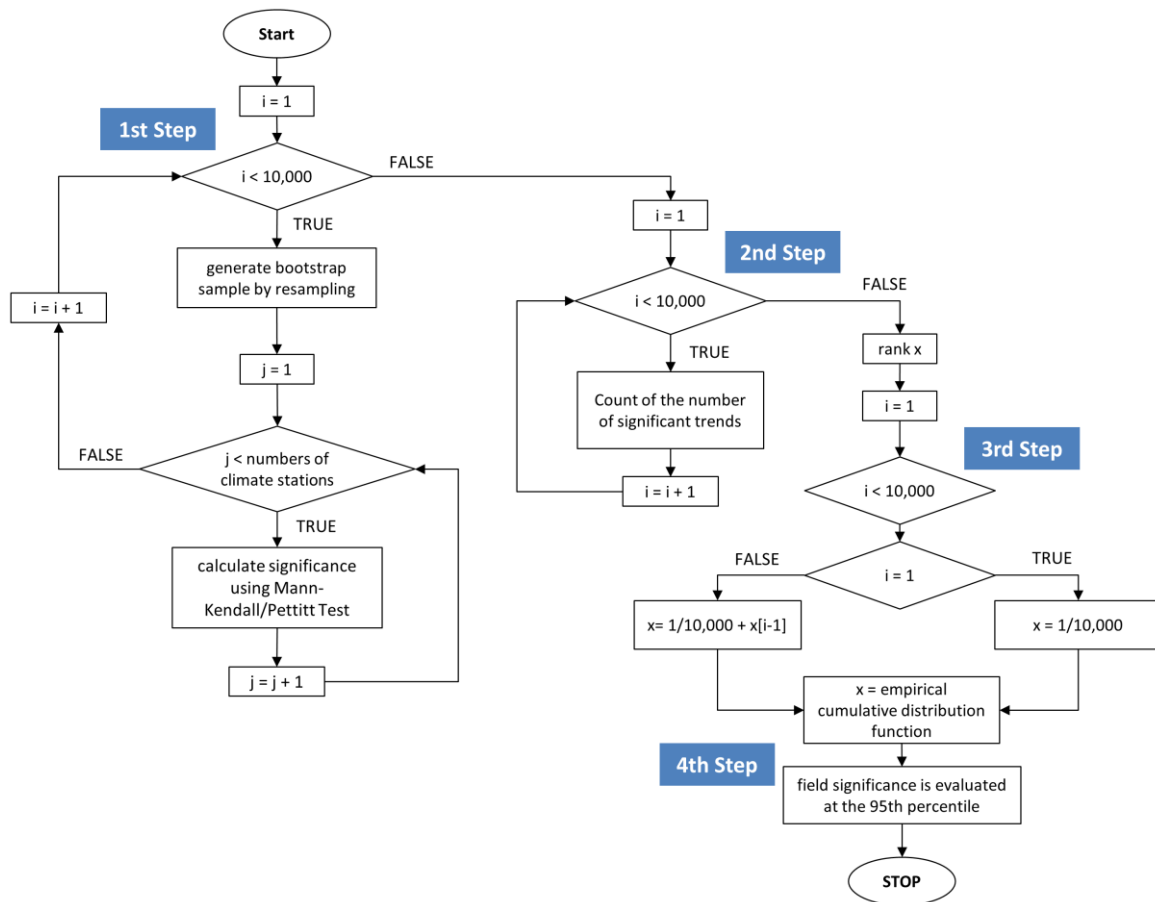


Figure 5-3: Approach to evaluate field significance of spatially correlated time series (i and j represent counters)

As a result, the field significance is expressed as a “number of stations”. This means that trends can only be regarded as truly significant on the catchment scale if the number of stations with significant trends is larger than the field significance.

5.2 Results

5.2.1 Autocorrelation

The presence of autocorrelation in the time series can alter the outcome of the Mann-Kendall trend test (section 2.1.2). The first order autocorrelation of the time series was evaluated for each month and each meteorological station considering field capacity of cross-correlated time series by a bootstrapping approach (Figure 5-3). Time series were pre-whitened (Appendix C, page C-3) before calculating the significance of trends using the Mann-Kendall test in month when autocorrelation is above field significance (Table 5-1).

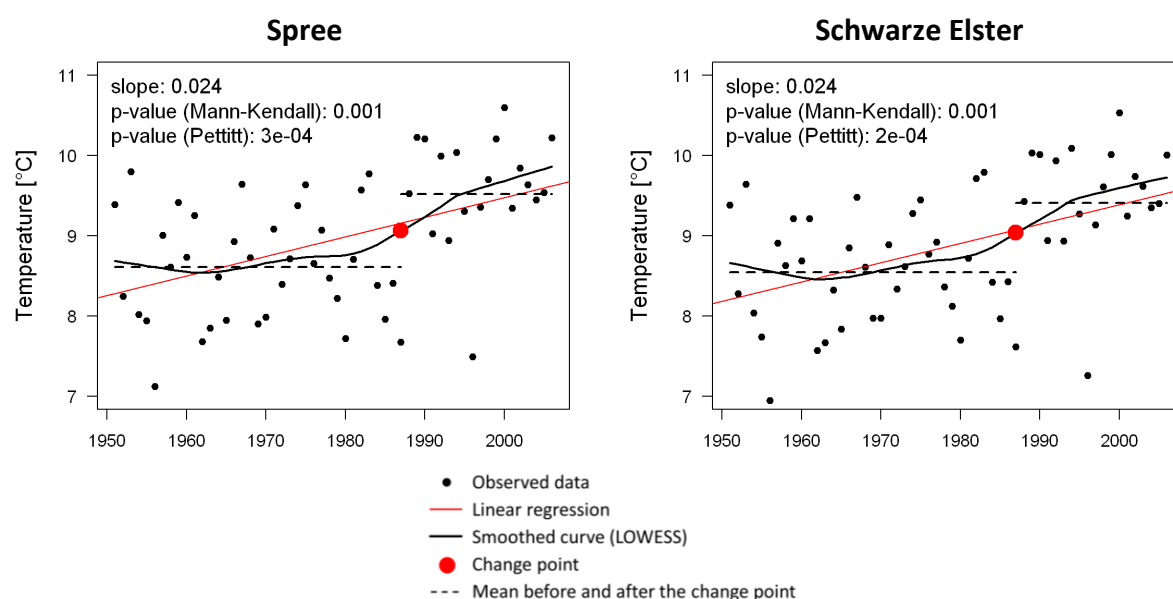
Table 5-1: Months with autocorrelation of time series above field significance in the Spree and Schwarze Elster river catchments

Variable	Spree	Schwarze Elster
Mean temperature	August, October	August, October
Maximum temperature	August	August
Minimum temperature	October	August, October
Potential evapotranspiration	-	June
Global radiation	-	June, November
Precipitation	July	July

5.2.2 Trend detection in the Spree and Schwarze Elster river catchments

Air temperature

The trend analysis conducted on the interpolated annual temperature time series revealed that there has been an increase in mean (Figure 5-4), minimum and maximum (Figure C-1 in Appendix C) temperature by + 1.3 °C, + 1.1 °C and + 1.3 °C, respectively, during the last 50 years in both the Spree and Schwarze Elster river catchments. In fact, the increasing temperature trends are significant for both the Mann-Kendall and Pettit test with change points in the year 1987 in both river catchments. Since both significant change points and gradual trends are detected, the change can be interpreted as a linear positive trend (represented by the linear regression line), as a step-wise change (represented by the change point) as well as a more complex form of change (represented by the LOWESS smoothed curve).

**Figure 5-4: Mean temperature (interpolated annual values, 1951-2006) in the Spree and Schwarze Elster river catchments and trend interpretation**

The results of the monthly station-wise analysis (Figure 5-5, a and b), which allows the determination of changes in the intra-annual distribution as well as the identification of spatial patterns, are presented in Figure 5-5 for mean temperature, Figure C-5 for maximum and Figure C-6 for minimum temperature in Appendix C. For mean temperature, the number of positive mean temperature trends (Spree: 472, Schwarze Elster: 434) significantly outweighs the number of negative trends (Spree: 20, Schwarze Elster: 10). A few negative trends can be identified in the months of:

- June
- September (only maximum temperature)
- November (only minimum temperature in the Spree river catchment)
- December (mean temperature in Schwarze Elster river catchment and minimum temperature in Spree river catchment).

During all other months, mean temperature trends are positive at all stations.

When accounting for field significance, significant positive mean temperature change points were detected in the Spree and Schwarze Elster river catchment (Figure 5-5, Figure C-5 and C-6 in Appendix C, c) in the months of:

- January (maximum (both river catchments) and mean (only Spree): 1987)
- March (minimum: 1971)
- April (mean (Spree: 1986, Schwarze Elster: 1991), maximum: Spree: 1986)
- May (mean and minimum: 1980, maximum: 1984)
- August (minimum (Spree: 1989, Schwarze Elster: 1988), mean and maximum: 1981).

Similarly, when accounting for field significance, significant gradual mean, maximum and minimum temperature trends were detected in the Spree and Schwarze Elster river catchment the months of:

- April (only mean temperature)
- May
- July (only minimum temperature in the Schwarze Elster river catchment)
- August.

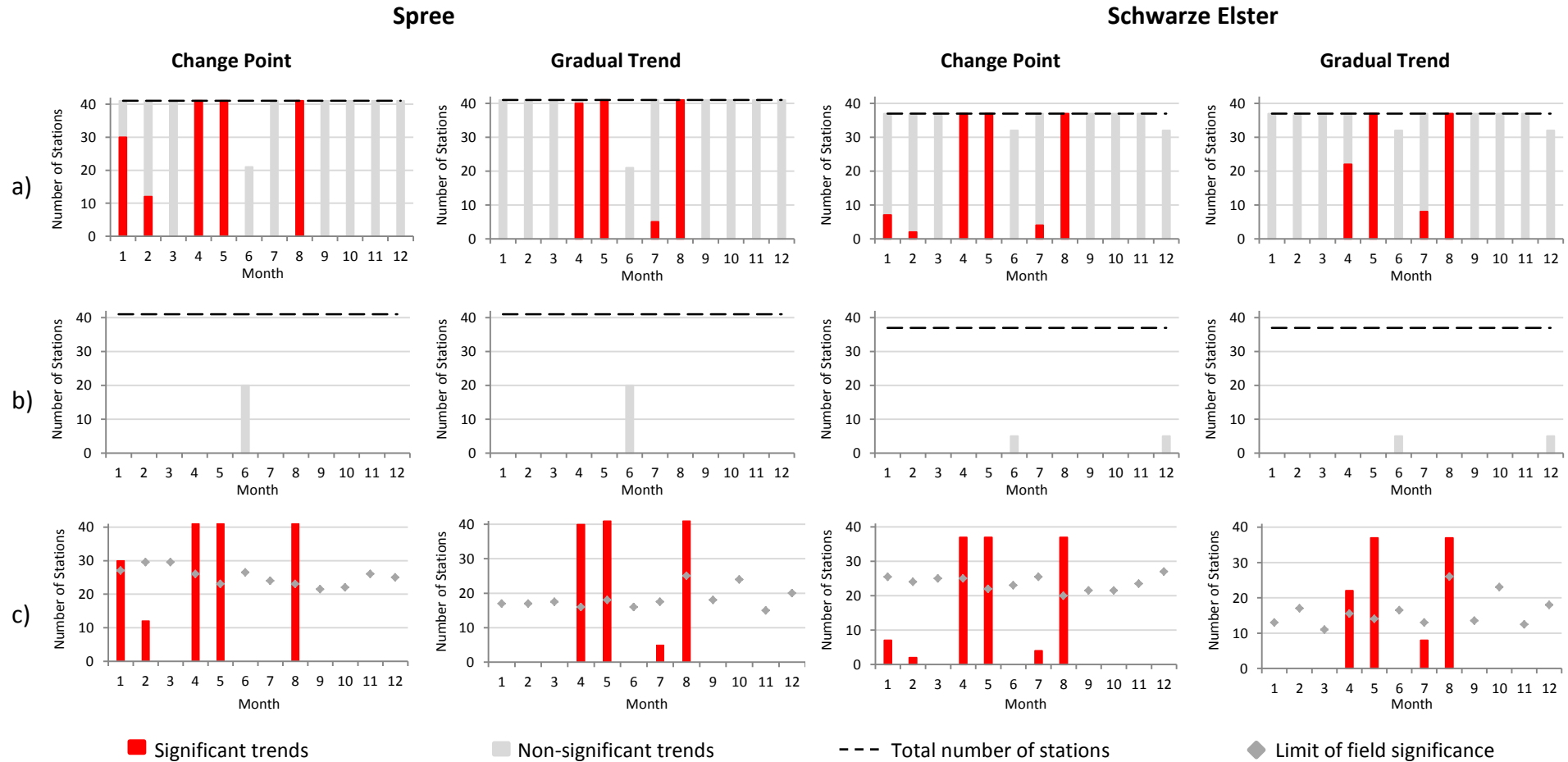


Figure 5-5: Mean temperature (1951-2006): number of stations with significant and non-significant (a) positive and (b) negative trends, (c) number of significant trends and field significance for change points and gradual trends in the Spree (left) and Schwarze Elster (right) river catchments

The magnitude of the detected significant gradual temperature increase averaged over all stations in the months of April, May, July and August is displayed in Table 5-2.

Table 5-2: Magnitude of significant mean (T_{mean}), minimum (T_{min}) and maximum (T_{max}) temperature [$^{\circ}\text{C}$] increase averaged over all stations (1951-2006)

	T_{mean}		T_{min}		T_{max}	
	Spree	Schwarze Elster	Spree	Schwarze Elster	Spree	Schwarze Elster
April	+ 1.8	+ 1.7	-	-	-	-
May	+ 2.2	+ 2.3	+ 1.3	+ 1.5	+ 2.4	+ 2.5
July	-	-	-	+ 1.1	-	-
August	+ 2.0	+ 2.0	+ 1.4	+ 1.4	+ 2.2	+ 2.1

Based on Table 5-2, minimum, mean and maximum temperature increase is strongest in May. For mean temperature, the significant increase amounts to 2.2 $^{\circ}\text{C}$ when averaged over all stations, ranging from 2.6 $^{\circ}\text{C}$ at the station Hohendubrau (Spree) and Oppach (Schwarze Elster) to 1.7 $^{\circ}\text{C}$ at Zahna (Schwarze Elster) and 1.6 $^{\circ}\text{C}$ at Berlin-Tempelhof (Spree). These results suggest that there is a south-easterly gradient of temperature increase in May (Figure 5-6).

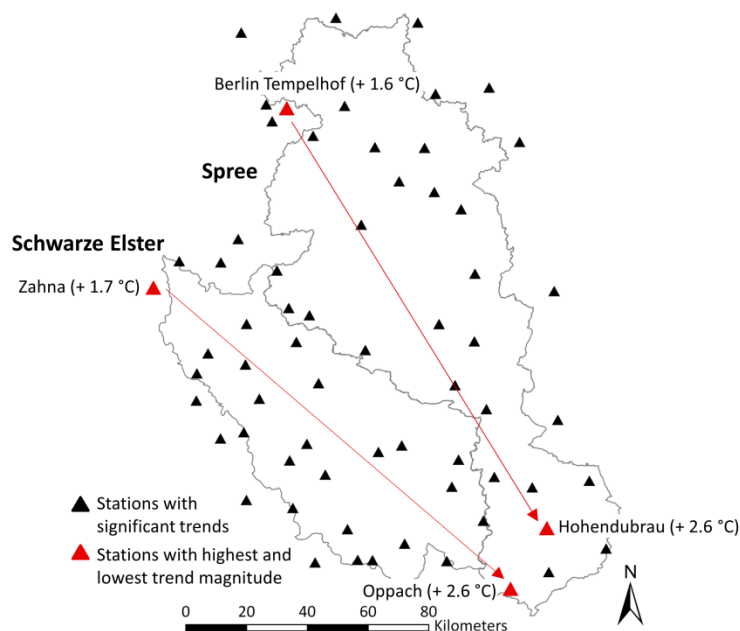


Figure 5-6: Mean temperature (1951-2006): spatial distribution of significant and non-significant gradual trends as well as gradient in trend magnitude in May

Significant positive mean temperature change points are clustered in the northern part of the Spree catchment in January (Figure 5-7).

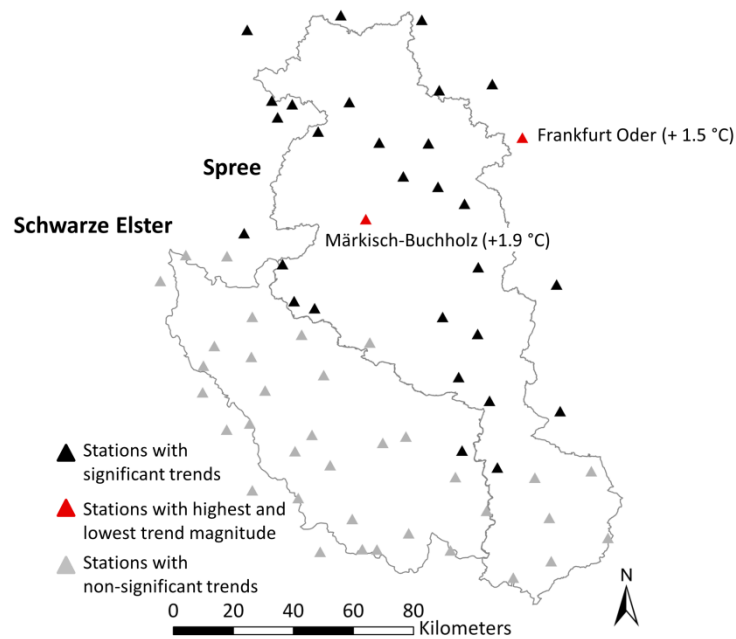


Figure 5-7: Mean temperature (1951-2006): spatial distribution of change points in the month of January (for Spree, trends are above field significance)

The station with the highest and lowest mean temperature increase in January are Märkisch-Buchholz (+ 1.9 °C) and Frankfurt Oder (+ 1.5 °C), respectively. A spatial gradient of mean temperature was not identified. During all other months, significant mean temperature trends/change points are evenly distributed throughout the study catchments and spatial gradients were not detected (Figure C-3 (change points), C-4 (gradual trends) in Appendix C). The spatial distribution of the maximum and minimum temperature change points and gradual trends is displayed in Appendix C (Figure C-7 and C-8 for maximum temperature and Figure C-9 and C-10 for minimum temperature).

On both the monthly and annual basis, both significant change points as well as gradual trends are in most cases detected at the same time (Figure 5-4 and 5-5), aggravating the differentiation between the natures of the trend. However, during the months of January and February, significant change is only detected for mean temperature by the Pettitt test (Figure 5-5, c), which is, however, below field significance except in January in the Spree river catchment. Visualizing the mean temperature time series from the station Seelow (Spree river catchment, Figure 5-8) reveals that the time series are characterised by a strong variation, similar to a phase shifted sinus function (smoothed curve LOWESS).

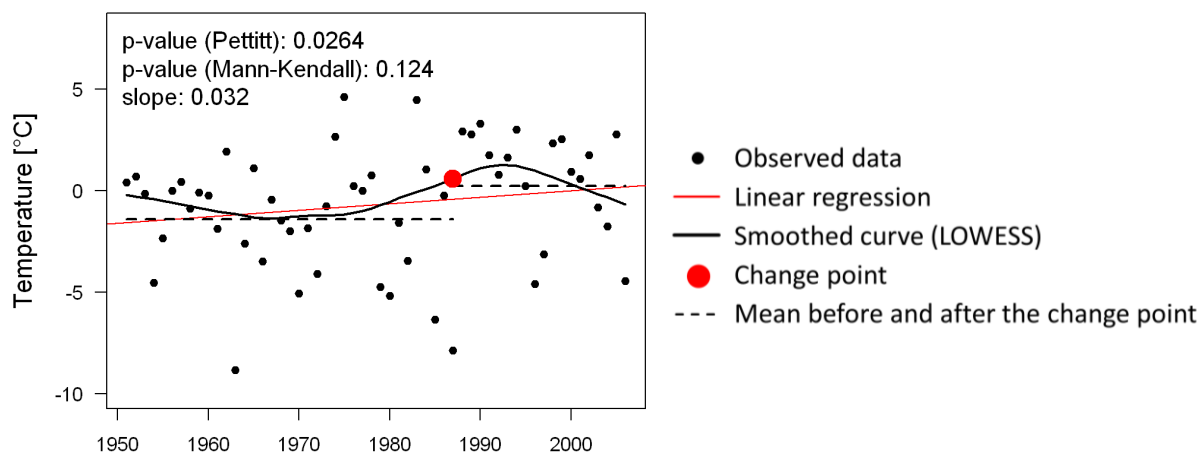


Figure 5-8: Mean air temperature in January: representative example (station Seelow, Spree river catchment) with significant mean temperature change point, but non-significant gradual trend

Consequently, a significant change point is detected while the overall gradual trend is not significant so far. As long as the cause for this variation cannot be attributed, the interpretation of the persistence of this behaviour is hampered and regional climate models might not replicate such behaviour.

Potential evapotranspiration

Potential evapotranspiration, driven by the increase in temperature (Figure 5-4) and global radiation (Figure C-2 in Appendix C), has increased by 24 mm and 27 mm in the Spree and Schwarze Elster river catchments, respectively, since the 1950s (Figure 5-9). The gradual increase is to date only significant in the Schwarze Elster based on the Mann-Kendall test. The detected change points in 1988 (Spree) and 1987 (Schwarze Elster) are significant in both catchments as a result of the shift from a negative to positive trend around the 1980s. In fact, potential evapotranspiration decreases until the 1980s by 1.3 mm/a after which it increased by around 1.8 mm/a (Figure 5-9). The decrease in potential evapotranspiration before the 1980s can be attributed to decreasing global radiation (Figure C-2 in Appendix C).

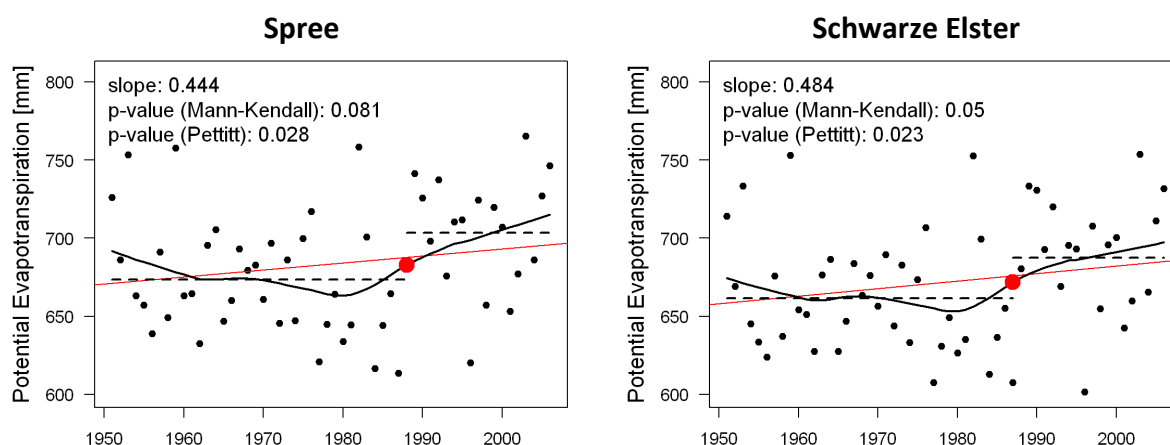


Figure 5-9: Potential evapotranspiration (interpolated annual values, 1951-2006) in the Spree and Schwarze Elster river catchments and trend interpretation

The monthly spatially explicit analysis shows that the number of positive trends (Spree: 351, Schwarze Elster: 304) outweighs the number of negative trends (Spree: 141, Schwarze Elster: 140) by 150 % in the Spree and by 120 % in the Schwarze Elster river catchment (Figure 5-10, a and b). The positive potential evapotranspiration trends during the winter months are mainly driven by an increase in global radiation (Figure C-15 in Appendix C) while the positive trends during the summer months are mostly a result of an increase in temperature (Figure 5-5). Negative gradual trends can be found during the months of:

- March
- June (all stations)
- July
- September (all stations)
- October (Figure 5-10, b).

The detected significant negative change points in June in the Spree and the negative gradual trends in the Schwarze Elster river catchments are well below field significance (Figure 5-10, b and c).

When accounting for field significance, positive change points are significant in the months of (Figure 5-10, c):

- January (1987)
- February (1987 only Spree)
- May (1974 (Spree), 1987 (Schwarze Elster))
- December (1981).

Field significant gradual trends can only be found in:

- December (Spree)
- August (Schwarze Elster).

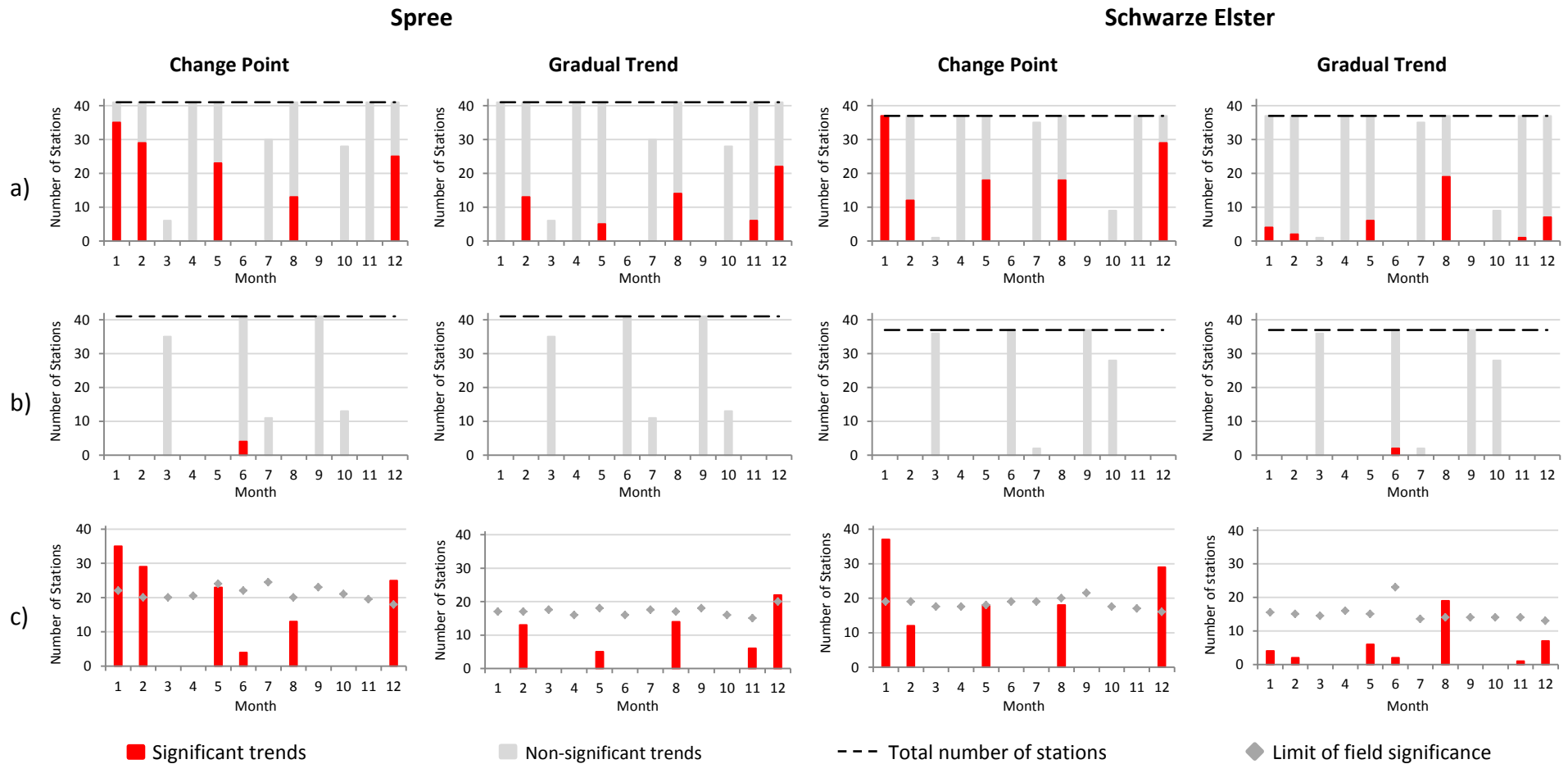


Figure 5-10: Potential evapotranspiration (1951-2006): number of stations with significant and non-significant (a) positive and (b) negative trends, (c) number of significant trends and field significance for change points and gradual trends in the Spree (left) and Schwarze Elster (right) river catchments

In accordance with temperature, the biggest increase in potential evapotranspiration can be identified in May (+ 10 mm) and the strongest decrease in June (- 11 mm) on average over all stations in the Spree and Schwarze Elster river catchments. The spatial distribution of significant, above field significant, positive potential evapotranspiration change points is displayed in Figure 5-11. In January, significant change points are relatively evenly distributed throughout the study catchments with a north-western gradient of increasing potential evapotranspiration and a relatively small increase in absolute terms (on average: 1.45 mm, Figure 5-11). In February, significant positive change points cluster themselves in the northern and centre part of the Spree catchment with a gradient of increasing potential evapotranspiration from south to north. In May, significant positive change points are located in central (both catchments) and southern part (only in the Spree) with a south-easterly gradient, similar to that of temperature presented in Figure 5-6.

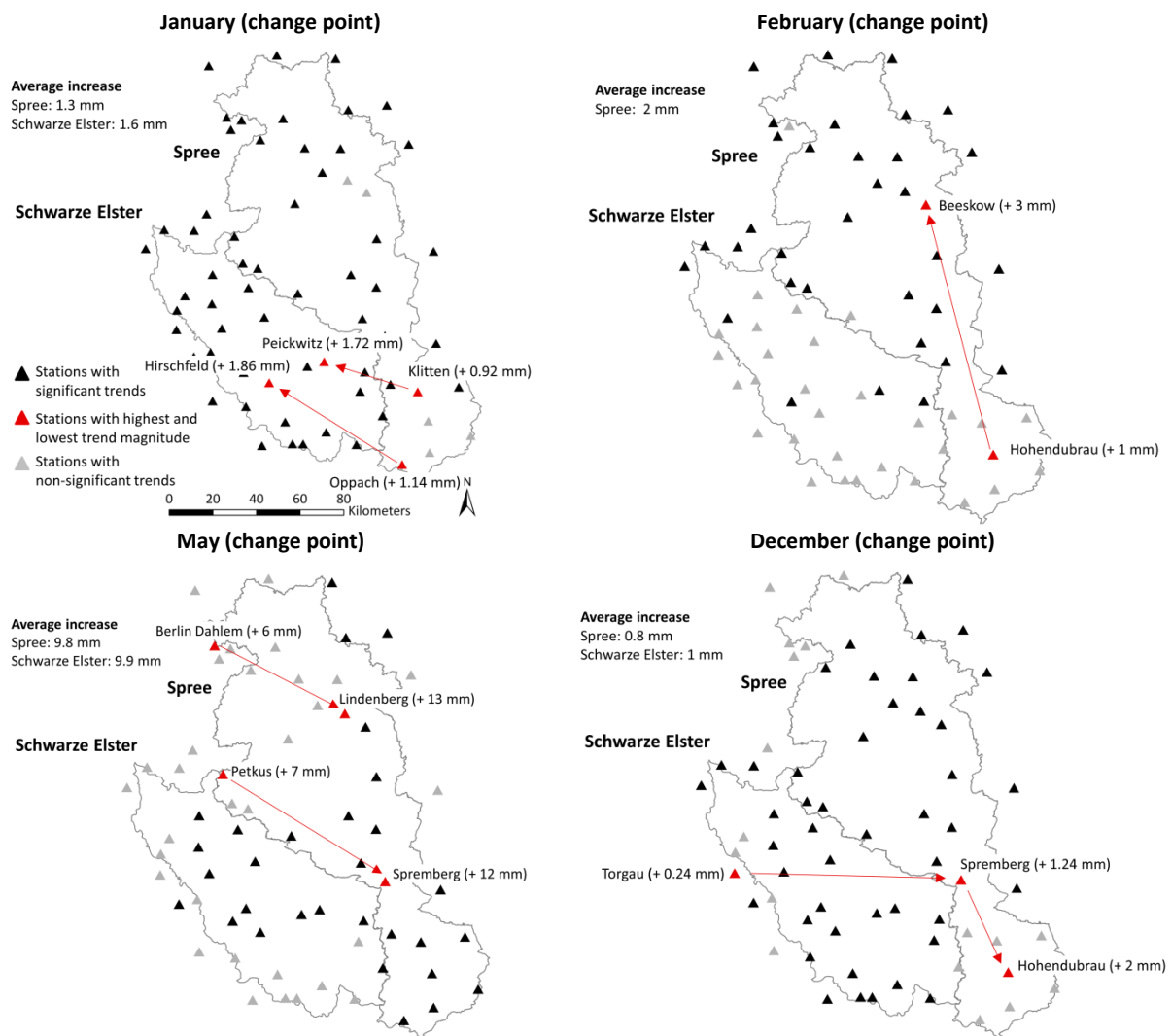


Figure 5-11: Potential evapotranspiration (1951-2006): spatial distribution of significant and non-significant change points as well as gradient in trend magnitude

In December, significant change points are evenly distributed in the Schwarze Elster river catchment, while they are clustered in the northern part of the Spree river catchment. A clear gradient cannot be identified. Similarly to the change points, the spatial distribution of significant, above field significant, positive potential evapotranspiration gradual trends is displayed in Figure 5-12. In December, similar to the change points, significant gradual trends are encountered in the centre to northern part of the Spree river catchment. Opposite to the change points, no significant gradual trends were detected in the Schwarze Elster river catchment. In August, significant gradual trends are clustered in the northern (only Schwarze Elster) and centre part of the catchments with a north-south gradient and an absolute increase of potential evapotranspiration of 9 mm.

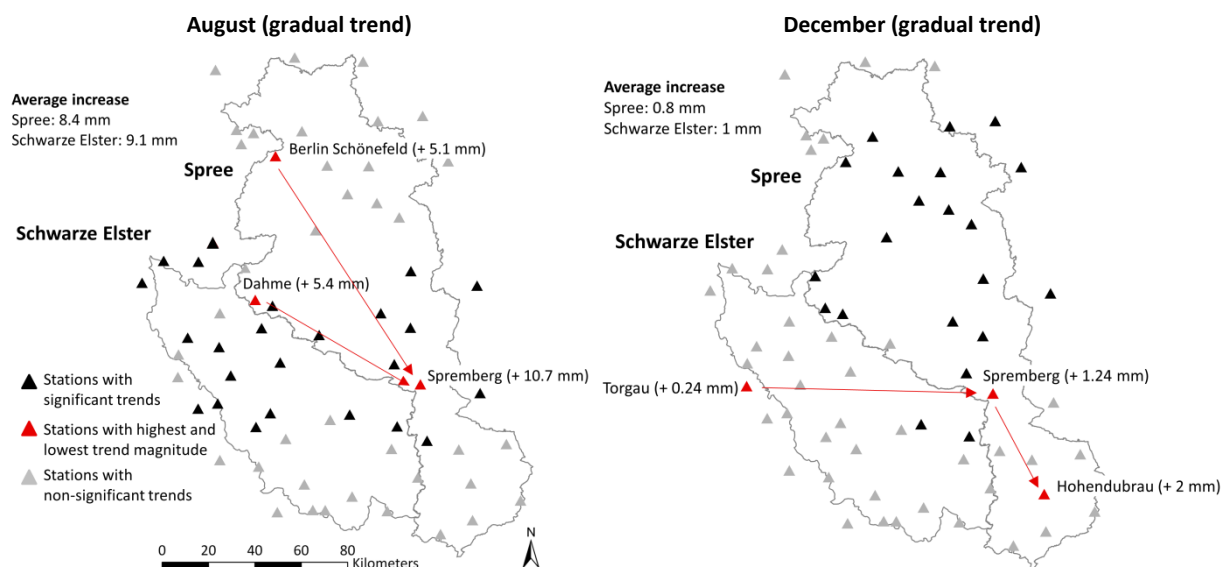


Figure 5-12: Potential evapotranspiration (1951-2006): spatial distribution of significant and non-significant gradual trends as well as gradient in trend magnitude

The spatial distribution of significant and non-significant gradual trends (Figure C-12) and change points (Figure C-11) during all other months is presented in Appendix C.

Precipitation

Precipitation has decreased by 13 mm in the Spree and by 10 mm in the Schwarze Elster river catchments since the 1950s (Figure 5-13). Both gradual trends and change point are non-significant.

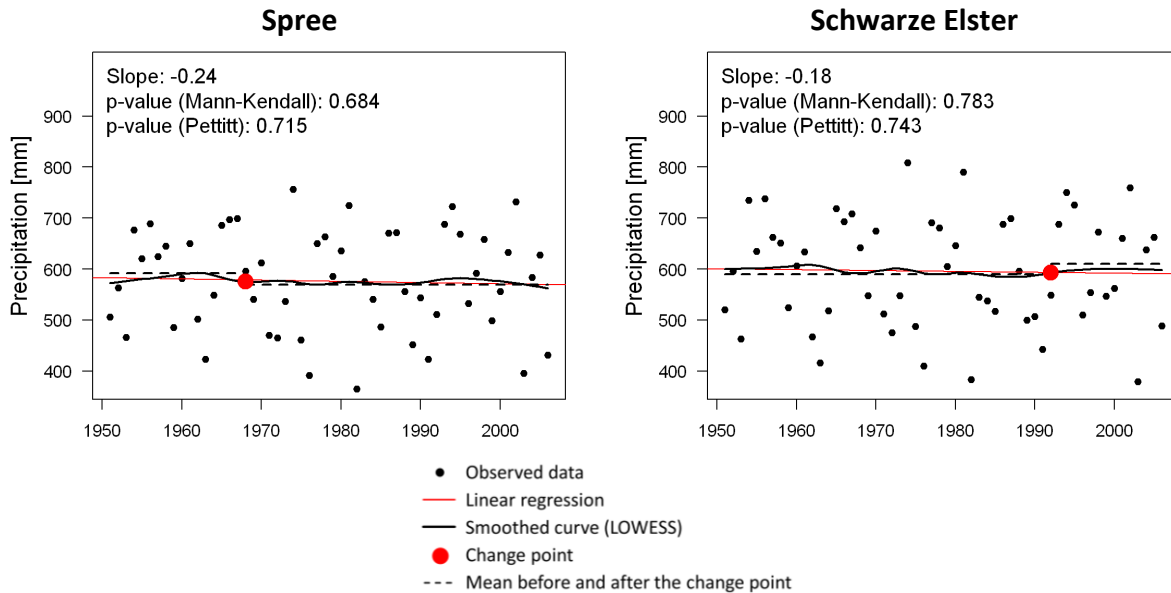


Figure 5-13: Precipitation (interpolated annual values, 1951-2006) in the Spree and Schwarze Elster river catchments and trend interpretation

Opposite to the slight decrease in precipitation based on the interpolated precipitation time series (Figure 5-13), the monthly analysis shows that the number of stations with positive trends (Spree: 254, Schwarze Elster: 251) exceeds the number of stations with negative trends (Spree: 238, Schwarze Elster: 193) by 7 % in the Spree and by 30 % in the Schwarze Elster river catchment (Figure 5-14, a and b). This result highlights the impact of spatial interpolation on the outcome of the analysis. The monthly station wise trend analysis shows a tendency of a shift in precipitation towards decreasing summer and increasing winter precipitation, which is not yet significant in the study catchments. Significant change points as well as gradual trends are all well below field significance (Figure 5-14, c). Spatially, no patterns could be detected (Figure C-13 and C-14 in Appendix C).

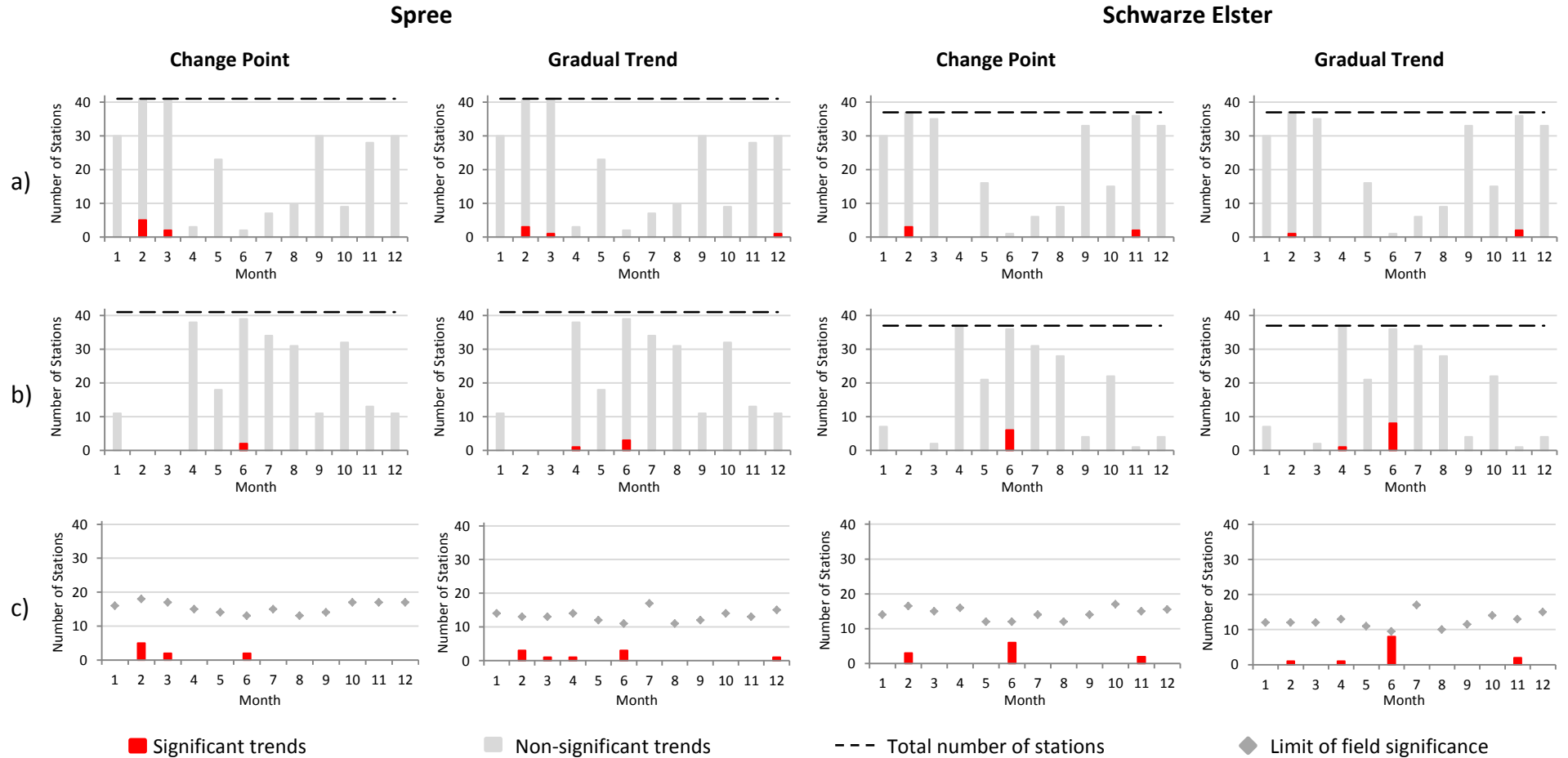


Figure 5-14: Precipitation (1951-2006): number of stations with significant and non-significant (a) positive and (b) negative trends, (c) number of significant trends and field significance for change points and gradual trends in the Spree (left) and Schwarze Elster (right) river catchments

5.2.3 Trend detection in the subcatchments

Similar to the Spree and Schwarze Elster river catchments, mean annual temperature increased in all subcatchments (Figure C-16 in Appendix C). The strongest increase in annual temperature can be observed in the Dahme river catchment (1.5 °C, 1961-2006), followed by the Weißer Schöps (1.4 °C, 1963-2006) and the Pulsnitz river catchment (1.3 °C, 1951-2006). The increase is significant for both the Pettitt, change points also occurring in the year 1987, and Mann-Kendall test. On the seasonal basis, time series of temperature also show a positive trend during all seasons and in all subcatchments, with the strongest increase in winter (Dahme: 2.3 °C) and the lowest in autumn (Pulsnitz: 0.5 °C, Table C-1 in Appendix C, slope). In winter, the positive temperature trends are statistically significant only for the Pettitt test in all study catchments matching the results presented in Figure 5-8 for the Spree river catchment. In spring, trends are significant for both gradual trends and change points at significance level 0.01 in all subcatchments, even though the overall trend magnitude is lower (Weißer Schöps 7 %, Dahme 24 %) compared to the winter months. In the Pulsnitz river catchment, trend magnitude between winter and spring does not differ (Table C-1 in Appendix C). Also during the summer months, both gradual trends and change points are significant with a temperature increase of 1.4 °C on average. In autumn, trends are non-significant.

Similar to temperature, potential evapotranspiration shows an increase of 19 mm, 48 mm and 40 mm in the Pulsnitz, Weißer Schöps and Dahme river, respectively (Figure C-16 in Appendix C). So far, positive potential evapotranspiration trends are statistically significant in the Weißer Schöps and Dahme river catchments for both the Mann-Kendall and Pettitt test on the annual basis (Figure C-16 in Appendix C). Change points again occur in the years 1987 (Pulsnitz and Dahme) and 1988 (Weißer Schöps). Shortening the time series length of the Pulsnitz river catchment also increases the slope of the trend and reduces the corresponding p-value of the significance tests, demonstrating how sensitive the trend tests react to changes in the time series length. In line with the analysis for the Spree and Schwarze Elster river catchments, a shift from negative trends to positive trends around the 1980s is detected. On the seasonal basis, potential evapotranspiration trends are also positive except in autumn in the Pulsnitz river catchment (Table C-1 in Appendix C). Trend magnitude is largest (+ 27 mm) in spring in the Weißer Schöps river catchment and lowest (- 2.2 mm) in winter in the Pulsnitz river catchment. In winter, the positive trend in potential evapotranspiration (+ 6 mm) is significant in all study catchments for the Pettitt test. For the Mann-Kendall test, it is only significant in the Dahme river catchment. In spring, the increase in potential evapotranspiration (+ 18 mm) is significant for both gradual trend and change

point in the Weißer Schöps and Dahme river catchment. During summer and autumn trend of potential evapotranspiration are non-significant.

Precipitation shows a non-significant downward trend in the Pulsnitz (- 1.8 mm) and Weißer Schöps (- 39 mm) river catchments and a non-significant upward trend (+ 2.3 mm) in the Dahme river catchment on the annual basis (Figure C-16 in Appendix C). Trend magnitude is largest in winter (+ 27 mm) and lowest in summer (- 45 mm) in the Pulsnitz river catchment.

On the seasonal basis, trends are also non-significant (Table C-1 in Appendix C). For the Pulsnitz river catchment, a tendency towards a redistribution of precipitation towards an increase in autumn (+ 24 mm) and winter (+ 27 mm) and a decrease in spring (- 7 mm) and summer (- 45 mm) is evident, matching the results from the analysis of the Spree and Schwarze river catchment (Table C-1 in Appendix C). Due to the difference in the time series lengths, this phenomenon is not observed in the Dahme and Weißer Schöps river catchments. Considering the same time period (1951-2006), however, confirms the redistribution from summer to winter also in these subcatchments.

Mainly driven by the increase in temperature and potential evapotranspiration, runoff is decreased by 24 mm, 38 mm and 33 mm in the Pulsnitz, Weißer Schöps and Dahme river catchments, respectively. Trend magnitude is, in accordance to precipitation, largest in winter (+ 6 mm) and lowest in summer (- 21 mm) in the Pulsnitz river catchment. The decrease in runoff is non-significant in the Pulsnitz and Weißer Schöps river catchments on the annual basis (Figure C-16 in Appendix C). In the Pulsnitz river catchment, an increase in runoff up to the beginning of the 1970s and a decrease during the 1980s with an almost significant change point in the year 1988, an indication of most probably anthropogenic influence, can be identified (Figure C-16 in Appendix C). Similarly, the significant downward trend in the Dahme river catchment is most likely of anthropogenic origin and confirms the analysis presented in section 4.4. On the seasonal basis, runoff shows a negative trend in the Pulsnitz river catchment, except during the winter (Table C-1 in Appendix C). In the Weißer Schöps and Dahme river catchments, runoff decreased during all seasons. Due to the anthropogenic impact in the Dahme river catchment, negative trends in runoff are significant during all seasons except in summer when only the change point is significant.

5.2.4 Consistency of observed changes with climate change scenarios

The temperature and precipitation trends based on measurements and simulations by the DAs are presented on annual and seasonal basis in Figures 5-15, 5-16 (Spee and Schwarze Elster) and Figures C-17, C-18 (subcatchments) in Appendix C. The boxplots are a result of the realisations used for each DA.

Concerning mean annual temperature, all DAs underestimate (averages: REMO: \approx - 80 %, CCLM: \approx - 50 %, WettReg: \approx - 90 %) the trend magnitude of the measurements (on average

+ 0.032 °C) in the Spree and Schwarze Elster (Figure 5-15, top) and their subcatchments (Figure C-17 in Appendix C, top). Apart from winter (all DAs), where temperature increase is largest for the measurements, and spring (only WettReg on average), the DAs and the measurements agree on a positive temperature trend during the period 1961-2006. In autumn, the DAs overestimate the trends in the measurements.

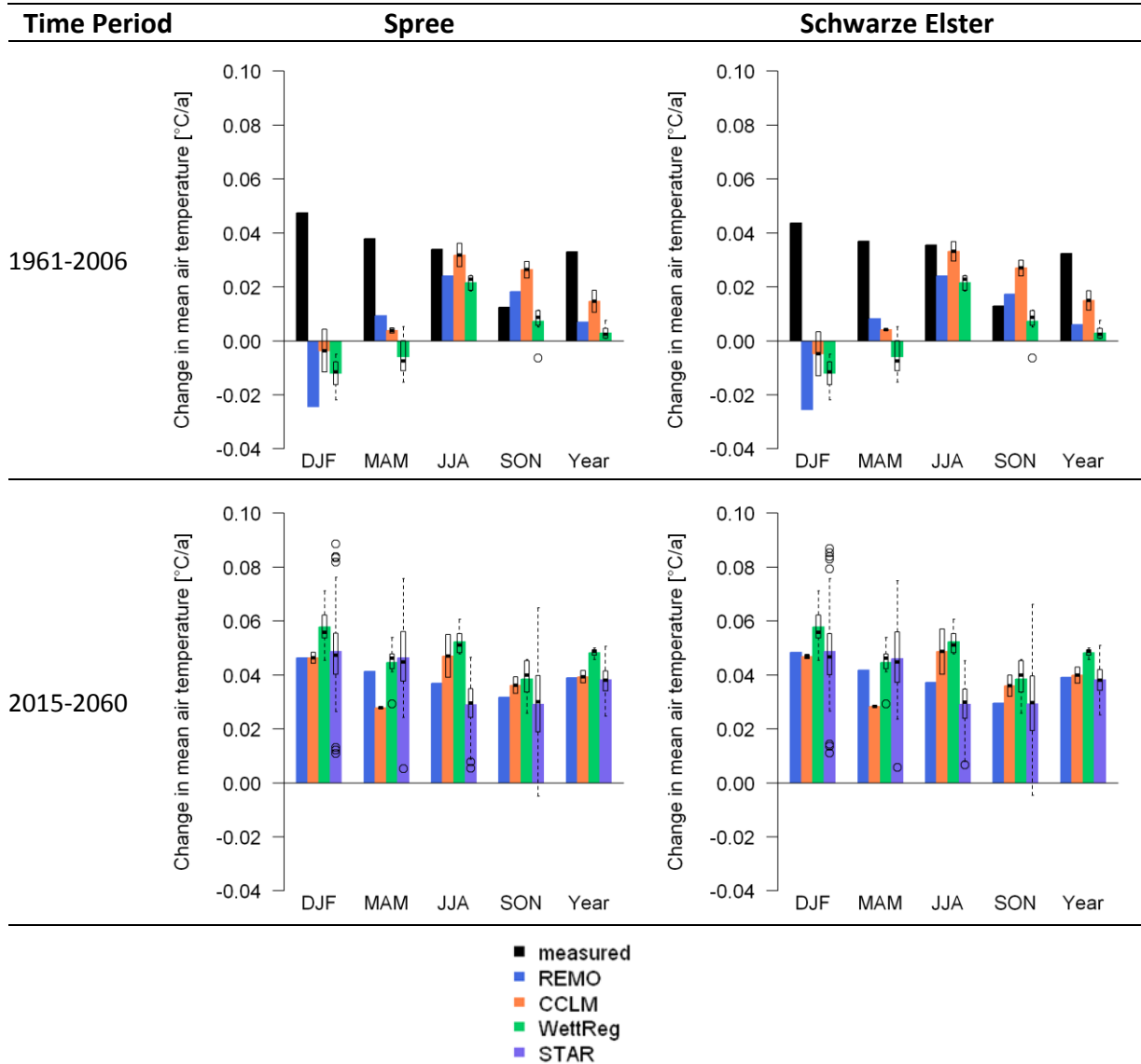


Figure 5-15: Mean temperature: Comparison of trend magnitude between measured and simulated temperature for the period 1961-2006 (top) and between simulations for the period 2015-2061 (bottom) in the Spree and Schwarze Elster river catchments

For the period 2015-2060, all DAs simulate positive temperature trends in all study catchments on the annual as well as on the seasonal bases (Figure 5-15 and Figure C-17 in Appendix C, bottom). Simulated increase in temperature is largest during winter (on average 0.05 °C/a) and lowest (on average 0.033 °C/a) during autumn in the study catchments. CCLM

computes lower temperature increase in spring (MAM) compared to the other DAs. WettReg computes, on average, the strongest increase in temperature (0.05 °C/a).

Measured precipitation decreased in the Spree (- 0.19 mm/a) and Weißer Schöps (- 0.40 mm/a) river catchments while it increased in the Schwarze Elster (+ 0.22 mm/a), Pulsnitz (+ 0.93 mm/a) and Dahme (+ 0.05 mm/a) river catchments during 1961-2006 on the annual basis (Figure 5-16 and Figure C-18 in Appendix C, top).

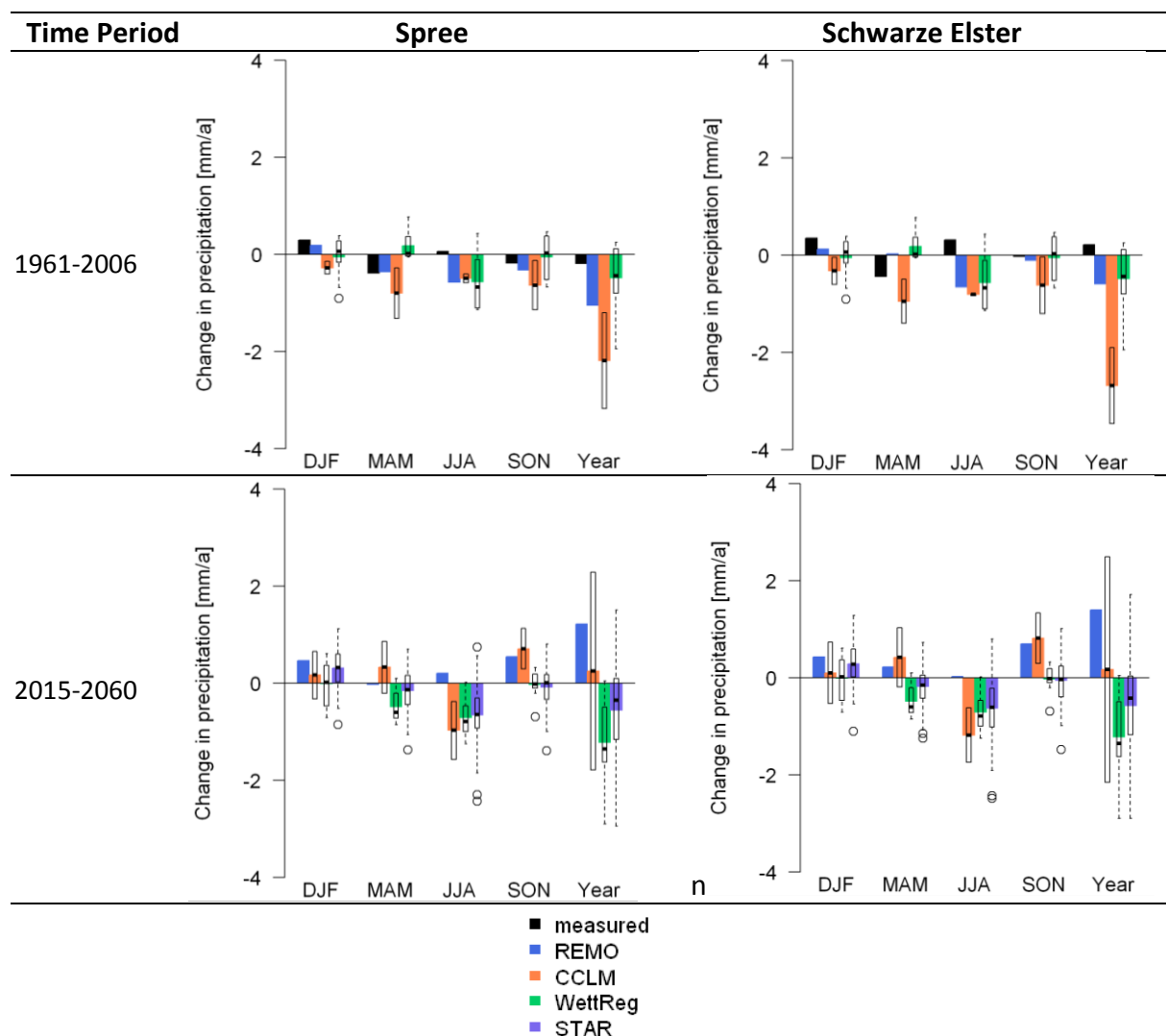


Figure 5-16: Precipitation: Comparison of trend magnitude between measured and simulated temperature for the period 1961-2006 (top) and between simulations for the period 2015-2061 (bottom) in the Spree and Schwarze Elster river catchments

These results differ from the trends presented in Figure 5-13 (Spree) and Figure C-16 in Appendix C (Pulsnitz) for the Spree and Pulsnitz river catchments and again highlight the influence of the time series length on the results. On the annual basis, the DAs agree on simulating on average a decreasing precipitation but differ in magnitude in all study catchments during the period 1961-2006. Seasonally, a redistribution of measured

precipitation from summer to winter cannot be observed and none of the DAs consistently agrees with the direction of the measured trends. In summer, all DAs simulate decreasing precipitation which is in contrast to the measurements (Figure 5-16, Figure C-18 in Appendix C, top).

For the period 2015-2061, REMO computes a positive trend, CCLM on average no considerable change and the statistical DAs, again especially WettReg, on average a strong decrease in precipitation on the annual basis (Figure 5-16 and Figure C-18 in Appendix C, bottom). Seasonally, the dynamical DAs, tend to simulate positive trends, except for CCLM during the summer, while the statistical DAs, especially WettReg, tend to simulate decreasing precipitation trends in all seasons except in winter. Due to the nature of the STAR algorithm, the expected redistribution of increasing precipitation during winter and decreasing precipitation during summer was confirmed (see section 3.2.2).

5.3 Discussion

Regardless of the method used for the trend analysis, temperature and potential evapotranspiration have increased in the study catchments of Spree, Schwarze Elster as well as in their subcatchments of Pulsnitz, Weißer Schöps and Dahme since the 1950s. The intra-annual analysis showed that the temperature increase is significant especially during the spring and summer months. Change points for both temperature and potential evapotranspiration occurred in the year 1987 or 1988. In fact, global radiation and consequently also potential evapotranspiration show a negative trend before the 1980 and a positive trend after 1980. The decrease before 1980 may be attributed to the effect of increased industrial pollution during the times of the German Democratic Republic in Eastern Germany. This effect is also referred to as the global dimming (CALANCA et al., 2006; TELISCA, 2013; WILD, 2009). A further investigation therefore has, however, been outside the scope of this thesis. Precipitation trends are not significant in a statistical sense but show a tendency towards increasing winter and decreasing summer precipitation for the time period 1951-2006. This, along with increasing temperature and potential evapotranspiration, could further aggravate agricultural practises, low-flows and consequently water user conflicts in the Lusatian river catchments in summer.

When both non-significant positive and negative trends were detected, trends are generally very close to zero, such as for precipitation in May in the Spree and Schwarze Elster river catchments (Figure 5-14 a and b). In most cases, both the Pettitt and Mann-Kendall test identified significant trends at the same time, aggravating a clear differentiation between the nature of the change. In order to test if the existence of a change point has affected the existence of a gradual trend in a time series, the Mann-Kendall test was applied before and after the change point, such as proposed by VILLARINI et al. (2011). It is assumed that the

change point can be interpreted as a “true” change point if there exists no significant gradual trend before and after the change point. The analysis of the existence of gradual trends before and after the change point showed, however, that in some cases, gradual trends were still significant before or after the change point. In other cases, as it would be expected, gradual trends were non-significant before or after the change point which would consolidate the assumption that change must have occurred step-wise. However, by shortening the time series length itself, gradual trends may no longer be significant as well. These results are supported by GUERREIRO et al. (2014) who drew similar conclusions in their study on changes in precipitation in transnational basins in the Iberian Peninsula. Consequently, the results of statistical analysis performed in this study suggest that a clear differentiation between a change point and gradual trend is not always possible using Pettitt and Mann-Kendall test statistics. In fact, the pattern of change can be more complex than the two simplistic categories of gradual change and change point (as shown for example in Figure 5-8, represented by LOWESS (GUERREIRO et al., 2014; KUNDZEWICZ and ROBSON, 2004; ROUGÉ et al., 2013)). Therefore, the results based on the two methods presented should rather be regarded as complementing each other and in that way increasing the confidence in the final results. In general, a change point resulting from changes in the measurement technique/procedure is highly unlikely since a large number of stations were evaluated simultaneously.

The analyses further proofed the importance of considering different correlation structures of the data. Similarly to the studies by DOUGLAS et al. (2000) and GUERREIRO et al. (2014), the spatially explicit trend analysis in the Spree and Schwarze Elster river catchments would have overestimated the significance of the trends if field significance and cross-correlation had been ignored. Moreover, when accounting for autocorrelation and conducting the pre-whitening, it could be observed that the limit of field significance is generally larger compared to the months when pre-whitening was not necessary to be carried out (for example Figure 5-5, c, in August). Nevertheless, the overall result, whether or not a trend is regarded as significant or non-significant, has not been affected by the pre-whitening procedure.

Since the results of the analysis of the measured time series suggest consistent temperature increase but no significant precipitation changes, the DAs should be able to reflect this development. In fact, the increase in temperature is reproduced by the different climate DAs, even though differences in magnitude exist. For precipitation, on the other hand, uncertainties are larger. This result is supported by BLÖSCHL and MONTANARI (2010) who pointed out that scenarios concerning future temperature are more robust compared to precipitation. Considering the fact that precipitation has not changed considerably during the last centuries, or even has tended to a slight increase in some catchments, the strong

decrease in precipitation simulated by the statistical DAs should be interpreted with care by considering the nature of the statistical downscaling algorithms (section 3.2.2 and 3.2.3). The dynamical DAs, on the other hand, are too wet without bias correction.

Finally, the dependence of the time series length on the results of trend tests needs to be stressed. An increase or reduction in time series length can lead to a different outcome as highlighted multiple times in the analyses.

6 Hydrological modelling

6.1 Materials and methods

6.1.1 The hydrological simulation models WaSiM-ETH and HBV-light

Two conceptually different hydrological models, the process and raster-based Water Balance Simulation Model developed at the ETH Zurich (WaSiM-ETH, (SCHULLA, 1997; SCHULLA and JASPER, 2012) and the conceptual model Hydrologiska Byråns Vattenbalansavdelning in its light version (HBV-light, (SEIBERT, 2003), were used. Both models are characterised by different process descriptions and input data requirements (Table D-1 in Appendix D). Simulations were carried out in a daily time step with both hydrological models for all analyses presented in chapters 6, 7 and 8.

WaSiM-ETH

WaSiM ETH is a deterministic process-based spatially distributed model based on a regular grid. The model was originally developed by SCHULLA (1997) to investigate climate change impacts on the hydrological cycle in alpine catchments. Since then, the model has continuously been developed further and applied in different studies at different spatial scales (GRAHAM et al., 2007b; HÖLZEL and DIEKKRÜGER, 2011; HÖLZEL et al., 2013) and at different geographical settings, including mountainous (GURTZ et al., 2003; JASPER et al., 2002; VERBUNT et al., 2005) and lowland catchments (KRAUSE and BRONSTERT, 2007). Due to its spatially distributed character, WaSiM-ETH facilitates the analysis of spatial patterns and processes. Temporally, the model can be used in continuous or event-based applications. A detailed model description can be found in SCHULLA (1997), JASPER (2005) as well as in SCHULLA and JASPER (2012). In this study, the model version 8.5 is used. Due to its modular structure, the application of WaSiM-ETH permits a large flexibility in application (Figure 6-1). Each module represents a hydrological process. Depending on the aim of the study and the data availability, modules can flexibly be included or excluded. The minimum spatial input data required to run WaSiM-ETH include:

- Digital Elevation Model (DEM)
- Land use map
- Soil map

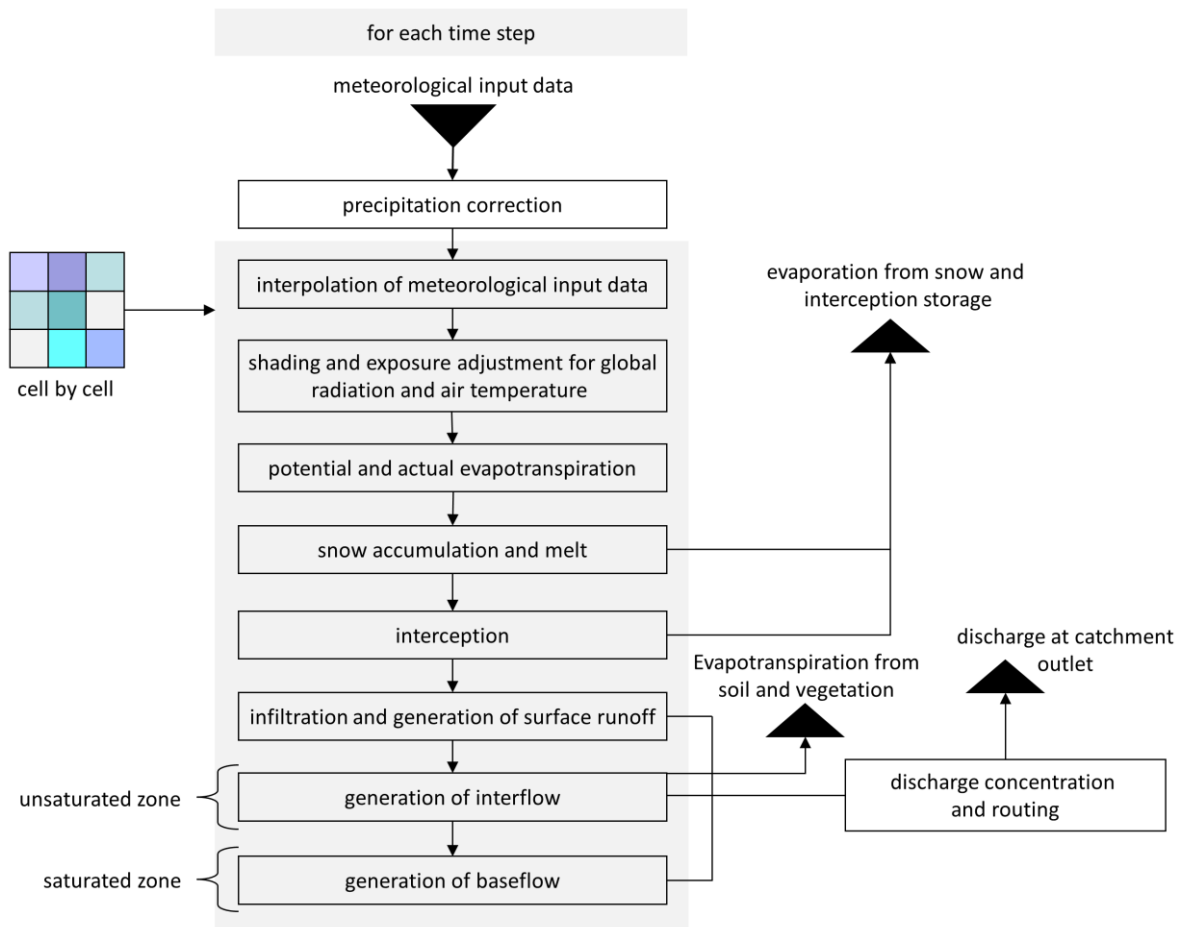


Figure 6-1: Schematic structure of the WaSiM-ETH model (modified after SCHULLA (1997) and HÖLZEL (2011))

Meteorological input time series form the climatic boundary conditions. Before the meteorological input data are interpolated, WaSiM-ETH internally corrects precipitation separately for solid and liquid precipitation using the wind dependent correction after SEVRUK (1986). A topography dependent adjustment of radiation and temperature can be carried out for each grid cell using an approach after OKE (1987) which is recommended for the application in mountainous regions. After this step, potential actual evapotranspiration is calculated using a two-step approach. At first, potential evapotranspiration is computed based on the MORECS-Scheme (THOMPSON et al., 1981), which uses the physically based Penman-Monteith formula (MONTEITH, 1975; MONTEITH and UNSWORTH, 1990) and considers vegetation coverage. Using the Penman-Monteith formula (Equation D-1 in Appendix D), the meteorological conditions in the atmosphere are characterised by the effective radiation balance ($R_N - G$), the saturation deficit of the air ($e_s - e$) and the temperature dependent slope of the saturated vapour pressure curve. The aerodynamic resistance r_a and the vegetation surface resistance r_s are computed based on the approach of THOMPSON et al. (1981). In a second step, potential evapotranspiration is reduced to actual

evapotranspiration using a linear suction approach depending on the matrix potential in the root zone (Equation D-2 in Appendix D, (FEDDES et al., 1976)). Using this approach, potential evapotranspiration is not only reduced when there is too little water available but also when there is too much water and anaerobic conditions prevail. Snow melt is simulated using the degree-day method. Interception is computed with a simple bucket approach depending on the LAI, the vegetation coverage degree, as well as a user-defined parameter describing the maximum layer thickness of the water on the leaves. Infiltration, which constitutes the upper boundary conditions for the calculation of water fluxes within the unsaturated zone, is calculated based on the Richards equation. For each grid cell, 1D vertical water fluxes within the unsaturated zone are computed based on the Richards equation parameterised after VAN GENUCHTEN (1980). In order to solve the Richards equation by a finite difference scheme, the soil column is discretised into different computational layers. Each computational layer may exhibit different hydraulic properties. At each soil layer boundary, interflow can be generated as a function of the saturated hydraulic conductivity (k_{sat}), the drainage density for interflow (d_i) and the hydraulic gradient (Equation D-3 in Appendix D). As a prerequisite for interflow generation, the water content has to be higher than the water content at field capacity. Interflow is directly discharged to the next river branch using an isocronic approach (Equation D-4 in Appendix D). This implies that interflow is not explicitly routed from one cell to the next cell. Additionally, WaSiM-ETH considers the effect of decreasing saturated hydraulic conductivity with depth (Equation D-5 in Appendix D). For solving the Richards equation, the upper boundary layer constitutes the calculated infiltration rate (Neumann boundary condition) while the lower boundary condition is determined by the groundwater table (Dirichlet boundary condition) which is calculated within the unsaturated zone model. The Richards equation is only valid for the soil matrix. Macropores, regarded as an additional water storage in contact with both the soil surface and the soil matrix, are considered using a modified bypass approach (JANSSON and KARLBERG, 2001). The infiltration into macropores is tied to a user-defined precipitation threshold value.

Groundwater flow is described two dimensionally by the continuity and Darcy's flow equation solved by an implicit finite difference approach: the Gauss-Seidel algorithm with automatic estimation of Successive Over Relaxation factors (SOR). Groundwater is connected to surface water by leakage approaches within the unsaturated zone model. The leakage approach implemented in WaSiM-ETH is based on a semipermeable layer (colmation layer) with a user-defined hydraulic conductivity and describes groundwater exfiltration one dimensionally (Figure 6-2).

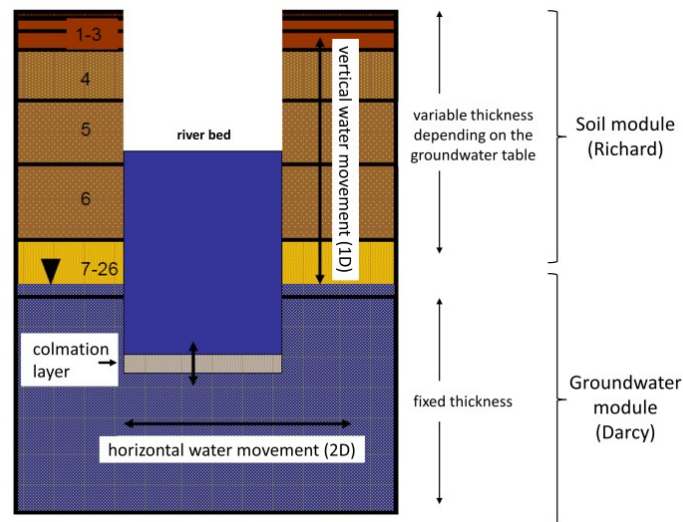


Figure 6-2: Schematic illustration of the interaction between unsaturated and saturated zone in WaSiM-ETH (modified after GAUGER (2007))

Surface water runoff can be generated at each grid cell. Infiltration excess overland flow takes place when the intensity of precipitation is higher than the saturated hydraulic conductivity of the upper soil layer. Apart from this, surface runoff can be generated from snow melt. When the 2D groundwater approach is used, saturation overland flow can also be caused by the groundwater table reaching the soil surface. Once surface water runoff is generated, reinfiltration is not considered in the model.

Surface runoff and interflow are each transformed separately by a single reservoir cascade using an isochronic approach with additional retention (Equation D-4 in Appendix D). Base flow generation takes only place by groundwater exfiltration into the surface river system at defined river grid cells. The total runoff, which constitutes the input to the routing model, is computed by summing up the average value of each runoff component. In the routing model, total runoff is routed through predefined routing sections using a kinematic wave approach based on flow velocity of the Manning-Strickler equation (MANNING, 1890; STRICKLER, 1923).

HBV-light

HBV-light is a conceptual, user-friendly hydrological model which has been developed for educational purposes (SEIBERT, 2003; SEIBERT and VIS, 2012). The original HBV model was developed by BERGSTRÖM (1976) and has become a standard model for simulating runoff in Nordic countries during the last decades. Model development was driven by the aim to design a simulation tool which represents the most important runoff generation processes in a simple and robust way. Since its development, HBV has been applied in more than 30 countries for research purposes, as well as for water engineering and operational hydrology (MACHLICA et al., 2012). Recently, also several model applications of HBV-light have been

reported in literature for different research purposes in different geographical settings (BIRKEL et al., 2012; GAO et al., 2012; MACHLICA et al., 2012; PLESCA et al., 2012). The basic equations implemented in HBV-light correspond to the HBV-6 version of BERGSTRÖM (1992). A detailed model description of the HBV-light model can be found in SEIBERT (1997), SEIBERT (1999) and SEIBERT and VIS (2012).

As depicted in Figure 6-3, the model consists of four routines: snow, soil, response and routing routine.

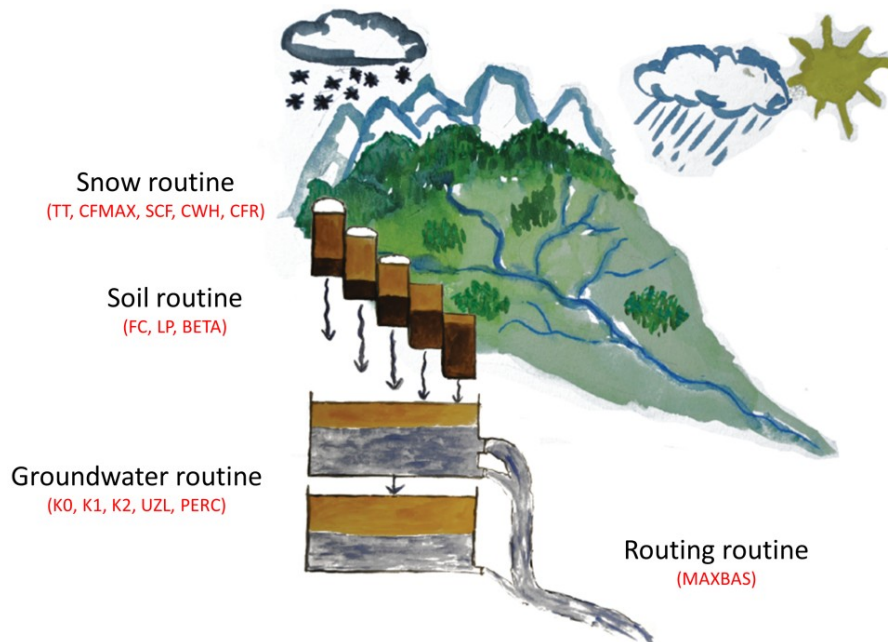


Figure 6-3: Schematic structure of the HBV-light model (SEIBERT and VIS, 2012)

i) Snow Routine

The snow routine controls the processes of snow accumulation and melt. Precipitation is simulated as either snow or rain depending on a user-defined threshold temperature (TT). Precipitation falling as snow is multiplied by a snowfall correction factor (SCF). Snow melt is computed with the degree-day method using the degree-day factor (CFMAX). Until a certain fraction (CHW) of the water equivalent of snow is exceeded, meltwater and rainfall are retained within the snowpack. Refreezing of snow melt is also considered by the model. When temperatures drop below TT, a refreezing coefficient (CFR) determines the amount of liquid water that is refrozen within the snowpack.

ii) Soil Routine

Within the soil routine, actual evapotranspiration, soil moisture content and groundwater recharge are calculated as a function of actual water storage in the soil box. Depending on the relation between the water content in the soil box and its maximum value (FC), precipitation is divided into water filling the soil box and groundwater recharge. The shape

parameter BETA determines the relative contribution to runoff from rain or snowmelt (Figure 6-4, left). Actual evapotranspiration is deduced from the soil box at the potential evapotranspiration rate if soil moisture storage divided by field capacity is above LP while a linear reduction is used when the ratio of soil moisture storage and field capacity is below LP (Figure 6-4, right).

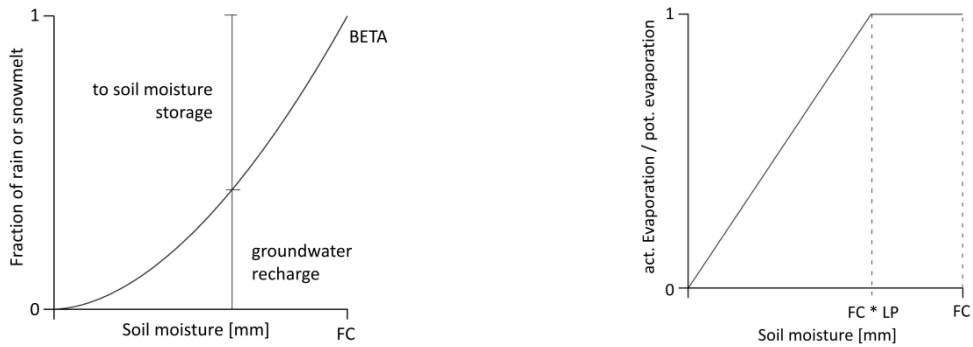


Figure 6-4: Soil routine in HBV-light: Contribution from rainfall or snowmelt to soil moisture storage/groundwater recharge (left) and reduction of potential evaporation depending on soil moisture storage (right, (SEIBERT, 2005)

iii) Runoff Response Routine

The runoff response function is represented by two conceptual groundwater storage reservoirs (Figure 6-5).

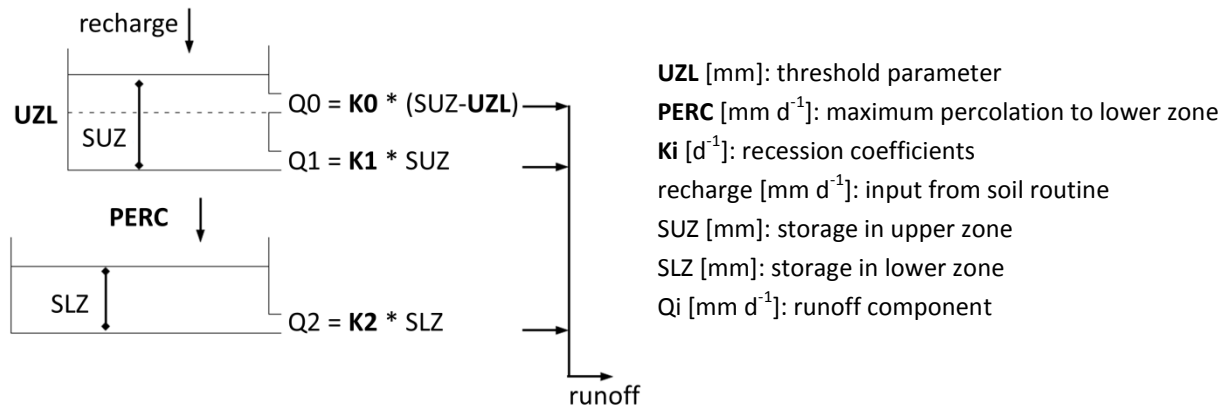


Figure 6-5: Runoff response routine in HBV-light (SEIBERT, 2005)

The groundwater recharge computed in the soil moisture routine is added to the upper groundwater box. A user-defined parameter (PERC) defines the maximum percolation rate from the upper to the lower groundwater storage box. Runoff is computed based on three linear reservoir equations, representing a fast, a slow and a very slow runoff component, which depend on user-defined recession coefficients (K0, K1, K2). The fast runoff component Q0 is only generated when water storage in the upper groundwater storage (SUZ) is above a threshold parameter (UZL).

iv) Routing Routine

Runoff transformation is realized by combining the three runoff components using a triangular weighting function where the flow generated in one time step is redistributed over a certain number of consecutive time steps depending on a user-defined parameter (MAXBAS).

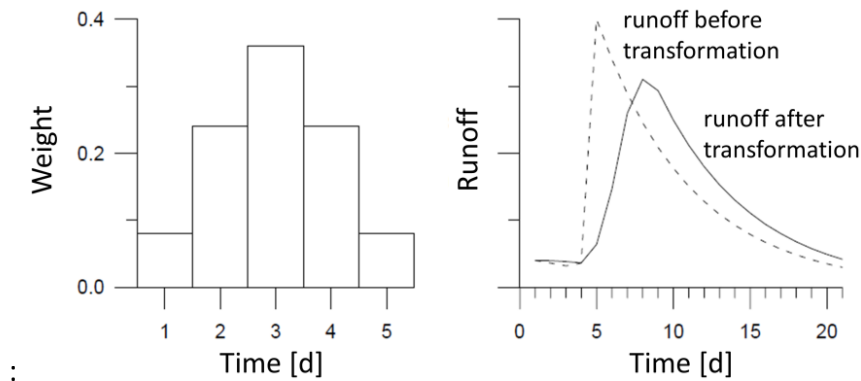


Figure 6-6: Routing routine HBV-light: example of runoff transformation with MAXBAS = 5 (SEIBERT, 2005)

6.1.2 Evaluation of hydrological model performance

The purposes of evaluating hydrological model performances are:

- To estimate a hydrological models ability to reproduce measurements
- To asses model improvements
- To compare the performance of different hydrological models (KRAUSE et al., 2005).

Hydrological model evaluation can be done subjectively and/or objectively. Subjective model assessment generally includes the analysis of the systematic (e.g. over or under prediction) and dynamic (e.g. timing, rising limb, falling limb, and base flow) runoff behaviour. Objective assessment, on the contrary, generally uses a form of a mathematical estimate, such as a statistical performance criterion of the error between simulated and measured hydrological variables, typically discharge. In this study, a number of different performance criteria are used for the comparison between measured and simulated discharge data (Table D-2 in Appendix D). Each criterion has its strengths and weaknesses and places emphasis on a certain aspect of the hydrograph, such as low-flows, peaks, the overall dynamic or the volumetric error. Thus, it is generally recommended to use a variety of different performance criteria to have a profound basis for judging model performance. This approach is generally referred to as multi-criteria evaluation.

The Nash-Sutcliffe Efficiency index (NSE, (NASH and SUTCLIFFE, 1970) is a normalized measure ranging from $-\infty$ to 1 (perfect fit). A NSE value below zero indicates that the mean of the measured discharge is a better indicator than the simulated discharge. Due to the

normalization of the variance of the measured discharges, higher NSE values are obtained in catchments with a higher discharge dynamic compared to catchments with a lower dynamic (KRAUSE et al., 2005). Furthermore, peak discharges receive more weight compared to low-flows because the differences between the measured and simulated discharges are computed as squared values (LEGATES and MCCABE, 1999). The application of Logarithmic values (discharges) to the NSE (LNSE) has the advantage that the extreme discharges are flattened and consequently the influence of low-flow is increased. This makes the LNSE useful for studies focussing on low-flows. The coefficient of determination, r^2 , ranges between 0 (no correlation) and 1 (perfect fit). The r^2 is based on the assumption of linearity and quantifies “how much of the observed dispersion is explained by the predictions” (KRAUSE et al., 2005). Consequently, a model which systematically over- or underpredicts measured discharge may still result in very high values for the r^2 . The NSE, LNSE and r^2 focus on the representation of the discharge dynamic and do not explicitly take into account volumetric errors. Therefore, the minimization of the Mean Absolute Relative Error (MARE) and the Mass Balance Error (MBE) is of high relevance for long term water balance simulations and their minimization constitutes the first step when parameterising and calibrating a hydrological model.

6.2 Set up of specific hydrological models

6.2.1 Parameterisation of site specific WaSiM-ETH models

The meteorological input variables used for WaSiM-ETH are displayed in Table D-3 in Appendix D. The station based meteorological input data were interpolated using the Inverse Distance Weighting (IDW) approach. Spatially, after testing different grid cell sizes ranging from 50 m to 500 m, 100 m was chosen as a good compromise between the resolution of the spatial input data of topography, land use, and soil properties, computational effort and the overall study aim. In order to generate consistent input raster data sets, several pre-processing steps are necessary. Using the programme TANALYS (Topographic ANALYSIS; SCHULLA and JASPER, 2012), a topographic analysis was carried out based on the DEM. As a result, several raster data sets, such as flow direction, flow accumulation, river network and subcatchment structure are generated which serve as input data sets for several WaSiM-ETH modules. Land use maps were constructed for each catchment based on the CORINE land cover dataset (Table A-1 in Appendix A, (CLC, 2006)) from which 12 land use classes, each being characterised by a specific, however static, seasonal evolution, were defined (Table 4-1). Land use parameters (Table D-4, Appendix D) were obtained for each land use class separately from literature (SCHERZER et al., 2006; SCHULLA, 1997; SCHULLA and JASPER, 2007). The land use parameters also include the

empirical parameters of the Penman-Monteith formula (MONTEITH, 1975; MONTEITH and UNSWORTH, 1990), such as the albedo, the aerodynamic resistance and the leaf area index. Soil maps and soil types were derived from the available standard soils maps for each catchment (BÜK 200, 2007; BÜK 300, 2007). The DIN 4220 (2008) was used as a source for the van Genuchten soil hydraulic parameters Θ_s , Θ_r , α and n for each soil type (Table D-4 in Appendix D). Parameterisation of macropores was based on standard parameter values suggested by SCHULLA and JASPER (2007) as well as by SCHERZER et al. (2006). Soil information, based on the available soil maps, was limited to the upper 2 m. However, when applying WaSiM-ETH with the integrated 2D groundwater model, the complete first unconfined aquifer has to be included in the unsaturated zone because otherwise model instabilities occur (GAUGER, 2007; JASPER, 2010). In addition, the groundwater table, which is variable, is calculated within the unsaturated zone model. Hence, the unsaturated zone was parameterised up to a depth of 12 m. The upper two meters were parameterised based on the available soil maps (BÜK 200, 2007; BÜK 300, 2007) and the lower ten meters based on the hydrological maps (HÜK 200, 2007), Table 6-1).

Table 6-1: Discretisation of unsaturated zone in the study catchments

	Number of different soils types	Number of layers / thickness [m]*
Pulsnitz	53	12 / 0.3 and 2 / 5
Weißer Schöps	35	30 / 0.3
Dahme	12	12 / 0.3 and 2 / 5

* in Pulsnitz and Dahme river catchment, a differentiation between upper thinner and lower thicker layers was made

Due to the fact that the process of surface and groundwater interaction is especially important for the water cycle in plane landscape areas, the 2D groundwater approach was preferred over the simple conceptual linear storage approach which is more frequently applied (HÖLZEL and DIEKKRÜGER, 2011; HÖLZEL et al., 2011; RÖSSLER et al., 2012). The integrated 2D groundwater model requires a number of additional spatial data sets (Table 6-2).

Table 6-2: Spatial data input requirements and parameterisation basis for 2D groundwater model

Input data set	Parameterisation Basis/Value
saturated hydraulic conductivity [m/s]	HÜK200 (anisotropy was not considered)
boundary conditions (Neumann [m/s] or Dirichlet [m a.s.l.])	not specified, boundary conditions are assumed to be identical to the surface
specific storage coefficient [m ³ /m ³]	0.1 (HÖLTING and COLDEWEY, 2009; JASPER, 2010)
leakage factors [1/s] (colmation layer)	$5 \cdot 10^{-6} - 1 \cdot 10^{-6}$ (SCHULLA 2010)
aquifer thickness [m]	9 – 13

The hydrogeological map (HÜK 200, 2007), which has been used as the basis for parameterising the groundwater model, only contains information on the upper large scale coherent unconfined aquifer. Due to this limitation, the groundwater model can only be regarded as a simplified representation of the saturated zone. Since information about aquifer thickness is not contained in the HÜK200, it was estimated and adjusted during model parameterisation by a sensitivity analysis. Also information on the catchments subsurface boundaries was not available. Thus, surface and subsurface catchments boundaries were considered to be identical which can be regarded as a rough estimation, especially in the plane landscape of the Dahme river, and may be a source of additional model uncertainty. The proportion of baseflow to total runoff is mainly controlled by the highly sensitive parameters of saturated hydraulic conductivity, leakage factor of the colmation layer and the width and depth of the river system. The influence of these parameters on the baseflow proportion was analysed for each study catchment. The parameters were then adjusted in such a way that the distribution of the runoff components roughly agrees with the values suggested by DIFGA which separates total runoff in faster and slower components. The comparison between the runoff components simulated with WaSiM-ETH and DIFGA can, however, only be regarded as a reference since the conceptual basis of the approaches differs (GAUGER, 2007; UHLENBROOK, 1999). However, the groundwater model parameters do not only influence the proportion of the runoff components to total runoff, but they also affect catchment functioning and runoff dynamic in the study catchments. Spatially distributed data on the saturated hydraulic conductivity are based on the HÜK200, whose values range between two decimal powers. Hence, the values had to be adjusted during model parameterisation. High values of the saturated hydraulic conductivity increase base flow (Figure 6-7). Lower values, on the other hand, decrease baseflow but increase water storage in the catchments valley. Consequently, groundwater can rise up to the ground surface where, during a rainfall event, surface runoff

is generated. Therefore, runoff peaks and the overall runoff variability can be more pronounced when saturated hydraulic conductivities are lower. Similarly to the saturated hydraulic conductivity, a large leakage factor, which regulates the exchange between groundwater and surface water in WaSiM-ETH, leads to a larger proportion of baseflow as the resistance for groundwater exfiltration decreases.

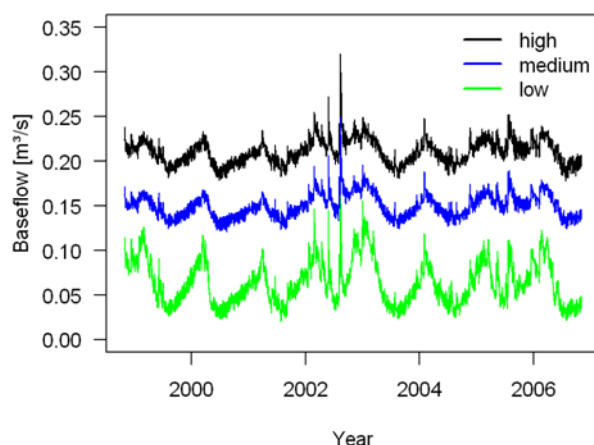


Figure 6-7: Sensitivity of baseflow as a function of saturated hydraulic conductivity in WaSiM-ETH (example Dahme river catchment); high represents the upper limit of the saturated hydraulic conductivity, low the lower limit and medium the average

The river system grid cells, where groundwater infiltration and exfiltration takes place, is generated during pre-processing using the TANALYS programme, but was further adjusted during model parameterisation. As recommended by SCHULLA (2010), also all other grid cells were defined as river grid cells with lower width and depth compared to the river system. This is due to the fact, that in reality an area of $100\text{ m} \cdot 100\text{ m}$ (= grid cell size) is not a flat plane but contains small trenches or depressions where water can drain.

6.2.2 Parameterisation of site specific HBV-light models

HBV-light is used as a lumped conceptual model. The model only requires temperature, precipitation and potential evapotranspiration as driving variables to simulate discharge. Interpolation of the meteorological input data was initially conducted based on Thiessen polygons. A former study showed that using different interpolation methods for the meteorological input data causes large deviations in the modelling results between WaSiM-ETH and HBV-light (GÄDEKE et al., 2012a). Therefore, the interpolated meteorological variables temperature, precipitation and potential evapotranspiration by WaSiM-ETH were used as meteorological input to HBV-light and uncertainties related to the input data were avoided. Consequently, the model comparison between the hydrological

models only focusses on structural model differences. In total, HBV-light contains 14 model parameters in its lumped version which were adjusted during model calibration.

6.2.3 Calibration and validation

In the process of hydrological model calibration, the model parameters are adjusted in such a way that the best possible fit between simulation and observation is achieved. Subsequently, during model validation, the model performance is evaluated for an independent time period. Thus, the split sample test is applied (KLEMES, 1986). If the hydrological model performance does not differ considerably between model calibration and validation, it is assumed that the model is also valid outside of calibration and validation periods (BEVEN, 2001).

Model calibration and validation is carried out on measured discharge at gauge Ortrand (Pulsnitz), at the gauge Särichen (Weißer Schöps) and at gauge Prierow (Dahme, for location see section 4.1.2 to 4.1.4). Due to its distributed character, WaSiM-ETH was additionally calibrated on discharge gauges located within the study catchments to assess whether internal catchment processes are simulated reliably.

For both hydrological models, the hydrological years 1999-2001 were used for model calibration and the years 1997-1999 for model initialization. The model validation was subdivided into two separate steps: at first, the hydrological models were validated on daily measured discharge for the hydrological years 2002-2006. Calibration and validation on daily measured discharge was restricted to the period 1999-2006 due to initial data availability. However, this period includes both wet (e.g. 2002) and dry (e.g. 2003) years compared to the long term average and was therefore regarded suitable for model calibration and validation on daily discharge. Secondly, the hydrological models were additionally validated on long term mean monthly measured discharge values for the reference period 1963-1992 in the Weißer Schöps and Dahme river catchments and for the period 1988-2006 in the Pulsnitz river catchment. This period was determined by the discharge data availability (Table A-1 in Appendix A). The model calibration strategy differs between the two hydrological models (Figure 6-8).

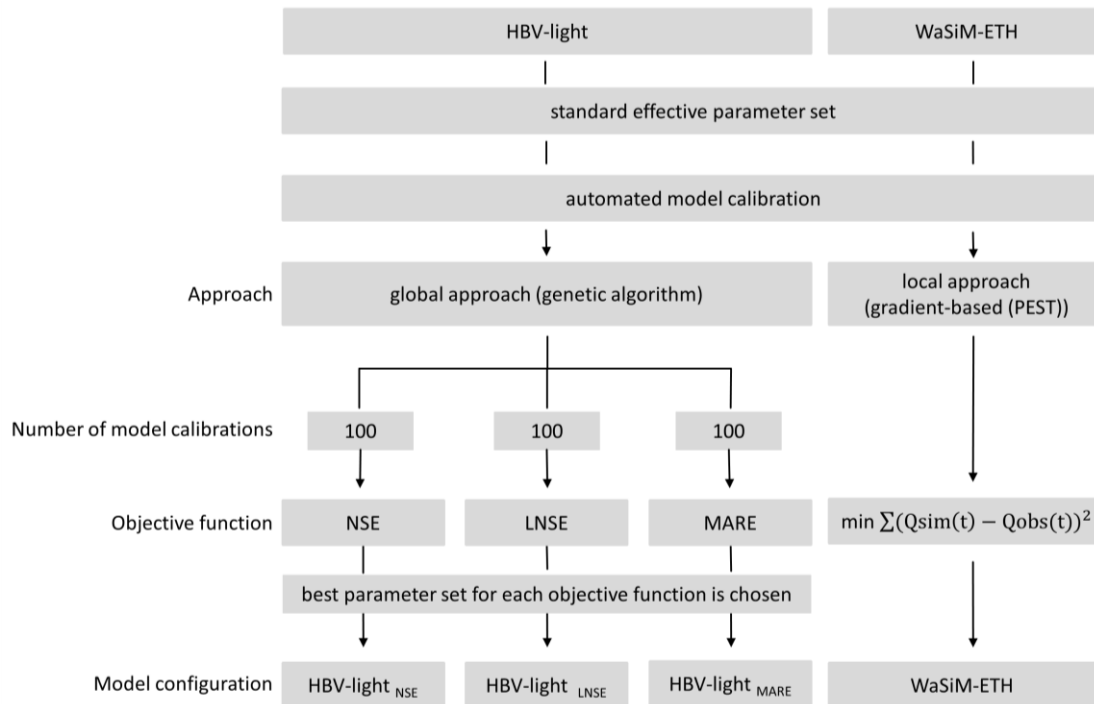


Figure 6-8: Calibration strategy for HBV-light and WaSiM-ETH

The parameterised WaSiM-ETH models (section 6.2.1) were calibrated automatically by inverse modelling using the Model Independent Parameter ESTimation program PEST (DOHERTY, 2004), a gradient-based local search approach. Only four conceptual model parameters were chosen for calibration (Table 6-3).

Table 6-3: WaSiM-ETH parameters chosen for hydrological model calibration and their ranges used for calibration (k_{rec} global value for all soil types, $qd_{rec} < qi_{rec}$)

Parameter	Definition	Units	Range	Equation in Appendix D
qd_{rec}	recession parameter for direct flow	h	24 – 96	Equation D-4
qi_{rec}	recession parameter for interflow	h	48 – 120	Equation D-4
d_r	drainage density for interflow	m^{-1}	5 – 35	Equation D-3
k_{rec}	recession constant of the saturated hydraulic conductivity with depth	-	0.1 – 0.9	Equation D-5

All other model parameters describing the physical characteristics of the catchment on a spatially distributed basis, such as land use and soil parameters (Table D-4 in Appendix D), were not calibrated. At first, automated calibration was performed for the gauging stations located within the study catchments. Afterwards, the discharge at the outlet gauges was calibrated.

For HBV-light, 12 model parameters were chosen for model calibration (Table 6-4) based on a literature review (GAO et al., 2012; SEIBERT, 1997; SEIBERT, 2000; STEELE-DUNNE et al., 2008).

Table 6-4: Characteristics of HBV-light parameters chosen for hydrological model calibration

Routine	Parameter	Definition	Units	Range
Snow	TT	threshold temperature	°C	-2 – 0.5
	CFMAX	degree – day factor	mm °C ⁻¹ d ⁻¹	0.5 – 4
	SFCF	snowfall correction factor	-	0.5 – 0.9
Soil Moisture	FC	maximum value of soil moisture storage	mm	100 – 550
	LP	fraction of FC above which ETA equals ETP	-	0.3 – 1
	BETA	shape coefficient	-	1 – 5
Runoff Response	K0	recession coefficient (upper box)	d ⁻¹	0.1 – 0.5
	K1	recession coefficient (upper box)	d ⁻¹	0.01 – 0.2
	K2	recession coefficient (lower box)	d ⁻¹	5·10 ⁻⁵ – 0.1
	PERC	maximum rate of recharge between the upper and lower groundwater boxes	mm d ⁻¹	0 – 4
	UZL	threshold for Q ₀ flow	mm	0 – 70
Routing	MAXBAS	length of triangular weighting function in routing routine	d	1 – 2.5

Model calibration of HBV-light was performed automatically three times on three different objective functions using a global approach in the form of a genetic algorithm (SEIBERT, 2000) with subsequent local optimisation using Powell's quadratically convergent method (PRESS et al., 1992; Figure 6-8). The objective functions include the NSE, the LNSE and the MARE measures (Table D-2 in Appendix D). Therefore, the focus was not only set on the differences of the results between a conceptual and process-based hydrological model but also on different parameterisations of the conceptual model HBV-light that target different portions of the hydrograph. For each objective function, HBV-light was calibrated 100 times to consider parameter uncertainty. Each time, 5000 model runs were performed for the genetic algorithm followed by 5000 additional model runs for local optimisation. From the 100 parameter sets, one parameter set was chosen that performed reasonably well for all objective functions considered (Figure 6-8).

As presented in section 4.4, due to the anthropogenic impact on measured discharge in the Dahme river catchment, hydrological model calibration and validated was aggravated. Thus,

in the Dahme river catchment, WaSiM-ETH was manually parameterised and no automated calibration was performed. The model performance was only evaluated subjectively as well as using the coefficient of determination (r^2) in order to evaluate if the discharge dynamic is simulated reliably. The simulated discharge of WaSiM-ETH was then used for automatic calibration of HBV-light. After model calibration and validation, four different hydrological model configurations (WaSiM-ETH (1) and HBV-light (3)) were available for each study catchment.

6.3 Results

6.3.1 Mean discharge analysis

The final calibrated model parameters are displayed in Table D-5 for WaSiM-ETH and Table D-6 for HBV-light in Appendix D. The preliminary manual model parameterisation of WaSiM is complex, particularly when applying the 2D groundwater model. However, already after careful model parameterisation, the modelling results, including base flow and flow recession after peak events, match well with the observations (Figure D-1 to D-6 in Appendix D, uncalibrated model WaSiM-ETH). This is also reflected in the high values of the LNSE and r^2 efficiency criteria in Table 6-5 for the outlet gauges (Ortrand, Särichen, Prierow) and Table D-7 in Appendix D for the internal discharge gauges (column: “WaSiM without calibration”). Consequently, the automated model calibration of the conceptual WaSiM-ETH model parameters (Table 6-3) using PEST primarily only improves the simulated height of the peak discharges. In the Pulsnitz and Dahme river catchments, the recession constants for direct flow are increased (Table D-5 in Appendix D). This reduces the runoff peaks (Figure D-1, D-2, D-5, D-6 in Appendix D) and improves the NSE efficiency criterion. Due to plane landscapes with large permeable aquifers, the recession of interflow is increased in the Dahme (all gauges) and Pulsnitz river (only gauge Ortrand) catchments leading to reduced interflow peaks and a longer recession. Opposite to that, in the low mountain range catchments, the recession of interflow is decreased in the Weißer Schöps (all gauges) and the Pulsnitz river (gauge Königshain) catchment. The proportion of interflow to total runoff is reduced in all study catchments by decreasing the drainage density for interflow (d_r). In order to reduce calibration efforts, the recession constant of the saturated hydraulic conductivity with soil depth, was set equal for each soil type and depth. Concerning HBV-light only poor efficiency criteria are achieved without calibration (Table 6-5, “HBV without calibration”). The automated model calibration using the genetic algorithm significantly increases model performance (Table 6-5, columns: HBV NSE, LNSE, MARE). Due to the fact that conceptual model parameters do not have a physical basis, different parameter combinations can lead to similar model performance.

Table 6-5: Performance criteria of discharge calibration and validation based on *daily and ** long-term mean monthly time step (Pulsnitz: 1989-2006; Weißer Schöps, Dahme: 1963-1992)

Performance Criteria	Calibration* (1999-2001)						Validation* (2002-2006)						Validation **					
	WaSiM without calibration	WaSiM calibrated	HBV without calibration	HBV NSE	HBV LNSE	HBV MARE	WaSiM without calibration	WaSiM calibrated	HBV without calibration	HBV NSE	HBV LNSE	HBV MARE	WaSiM without calibration	WaSiM calibrated	HBV without calibration	HBV NSE	HBV LNSE	HBV MARE
Pulsnitz (gauge Ortrand)																		
r ²	0.82	0.87	0.27	0.85	0.83	0.84	0.67	0.74	0.14	0.75	0.62	0.65	0.82	0.96	0.79	0.9	0.97	0.95
NSE	0.37	0.74	-0.48	0.84	0.81	0.72	0.53	0.73	-0.52	0.75	0.60	0.60	0.74	0.86	0.78	0.86	0.90	0.95
LNSE	0.76	0.80	0.26	0.56	0.82	0.61	0.77	0.80	0.16	0.61	0.55	0.56	0.77	0.77	0.70	0.85	0.89	0.90
MBE	4.40	-6.20	-6.95	-4.08	-0.56	2.24	9.59	1.07	3.93	4.37	9.15	13.56	-6.29	-12.12	-5.42	-5.42	-3.84	0.18
Weißer Schöps (gauge Särichen)																		
r ²	0.74	0.81	0.16	0.8	0.85	0.80	0.69	0.78	0.11	0.72	0.74	0.70	0.75	0.98	0.70	0.83	0.77	0.79
NSE	0.74	0.81	0.09	0.76	0.85	0.79	0.66	0.77	0.07	0.71	0.74	0.70	0.73	0.95	0.08	0.81	0.70	0.74
LNSE	0.81	0.82	0.07	0.79	0.80	0.80	0.71	0.65	-0.09	0.66	0.54	0.60	0.81	0.87	0.05	0.77	0.67	0.78
MBE	5.91	-3.53	-2.94	2.35	-0.47	-10.80	9.23	5.37	10.72	-0.83	5.75	-4.84	-0.11	-5.31	69.08	-3.48	-5.47	2.48
Dahme (gauge Prierow)																		
r ²	0.69	0.80	0.14	0.66	0.65	0.62	0.51	0.62	0.19	0.51	0.48	0.49	0.56	0.78	0.33	0.39	0.52	0.49

Coefficient of determination (r²), Coefficient of model efficiency (NSE), Coefficient of model efficiency using logarithmic runoff (LNSE), Mass balance error (MBE) [%]

This is confirmed by the wide range of parameter values for the calibrated HBV-light models in Table D-6 in Appendix D. With the calibrated model parameters (Table D-5 and D-6 in Appendix D), both hydrological models proved to be suitable tools for simulating measured runoff as reflected by the efficiency criteria in Table 6-5 during both model calibration and validation. In general, model performance decreases during validation compared to calibration:

- In the Pulsnitz river catchment, the hydrological models WaSiM-ETH and HBV-light simulated on average a r^2 of 0.85, a NSE of 0.78 and a LNSE of 0.70 during model calibration. Simulated discharge is on average underestimated by -2.2 % ranging from -6.2 % by WaSiM-ETH to +2.2 % by HBV-light MARE. During validation on daily discharge, the performance of the hydrological models decreases by more than 10 % on average for all performance criteria while the MBE increases by 9 %. Within the second validation period, based on long term mean monthly discharge, the performance criteria are above 0.8 and discharge is on average underestimated by 5.3 %.
- In the Weißer Schöps river catchment, the performance criteria (r^2 , NSE, LNSE) are on average above 0.8 for WaSiM-ETH and HBV-light during model calibration. Simulated discharge is on average underestimated by 3.1 % ranging from -10.8 % by HBV-light MARE to +2.4 % by HBV-light NSE. During validation on daily discharge, the performance of the hydrological models decreases by more than 9 % (NSE) up to 24 % (LNSE) while the MBE increases by 4 %. During the second validation period, performance criteria are above 0.8 and discharge is on average underestimated by 3.0 %.
- In the Dahme river catchment, the hydrological models WaSiM-ETH and HBV-light simulate a r^2 of 0.82 during model calibration which is reduced by 23 % to 0.53 during model validation. During the second validation period, r^2 accounts to 0.55.

For the internal gauging stations, model performance of WaSiM-ETH is on average lower (Table D-7 in Appendix D).

- Pulsnitz river catchment: The statistical performance indicators (r^2 , NSE, LNSE) are on average about 32 % lower during calibration, 54 % during validation based on daily discharge and 67 % based on long term mean monthly discharge at the internal gauge Königshain compared to the outlet gauge Ortrand. The strong reduction is mainly due to the poor performance concerning the LNSE during validation at the internal gauge Königshain. The MBE increases for the internal gauge Königshain compared to the outlet gauge Ortrand.
- Weißer Schöps river catchment: The hydrological model performance is comparable between the gauging station Särichen and Holtendorf. For the internal gauging station Königsbrück, the statistical performance indicators (r^2 , NSE, LNSE) are 19 % lower during

calibration, 23 % during validation based on daily discharge and 20 % during validation based on long term mean monthly discharge. The MBE deviates considerably for Königsbrück compared to Särichen (> 200 %).

- Dahme river catchment: The r^2 is 15 % lower during calibration, 58 % during validation based on daily discharge at gauge Dahme Stadt compared to the outlet gauge Prierow.

Comparing the performance of the different hydrological models, no model configuration can be identified that consistently outperforms the others model configurations concerning all performance criteria and during all simulation periods in the Pulsnitz river catchment (Figure 6-9 and Table 6-5).

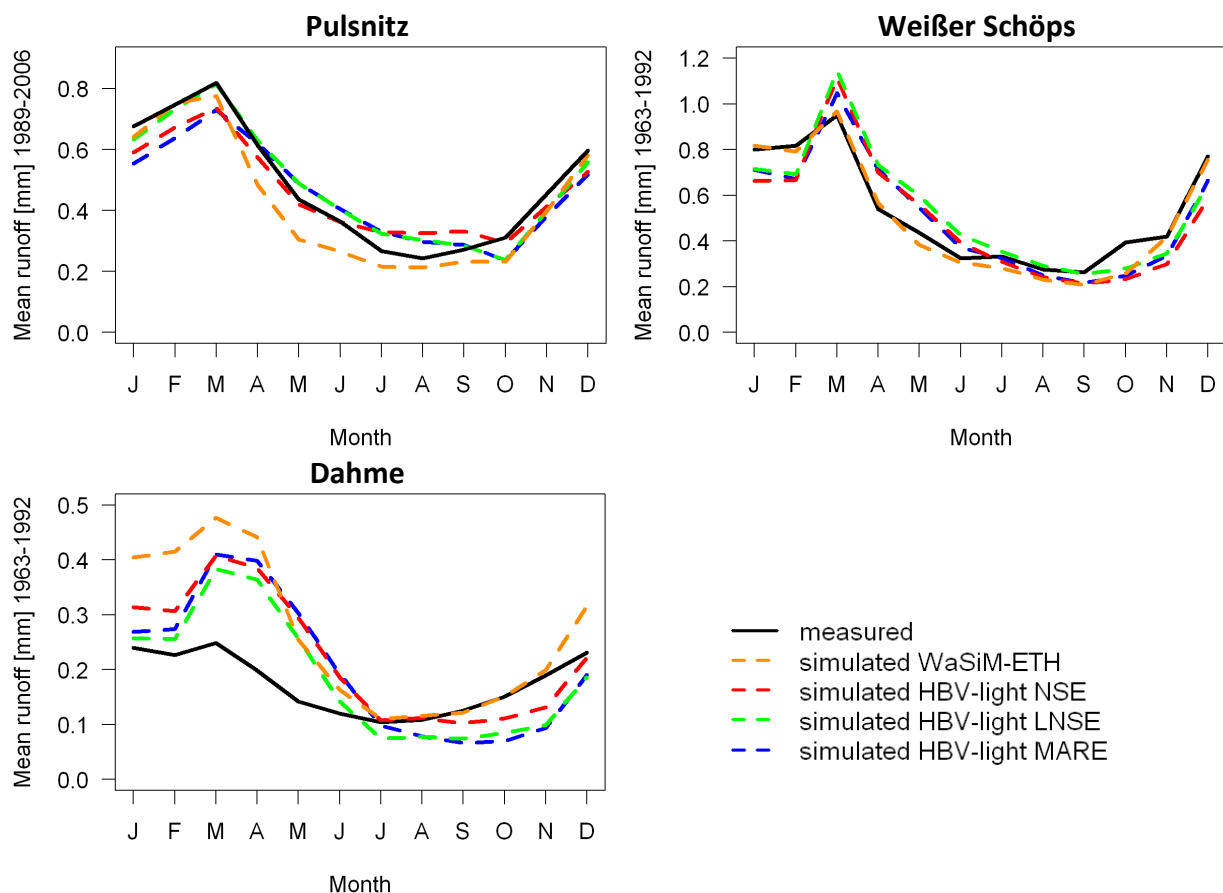


Figure 6-9: Comparison between measured and simulated mean monthly runoff for the Pulsnitz (1988-2006), Weißer Schöps (1963-1992) and Dahme (1963-1992)

During each analysis period, another model performs best when considering the average of the performance criteria r^2 , NSE and LNSE (calibration: HBV-light LNSE, validation on daily discharge: WaSiM-ETH, validation on long term mean monthly discharge: HBV-light MARE). The comparison of the water balance components between the two hydrological models reveals that WaSiM-ETH simulates higher actual evapotranspiration rates and consequently lower discharge compared to HBV-light during all periods in the Pulsnitz river catchment (Table 6-6).

Table 6-6: Water balance components: corrected precipitation (P_{cor} [mm/a]), actual evapotranspiration (ETA [mm/a]), runoff (R [mm/a]), change in storage (ΔS [mm/a]) for the calibration and validation periods

		Calibration (1999-2001)				Validation (2002-2006)				Validation*			
		P	ETA	R	ΔS	P	ETA	R	ΔS	P	ETA	R	ΔS
Pulsnitz (gauge Ortrand)													
	WaSiM-ETH	713	603	135	-25	714	583	129	2.0	707	594	120	-7.0
	HBV-light _{NSE}		540	180	-7.0		517	174	23		529	167	11
	HBV-light _{LNSE}		551	186	-24		530	182	2.0		540	169	-2.0
	HBV-light _{MARE}		542	192	-21		521	189	4.0		531	176	0
Weißer Schöps (gauge Särichen)													
	WaSiM-ETH	719	568	160	-9.0	681	559	162	-40	727	557	195	-25
	HBV-light _{NSE}		566	168	-15		537	173	-29		537	173	17
	HBV-light _{LNSE}		569	168	-18		549	158	-26		550	183	-6.0
	HBV-light _{MARE}		582	150	-13		566	144	-29		567	167	-7.0
Dahme (gauge Prierow)													
	WaSiM-ETH	602	549	83	-30	684	587	116	-19	652	569	109	-26
	HBV-light _{NSE}		520	61	21		575	80	29		536	76	40
	HBV-light _{LNSE}		509	70	23		564	86	34		528	83	41
	HBV-light _{MARE}		516	66	20		568	79	37		530	69	53

* Pulsnitz: 1989-2006, Weißer Schöps, Dahme: 1963-1992

In the Weißer Schöps river catchment, using both hydrological models, high performance indicators are attained during calibration (Table 6-5). In the validation period based on daily discharge (2002-2006), WaSiM-ETH performs better compared to the average of the three HBV-light model configurations. The difference in the performance between the hydrological models becomes even more visible when their performance is evaluated for the period 1963-1992 on long term mean monthly runoff (Figure 6-9, Table 6-5). This is reflected in the statistical performance criteria (r^2 , NSE, LNSE) which are on average 20 % higher for WaSiM-ETH compared to HBV-light. Only the MBE is on average lower for HBV-light compared to WaSiM-ETH. The water balance components between WaSiM-ETH and the model configurations of HBV-light are comparable (Table 6-6).

The modelling results in the Dahme river catchment are afflicted with considerable uncertainty due to the fact that model calibration is aggravated by the anthropogenic impact on runoff (section 4.4 and Figure C-16) which has to be considered during the analysis and interpretation of the modelling results. Consequently, the simulated runoff differs considerably from the measured runoff during 1963-1992 (Figure 6-9). Also the different model configurations among themselves show distinct differences even though calibration of HBV-light was based on the simulated discharge by WaSiM-ETH. These differences are also reflected in the water balance components: WaSiM-ETH, in contrast to HBV-light, simulates higher actual evapotranspiration and discharge. Consequently, WaSiM-ETH and HBV-light simulate a negative and positive storage change component, respectively (Table 6-6, ΔS).

6.3.2 Low-flow analysis

In order to evaluate the models ability to simulate low-flow conditions, the FDC as well as the mean of the AM(7) (MAM(7), section 2.4) of measured and simulated discharges were compared. The FDC was built for the calibration and validation period 1999-2006 and the MAM(7) time series for the low-flow years 1999-2005 based on daily discharge (Figure 6-10 and 6-11). Since the study catchments are characteristic for pluvial river systems (section 4.3), splitting the time series into different low-flow seasons was not necessary and, as suggested by the DVWK (1983), the low-flow year (01.04.-31.03.) was chosen for the MAM(7) analysis.

Figure 6-10 displays the FDCs for measured and simulated discharge for the study catchments for the period 1999-2006. In general, the analysis of the FDCs suggests that the simulations overestimate the measurements that are exceeded 80 % of the times. In the Pulsnitz river catchment, the HBV-light model configurations MARE and NSE even outperform WaSiM-ETH and HBV-light LNSE which has not been expected since during calibration of HBV-light LNSE, low-flow is given higher relevance. In the Weißer Schöps river

catchment, on the other hand, the differences between the hydrological models are lower. In the Dahme river catchment, a direct comparison of the simulations to the measurements is not possible due to the anthropogenic impact. Nevertheless, the discharge simulated by the different hydrological models differs considerably, especially the flows that are exceeded 60 % of the times. Contrary to the large differences in low-flow, all model configurations simulate high flows precisely, especially in the Pulsnitz and Weißer Schöps river catchments.

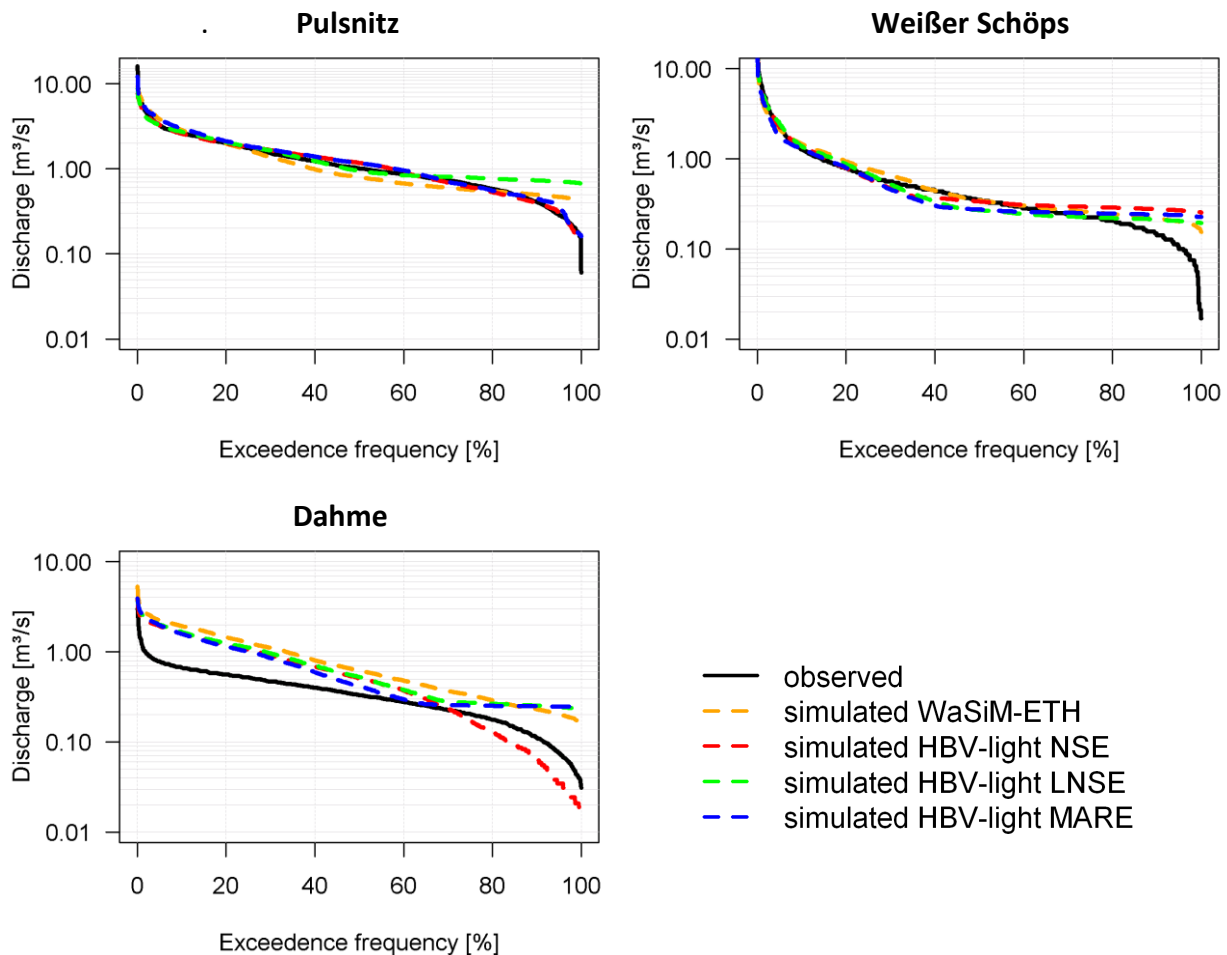


Figure 6-10: Flow duration curve for measured and simulated discharge for the Pulsnitz, Weißer Schöps and Dahme river catchments for the period 1999-2006

The FDC cannot only be used to visualize the differences between the hydrological models in capturing the flow regime, but also to analyse the combined effect of physiographic and climatic influence on discharge, and hence on catchment response. The FDCs of the Weißer Schöps river catchment, has a steeper gradient compared to the other catchments, especially for the flows that are exceeded 80 % of the times. This is representative for catchments with a high variability of daily discharges (Figure 4-2) and is according to WMO (2008) typical of an impermeable catchment with little storage and a quick response to rainfall. The FDC of the Dahme river catchment is representative for highly permeable

catchments as well as for catchments that are strongly regulated anthropogenically (WMO, 2008).

Figure 6-11 displays the measured and simulated MAM(7) for the low-flow years 1999-2005 for the study catchments. In the Pulsnitz river catchment, HBV-light LNSE overestimates the measured MAM(7). HBV-light NSE, MARE and WaSiM-ETH, on the other hand, underestimate the measurements up to the year 2000, after which they overestimate them, except HBV-light MARE and NSE who fit the measurements in the year 2003. In the Weißer Schöps river catchment, the overall dynamic of the measured MAM(7) is simulated well by all hydrological models, even though the MAM(7) after 2002 is overestimated. In the Dahme river catchment, HBV-light MARE and LNSE overestimate the measurements but simulate the overall dynamic well. WaSiM-ETH and HBV-light NSE are characterised by a larger dynamic overestimating the peaks considerably.

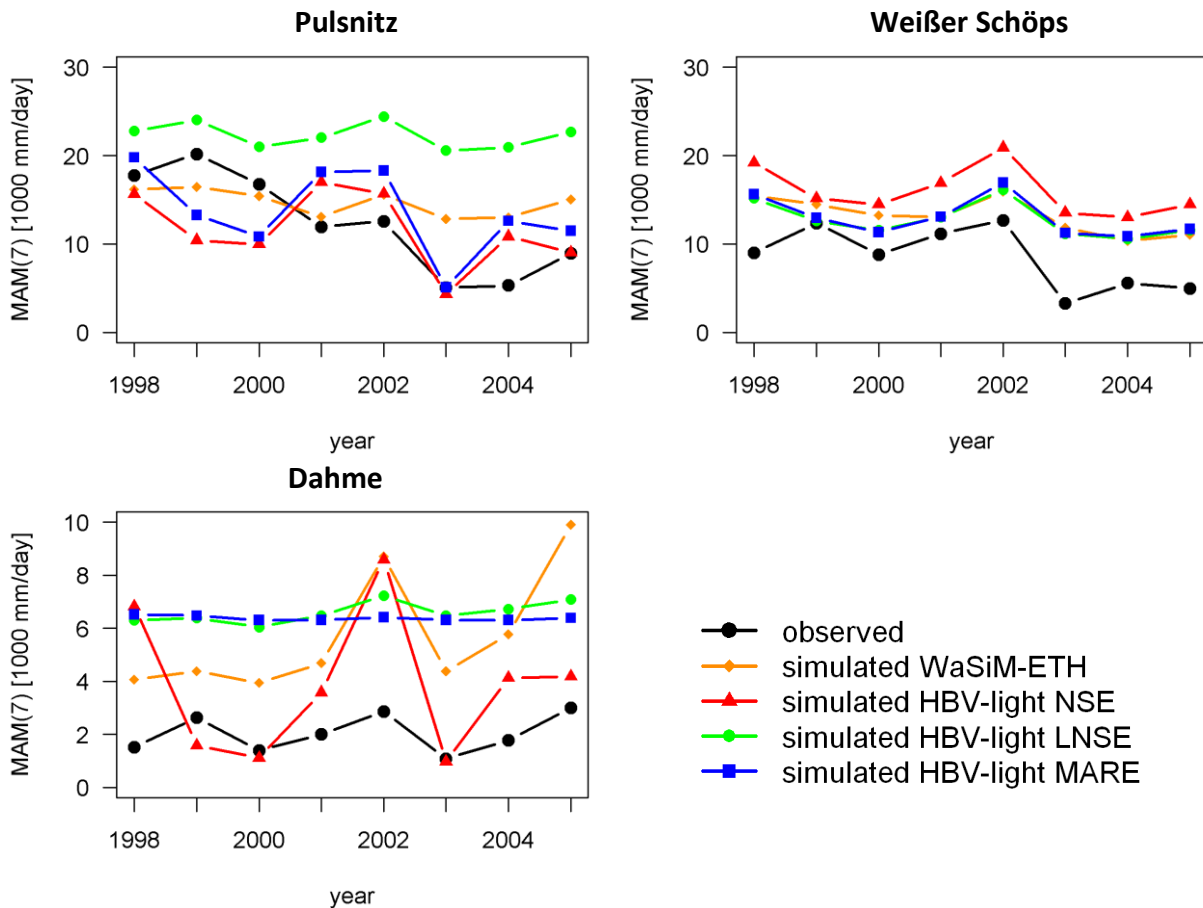


Figure 6-11: Comparison of measured and simulated MAM(7) for the low-flow years 1999-2005 for the Pulsnitz, Weißer Schöps and Dahme river catchments

6.4 Discussion

The multi-criteria calibration and validation showed that both models are suitable to simulate the hydrological catchment behaviour. In fact, concerning the statistical performance criteria, WaSiM-ETH and HBV-light performed almost equally even though

i) different calibration strategies were used and ii) the portioning of precipitation in actual evapotranspiration and discharge differs between both hydrological models. This is especially true in the Pulsnitz and Dahme river catchments where an anthropogenic impact on discharge was identified which increases the uncertainty related to the hydrological model parameterisation.

In terms of calibrating conceptual hydrological models, MERZ et al. (2009) recommended a calibration of at least five years in order to capture most of the hydrological variability in a catchment. However, the three years chosen for calibration in this study are regarded as sufficient since high efficiency criteria were obtained during both model calibration and validation. Also the validation of the HBV-light models on long-term mean monthly discharge (second validation period) proved that the models perform adequately outside of their calibration period. The automated calibration of HBV-light using a genetic algorithm, resulting in 100 parameter sets for each objective function, showed that different parameter combinations can result in similar high model performance. This phenomena was described by BEVEN (2006) as equifinality and has numerously been discussed in literature (BEVEN, 1993; BEVEN and BINLEY, 1992; DUAN et al., 1992; FREER et al., 1996; MEIN and BROWN, 1978; SEIBERT, 1997; STEELE-DUNNE et al., 2008; VAN DER PERK and BIERKENS, 1997). Including additional parameter sets into this study could give an additional uncertainty assessment of the parameterisation of HBV-light. The choice of three different parameter combinations that target different aspects of the hydrograph was, however, regarded as sufficient in the context of this study focussing on long term changes in water balance components due to climate change. In contrast to the lumped HBV-light model, the calibration of WaSiM-ETH using PEST only marginally increased model performance. This is due to the thorough model parameterisation which is especially challenging and time consuming when applying the 2D groundwater model. In fact, the model parameterisation can be regarded as a preliminary manual model calibration especially concerning the parameters of the groundwater model (Table 6-2). Also unlike HBV-light, WaSiM-ETH was additionally calibrated and validated on internal catchment gauging stations where model performance is, however, lower compared to the outlet gauges. The relation between catchment size and hydrological model performance with lower model fit for smaller catchments, is confirmed in literature (ANDERSEN et al., 2001; CONRADT et al., 2012; MERZ et al., 2009; MOUSSA et al., 2007). The large MBE of on average > 10 % for the internal catchment gauges (Table D-7 in Appendix D, calibrated model versions) is caused by several factors: i) location of precipitation station, ii) interpolation of precipitation using the IDW method, iii) scaling and regionalisation errors of input data and iv) the MBE is represented in percentage, which means that small differences show relatively large percent differences especially when discharges are low in absolute terms. For example, the gauging station

Königshain (Weißer Schöps), with a mean discharge of 0.06 m³/s (1999-2006), is located in low mountain range without an internal precipitation station. Since the IDW, as a pure geometric interpolation method, does not consider terrain effects, precipitation is expected to be underestimated and consequently, the MBE at the gauge Königshain is negative (Table D-7 in Appendix D).

Overall, the calibrated model configurations can be regarded as a good compromise between low, mean and high flow representation. Therefore, the lower model performance concerning low-flows should not be overrated, especially since low-flows were not the primary focus during model calibration.

Finally, a complete agreement between measurements and simulations is not attainable due to the fact that each model represents reality in a simplified form. Moreover, data availability is always limiting model parameterisation. These factors result in different model uncertainties (Figure 1-1) of which some important are highlighted:

Model structure:

- The soil macropore module in WaSiM-ETH is only controlled by a precipitation threshold even though soil wetness also plays a considerable role (PLATE and ZEHE, 2008).
- No explicit cell to cell routing of interflow exists in WaSiM-ETH.
- HBV-light, as a conceptual model, neglects several hydrological processes, such as interception, and is used as a lumped model.

Model parameters:

- Both models are characterized by a large number of model parameters. Thus, the degrees of freedom in model parameterization are large and different parameter combinations may lead to similar modelling outcome (equifinality).
- In WaSiM-ETH, the catchment surface roughness is represented by a uniform roughness coefficient, a differentiation based on land use is not possible.

Measurements:

- The quality of the measurements was pre-checked before applying it for the hydrological modelling. Nevertheless, uncertainties related to the quality of measurements remain.
- Additional data could improve model parameterisation, especially related to the saturated zone for the parameterisation of the groundwater model in WaSiM-ETH. Information on aquifer quickness and more precise data on saturated hydraulic conductivity could facilitate model parameterisation. The same is true for soil hydraulic parameters which also impact model performance considerably.

7 Hydrological climate change impact assessments

7.1 Materials and methods

Based on the validated hydrological models, the climate change impact assessments were performed for each catchment separately using the modelling chain displayed in Figure 7-1.

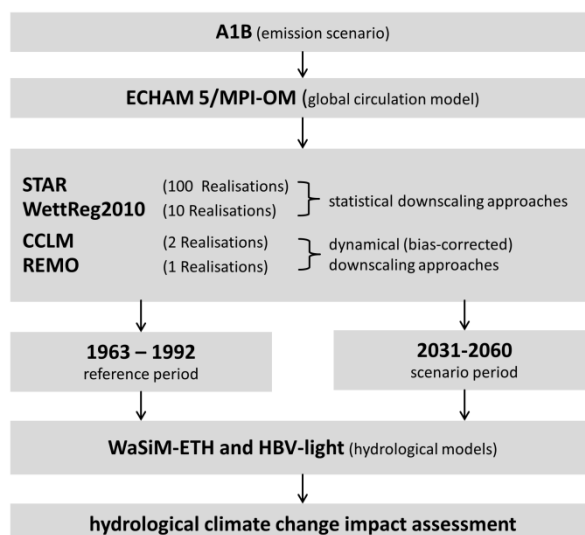


Figure 7-1: Model chain for hydrologic climate change impact assessments

The hydrologic climate change impact assessments were subdivided into four steps:

- 1) The statistical distribution of the meteorological variables temperature and precipitation, as the two most relevant climatic variables to hydrological simulations, simulated by REMO, CCLM and WettReg were used i) to test their suitability for climate change impact assessments and ii) to evaluate the effectiveness of the bias correction for REMO and CCLM for the reference period. The reference period 1963-1992 differs temporally from the control period chosen for the bias correction (section 3.3, CCLM: 1961-2006, REMO: 1951-2006) and was therefore regarded as suitable to analyse the effectiveness of the bias correction. The analyses were carried out on a daily, monthly and annual basis. The realisations of CCLM (2) and WettReg (10) were included each to the same degree in the distribution building, so that the resulting distribution contains the information from all realisations.
- 2) The long term mean water balance components and discharge simulated by the hydrological models (WaSiM-ETH, HBV-light) driven by: i) the meteorological output of the DAs REMO, CCLM and WettReg and the meteorological measurements for the reference period (1963-1992) and ii) the DAs REMO, CCLM, STAR and WettReg for the scenario period (2031-2060) were compared on the annual and intra-annual basis. The hydrological climate change impact was assessed by comparing the results of the scenario with the reference

period for each hydrological model and DA, thereby concentrating on the individual change pattern of each DA. Due to the fact that data input is identical between WaSiM-ETH and HBV-light (section 6.2.2), the three variables of temperature, potential evapotranspiration and precipitation do not differ between the hydrological models on the long term annual basis. Differences of the modelled long term mean water balance components and discharge between the different model chains, based on 26 simulations for the reference and 226 simulations for the scenario period for each catchment, were considered as uncertainties (section 7.2.2).

3) Changes in low-flows simulated by WaSiM-ETH and HBV-light driven by the DAs between the reference and scenario period were estimated for: i) statistical low-flow indicators Q95 and MAM(7), ii) the FDC, iii) low-flow frequency analysis and iv) Wilcoxon-Mann-Whitney test based on mean and minimum discharge as well as AM(7) between HBV-light and WaSiM-ETH. For HBV-light, only the LNSE version was considered. All low-flow analyses were implemented into the software environment R for statistical computing (R, 2011) using the MASS package (R MASS PACKAGE, 2013) which contains functions and datasets based on VENABLES and RIPLEY (2002). The low-flow indicators MAM(7) and Q95 were calculated for the:

- Reference period (01.04.1963-31.03.1991): measured discharge, simulated discharge by hydrological models based on:
 - meteorological measurements
 - meteorological output of DAs
- Scenario period (01.04.2032-31.03.2060): simulated discharge by hydrological models based on meteorological output of DAs.

In order to determine the Q95, the Flow Duration Curve (FDC) was estimated. The FDC was calculated for each model chain member. For CCLM, STAR and WettReg, only one FDC was constructed containing each realisation to the same degree.

The low-flow frequency analysis was carried out in accordance with the DVWK (1983) as well as the WMO (2008). The following procedure was chosen:

- a) The AM(7) time series was used to construct the low-flow frequency curve.
- b) The Weibull probability distribution (Equation 7-1) was fitted to the AM(7) time series with parameter estimation using Maximum likelihood parameter estimation.

$$F(x) = 1 - \exp \left[- \left(\frac{x - \xi}{\alpha} \right)^\kappa \right] \quad \text{Equation 7-1}$$

- with α scale parameter
 ξ location parameter
 κ shape parameter which controls the tail of the distribution

- c) After fitting the Weibull probability distribution to the simulated discharge of the reference period, the AM(7) of a 50 year return period was estimated (Figure 7-2).

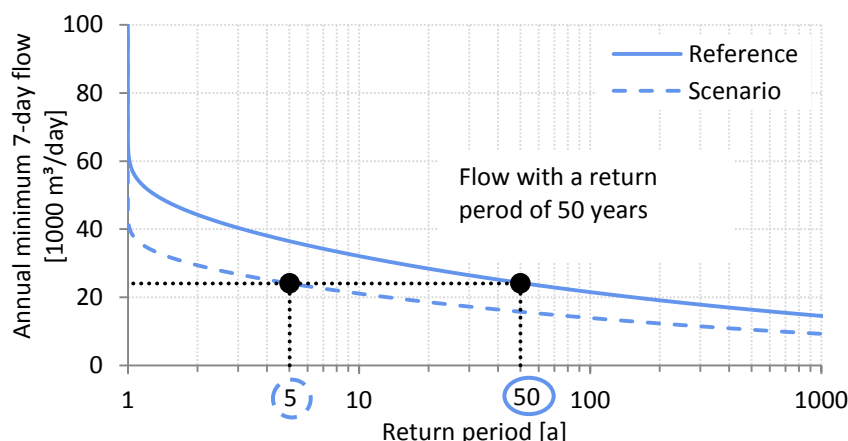


Figure 7-2: Approach for estimating the change in the return period of the 50-year AM(7) flow between reference and scenario period

- d) In the following, the Weibull probability distribution was fitted to the simulated discharges of the scenario period where the return period of the reference 50 year AM(7) flow was determined. Comparing the return periods between reference and scenario period shows whether the risk of the reference 50 year AM(7) increases or decreases in the scenario period. The example shown in Figure 7-2 illustrates that the 50 year low-flow event of the reference period ($\approx 0.27 \text{ m}^3/\text{s}$) will have a return period of only 5 years in the scenario period and therefore an increased low-flow risk. By definition of the AM(7), return periods below one year are not possible.

Using the Wilcoxon-Mann-Whitney test, the simulated mean and minimum discharge as well as the AM(7) by HBV-light and WaSiM-ETH were compared between the hydrological models. The aim of this analysis was to evaluate the independency/similarity of the results based on the choice of the hydrological model. For this purpose, the non-parametric Wilcoxon-Mann-Whitney test was chosen which performs a two-sided rank sum test of the null hypothesis stating that two series of data are independent samples from identical continuous distributions with equal medians. The alternative hypothesis assumes that the two series of data do not have equal medians.

- 4) For the development of climate change adaptation strategies, not only the impact of climate change on the mean water balance components is of great relevance but also the spatially differentiated catchment response to changes in the climatic drivers. In fact, the capacity of a catchment to buffer potential climate change impacts will mainly depend on the catchments physiographic characteristics, where the dominant one is to be identified in this analysis. The climate change impact on the spatial patterns of actual evapotranspiration and groundwater recharge was analysed for each DA using WaSiM-ETH due to its spatially

distributed character. The results are displayed as the differences between scenario minus reference period.

7.2 Results

7.2.1 Evaluation of uncertainties of downscaling approaches during reference period

Generally, the bias correction of REMO and CCLM results in a good agreement during the reference period (1963-1992). No DA could be identified that outperforms the other DAs consistently in all study catchments (Figure 7-3 and Table E-1 in Appendix E). For mean and median precipitation, the following results were obtained:

- In the Pulsnitz river catchment, REMO outperforms CCLM and WettReg concerning mean precipitation. REMO underestimates measured mean precipitation by less than 1 % on all time scales. CCLM and WettReg show on average deviations of + 2.2 % and - 6.0 % to the measurements, respectively. Concerning median precipitation, REMO also outperforms the other DAs except on the annual basis where CCLM shows the best fit.
- In the Weißer Schöps river catchment, WettReg outperforms REMO and CCLM concerning mean precipitation. WettReg deviates from the measured mean precipitation by less than + 0.5 % on all time scales. REMO and CCLM show on average deviations of about ± 1.0 %. Concerning median precipitation, WettReg also outperforms the other DAs on the daily basis. On the monthly basis, WettReg and CCLM perform equally while on the annual basis, REMO shows the best fit.
- In the Dahme river catchment, CCLM outperforms REMO and WettReg concerning mean precipitation. CCLM deviates from the measured mean precipitation by less than + 0.6 % on all time scales. REMO and WettReg overestimate mean measured precipitation on average by 5.1 % and 8.9 %, respectively. Concerning median precipitation, CCLM outperforms the other DAs on the annual basis. On the monthly basis, CCLM and REMO perform equally while on the daily basis, REMO shows the best fit.

The results of mean and median precipitation indicate that the best fit between the measurements and simulations can be observed in the Weißer Schöps river catchment.

Mean measured temperature is overestimated by REMO and WettReg by on average + 5 % and + 4 %, respectively, in the study catchments over all time scales. CCLM shows the best agreement with deviations from the measurements ranging from + 1.1 % to + 2.4 %.

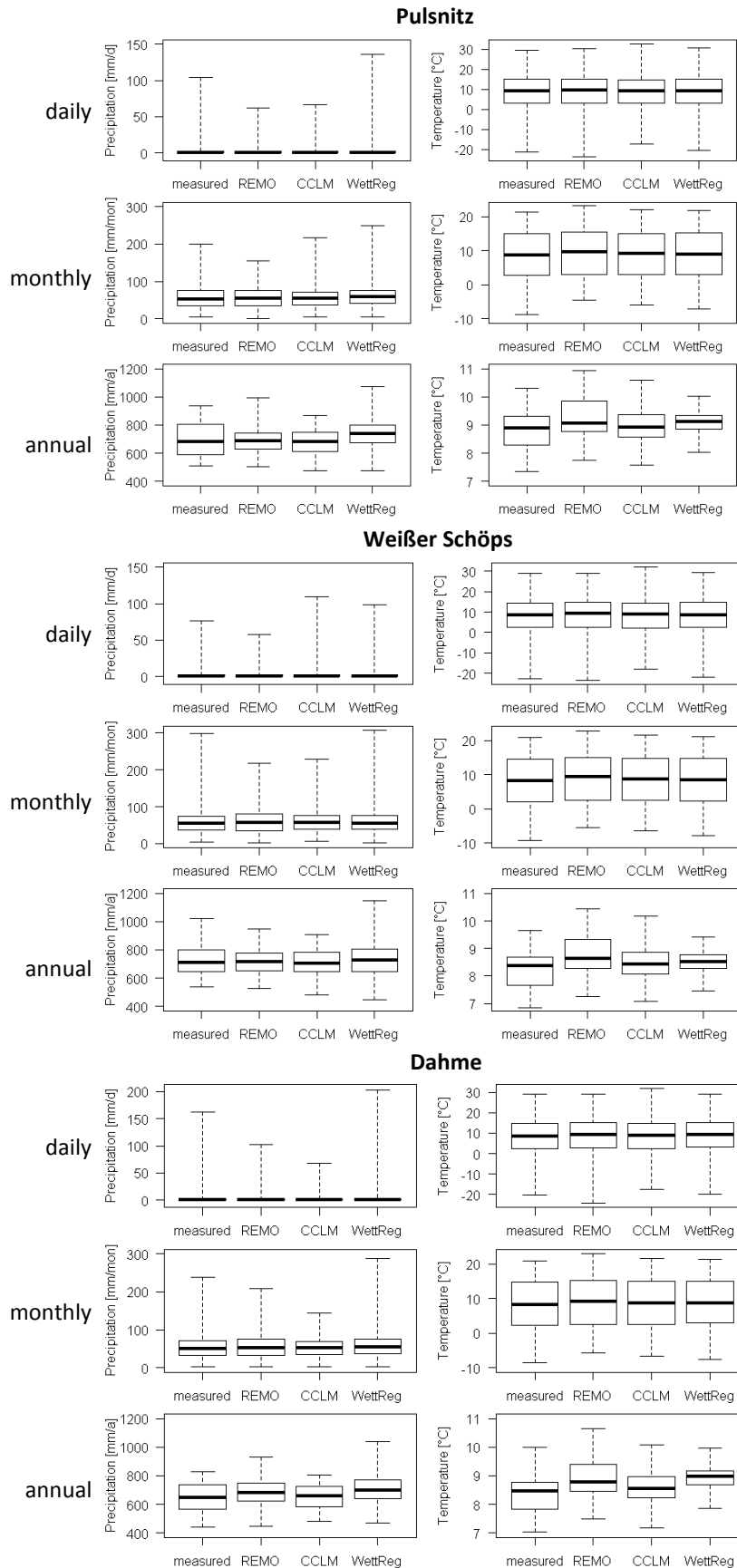


Figure 7-3: Measured and simulated precipitation and temperature distribution on a daily, monthly and annual basis during the reference period (1963-1992)

Concerning the statistical distribution, the analysis of the 25th and 75th percentiles (Figure 7-3) and the complete spread of the precipitation and temperature data partially show that the three DAs differ considerably from the measurements, as reflected in the standard deviation, maximum and minimum values in Table E-1 in Appendix E.

Concerning the distribution of precipitation, WettReg overestimates the spread of the precipitation measurements in all study catchments, especially on the annual basis and on the daily basis in the Pulsnitz and Dahme river catchment. Concerning the statistical distribution of temperature, the DAs show a good agreement with the 25th and 75th percentiles and the spread of the measured temperature distribution on the daily and monthly basis. On the annual basis, REMO overestimates the entire temperature distribution while WettReg underestimates the spread of the distribution.

Despite the deviations of the DAs to the measurements, all DAs are regarded as applicable for the hydrological modelling of climate change impacts, especially when focussing on long term averages; in this respect, the DAs perform satisfactory.

7.2.2 Simulations for the reference period and climate change impact during the scenario period

Precipitation and Temperature

During the reference period, the deviation between measured and simulated (by DAs) precipitation ranges from -2 % to +8 % in all study catchments (Table E-2 to E-4 in Appendix E). Intra-annually, the variability of the measured precipitation, lower precipitation during winter and higher precipitation during summer, is well reproduced by the DAs in all study catchments (Figure 7-4, compare “measurements” with simulations during reference period). However, all DAs overestimate summer precipitation. In accordance with the results presented in section 5.2.4, REMO and CCLM simulate an increase by 5 % and 1 % in precipitation while the statistical DAs STAR and WettReg simulate a decrease by 8 % and 12 % on average in the study catchments, respectively, in the scenario period (Figure 7-4). In all study catchments, REMO simulates the strongest increase in precipitation (+4 % to +5 %). Except in the Weißer Schöps river catchment where precipitation decrease based on STAR dominates (-16.5 %), WettReg simulates the strongest decrease in precipitation (-9 % to -14 %). Except for REMO and CCLM (only in the Weißer Schöps river catchment), a strong reduction of summer precipitation is identified.

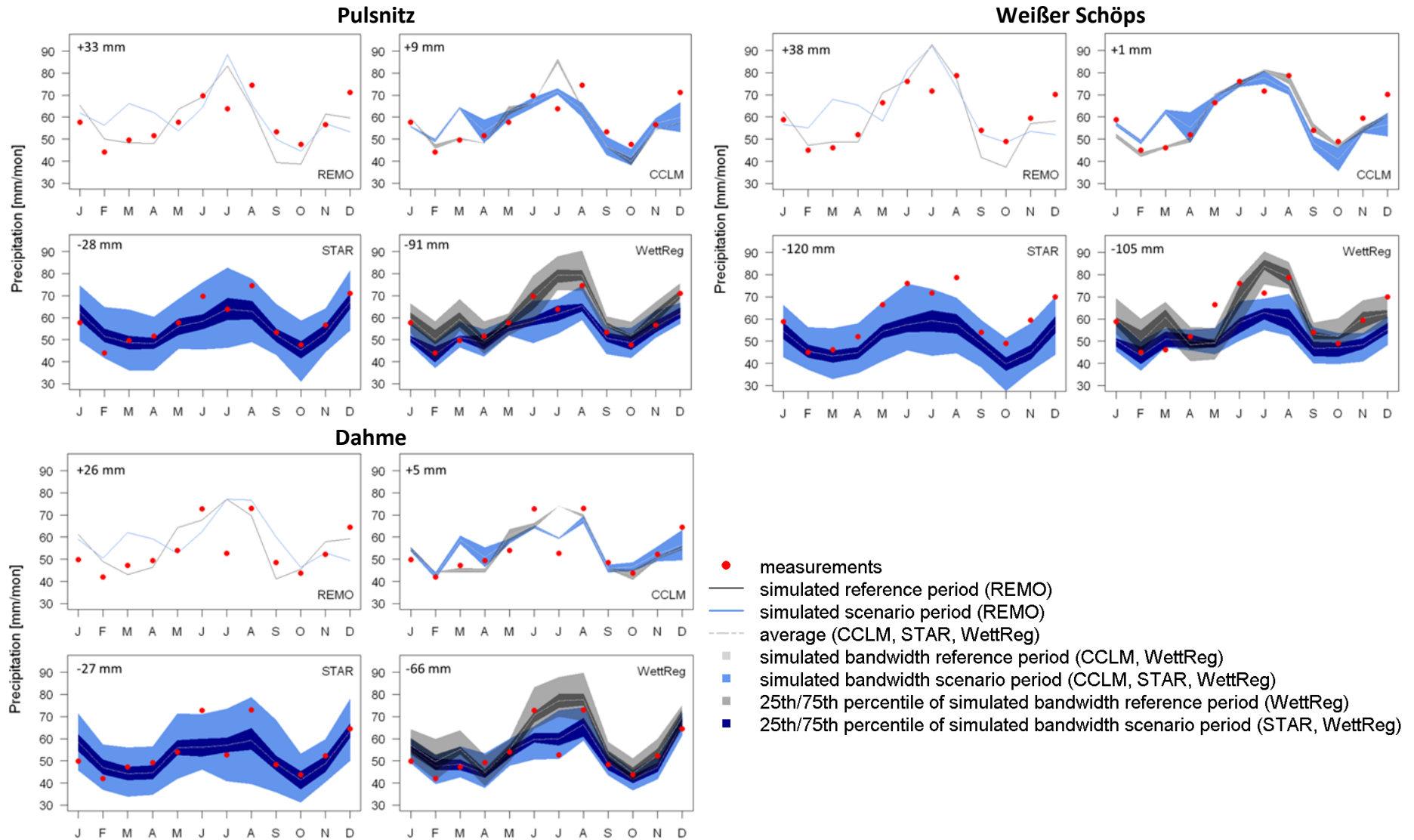


Figure 7-4: Precipitation: Intra-annual variability of measurements and simulations as well as the absolute difference between both (upper left corner) for the Pulsnitz, Weißer Schöps and Dahme river catchments

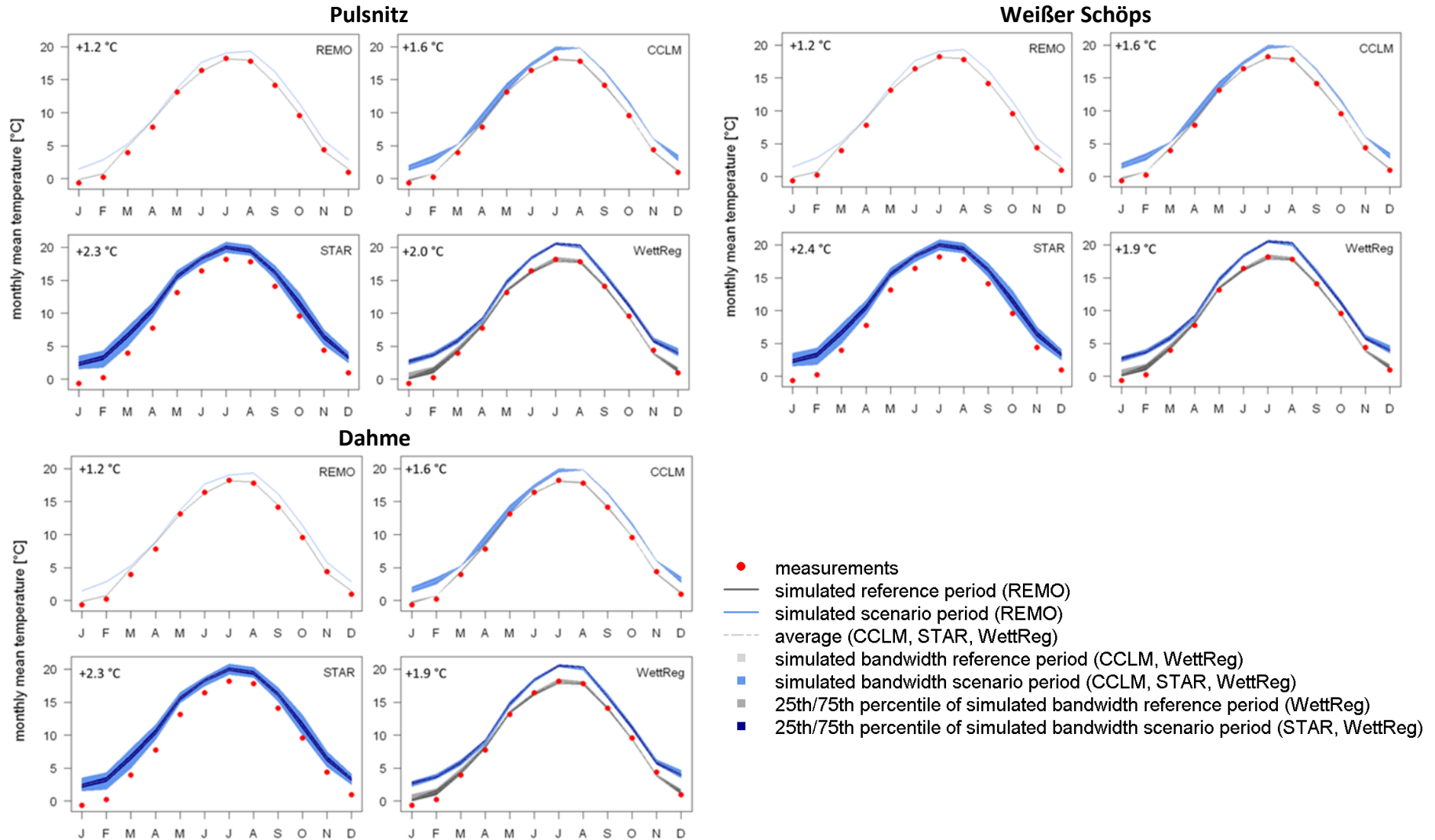


Figure 7-5: Mean temperature: Intra-annual variability of measurements and simulations as well as the absolute difference between both (upper left corner) for the Pulsnitz, Weißer Schöps and Dahme river catchment

The deviations between the measured and simulated annual temperature cycle of WettReg, CCLM and REMO are negligible during the reference period, even though the DAs tend to overestimate temperatures in winter (Figure 7-5, compare “measurements” with simulations during reference period). Concerning the simulated mean temperature for the scenario period which again confirms the results presented in section 5.2.4, all DAs calculate an increase both intra-annually and on the long term annual basis. The results based on STAR and REMO show on average the highest (+28 %) and lowest (+19 %) temperature increases, respectively (Figure 7-5).

Potential and actual evapotranspiration

During the reference period, the difference between measured and simulated (by DAs) potential evapotranspiration is below 5 % in all study catchments (Table E-2 to E-4 in Appendix E). During the scenario period, potential evapotranspiration increases for all model chains (Table E-2 to E-4 in Appendix E). WettReg computes the strongest increase (+ 19 % to + 24 %) in potential evapotranspiration in all study catchments, which is because it simulates on average i) the strongest temperature increase during the summer months (Figure 7-5), ii) the strongest increase in global radiation and iii) the lowest air humidity. Also STAR simulates a stronger increase in temperature, global radiation and less air humidity compared to CCLM and REMO. The interplay of these three variables leads to an average increase in potential evapotranspiration of around 19 % by STAR and 22 % by WettReg in comparison to 2 % by REMO and 4 % by CCLM in the study catchments.

For actual evapotranspiration, WettReg computes on average the largest deviations to the measurements (6 %) followed by REMO (4 %) and CCLM (1 %) for all study catchments during the reference period (Table E-2 to E-4 in Appendix E). During the scenario period, the model chains driven by the dynamical RCMs REMO and CCLM simulate a slight increase in actual evapotranspiration of 3 % and 1 %, respectively. Based on the statistical DAs, on the contrary, a slight decrease (STAR: - 1 %, WettReg: - 3 %) is simulated. Independently of the DA used, WaSiM-ETH simulates higher actual evaporation rates compared to the mean of the three HBV-light model parameterisations in the Pulsnitz and Dahme river catchments. In the Weißer Schöps river catchment, HBV-light MARE simulates the highest actual evapotranspiration, except when based on WettReg (Table E-2 to E-4 in Appendix E). The difference in actual evapotranspiration between the two hydrological models is most distinct in the Pulsnitz and least distinct in the Weißer Schöps river catchment.

Discharge

The comparison of the mass balance error between simulated long term mean discharge driven by the meteorological measurements and by the DAs output shows that the fit is best for

WettReg in the Weißer Schöps with an underestimation of discharge by 10 % for WaSiM-ETH and by 0.7 % for HBV-light during the reference period (Table 7-1). In the Dahme river catchment, simulations based on CCLM show the best fit with an underestimation of 1 % and 3 % for WaSiM-ETH and HBV-light, respectively. These results are in accordance with the analysis of precipitation in section 7.2.1. In the Pulsnitz river catchment, the best fit is based on WettReg with an overestimation of 4 % and 7 % for WaSiM-ETH and HBV-light, even though mean precipitation was best fitted by REMO (section 7.2.1). However, REMO overestimates potential and actual evapotranspiration. One reason for that is that global radiation, which is necessary for calculating potential evapotranspiration after Penman-Monteith, had to be estimated from simulated cloud cover and humidity by REMO (section 3.2). This approach certainly adds additional uncertainty to the calculated results obtained by REMO and results in larger deviations to measured discharge.

Table 7-1: Mass Balance Error [%] between simulated long term mean discharge driven by the meteorological measurements and by the meteorological output of the DAs during the reference period (1963 1992) for WaSiM ETH (wasim) and HBV light (hbv – mean of the three model configurations)

	REMO _{wasim}	Remo _{hbv}	CCLM _{wasim}	CCLM _{hbv}	WettReg _{wasim}	WettReg _{hbv}
Pulsnitz	-15.0	-11.0	-7.4	-6.6	4.3	6.9
Weißer Schöps	-28.0	-22.0	-17.0	-9.1	-10.0	-0.7
Dahme	2.4	2.3	-0.9	-3.0	9.6	9.9

The mass balance errors presented in Table 7-1 also highlight that the difference between the hydrological models are substantial. In fact, the mean of the three HBV-light model configurations generally performs better compared to the WaSiM-ETH simulations, except when WaSiM-ETH is driven by CCLM and WettReg in the Dahme and by WettReg in the Pulsnitz river catchment.

In addition to the analysis of the mass balance error, the comparison of the water balance components (Table E-2 to E-4 in Appendix E) between WettReg and the meteorological measurements in the reference period reveals that WettReg overestimates precipitation by 45 mm/a (6 %) in the Pulsnitz and by 55 mm/a (8 %) in the Dahme river catchments. In the Weißer Schöps river catchment, the deviation between measured and simulated precipitation by WettReg is negligible. At the same time, actual evapotranspiration is also overestimated by WettReg, compensating the overestimated precipitation. CCLM, on the other hand, underestimates both precipitation (except in the Dahme river catchment 0.15 %) and potential evapotranspiration by 2 %.

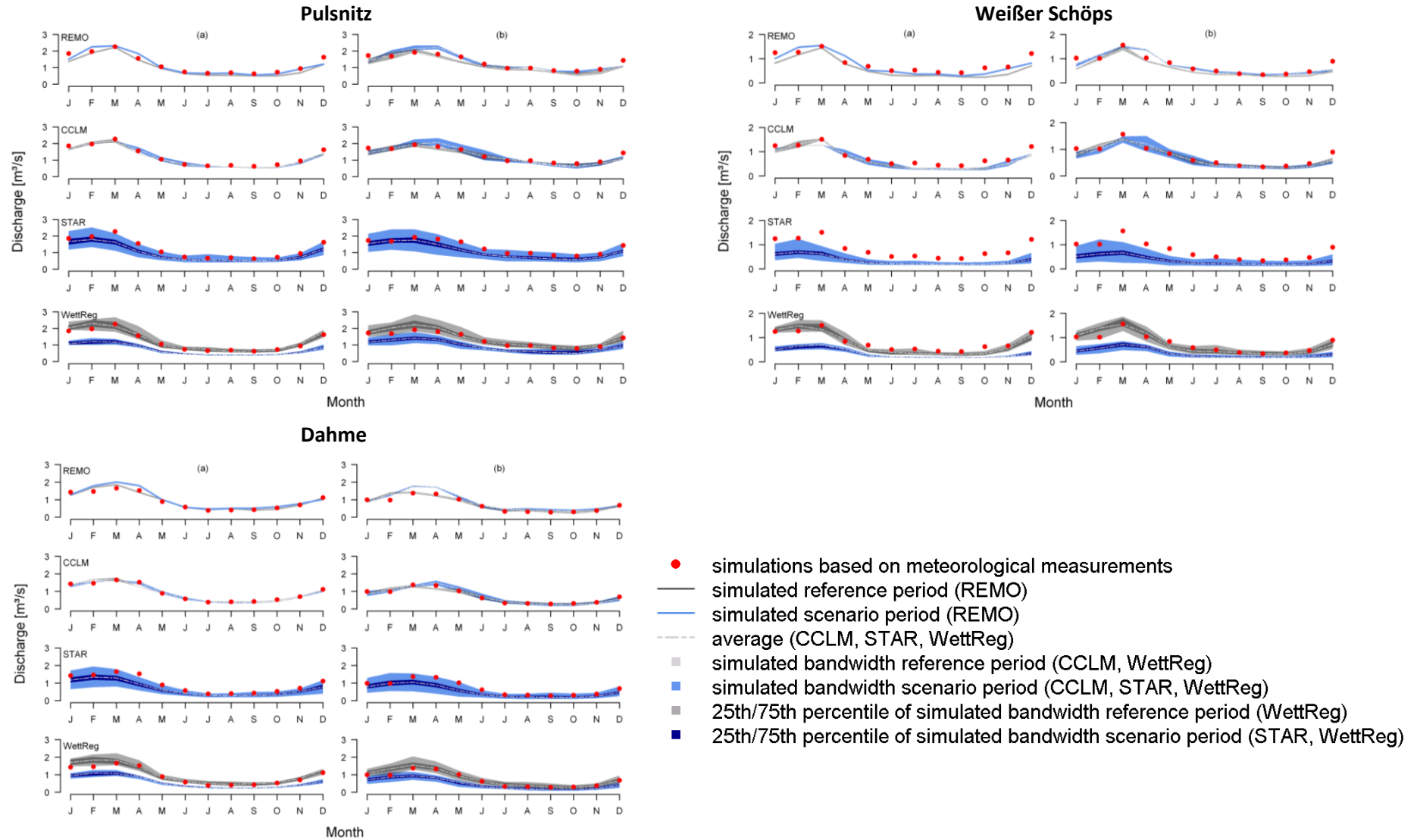


Figure 7-6: Intra-annual variability of simulated discharge of a) WaSiM-ETH and b) HBV-light driven by meteorological measurements, meteorological output from DAs for the reference period and scenario period (HBV-light bandwidth includes all three model configurations)

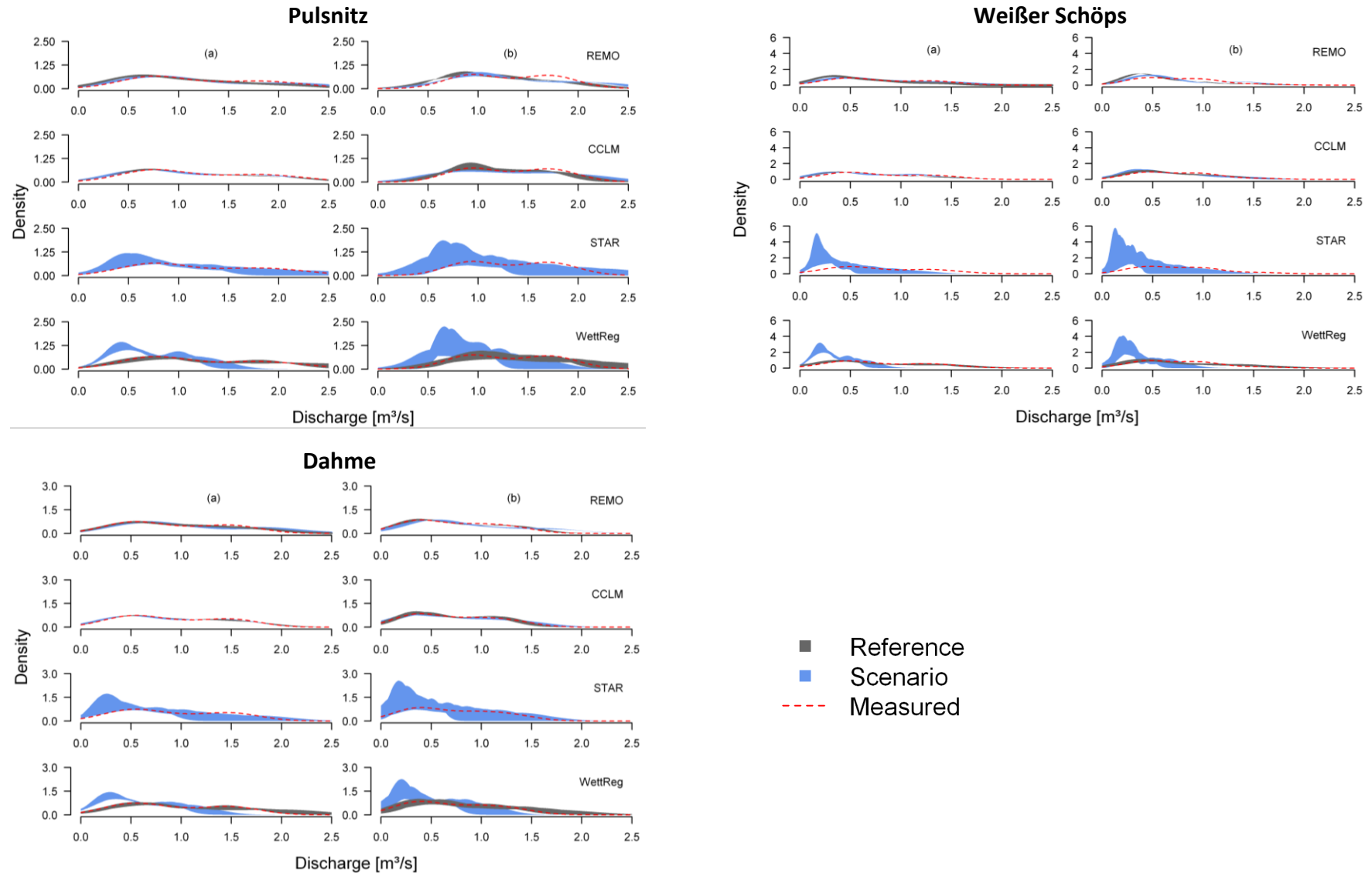


Figure 7-7: Density function of discharge for a) WaSiM-ETH and b) HBV-light driven by the meteorological measurements (“Measured”), meteorological output from the DAs for the reference and scenario period (HBV-light bandwidth includes all three model configurations)

For both DAs (CCLM, WettReg), the good agreement between measured and simulated discharge is also a result of the interplay between precipitation and evapotranspiration, the errors of which compensate each other. These results highlight the importance of analysing the entire water balance because simulations can give good results for the wrong reasons.

Concerning the intra-annual variability of discharge, both hydrological models driven by the DAs agree well with the overall discharge variability based on the meteorological measurements (Figure 7-6, compare “simulations based on meteorological measurements” with simulation results during reference period) during the reference period. The peak discharge, which occurs in March, is well matched as well as the low-flows in summer.

Similarly, when the hydrological models are driven by the DAs, the density function of the simulated discharge based on the meteorological measurements is well reproduced during the reference period (Figure 7-7, compare “Measured” with “Reference”).

In the scenario period, simulations based on the statistical DAs STAR and WettReg show a considerable decrease in runoff by 34 % and 43 %, respectively, as a consequence of lower precipitation and higher potential evapotranspiration in the study catchments (Table E-2 to E-4 in Appendix E). Contrary to that, runoff increases by 1 % based on CCLM and by 17 % based on REMO.

Besides the opposing discharge trends as a result of using a statistical or dynamical DA, the results based on WaSiM-ETH and HBV-light also show distinct differences in the water balance components in the scenario period, especially in the Pulsnitz and Dahme river catchments where calibration was aggravated due to anthropogenic impact. In the Pulsnitz river catchment, WaSiM-ETH computes, in accordance with the reference period, lower runoff, higher actual evapotranspiration and a negative change in storage compared to HBV-light. In the Dahme river catchment, WaSiM-ETH computes higher runoff and actual evapotranspiration compared to HBV-light. In the Weißer Schöps, the difference between the results based on the hydrological models is less pronounced and both hydrological models close the water balance better compared to the other study catchments. These results are in line with the analysis during model calibration and validation (section 6.3.1).

Intra-annually, the simulated discharge based on REMO increases throughout the year, especially during the winter months when evapotranspiration plays only a minor role and in spring when precipitation increases (Figure 7-6, compare simulation results from the scenario to the reference period). When CCLM is used as a driver for the hydrological models, the intra-annual discharge distribution does not change considerably. As a consequence of increasing temperature and decreasing precipitation during the summer months (Figure 7-4), discharge decreases by more than 20 % based on the statistical DAs. Based on STAR, the peak discharge occurs earlier in spring, as more runoff is generated during the winter months when higher temperatures lead to less precipitation falling as

snow and consequently less water storage in the catchment. For WettReg, the decrease in discharge is computed throughout the whole year with a significant reduction during the months of November to April, which leads to a decrease in the overall annual discharge variability. The large uncertainty bandwidth due to the 100 STAR/10 WettReg realisations can effectively be reduced by considering only the 25th and 75th percentiles (Figure 7-6).

The comparison of the simulated discharge density between the reference and scenario period shows that the changes in discharge distribution are comparably low when the dynamical RCMs are used to drive the hydrological models (Figure 7-7, compare “Scenario” with “Reference”). The probability of lower discharge values decreases while the probability of higher discharge values slightly increases during the scenario period. In contrast, when the statistical DAs are used as drivers, the opposite behaviour can be observed. In addition, the spread of the discharge distribution is significantly reduced, especially for the results based on WettReg. WaSiM-ETH and HBV-light simulate the intra-annual discharge distribution comparable.

7.2.3 Low-flow analysis under climate change impact

The statistical low-flow indicators MAM(7) and Q95, computed for both measurements and simulations (WaSiM-ETH and HBV-light driven by the meteorological output of the DAs) are displayed in Table E-5 in Appendix E for the reference and scenario period. The comparison between measurements and simulations confirms the results from section 6.3.2 that the hydrological models, in their current parameterisation, have difficulties in capturing well low-flow events. In the Weißer Schöps river catchment, simulations based on WaSiM-ETH agree better with the measured Q95 and MAM(7) compared to HBV-light. For example, the simulated MAM(7) based on WaSiM-ETH deviates from the measurements between 0.07 m³/s (REMO -> WaSiM-ETH) and 0.10 m³/s (STAR -> WaSiM-ETH) while the simulations based on HBV-light differ between 0.14 m³/s (REMO -> HBV-light) and 0.18 m³/s (CCLM -> HBV-light). Similar results are obtained for the Q95. In the Dahme river catchment, the differences in the MAM(7) and Q95 between the hydrological models is less pronounced because HBV-light was calibrated based on the simulated discharge of WaSiM-ETH. For the Pulsnitz river catchment, a comparison between measurements and simulation results was not possible due to the unavailability of measured discharge data for the reference period at gauge Ortrand.

The impact of potential climate change on the MAM(7) and the Q95 is similar to the mean flow presented in section 7.2.2. Based on REMO, the strongest increase in the MAM(7) and Q95 is identified in the Weißer Schöps (MAM(7): 14 %, Q95: 25 %) followed by the Pulsnitz (MAM(7): 5 %, Q95: 12 %) and the Dahme river catchment (MAM(7): 0.4 %, Q95: 7 %) on average over WaSiM-ETH and HBV-light in the scenario compared to the reference period.

When using CCLM, the MAM(7) and Q95 do not change considerably in the Pulsnitz and Weißer Schöps river catchments (- 3 % to 0 %), but decrease by 8 % in the Dahme river catchment. Based on the statistical DAs, the low-flow indicators decrease from 15 % up to 39 % (Table E-5 in Appendix E). In the Pulsnitz and Dahme river catchments, WaSiM-ETH simulates lower values for the indicators compared to HBV-light.

Visualizing the FDC on a logarithmic scale for each member of the model chain in each study catchment supports the fact that the differences between the hydrological models become larger for lower flows (Figure 7-8 (Weißer Schöps), Figure E-1 in Appendix E (Pulsnitz, Dahme)).

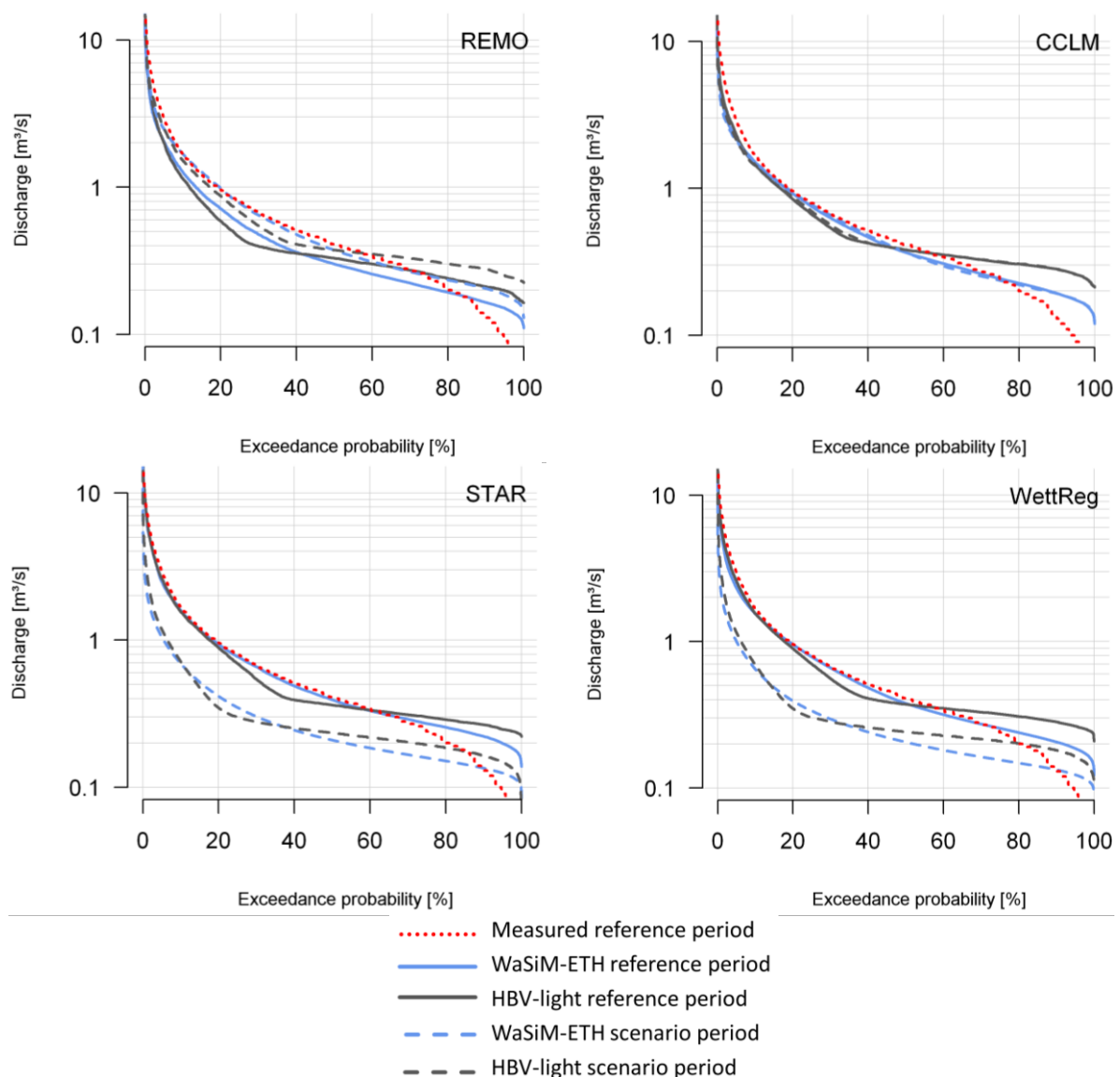


Figure 7-8: Flow duration curve based on WaSiM-ETH and HBV-light driven by the DAs in the reference and the scenario period for Weißer Schöps river catchment (Pulsnitz and Dahme river catchments in Appendix E)

For the gauging station Särichen (Weißer Schöps) measured discharge is available which can be used to compare to the simulation results in the reference period (Figure 7-8). Again, it

can be seen that the hydrological models are not able to simulate the lowest flows satisfactorily (< 80 per cent). This analysis also confirms that low-flows increase based on REMO, do not change based on CCLM and decrease significantly based on the statistical DAs in the scenario compared to the reference period. In fact, for all DAs, WaSiM-ETH and HBV-light start to deviate for flows that are exceeded in 40 % of all times with WaSiM-ETH simulating lower flows compared to HBV-light. The difference in high flows between the hydrological models is almost negligible.

The extreme value analysis was used to assess the change in the 50 year return period of the reference AM(7) low-flow in the scenario period. The results are presented in Figure 7-9 (Weißer Schöps) and Figure E-2 in Appendix E (Pulsnitz and Dahme).

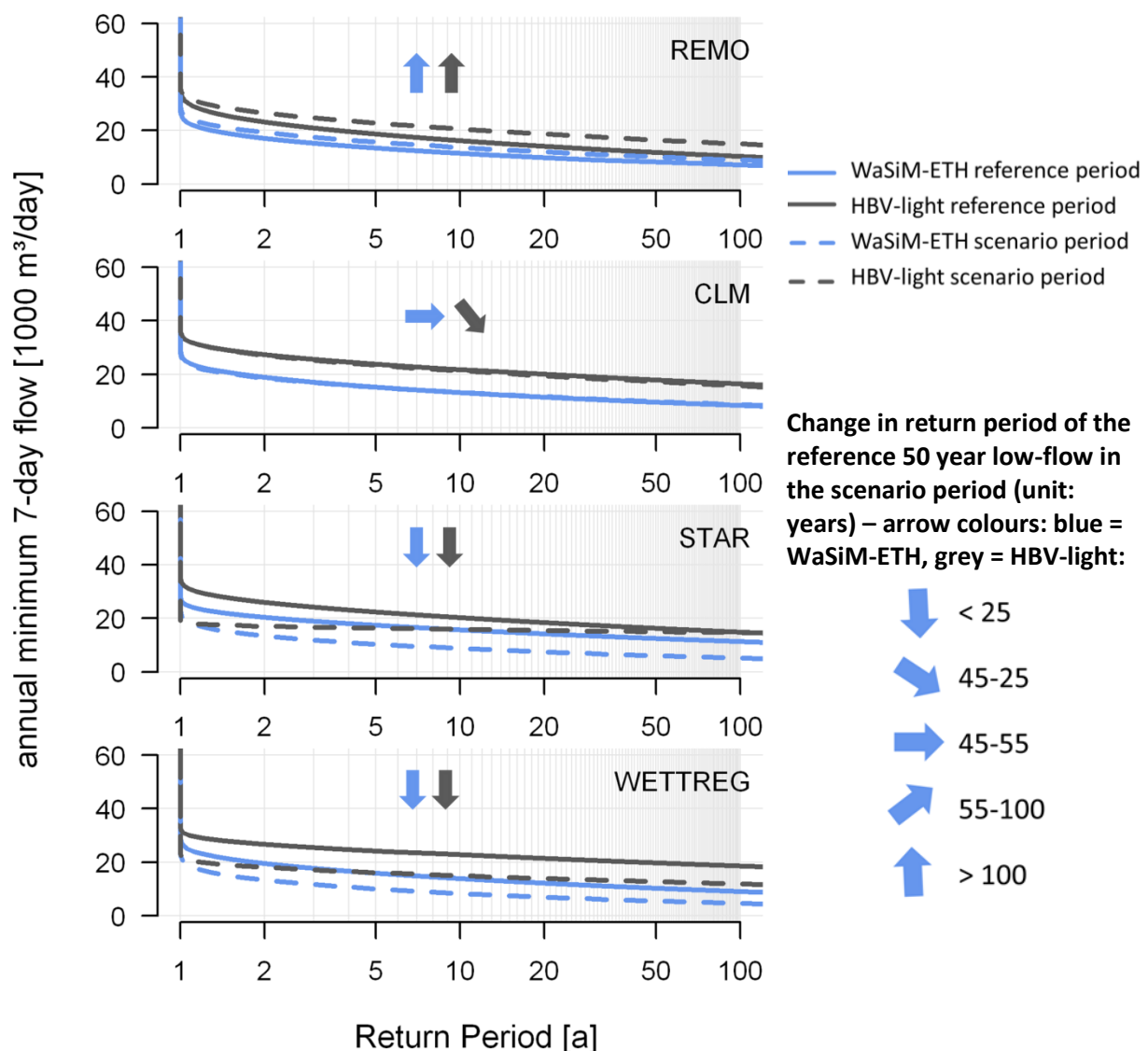


Figure 7-9: Change in the return period of the 50-year AM(7) between reference and scenario period for the Weißer Schöps river catchment. The arrows in the Figure display the change in occurrence of the return period of the reference 50 year low-flow in the scenario period (blue arrows: WaSiM-ETH; grey arrows: HBV-light, Pulsnitz and Dahme river catchments in Appendix E)

Using REMO, both hydrological models simulate less severe low-flow conditions in the Pulsnitz (Figure E-2 in Appendix E) and Weißer Schöps (Figure 7-9) river catchments. In fact, the 50 year low-flow of the reference period becomes a 100 year low-flow or even of less frequency during the scenario period. Due to the fact that the 50 year low-flow based on REMO in the Dahme river catchment is already very low, no considerable change in the frequency of the return period is simulated (Figure E-2 in Appendix E). Nevertheless, the results of the hydrological models differ. While HBV-light simulates an increase in return period, WaSiM-ETH simulated no considerable change.

When CCLM is used to drive the hydrological models, the direction of change in low-flow frequency also differs between the hydrological models and the study catchments. While WaSiM-ETH simulates a longer return period in the scenario period, implying less severe low-flow conditions, HBV-light simulates an increase in frequency of the 50 year low-flows in the Pulsnitz river catchment. In the Weißer Schöps river catchment, WaSiM-ETH computes no change in return period while HBV-light tends to increased low-flows frequency. In the Dahme river catchment, the hydrological models agree on the fact that 50 year low-flow occurs less frequent.

Using STAR, the change return period is also highly inconsistent. In the Pulsnitz river catchment, the reference AM(7) will have a return period of 47 years based on WaSiM-ETH implying no real change. In contrast, based on HBV-light, the return period will be larger than 100 years implying lower frequency. Similarly, in the Dahme river catchment, the return periods between WaSiM-ETH and HBV-light vary between 47 years and longer than 100 years, respectively. Only in the Weißer Schöps river catchment, the hydrological models agree on the fact that the reference AM(7) will become more frequent having a 2 to 8 year return period.

Only on the basis of the WettReg model, the 50 year return period flow is simulated consistently to be more frequent (1-14 years) in all study catchments for the scenario period. Similarly to the FDC analysis, the extreme value analysis underlines the fact that not only the uncertainty related to the choice of the DA is considerable but that the uncertainty related hydrological model increases when analysing low-flows in climate change impact assessments. In order to proof statistically that the uncertainty related to the hydrological model increases when considering low-flows, the Wilcoxon-Mann-Whitney test was used to compare the simulated time series of the mean annual discharge, the minimum annual discharge and the AM(7) between WaSiM-ETH and HBV-light (Table E-6 in Appendix E).

The null hypothesis, which denotes that two time series of data are independent samples from identical continuous distributions with equal medians, is rejected for:

- Mean annual discharge based on STAR in the scenario period (all study catchments)
- Mean annual discharge based on WettReg in the Dahme (only reference period) and in the Pulsnitz river catchment (only scenario period)
- Minimum annual discharge in the Pulsnitz and Weißer Schöps river catchment (all model chains)
- AM(7) in the Pulsnitz and Weißer Schöps river catchment (all model chains).

For the Dahme river catchment, the null hypothesis is rejected for minimum annual discharge for all model chains except for REMO and WettReg (only reference period). Concerning the AM(7), only the simulations based on STAR and WettReg in the scenario period are rejected by the Wilcoxon-Mann-Whitney test. Therefore, the hydrological models seem to better agree in the Dahme river catchment considering the low-flow indicators which results from the fact that HBV-light was calibrated based on the simulated discharge of WaSiM-ETH in the Dahme river catchment due to its strong anthropogenic impact. Nevertheless, the results of the Wilcoxon-Mann-Whitney test emphasize that the uncertainty related to the choice of the hydrological models increases when low-flows are considered.

It can be argued that the low-flow analysis is not representative as the hydrological models do not match well the measurements (Table E-5 in Appendix E). Since the results focus only on the change signals, they are regarded as valuable for uncertainty exploration, showing the increasing importance of the hydrological model and its parameterisation when dealing with low-flows. Moreover, the results show that climate change impact assessments focussing on low-flows are highly uncertain.

7.2.4 Climate change impact analysis on spatial patterns of actual evapotranspiration and groundwater recharge

The analysis of the impact of climate change on the spatial patterns of actual evapotranspiration on the long term annual basis is presented in Figure 7-10 (Pulsnitz), Figure E-3 (Weißer Schöps) and E-4 (Dahme) in Appendix E. Due to increasing precipitation and temperature based on the simulations with REMO, actual evapotranspiration increases on forested by on average 22 mm and on agriculturally used areas by 8 mm in the study catchments. In contrast to the results based on REMO, actual evapotranspiration decreases on forested areas based on the simulations with STAR (on average – 27 mm) and WettReg (on average – 50 mm) due to a stronger increase in temperature and potential evapotranspiration during the summer months. Actual evapotranspiration from agricultural areas increases, especially in the Pulsnitz (STAR: + 18 mm, WettReg: + 1 mm) and Dahme

(STAR: + 16 mm, WettReg: + 10 mm) river catchments. This may be due to increased temperatures during especially the winter and spring months. A monthly explicit analysis is necessary to confirm these hypotheses. Based on CCLM, no clear change in the spatial patterns of actual evapotranspiration can be identified which is mainly due to the fact that the actual evapotranspiration rates between reference and scenario period do not change. Overall, actual evapotranspiration increases based on REMO (+ 11 mm/a), CCLM (+ 3 mm/a) and STAR (- 1 mm/a), but decreases based on WettReg (- 12 mm/a) on average in the study catchments.

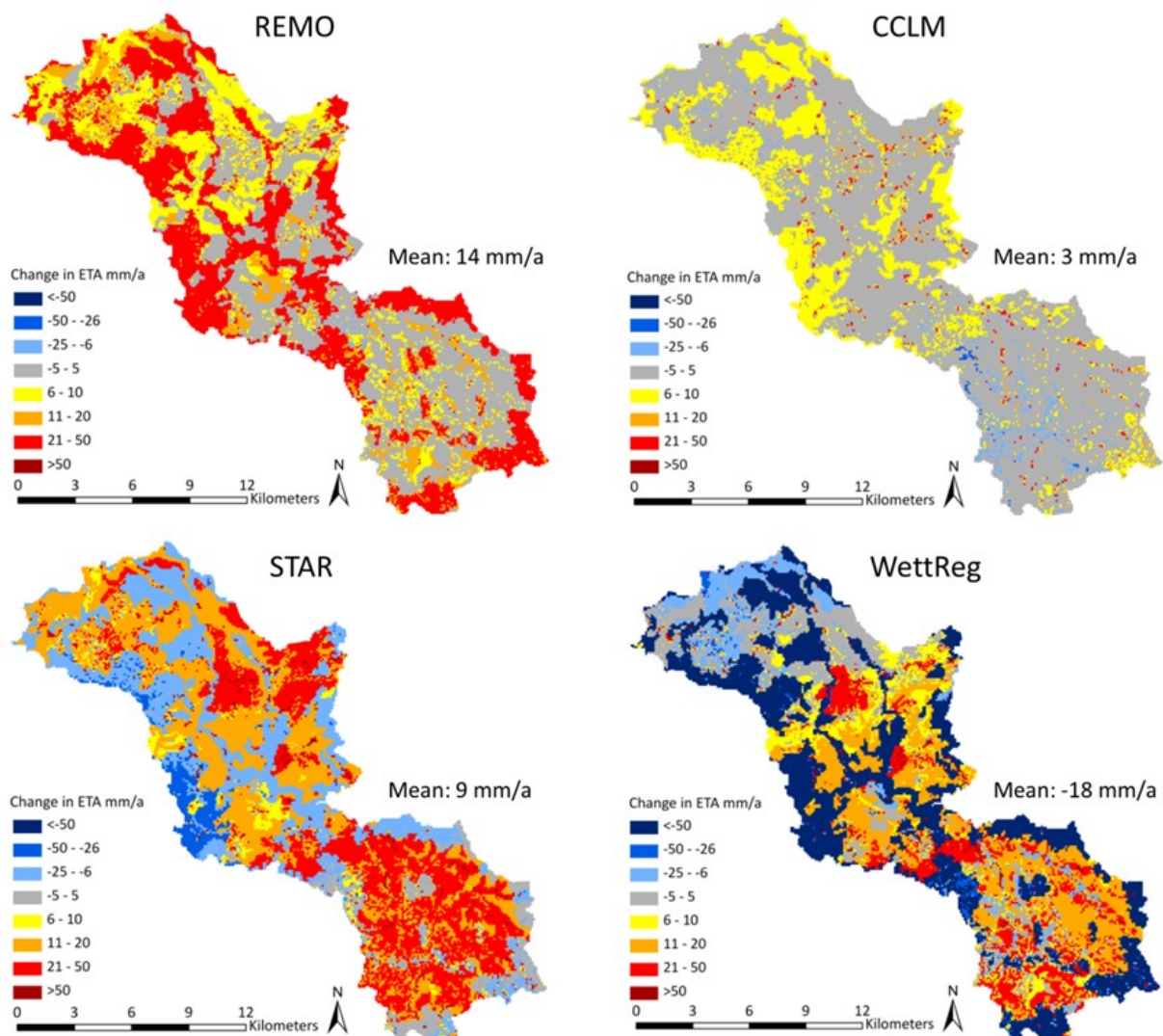


Figure 7-10: Difference in actual evapotranspiration (ETA) based on REMO (top left), CCLM (top right), STAR (bottom left) and WettReg (bottom right) between the scenario and reference period for the Pulsnitz river catchment. The average change is displayed in each figure (Weißer Schöps and Dahme river catchments in Appendix E)

The impact of climate change on the spatial patterns of groundwater recharge is displayed in Figure 7-11 (Pulsnitz) and Figure E-5 (Weißer Schöps), E-6 (Dahme) in Appendix E. Based on REMO, groundwater recharge increases over agriculturally used areas by 11 mm, 22 mm and 42 mm in the Pulsnitz, Weißer Schöps and Dahme river catchments, respectively. This fact also confirms that plants must already be well supplied with water during the reference period and the additional precipitation simulated by REMO during the scenario period cannot be utilized by the plants.

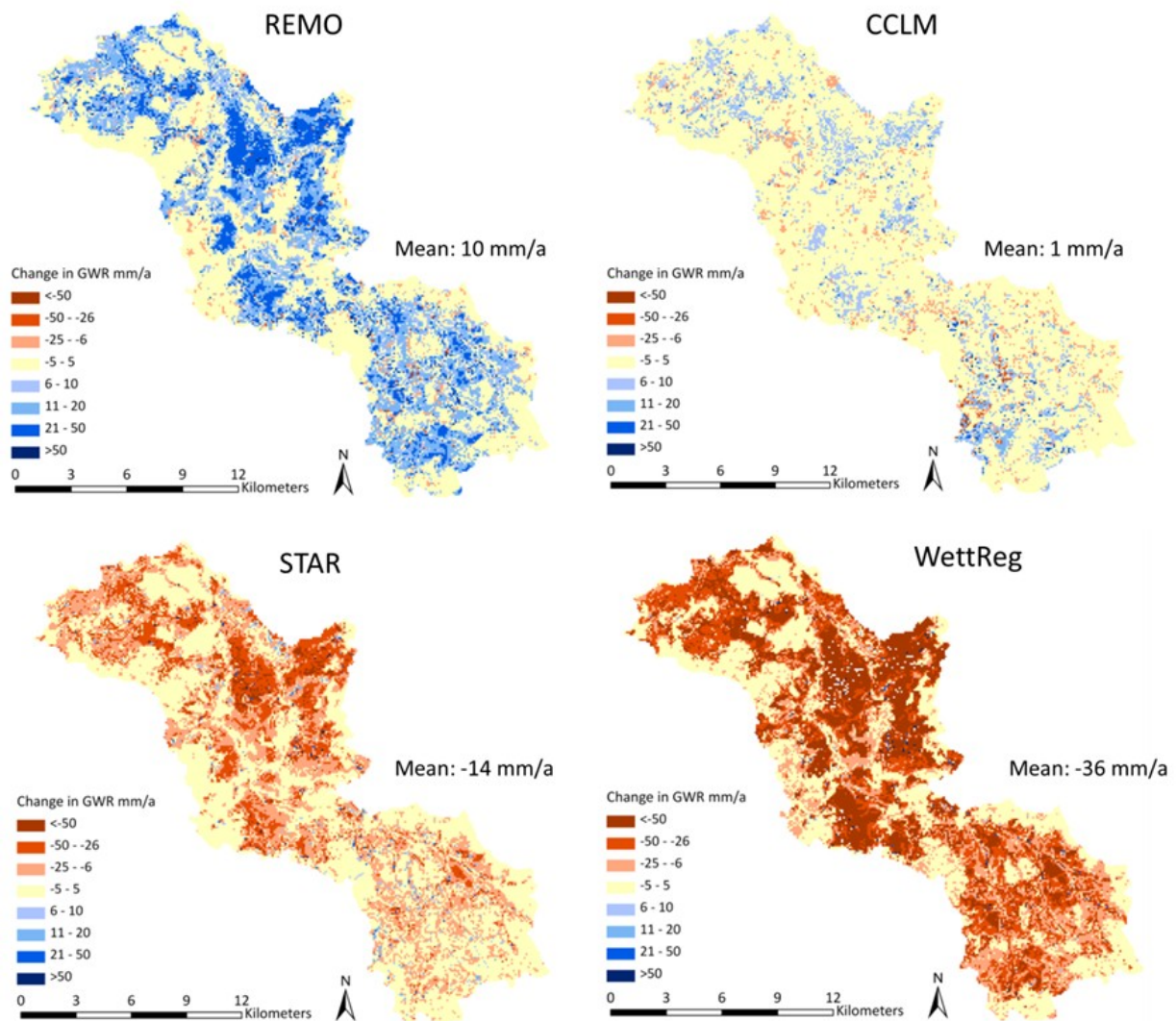


Figure 7-11: Difference in groundwater recharge (GWR) based on REMO (top left), CCLM (top right), STAR (bottom left) and WettReg (bottom right) between the scenario and reference period for the Pulsnitz river catchment. The average change is displayed in each figure (Weißer Schöps and Dahme river catchments in Appendix E)

Even on forested areas, groundwater recharge increases by on average 10 mm based on REMO. Similarly to actual evapotranspiration, the patterns of groundwater recharge remain the same based on the result of CCLM except in the Dahme river catchment where

groundwater recharge increases up to 10 mm/a over agricultural areas due to the low water holding capacity of sandy soils. For the statistical DAs, a strong decrease of groundwater recharge is simulated over agriculturally (- 35 mm/a) used areas as a result of increasing actual evapotranspiration and decreasing precipitation in the study catchments. On forested areas, groundwater recharge is further reduced in the scenario period (- 13 mm/a). Overall, groundwater increases on average by 21 mm/a based on REMO, and decreases on average by 2 mm/a, 30 mm/a and 35 mm/a based on CCLM, STAR and Wettreg in the study catchments, respectively.

The spatial-temporal analysis of actual evapotranspiration and groundwater recharge revealed that land use is the main driver for the formation of spatial patterns in the study catchments. This result was expected because land use is a function of other physiographic catchment characteristics, such as soil and topography.

7.3 Discussion

The analysis of the impact of climate change on hydrology was carried out using an ensemble approach consisting of 113 Realisations of four different DAs and four different model configurations of two different hydrological models. In total, 452 simulations were performed for each study catchment. The results reveal that the uncertainty at the end of the model chain is substantial confirming the “uncertainty explosion” (HENDERSON-SELLERS, 1993).

Concerning the hydrological models and their parameterisation, one focus of this study was to evaluate whether a large difference exists between the output of a process-based spatially distributed model and a lumped conceptual model in a climate change impact assessment. In this context, the analysis of the long term mean of the water balance components as well as its seasonal dynamic showed that the difference between the two hydrological models and their parameterisation is comparably low, especially in the Weißer Schöps river catchment. One reason for the similarity of the results based on the two hydrological models is seen in the fact, that the runoff regime of the study catchments is heavily dominated by evapotranspiration which is represented by the same modelling approach (Penman-Monteith). BORMANN (2011) showed that different approaches to model potential evapotranspiration respond significantly different to observed climate change in Germany. Therefore, larger differences between the results of the hydrological models are likely if different approaches for modelling potential evapotranspiration were used by the hydrological models. Even though the difference in discharge between the hydrological models seems insignificant, the differences in the water balance components are considerable, especially in the Pulsnitz and Dahme river catchments. However, the anthropogenic impact aggravates the analysis and interpretation of the results. Recently,

also other studies have investigated the uncertainty related to the choice of the hydrological models within the climate change modelling chain. While JIANG et al. (2007) showed that there are considerable differences in the projected change simulated by six different hydrological models, NAJAFI et al. (2011) and VELÁZQUEZ et al. (2013) also conclude that the uncertainty related to the hydrological model is rather low compared to the uncertainty of the climate input, except during low-flow conditions. This is confirmed by this study where the difference between the modelling results of the hydrological models become larger when low-flow conditions are analysed as statistically confirmed by the analysis using the Wilcoxon-Mann-Whitney test. Even though both hydrological models have difficulties in simulating the measured low-flow regime reliably, it was shown that WaSiM-ETH performed better compared to HBV-light. This can be attributed to the fact that groundwater flow in HBV-light is based on three different conceptual linear storage boxes where the outflow rate is a linear function based on storage. In WaSiM-ETH, on the other hand, groundwater flow is described physically based two dimensionally (see section 6.1.1). Eventually, the choice of the type of hydrological model needs to be answered for each study individually, depending on the aim of the study and the available resources. The main advantage of process-based spatially distributed models is their ability to simulate the response of internal catchment processes to a change in the climate forcing as conducted for actual evapotranspiration and groundwater recharge in this study. Such analyses can be utilized for an integrated river catchment planning and management and the formulation of climate change adaptation strategies.

The analysis of the effectiveness of the bias correction for the meteorological input to the hydrological model showed that a good agreement between measured and simulated mean and median temperature and precipitation could be obtained during the reference period. However, concerning the statistical distribution and the 25th and 75th percentiles larger differences were identified. These results were expected since the linear scaling approach was used, which adjusts only monthly mean values and which is regarded as sufficient for studies focussing on long term average changes in water balance components. It needs to be pointed out as well, that all bias correction methods assume stationarity, which implies that the correction algorithm and its parameters, which are valid under current climate conditions, are also valid under future climate conditions. Furthermore, the bias correction, even though it improves the overall applicability of the RCMs, certainly adds additional uncertainty to the model chain results, especially because the internal physical consistency between the parameters is destroyed. However, TEUTSCHBEIN and SEIBERT (2012a) note that the bias correction method adds the smallest portion of uncertainty to the modelling chain, justifying the choice of only one method in this study, the simple linear scaling approach.

The DA is the largest source of uncertainty when long term mean flow was considered. Especially the choice of a statistical or dynamical approach has a large impact on the modelling results. This is in accordance with the results by TEUTSCHBEIN and SEIBERT (2012a), who showed that the DA is the largest source of uncertainty in their analysis, even though only using dynamical RCMs from the EU ENSEMBLES Project (VAN DER LINDEN and MITCHELL, 2009). KAY et al. (2009) also conclude that the DA adds significant uncertainty to the climate change impact if the uncertainty related to the GCM is neglected. In fact, many studies agree on the fact that the GCM is by far the largest source of uncertainty within the modelling chain (GRAHAM et al., 2007a; GRAHAM et al., 2007b; KAY et al., 2009; WILBY and HARRIS, 2006; WILBY et al., 2006) which are directly transferred to the DA in the form of boundary and initial conditions because no bias correction is done at this step in the modelling chain. The DAs used in this study are all based on the same GCM, but each DA to a different degree. The dynamic models REMO and CCLM use most of the information of the driving GCM in the form of initial and boundary conditions, which explains their similarity in the final results. WettReg and STAR, on the other hand, are much less dependent on the driving GCM, which partly explains their difference to the dynamic RCMs. This fact, however, does not allow a judgement regarding model performance as each approach has its strength and weaknesses (Table 2-1). Generally, it remains questionable whether the variability of results at the end of the modelling chain would increase or decrease if other DAs based on different GCMs were included in this study. According to MERZ et al. (2012), the meaningfulness of the variability of the final result depends on the fact whether or not the chosen representatives of the model chain represent an adequate sample of the whole population. Consequently, an ensemble-based approach alone may not necessarily lead to an increase in the confidence of the final results. Nevertheless, the large variability of the results at the end of the model chain questions the validity of impact studies that are based only on a single DA or a single approach (dynamical or statistical), which can only be regarded as an indication of a possible future or even only as one random event.

The estimation of the vulnerability of the study catchments to hydrological change is aggravated by the large variability of the modelling results. This fact may reduce the local stakeholders' confidence in the results and their willingness to develop and implement suitable climate change adaptation strategies, as also discussed by BORMANN et al. (2012) and FÜSSEL (2007). Even opposing trends are simulated for discharge (- 43 % to + 17 %), actual evapotranspiration (- 3 % to + 3 %) and precipitation (- 12 % to + 5 %, average over all subcatchments). The large variability of results confirms the concerns already expressed by BEVEN (2011) in which he questioned "how precautionary do we need to be in planning for the future" considering the large uncertainties inherent in the current regional climate models. Generally, stakeholders can only be advised that processes controlled by future

temperature changes are more certain than hydrological processes controlled by precipitation, and that the uncertainty in the hydrological response to climate change is larger for smaller catchments (< 200 km²) compared to larger ones (BLÖSCHL and MONTANARI, 2010). Moreover, as the analysis of the low-flow indicators suggested, the uncertainty related to extremes, especially low-flows, increases compared to long term averages. Especially smaller headwater catchments may, however, be used to get a better understanding of how changes in the climatic forcing impact the hydrological functioning of a catchment which will depend among others on the characteristics and spatial arrangements of geology, topography, soils and vegetation communities (ALI et al., 2012; TETZLAFF et al., 2013). In this modelling study, land use was certainly the main catchments characteristic influencing the internal catchment response to climate change and can therefore be regarded as a promising trigger for natural based climate change adaptation strategies. To what extent changes in land use could counteract climate change impact on the catchment scale needs to be further verified (chapter 8).

8 Land use change analysis as a climate change adaptation strategy

8.1 Material and methods

For the land use change analysis, the process based spatially distributed hydrological model WaSiM-ETH was used. The simulations based on the status quo model version (“current land use”, parameterisation as described in section 6.2.1) were compared to the model versions with the change in land use (Table 8-1).

Table 8-1: Overview of land use change scenarios

Land Use Change Scenario	Characteristics	Catchment	Climate
Extreme scenarios	<ul style="list-style-type: none"> - entire catchment area parameterised as coniferous forest - entire catchment area parameterised as uncultivated land 	Pulsnitz, Weißer Schöps, Dahme	- current climate conditions (1963-1992)
Change in crop cultivation	- shift in the agricultural growing season towards earlier start and later end, overall less intensity	Pulsnitz, Weißer Schöps, Dahme	<ul style="list-style-type: none"> - current climate conditions (1963-1992) - dry, moderate and wet STAR scenario (2031-2060)
Combination of forest conversion and change in crop cultivation	<ul style="list-style-type: none"> - all forested areas is parameterised as deciduous forest - shift in the agricultural growing season towards earlier start and later end, overall less intensity 	Pulsnitz, Dahme	<ul style="list-style-type: none"> - current climate conditions (1963-1992) - dry, moderate and wet STAR scenario (2031-2060)

In the extreme scenarios (Table 8-1), which were only evaluated under current climate conditions, the entire catchment is parameterized as i) coniferous forest and ii) as uncultivated area. This serves as a mean to understand how much change in the water balance components can be triggered by maximum land use changes in the study catchments.

In the second land use change scenario “change in crop cultivation”, the impact of an earlier start and a later end of the growing season was investigated. Due to the large proportion of agricultural area (> 50 %, Figure 4-9) in the subcatchments, a change in agricultural parameterisation should results in a noticeable effect on the water balance on the catchment scale. In the context of climate change, crop growth may be shifted to periods which are currently not yet favourable. Due to observed (section 5.2) and projected

temperature increase (section 7.2.2), an earlier start of the growing may become feasible in the future. In the status quo scenario, the vegetation period starts in the middle of April and ends in the middle of September (see Table F-1 in Appendix F). During that period, the land use is quite intensive which is reflected in high values of the vegetation covered fraction (VCF), roughness length, LAI and leaf surface resistance. In the changed agricultural parameterisation, these parameters are reduced and the growing season already starts in the middle of March. The first growing season, which is overall less intensive, ends already in the middle of June. After that, an even less intensive growing cycle starts and lasts until the middle of October. At the same time, it is assumed that the crops grown in the changed agricultural parameterisation have deeper roots so that they are able to reach water from deeper soil layers. Overall, the vegetation period starts earlier, lasts longer and is less intensive, especially during the summer months.

The third land use change scenario is a combination of the “change in crop cultivation” scenario with additional forest change from coniferous to deciduous forest which is characterised by less water demand (REYER et al., 2011; WATTENBACH et al., 2007). In this scenario, all forested areas are parameterized as deciduous forest. The forest parameterisation is based on the standard WaSiM-ETH parameters suggested by the model developers in model version 8.10.0 (Table F-1 in Appendix F). The combination of forest conversion and change in crop cultivation is only applied in the Pulsnitz and Dahme river catchments where forest covers more than 30 % of the catchment area, because in the Weißer Schöps river catchment, the proportion of forest is too low ($\approx 10\%$, see Figure 4-9) to expect any noticeable effect on the water balance. In addition to that, the Dahme and Pulsnitz river catchments represent the Spree and Schwarze Elster river catchment, respectively, better in terms of land use distribution as the analysis in section 4.2 demonstrated.

The analysis focusses on the difference in the water balance components, discharge and potential evapotranspiration on the annual and monthly basis. For the scenario “combination of forest conversion and change in crop cultivation”, spatial patterns of actual evapotranspiration and groundwater recharge are also evaluated. Except for the extreme scenarios, all land use change scenarios are simulated for both current climate and climate change conditions in order to analyse whether the land use change can compensate possible climate change impacts. For this purpose the DA STAR was chosen, as STAR represents the standard DA used within the INKA BB project framework and as analyses from chapter 5 and 7 have shown, STAR can be characterised as a medium-dry DA and is therefore regarded as suitable for the evaluation of land use change as an adaptation strategy to a potentially warmer and dryer climate in the future. In order to reduce simulation time, from the 100 available STAR realisations, three realisations were chosen which have the lowest deviation

from the 10th percentile, the median, and the 90th percentile of the measurements at the climate station Cottbus (realisations 3, 50 and 76), referred to as dry, moderate and wet realisations. The analysis is carried out for the hydrological years 1963-1992 and 2031-2060.

8.2 Results

8.2.1 Extreme land use scenarios as boundary conditions

The simulations of the extreme land use scenarios reveal that based on the coniferous forest model parameterisation (Figure 8-1 (green) and Table F-2 in Appendix F), the highest potential and actual evapotranspiration and lowest runoff is simulated during all months in all study catchments. Contrary to that, the highest runoff and lowest potential and actual evapotranspiration is simulated for the uncultivated land scenario (red). In fact, annual actual evapotranspiration is reduced by about 40 % for the uncultivated scenario compared to the coniferous forest scenario in all study catchments. At the same time, runoff is increased by about 500 % in the Pulsnitz and by about 800 % in the Weißer Schöps and Dahme river catchments (Table F-2 in Appendix F). This implies that the relation between change in evapotranspiration and runoff is highly non-linear. The intra-annual runoff dynamic is highest for the uncultivated scenario, with high runoff in winter and lower runoff in summer. Vice versa, for coniferous land use, runoff is low and quite equilibrated throughout the year while the dynamics of potential and actual evapotranspiration is larger. These facts highlight the retention capacity potential of forested compared to uncultivated land use in catchments. At the same time, forest are characterised by higher evapotranspiration.

The simulations based on the original land use parameterisation (Figure 8-1, blue) lie in between the two extreme scenarios reflecting both the current land use and climate conditions of the study catchments. In the Weißer Schöps river catchment, with currently less than 10 % forest proportion (Figure 4-9), the simulated runoff is closer to the runoff based on the uncultivated land use distribution, especially during the winter months.

Overall, it can be concluded that land use can have significant impact on the water balance components in the study catchments, theoretically being at least of the same magnitude than the investigated impact of changes in the climate forcing analysed in section 7.2.

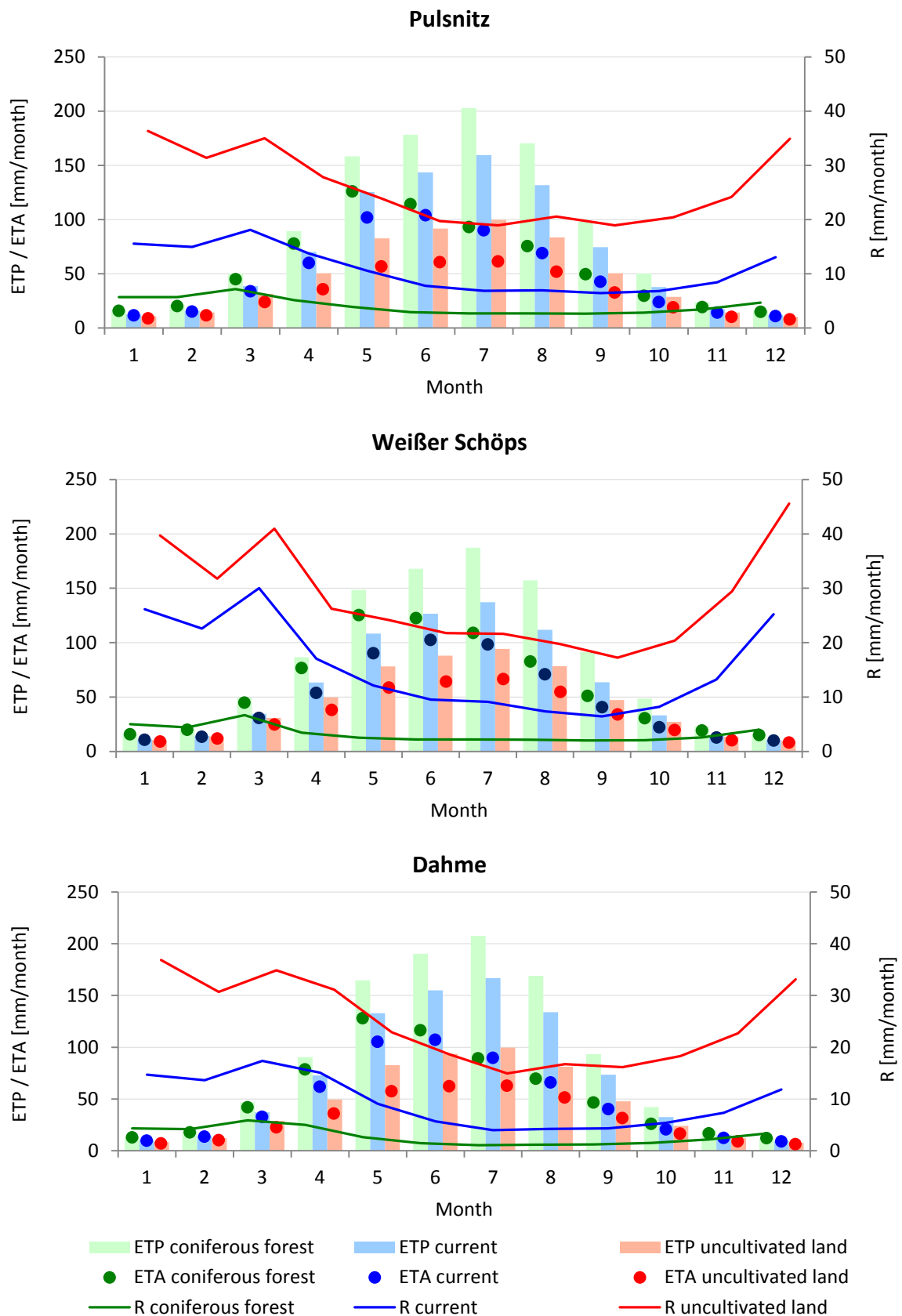


Figure 8-1: Long term potential evapotranspiration (ETP), actual evapotranspiration (ETA) and runoff (R) for extreme land use scenarios (all area coniferous forest or uncultivated land) as well as current land use under current climate conditions

8.2.2 Change in crop cultivation

For the change in crop cultivation practises (Table F-1 in Appendix F), a decrease in actual evapotranspiration is simulated in all study catchments on the long term annual basis (Table F-3 in Appendix F). The effect that crop change has on actual evapotranspiration decreases from the current over the wet and moderate to the dry climate scenario. In fact, under current climate conditions, actual evapotranspiration decreases by 8 mm/a in the Pulsnitz and by 14 mm/a in the Weißer Schöps and Dahme river catchments. For the dry climate scenario, actual evapotranspiration decreases by only 4 mm/a, 8 mm/a and 7 mm/a in the Pulsnitz, Weißer Schöps and Dahme river catchments, respectively. More relevant than the decrease of actual evapotranspiration due to crop change is its change due to climate change. In the Dahme river catchment, these changes are largest with an increase for the wet climate scenario by 29 mm/a and a decrease for the dry climate by 37 mm/a when crop change is considered (Table F-3 in Appendix F). For the moderate climate scenario, the change in actual evapotranspiration is negligible (6 mm/a) in the Dahme river catchment.

Long term mean annual runoff increases for the crop change scenarios in all study catchments (Table F-3 in Appendix F). Under current climate conditions, the increase accounts to 15 mm/a, 8 mm/a and 5 mm/a while, under the dry climate scenario, the increase in runoff due to crop change accounts to only 9 mm/a, 5 mm/a and 2 mm/a in the Dahme, Pulsnitz and Weißer Schöps river catchments, respectively. Again, the impact of climate change on runoff is larger than the impact of crop change. In the dry climate scenario under consideration of crop change, runoff reduces by 51 mm/a, 136 mm/a and 59 mm/a in the Pulsnitz, Weißer Schöps and Dahme river catchments, respectively, compared to the current climate conditions.

Intra-annually, higher potential evapotranspiration is simulated from March to June in all catchments when considering crop change (Figure 8-2, Figure F-1 and F-2 in Appendix F, top). Similarly, actual evapotranspiration increases from March to May, but decreases from June to August for all scenarios in comparison to current land use conditions (Figure 8-2, Figure F-1 and F-2 in Appendix F, centre). Runoff increases during all month expect during spring (Figure 8-2, Figure F-1 and F-2 in Appendix F, bottom). These results were expected since, in the model parameterisation, the growing season was shifted from summer to spring with reduced agricultural cultivation intensity. The analysis proves that shifting the vegetation period from the summer months to spring and late autumn is an effective trigger to counteract severer low-flow periods during summer as simulated by the hydrological models based on the DA STAR 2 K (section 7.2.3).

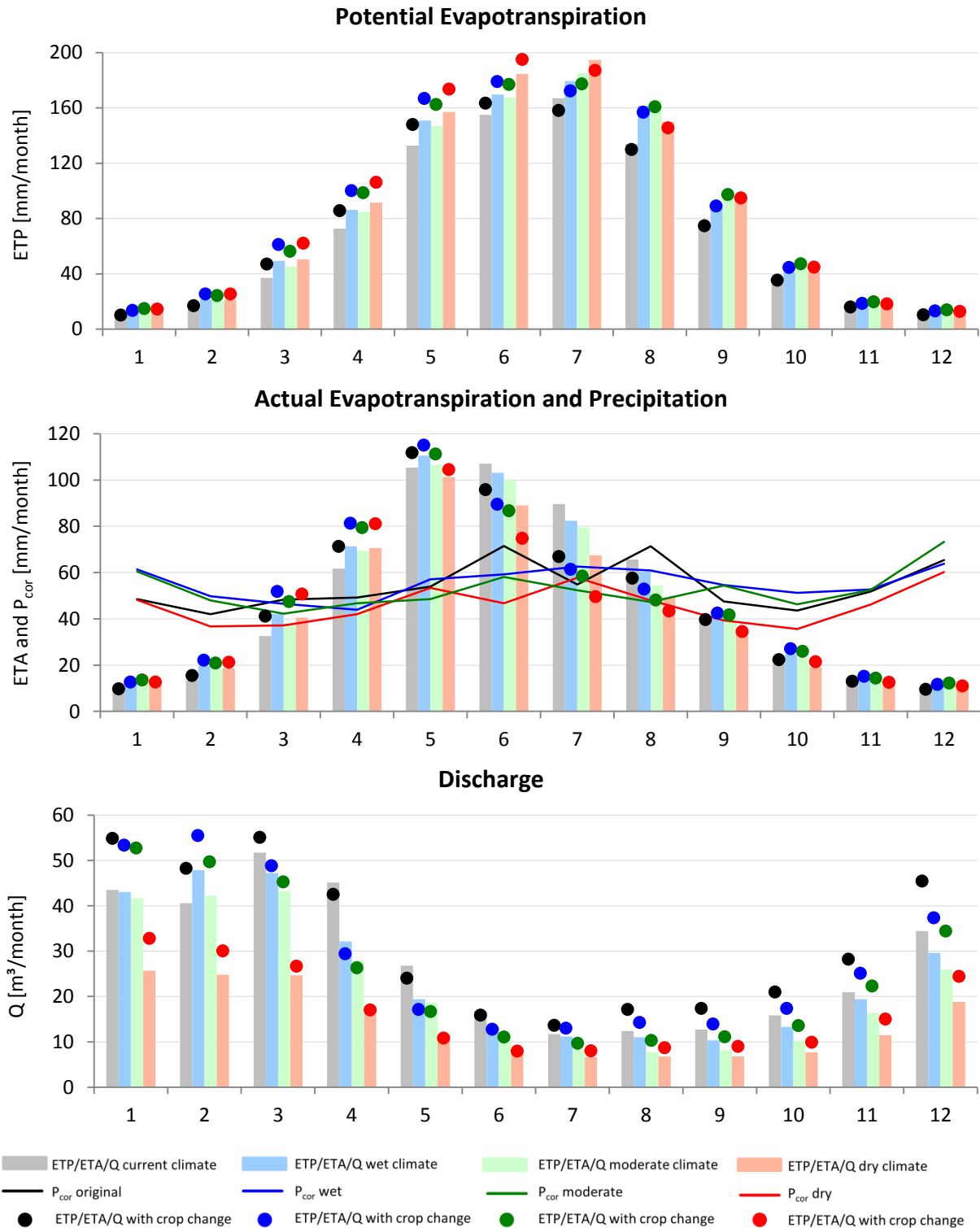


Figure 8-2: Potential (ETP), actual evapotranspiration (ETA) and discharge (Q) for current land use and changed agricultural parameterisation under current climate conditions (1963-1992) as well as the dry, moderate and wet climate realisation of STAR 2 K (2031-2060) in the Dahme river catchment (Pulsnitz and Weißer Schöps river catchments in Appendix E)

8.2.3 Combination of change in crop cultivation and forest conversion

The results of the combined effects of crop and forest conversion are in accordance with those of section 8.2.2. Actual evapotranspiration decreases on the annual basis with the forest conversion leading to an additional reduction of around 2 % (Table F-4 in Appendix F). The biggest decrease in actual evapotranspiration due to crop change is simulated under the wet climate scenario (-19 mm/a) in the Pulsnitz and under current climate conditions (-18 mm/a) in the Dahme river catchment. Again, the climate change impact is larger than the impact of land use change. The effect of the combination of forest conversion and change in crop cultivation was further investigated on the spatial patterns of actual evapotranspiration and groundwater recharge under current climate conditions (Figure 8-3).

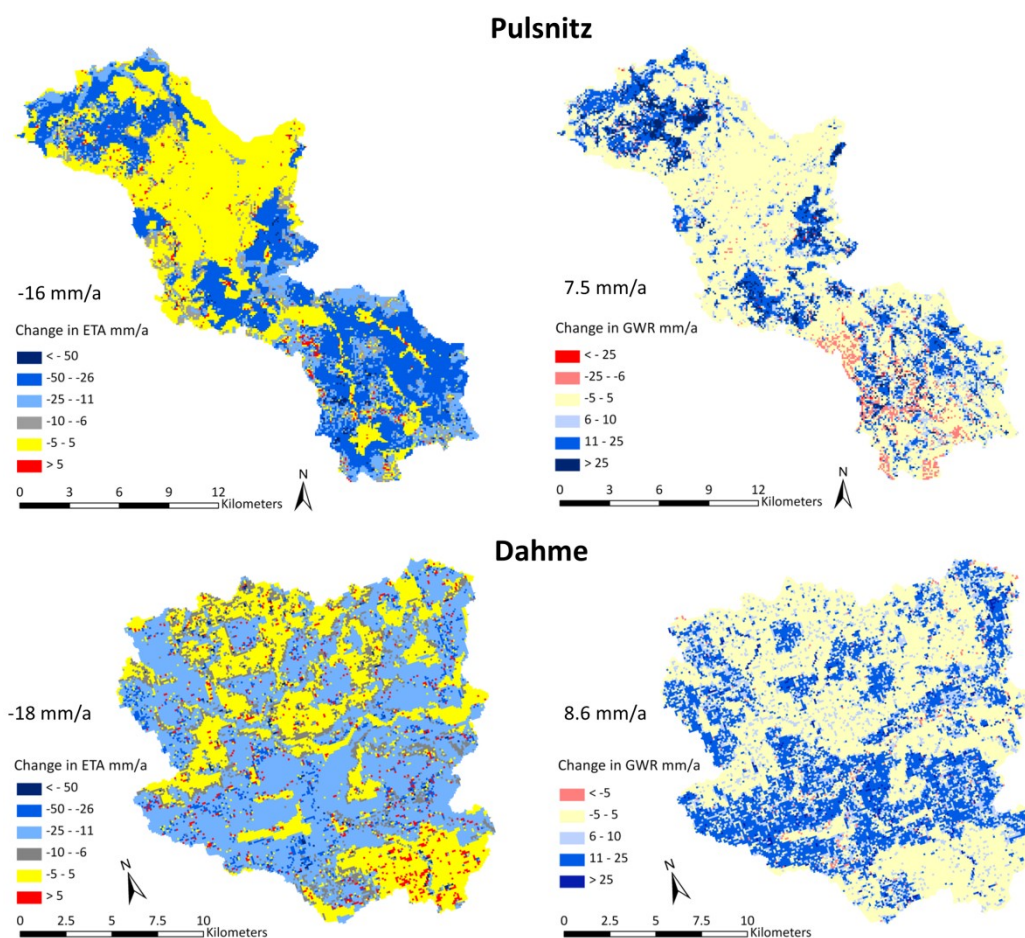


Figure 8-3: Difference in long term actual evapotranspiration (ETA, left) and groundwater recharge (GWR, right) between the simulations with and without land use change (forest and crop change) based on the moderate climate change scenario in the Pulsnitz (top) and Dahme (bottom) river catchments

In the Pulsnitz and Dahme river catchments, actual evapotranspiration decreases by on average 9 mm/a and 7 mm/a on forested and by 25 mm/a and 16 mm/a on agricultural areas, respectively. These results suggest that changes in agricultural cultivation have a

greater potential to impact the water balance. In total the decrease in actual evapotranspiration is larger (by 12 %) in the Dahme compared to the Pulsnitz river catchment. Groundwater recharge increases by on average 11 mm/a on agricultural and by 4 mm/a on forested areas in both river catchments. In total the increase in groundwater is again larger (by 15 %) in the Dahme compared to the Pulsnitz river catchment. It has to be pointed out, however, that more area is affected by land use change in the Dahme (94 %) compared to the Pulsnitz river catchment (75 %) so that the relative land use change impact cannot directly be compared between the catchments.

The intra-annual dynamics of evapotranspiration and runoff is again comparable to the results presented in section 8.2.2 (Figure F-3 in Appendix F).

Long term mean annual runoff also increases for all scenarios (> 10 %) in all study catchments (Table F-4 in Appendix F). The additional forest conversion accounts to a discharge increase of on average 6 % in the Pulsnitz and 2 % in the Dahme river catchments compared to the results presented in section 8.2.2.

8.3 Discussion

The extreme land use change scenarios presented in this chapter suggest that land use change scenarios can have a substantial impact on the partitioning of precipitation into evapotranspiration and runoff in the study catchments. In fact, the water balance components differ considerably between the coniferous forest and the uncultivated land model parameterisation. These differences were expected since coniferous forest are characterised by a higher surface roughness, vegetation coverage, leaf area and a deeper root depth and thus a higher retention potential compared to the uncultivated land parameterisation. The magnitude of the impact, however, also depends on the catchments physiographic characteristics as well as the seasonal distribution of precipitation. Moreover, the simulations of the extreme land use scenarios highlight that land use change can be as important as climate change in affecting the regional water balance. In fact, studies agree that vegetation is one of the most responsive catchment characteristics to climate change affecting hydrological catchment functioning such as storage, mixing and release of water water (DONOHUE et al., 2007; TETZLAFF et al., 2013). This is in agreement with the results of the climate change impact assessment presented in section 7.2.4, where land use, though depending on other physiographic catchment characteristics, has been the dominant driver of changes in spatial patterns of actual evapotranspiration and groundwater recharge. At the same time, land use change also has feedbacks to regional climate through changes in the surface energy and water balance (FOLEY et al., 2005) which is according to PIELKE (2005) yet only poorly recognized and understood and far beyond this thesis objectives.

A change in agricultural cultivation practises proved to be suitable to trigger an intra-annual shift of the water balance components promoting low-flow stabilization during the summer months. Low-flow stabilization during the summer months is of high relevance for the Lusatian river catchments, independent of the climate change impact, due to decreasing mining drainage water (Figure 4-2). In fact, extreme low-flows have already been observed during summer months in recent years in the Spree (KOCH et al., 2012) and Schwarze Elster river. Consequently, ecological requirements can already today not always be sufficiently met. Considering decreasing discharge variability, as simulated based on the statistical DAs (Figure 7-7), stream ecology will further be negatively impacted.

In the simulated crop change scenario, evapotranspiration decreased and runoff increased due to the overall reduction in agricultural intensification on the annual basis. The overall reduced agricultural intensity does, however, not necessarily imply reduced productivity and yield as elevated CO₂ levels are expected to positively influence plant growth (ROUNSEVELL et al., 2005). To which degree elevated CO₂ levels increase agricultural productivity remains questionable but experimental studies have already shown that the increase is unproportional which implies that a doubling of the CO₂ levels will not lead to halving the water use (BUNCE, 2004). Hence, an overall increase in agricultural productivity is not compatible with increasing temperatures and decreasing water yields. Moreover, the increasing cultivation of energy crops in the Lusatian river catchments, which are generally characterised by a high water demand during the summer, is doubtful. Several studies have already suggested that yield security of agricultural goods in the study region can only be maintained by irrigation which requires high investments (GERSTENGARBE et al., 2003; LISCHIED, 2013; WECHSUNG et al., 2008). Hence, their large-scale application is rather unlikely unless promoted by governmental authorities (e.g. European Union) in the form of subsidies.

The combination of forest conversion and change in agricultural cultivation increased runoff and decreased actual evapotranspiration. In the Lusatian river catchments, already today, an increasing share of mixed and deciduous forests can be detected (Table 4-1). Nevertheless, several studies have shown that the long term impact of forest change is rather low compared to climate change on the catchment scale ($A > 100 \text{ km}^2$, (GÄDEKE et al., 2012b; KÖPLIN et al., 2013)). Overall, the scenarios of crop change and the combination with forest conversion show that solely a change in agricultural land use strategy will not mitigate the projected climate change by the STAR 2 K scenario. Even though precipitation increases in the wet STAR realisation, the increase in actual evapotranspiration as a result of increasing temperatures cannot be compensated.

In general, the results disclose that land use change can be used as a policy instrument to moderate potential climate change impacts. In fact, depending on the severity of the climate

change impact, a change in, for example, agricultural cultivation practises, will be inevitable. However, knowledge on how natural vegetation responds to changes in climate is yet lacking (TROCH et al., 2009). For an overall adaptation strategy in the Lusatian river catchments, land use change should to be considered along with other, more technical based, adaptation strategies.

9 Summary and conclusion

In section 1.2, different research questions were addressed which can be answered based on the outcome of the analyses of this thesis.

- 1) **Change detection in the measurements:** *Which changes in the meteorological measurements can be detected? How have the observed changes in the measured meteorological variables affected the measured hydrological variables? Have these changes occurred gradually or step wise?*

The trend analysis showed that long term annual temperature (mean, maximum and minimum) and potential evapotranspiration have increased in the Lusatian river catchments since the middle of the last century. Precipitation, on the other hand, has not changed considerably on the annual basis but shows a tendency towards an increase in winter and decrease in summer. Due to increasing temperature and potential evapotranspiration, runoff shows a negative trend in the subcatchments of the Pulsnitz (- 24 mm during the period 1951 – 2006) and Weißer Schöps (- 37 mm during the period 1963 – 2006) where anthropogenic impact on discharge is comparably low. Through the monthly, spatially explicit investigations, intra-annual shifts as well as spatial hot spots of change could be identified. A clear differentiation between a change point and gradual trend was in most cases not possible based on the Pettitt and Mann-Kendall test as the pattern of change seems to be of more complex nature. However, especially in the Dahme river catchment, an anthropogenic impact was identified. Also, the dependence/sensitivity of outcome of trend tests on the time series length or analysis period was demonstrated as well as the importance of considering different correlations in the data, especially for the spatially-explicit analysis, justifying the methodological approach.

- 2) **Comparison between trends in measurements and DA output:** *Do the trends simulated by the climate DAs coincide with the trends in the meteorological measurements of temperature and precipitation during the period 1961-2006? Do the simulated temperature and precipitation trends based on the DAs for the period 2015-2060 agree with the direction of change if the measurements were extrapolated into the future?*

During the period 1961-2006, measurements and simulations (by DA) agree on a positive temperature trend on the annual basis even though differences in magnitude exist. On the seasonal basis, trends in the measurements and simulations are not consistent in winter and spring. During summer and autumn, measurements and simulations agree on increasing temperatures but again show differences in trend magnitude. For the future

period 2015-2060, the DAs agree on simulating increasing temperature on both annual and seasonal basis.

Concerning precipitation, the DAs simulate a negative precipitation trend during the period 1961-2006 on the annual basis in the study catchments. Measured precipitation, on the other hand, has slightly decreased in the Spree and Weißer Schöps and slightly increased in the Schwarze Elster, Pulsnitz and Dahme river catchments. Seasonally, trends in the measurements and simulations by DAs do not agree consistently.

In the future period 2015-2060, the dynamical DAs, which are statistically bias corrected, simulate increasing precipitation while the statistical DAs, especially WettReg, simulate a strong decrease in precipitation. Based on the trend analysis of measured precipitation, which revealed that precipitation has not changed considerable during the last decades, the strong decrease in precipitation simulated by the statistical DAs should be interpreted as a medium-dry climate scenario. Moreover, the nature of the algorithms, especially those of the statistical DAs, has to be considered because of not being open-ended.

3) **Comparison of conceptually different hydrological models:** *Do the results simulated by conceptual and process-based models differ during hydrological model calibration and validation?*

After model calibration, high values of statistical performance indicators are obtained with both hydrological models. It was demonstrated that using WaSiM-ETH, measured and simulated discharge fit already very well only after careful model parameterisation as reflected by the high values of the statistical performance indicators. This can mostly be attributed to the application of the 2D groundwater model. The parameterisation thereof is, however, complicated and requires considerable system understanding. The automated calibration using PEST only marginally increases model performance. WaSiM-ETH was additionally calibrated and validated on internal gauging stations where model performance is lower compared to the outlet gauge. HBV-light, on the other hand, requires intensive model calibration. For both hydrological models, model performance is lower during the validation compared to the calibration period. Concerning the partitioning of precipitation into evapotranspiration and runoff, the difference between the hydrological models is negligible in the Weißer Schöps river catchment, where anthropogenic impact is rather low. In the Pulsnitz and especially the Dahme river catchment, where discharge is anthropogenically impacted, model calibration is aggravated and consequently larger differences in the water balance components exist. Therefore, the uncertainty related to the results of the hydrological model increases. Concerning low-flows, the model parameterisations of WaSiM-ETH and HBV-light shows

deficiencies in simulating flows that have an exceedance probability larger 80 % with WaSiM-ETH performing better compared to HBV-light which can again be attributed to the 2D groundwater modelling approach.

- 4) **Climate change analysis:** *What is the uncertainty bandwidth of the simulated water balance components resulting from an ensemble-based climate change impact analysis? Which ensemble member, the climate DA or the hydrological model and its parameterisation, adds the largest share of uncertainty to the final results during mean and low-flow conditions? What does a large uncertainty bandwidth imply for the development of adaptation strategies? Is it possible to narrow the uncertainty bandwidth of the final results by, for example the integration of the results of the trend analysis?*

The results of the climate change analysis show that the uncertainty bandwidth of the final results is considerable which can reduce the willingness of regional stakeholder to develop and implement suitable climate change adaptation strategies. Opposing trends are simulated for the scenario compared to the reference period concerning long term average precipitation (- 12 % to + 5 %), actual evapotranspiration (- 3 % to + 3 %) and especially runoff (- 43 % to + 17 %). The large bandwidth results mostly from the choice of a statistical or dynamical DA. The uncertainty related to the choice of the hydrological models was identified as secondary within climate change impact studies when focussing on long term average changes in the study catchments. It has to pointed out, however, that larger difference related to the hydrological models are expected in the context of climate change studies when different approaches for computing potential evapotranspiration were used. When analysing low-flows, the uncertainty related to the choice of the hydrological model increases.

The combination of trend analysis and an ensemble-based modelling approach leads to a deeper process understanding of the complex interactions between a climate change and its impacts on regional water resources. In addition, regional stakeholders seem to have more trust in measurements than in simulation results. In fact, it was demonstrated that the results based on the statistical DAs, especially WettReg, represent medium-dry future scenarios. However, due to increasing temperatures and consequently increasing potential evapotranspiration, which were confirmed by the trend analysis on measured time series, precipitation would need to increase considerably for increasing runoff and groundwater recharge to take place. Therefore, a reduction in water yield is of high probability in the Lusatian river catchments in the future.

- 5) **Land use based adaptation to climate change:** *Which catchment characteristic dominates how catchments buffer potential climate change impacts on the hydrological cycle? What is the impact of land use change on the water balance components? Can land use change possibly compensate the simulated climate change impacts and therefore serve as a suitable climate change adaptation strategy in the Lusatian river catchments?*

Land use was identified to be the catchment characteristic that dominates how catchments partition, store and release water and consequently buffer potential climate change impacts. In general, the climate forcing dominates the hydrological response of a catchment. Nevertheless, the analysis of the extreme scenarios proofed, that land use can have a considerable impact on the partitioning of precipitation into evapotranspiration and runoff. As an adaptation strategy to climate change, a change in crop cultivation practises in the form of an earlier start and a later end of the growing season of overall less intensity showed that an intra-annual shift in actual evapotranspiration and runoff can be triggered. The impact of climate change based on the STAR + 2K scenario cannot, however, be compensated.

Based on the results of the trend analysis and the ensemble-based modelling approach, it can be concluded that a decrease in natural water yield is of high probability during the next decades, especially during summer months, in the Lusatian river catchments. The climate change impact will be further superimposed by the decrease in mining drainage discharge aggravating already existing water user conflicts. These facts highlight the necessity for long term planning for a sustainable river basin management under the consideration of climate change. A long term adaptation planning requires, however, the cooperation of authorities across different institutions and national states. The German federal system of responsibilities based on states rather than on the natural unit of a river catchment aggravates an integrated water management planning and calls for the establishment of the river basin association as for example already existing in other parts of Germany (ERFTVERBAND, 2014; RUHRVERBAND, 2014) which face, due to long term mining activities in the past, similar challenges (GRÜNEWALD, 2012a). In addition, the lack of sufficient resources both in term of funding as well as well-qualified human staff represents another big threat for a successful integrated catchment management and planning for climate change adaptation in the Lusatian river catchments. Already under current climate conditions, the local authorities are overstrained with the current challenges related to water quality (high concentration of sulphate and iron oxides in the river systems), quantity (flood and low-flow management, flooding of post mining lakes with surface water) and mining related hazards (stabilization of the dumped substrate).

Overall, land use change can serve as one part of an integrated climate change adaptation strategy. Such as strategy needs, depending on the severity of the climate change impact, to include other, especially technical measures of water resources management, such as additional water storage, different strategies to manage the existing and new reservoirs. It may also consider additional water transfers from neighbouring, more water rich, river catchments. These measures, requiring long term planning and high investment costs, should be implemented regardless of the impact of climate change by also considering the trans-regional relevance, for example for the water supply of the German capital of Berlin and lignite-fired power plants located in the study region.

Furthermore, the prevailing water quality issues, which are a result of the long term mining activities in Lusatia, need to be considered in the development of suitable adaptation strategies to climate change. Thus, so-called flexible “low-regret” adaptation strategies need to be considered that lead to an overall improvement of the tense water situation in the catchment and alleviate the already existing water user conflicts (FÜSSEL, 2007; GRÜNEWALD, 2012b). Adaptation strategies should also not only consider climate change but also other aspects of global change which may even be of higher relevance during the next decades than climate change.

Last but not least, in communication with stakeholders, it has to be stressed that scenario-based climate change impact studies will always remain highly uncertain. The uncertainty, should, however, not be used as a justification of no action because adaptation planning may also be based on other approaches, such as a risk or vulnerability based approach proposed by WILBY and DESSAI (2010) in order to ensure sustainable river basin management in the Lusatian river catchments.

10 Outlook

There is great potential to further extend the research presented in this study. Therefore, key future research needs are outlined:

- **Trend analysis for change detection:** The trend analysis could be extended by analysing not only changes in the mean, but also to changes in the variance and extremes. Changes in extremes are particularly relevant for regional stakeholder because they can potentially cause large economic damage. Another focus could be on analysing different time periods in order to judge the sensitivity of the results based on the time series length chosen. The MASH (moving average over shifting horizons) approach of ANGHILERI et al. (2014) seems also promising to simultaneously investigate changes in seasonality and to filter out effects of inter-annual variability. Moreover, long term persistence in the time series should be considered and its relation to trend significance testing as pointed out, among others, by KOUTSOYIANNIS and MONTANARI (2007). Including new approaches, such as the one proposed by ROUGÉ et al. (2013), that represent a combination of the Mann-Kendall and the Pettitt test directly focussing on differentiating between gradual changes and change points could also be included and provide further insight into the nature of the trends.
- **Hydrological modelling:** Concerning the hydrological models, structural model improvements, such as cell to cell routing of interflow, are seen as one option to improve the simulation results. In the context of climate change impact assessments, the implementation of dynamic parameters which are not static but change according to changes in the climate forcing would allow the direct consideration of non-stationarity in hydrological modelling. This would, however, require extensive knowledge on the interrelation of each parameter with the climatic forcing as well as the interrelation of the parameters with each other making a unique solution almost unfeasible. Therefore, in a simplified form, such an approach could be tested for a simple model having only few model parameters.

The existing model set up for WaSiM-ETH (and HBV-light) could further be validated on measured groundwater levels in order to further verify that internal catchment processes, related to, for example, surface-groundwater interaction are simulated reliably as well as to improve low-flow representation. Moreover, additional data, such as soil moisture measurements, refined soil and land use maps which would be especially beneficial for the land use change analysis as well as additional meteorological station data could further improve model parameterisation.

- **Hydrological climate change impact assessments:** Due to the complexity of the climate system, climate change impact assessments will always remain highly uncertain. Therefore, improving climate models, both GCMs and DA, especially in terms of structure and resolution is of high relevance for decreasing uncertainties related to climate change impact assessments. Moreover, feedback between the different modelling steps should be considered which would require coupling of all the models within the climate change modelling chain (GCM, DA, hydrological model etc). Such an approach is desirable but, in terms of computer power, not (yet) feasible. Moreover, most feedbacks, especially related to vegetation and those taking place across different system boundaries, are yet not or only poorly understood.

Apart from that, the incorporation of additional DAs, which should preferably be based also on different GCMs in order to meaningfully extend the ensemble, could i) even increase the uncertainty bandwidth or, as would be desired, ii) decrease the uncertainty when more model members agree on the same direction of change. Another way to improve the currently available RCMs is to bias-correct the GCMs output before it is used as boundary conditions to drive the RCMs. The bias-correction used in this study (linear scaling approach) could also be extended or substituted by more sophisticated bias-correction methods, such as distribution mapping for all meteorological variables. Such approaches are generally preferred over the simple linear scaling as the whole statistical distribution is adjusted which could improve the representativity of extremes, such as low-flows. Another option is to include probabilistic climate forecasts, consisting of several hundred model runs and therefore requiring large computation effort. According to RÖSSLER (2011), such an approach is favourable when working with regional stakeholders and practitioners as they have more experience dealing with probabilities than with bandwidth or ranges of possible values. However, if probabilistic climate forecasts are themselves more reliable remains questionable.

- **Land use change analysis:** The land use change analysis could be extended by different scenarios for crop rotation focussing on specific crops and spatial arrangements. The application of the dynamic vegetation module of WaSiM-ETH which allows the dynamic calculation of plant development is also promising with regard to climate change impact assessments. Using this module, temperature-induced variations in the timing of phenological phases are dynamically calculated (SCHULLA and JASPER, 2012). So far, feedback between vegetation and climate are not explicitly accounted for in WaSiM-ETH and land use parameterisation is based on a static approach. For the application, additional data on, for example length of dormancy, would be necessary for initial model validation. In addition, soil hydraulic parameters should be adjusted according to the land use type as suggested by RIEGER and DISSE (2013).

Apart from the modelling uncertainties related to the DA and the hydrological models which have been considered in this study, factors related to economic and social development are often extremely difficult to predict, not to mention to quantify, but may in many cases even be more relevant and have an even bigger impact on the water resources in a river catchment. Due to the complexity of the interplay between societies and water resources, the new PUB initiative “Phanta Rhei – Everything flows” (2013-2022) focusses on changes in the dynamics of the water cycle in connection with rapidly changing human systems (MONTANARI et al., 2013).

11 References

- Abbott, M.B., Bathurst, J.C., Cunge, J.A., O'Connell, P.E., Rasmussen, J., 1986. An introduction to the European Hydrological System - Systeme Hydrologique Europeen, "SHE", 1: History and philosophy of a physically-based, distributed modelling system. *Journal of Hydrology*, 87(1-2): 45-59.
- Abdul Aziz, O.I., Burn, D.H., 2006. Trends and variability in the hydrological regime of the Mackenzie River Basin. *Journal of Hydrology*, 319(1-4): 282-294.
- Adamowski, K., Prokoph, A., Adamowski, J., 2009. Development of a new method of wavelet aided trend detection and estimation. *Hydrological Processes*, 23(18): 2686-2696.
- Adger, W.N., Barnett, J., 2009. Four reasons for concern about adaptation to climate change. *Environment and Planning A*, 41(12): 2800-2805.
- Afzal, M., Mansell, M.G., Gagnon, A.S., 2011. Trends and variability in daily precipitation in Scotland. *Procedia Environmental Sciences*, 6: 15-26.
- Ali, G., Tetzlaff, D., Soulsby, C., McDonnell, J.J., Capell, R., 2012. A comparison of similarity indices for catchment classification using a cross-regional dataset. *Advances in Water Resources*, 40: 11-22.
- Allen, C.D., Macalady, A.K., Chenchouni, H., Bachelet, D., McDowell, N., Vennetier, M., Kitzberger, T., Rigling, A., Breshears, D.D., Hogg, E.H., Gonzalez, P., Fensham, R., Zhang, Z., Castro, J., Demidova, N., Lim, J.-H., Allard, G., Running, S.W., Semerci, A., Cobb, N., 2010. A global overview of drought and heat-induced tree mortality reveals emerging climate change risks for forests. *Forest Ecology and Management*, 259(4): 660-684.
- Almasri, A., Locking, H., Shukur, G., 2008. Testing for climate warming in Sweden during 1850–1999, using wavelets analysis. *Journal of Applied Statistics*, 35(4): 431-443.
- Andersen, J., Refsgaard, J.C., Jensen, K.H., 2001. Distributed hydrological modelling of the Senegal River Basin — model construction and validation. *Journal of Hydrology*, 247(3–4): 200-214.
- Anghileri, D., Pianosi, F., Soncini-Sessa, R., 2014. Trend detection in seasonal data: from hydrology to water resources. *Journal of Hydrology*, 511: 171-179.
- Arnell, N.W., 1992. Factors controlling the effects of climate change on river flow regimes in a humid temperate environment. *Journal of Hydrology*, 132(1–4): 321-342.
- Arnold, J.G., Allen, P.M., Bernhardt, G., 1993. A comprehensive surface-groundwater flow model. *Journal of Hydrology*, 142(1–4): 47-69.
- Arnold, J.G., Srinivasan, R., Muttiah, R.S., Williams, J.R., 1998. Large area hydrologic modelling and assessment part I: model development. *JAWRA Journal of the American Water Resources Association*, 34(1): 73-89.

- Askew, A.J., 1987. Climate change and water resources. The influence of climate change and climate variability on the hydrologic regime and water resources. IAHS Publication, 168: 421-430.
- ASTER DEM, 2009. Advanced spaceborne thermal emission and reflection radiometer, <http://asterweb.jpl.nasa.gov/gdem.asp> (last access: 11.12.2013).
- Bach, W., 1979. Impact of increasing atmospheric CO₂ concentrations on global climate: Potential consequences and corrective measures. *Environment International*, 2(4–6): 215-228.
- Barkhordarian, A., Bhend, J., von Storch, H., 2011. Consistency of observed near surface temperature trends with climate change projections over the Mediterranean region. *Climate Dynamics*, 38(9): 1695-1702.
- Bates, B., Kundzewicz, Z.W., Wu, S., Palutikof, J.P., 2008. *Climate Change and Water*. Technical Paper of the Intergovernmental Panel on Climate Change. IPCC Secretariat, Geneva, 210 pp.
- Beard, L.R., Maristancy, A., 1979. *Hydrological Effects of Climate Change*. Center for Research in Water Resources, Austin University of Texas, 52 pp.
- Bergström, S., 1976. Development and application of a conceptual runoff model for Scandinavian catchments. Swedish Meteorological and Hydrological Institute, Norrköping, 134 pp.
- Bergström, S., 1992. *The HBV Model: Its structure and applications*. Swedish Meteorological and Hydrological Institute Norrköping, 35 pp.
- Beven, K., 1993. Prophecy, reality and uncertainty in distributed hydrological modelling. *Advances in Water Resources*, 16(1): 41-51.
- Beven, K., 2001. *Rainfall-Runoff Modelling. The Primer*. John Wiley & Sons, Chichester, 360 pp.
- Beven, K., 2006. A manifesto for the equifinality thesis. *Journal of Hydrology*, 320(1-2): 18-36.
- Beven, K., 2011. I believe in climate change but how precautionary do we need to be in planning for the future? *Hydrological Processes*, 25(9): 1517-1520.
- Beven, K., Binley, A., 1992. The future of distributed models - Model calibration and uncertainty prediction. *Hydrological Processes*, 6(3): 279-298.
- Beven, K., Lamb, R., Quinn, P., Romanowicz, R., Freer, J., 1995. TOPMODEL. In: Singh, V.P. (Ed.), *Computer Models of watershed hydrology*. Water Resources Publications, Highlands Ranch, Colorado, USA, pp. 627-668.
- Beven, K.J., Kirkby, M.J., 1979. A physically based, variable contributing area model of basin hydrology / Un modèle à base physique de zone d'appel variable de l'hydrologie du bassin versant. *Hydrological Sciences Bulletin*, 24(1): 43-69.

- Birkel, C., Soulsby, C., Tetzlaff, D., 2012. Modelling the impacts of land-cover change on streamflow dynamics of a tropical rainforest headwater catchment. *Hydrological Sciences Journal*, 57(8): 1543-1561.
- Birsan, M.-V., Molnar, P., Burlando, P., Pfaundler, M., 2005. Streamflow trends in Switzerland. *Journal of Hydrology*, 314(1-4): 312-329.
- Bloomfield, P., Steiger, W.L., 1983. *Least Absolute Deviations: Theory, Applications, and Algorithms*. Progress in Probability and Statistics. Birkhäuser, Boston, Massachusetts, USA, 351 pp.
- Blöschl, G., Montanari, A., 2010. Climate change impacts – throwing the dice? *Hydrological Processes*, 24: 374-381.
- Böhm, U., Keuler, K., Österle, H., Kücken, M., Hauffe, D., 2008. Quality of a climate reconstruction for the CADSES regions. *Meteorologische Zeitschrift*, 17(4): 477-485.
- Boneau, C.A., 1960. The effects of violations of assumptions underlying the t test. *Psychological Bulletin*, 57(1): 49-64.
- Bormann, H., 2009. Analysis of possible impacts of climate change on the hydrological regimes of different regions in Germany. *Advances in Geosciences*, 21: 3-11.
- Bormann, H., 2011. Sensitivity analysis of 18 different potential evapotranspiration models to observed climatic change at German climate stations. *Climatic Change*, 104(3-4): 729-753.
- Bormann, H., Ahlhorn, F., Klenke, T., 2012. Adaptation of water management to regional climate change in a coastal region – Hydrological change vs. community perception and strategies. *Journal of Hydrology*, 454–455: 64-75.
- Bronstert, A., Kolokotronis, V., Schwandt, D., Straub, H., 2007. Comparison and evaluation of regional climate scenarios for hydrological impact analysis: General scheme and application example. *International Journal of Climatology*, 27(12): 1579-1594.
- Budyko, M.I., 1989. Empirical estimates of imminent climatic changes. *Soviet Meteorology and Hydrology*, 10: 1-8.
- BÜK 200, 2007. *Bodenübersichtskarte Sachsens 1:200000*. Sächsisches Landesamt für Umwelt, Landwirtschaft und Geologie (LFULG). Referat Bodenschutz: Abteilung Natur, Landschaft, Boden.
- BÜK 300, 2007. *Bodenübersichtskarte des Landes Brandenburgs 1:300000*. Landesamt für Geowissenschaften und Rohstoffe Brandenburg (LBGR) in Zusammenarbeit mit dem Landesvermessungsamt Brandenburg (LGB), Dezernat Bodengeologie.

- BÜK 1000, 1998. Bodenübersichtskarte der Bundesrepublik Deutschland 1:1000000, Bundesanstalt für Geowissenschaften und Rohstoffe. http://www.geoshop-hannover.de/is-bin/INTERSHOP.enfinity/WFS/port_bgr/de_DE/-/EUR/OG_ViewProductDetails-View;sid=Dq2QtNOuCqornYExC6n0t9Kk1FWpnVtuGCNSxN2BnuWxPJfEGL1BvvT8zN2emw==?ProductRef=bgr_DE-GD-0041%40port_bgr&OG_MainIDs=20602&PageableID=filteredCategories_Dq2QtNOuCqornYExC6n0t9Kk1FWpnVtuGCNSxN2BnuWxPJfEGL1BvvT8zN2emw%3d%3d&PageableName=Categories&PageID=0&Availability=true&CategoryID=Boden (last access: 03.12.2013).
- Bunce, J.A., 2004. Carbon dioxide effects on stomatal responses to the environment and water use by crops under field conditions. *Oecologia*, 140(1): 1-10.
- Burn, D.H., 1994. Hydrologic effects of climatic change in west-central Canada. *Journal of Hydrology*, 160(1-4): 53-70.
- Burn, D.H., Hag Elnur, M.A., 2002. Detection of hydrologic trends and variability. *Journal of Hydrology*, 255(1-4): 107-122.
- Burns, D.A., Klaus, J., McHale, M.R., 2007. Recent climate trends and implications for water resources in the Catskill Mountain region, New York, USA. *Journal of Hydrology*, 336(1-2): 155-170.
- Calanca, P., Roesch, A., Jasper, K., Wild, M., 2006. Global warming and the summertime evapotranspiration regime of the alpine region. *Climatic Change*, 79(1-2): 65-78.
- Chandler, R.E., Scott, E.M., 2011. *Statistical Methods for Trend Detection and Analysis in the Environmental Sciences*. Wiley, Chichester, United Kingdom, 368 pp.
- Christensen, J., Carter, T., Rummukainen, M., Amanatidis, G., 2007. Evaluating the performance and utility of regional climate models: the PRUDENCE project. *Climatic Change*, 81: 1-6.
- Clarke, R.T., 2010. On the (mis)use of statistical methods in hydro-climatological research. *Hydrological Sciences Journal*, 55(2): 139-144.
- CLC, 1990. CORINE Land Cover, European Environment Agency. <http://www.eea.europa.eu/data-and-maps/data/corine-land-cover-1990-raster-2> (last access: 03.12.2013).
- CLC, 2006. CORINE Land Cover, European Environment Agency. <http://www.eea.europa.eu/data-and-maps/data/corine-land-cover-2006-raster-2> (last access: 03.12.2013).
- Cleveland, W.S., 1979. Robust locally weighted regression and smoothing scatterplots. *Journal of the American Statistical Association*, 76: 829-836.
- Cleveland, W.S., Devlin, S.J., 1988. Locally weighted regression: an approach to regression analysis by local fitting. *Journal of the American Statistical Association*, 83: 596-610.

- Conradt, T., Koch, H., Hattermann, F., Wechsung, F., 2012. Spatially differentiated management-revised discharge scenarios for an integrated analysis of multi-realisation climate and land use scenarios for the Elbe River basin. *Regional Environmental Change*, 12(3): 633-648.
- Cooper, C.F., 1978. What might man-induced climate change mean? *Foreign Affairs*, 56: 500-520.
- Cullmann, J., Krausse, T., Saile, P., 2011. Parameterising hydrological models – Comparing optimisation and robust parameter estimation. *Journal of Hydrology*, 404(3–4): 323-331.
- Cunderlik, M.J., 2003. Hydrologic model selection for the CFCAS project: Assessment of water resources risk and vulnerability to changing climatic conditions. Project Report I. University of Western Ontario, Canada.
- Dai, A., 2013. Increasing drought under global warming in observations and models. *Nature Clim. Change*, 3(1): 52-58.
- Delgado, J.M., Apel, H., Merz, B., 2010. Flood trends and variability in the Mekong river. *Hydrology and Earth System Sciences*, 14(3): 407-418.
- Déqué, M., Rowell, D., Lüthi, D., Giorgi, F., Christensen, J., Rockel, B., Jacob, D., Kjellström, E., de Castro, M., van den Hurk, B., 2007. An intercomparison of regional climate simulations for Europe: assessing uncertainties in model projections. *Climatic Change*, 81: 53-70.
- Dessai, S., Hulme, M., Lember, R., Pielke Jr., R., 2009. Climate prediction: a limit to adaptation? In: Adger, W.N., Lorenzoni, I., O'Brien, K. (Eds.), *Adaptation to Climate Change: Thresholds, Values, Governance*. Cambridge University Press, Cambridge, pp. 64-78.
- Dietrich, O., Redetzky, M., Schwärzel, K., 2007. Wetlands with controlled drainage and subirrigation systems—modelling of the water balance. *Hydrological Processes*, 21(14): 1814-1828.
- Dietrich, O., Steidl, J., Pavlik, D., 2012. The impact of global change on the water balance of large wetlands in the Elbe Lowland. *Regional Environmental Change*, 12(4): 701-713.
- DIN 4220, 2008. Pedologic site assessment - designation, classification and deduction of soil parameters (normative and nominal scaling). Beuth Verlag, Berlin.
- Dingman, S.L., 2008. *Physical Hydrology*. Waveland Press, 656 pp.
- Doherty, J., 2004. PEST Model-independent parameter estimation. *Watermark Numerical Computing*, 279 pp.
- Donohue, R.J., Roderick, M.L., McVicar, T.R., 2007. On the importance of including vegetation dynamics in Budyko's hydrological model. *Hydrology and Earth System Sciences*, 11(2): 983-995.
- Douglas, E.M., Vogel, R.M., Kroll, C.N., 2000. Trends in floods and low flows in the United States: impact of spatial correlation. *Journal of Hydrology*, 240(1-2): 90-105.

- Drebenstedt, C., Möckel, R., 1998. Gewässer in der Bergbaufolgelandschaft. In: Pflug, W. (Ed.), Braunkohlentagebau und Rekultivierung. Springer, Berlin - Heidelberg - New York, pp. 610-624.
- Duan, Q., Sorooshian, S., Gupta, H.V., 1992. Effective and efficient global optimization for conceptual rainfall-runoff models. *Water Resources Research*, 28(4): 1015-1031.
- DVWK, 1983. Niedrigwasseranalyse Teil I: Statistische Untersuchung des Niedrigwasser-Abflusses. Deutscher Verbund für Wasserwirtschaft und Kulturbau, Fachausschuss "Niedrigwasser", Parey Verlag.
- Ehsanzadeh, E., Ouarda, T.B.M.J., Saley, H.M., 2011. A simultaneous analysis of gradual and abrupt changes in Canadian low streamflows. *Hydrological Processes*, 25(5): 727-739.
- Elfert, S., Bormann, H., 2010. Simulated impact of past and possible future land use changes on the hydrological response of the Northern German lowland 'Hunte' catchment. *Journal of Hydrology*, 383(3-4): 245-255.
- Engeland, K., Gottschalk, L., Tallaksen, L.M., 2001. Estimation of regional parameters in a macro scale hydrological model. *Nordic Hydrology*, 32(3): 161-180.
- Enke, W., Deutschländer, T., Schneider, F., Küchler, W., 2005a. Results of five regional climate studies applying a weather pattern based downscaling method to ECHAM4 climate simulation. *Meteorologische Zeitschrift*, 14(2): 247-257.
- Enke, W., Schneider, F., Deutschländer, T., 2005b. A novel scheme to derive optimized circulation pattern classifications for downscaling and forecast purposes. *Theoretical and Applied Climatology*, 82(1-2): 51-63.
- Erftverband, 2014. <http://www.erftverband.de/> (last access: 01.03.2014).
- Feddes, R.A., Kowalik, P., Kolinska-Malinka, K., Zaradny, H., 1976. Simulation of field water uptake by plants using a soil water dependent root extraction function. *Journal of Hydrology*, 31(1-2): 13-26.
- Feldmann, A.D., 2000. Hydrologic Modeling System HEC-HMS, Technical Reference Manual. U.S. Army Corps of Engineers, Hydrologic Engineering Center, HEC, Davis, California, USA.
- Feyen, L., Dankers, R., 2009. Impact of global warming on streamflow drought in Europe. *Journal of Geophysical Research: Atmospheres*, 114(D17): D17116.
- Foley, J.A., DeFries, R., Asner, G.P., Barford, C., Bonan, G.B., Carpenter, S.R., Chapin, F.S., Coe, M.T., Daily, G.C., Gibbs, H.K., Helkowski, J.H., Holloway, T., Howard, E.A., Kucharik, C.J., Monfreda, C., Patz, J.A., Prentice, I.C., Ramankutty, N., Snyder, P.K., 2005. Global consequences of land use. *Science*, 309(5734): 570-574.
- Fowler, H.J., Blenkinsop, S., Tebaldi, C., 2007. Linking climate change modelling to impacts studies: recent advances in downscaling techniques for hydrological modelling. *International Journal of Climatology*, 27(12): 1547-1578.

- Fowler, H.J., Ekström, M., Kilsby, C.G., Jones, P.D., 2005. New estimates of future changes in extreme rainfall across the UK using regional climate model integrations. 1. Assessment of control climate. *Journal of Hydrology*, 300(1–4): 212-233.
- Freer, J., Beven, K., Ambrose, B., 1996. Bayesian estimation of uncertainty in runoff prediction and the value of data: An application of the GLUE approach. *Water Resources Research*, 32(7): 2161-2173.
- Frei, C., Christensen, J.H., Déqué, M., Jacob, D., Jones, R.G., Vidale, P.L., 2003. Daily precipitation statistics in regional climate models: Evaluation and intercomparison for the European Alps. *Journal of Geophysical Research: Atmospheres*, 108(D3): 4124.
- Frei, C., Schöll, R., Fukutome, S., Schmidli, J., Vidale, P.L., 2006. Future change of precipitation extremes in Europe: Intercomparison of scenarios from regional climate models. *Journal of Geophysical Research: Atmospheres*, 111(D6): D06105.
- Fuhrer, J., Beniston, M., Fischlin, A., Frei, C., Goyette, S., Jasper, K., Pfister, C., 2006. Climate risks and their impact on agriculture and forests in Switzerland. *Climatic Change*, 79(1): 79-102.
- Füssel, H.M., 2007. Adaptation planning for climate change: concepts, assessment approaches, and key lessons. *Sustainability Science*, 2(2): 265-275.
- Gädeke, A., Hölzel, H., Koch, H., Grünewald, U., 2012a. Analysis of uncertainties related to regional climate and hydrological models on the water balance in a subcatchment of the Spree river, Germany. In: Hinkelmann, R. et al. (Eds.), *HIC 2012 - 10th International Conference on Hydroinformatics: "Understanding Changing Climate and Environment and Finding Solutions"*, July 14.-18. 2012, Hamburg.
- Gädeke, A., Pohle, I., Hölzel, H., Koch, H., Grünewald, U., 2012b. Analyse zum Einfluss des Landschafts- und Klimawandels auf den Wasserhaushalt in einem Teileinzugsgebiet der Spree. In: Grünewald, U. et al. (Eds.), *Wasserbezogene Anpassungsmaßnahmen an den Landschafts- und Klimawandel*. Schweizerbart, Stuttgart, pp. 81-94.
- Gao, H.K., He, X.B., Ye, B.S., Pu, J.C., 2012. Modeling the runoff and glacier mass balance in a small watershed on the Central Tibetan Plateau, China, from 1955 to 2008. *Hydrological Processes*, 26(11): 1593-1603.
- Gauger, C., 2007. *Wasserhaushaltsmodellierung in Flachlandinzugsgebieten der Weser unter spezieller Berücksichtigung der Oberflächen-Grundwasser-Interaktion*, Diplomarbeit, Albert-Ludwigs-Universität Freiburg, 120 pp.
- Gebremicael, T.G., Mohamed, Y.A., Betrie, G.D., van der Zaag, P., Teferi, E., 2013. Trend analysis of runoff and sediment fluxes in the Upper Blue Nile basin: A combined analysis of statistical tests, physically-based models and landuse maps. *Journal of Hydrology*, 482: 57-68.
- Gellens, D., 2000. Trend and correlation analysis of k-day extreme precipitation over Belgium. *Theoretical and Applied Climatology*, 66(1-2): 117-129.

- Germer, S., Kaiser, K., Bens, O., Hüttl, R.F., 2011. Water balance changes and responses of ecosystems and society in the Berlin-Brandenburg region - a review. *Erde*, 142(1-2): 65-95.
- Gerstengarbe, F.W., Badeck, F., Hattermann, F., Krysanova, V., Lahmer, W., Lasch, P., Stock, M., Suckow, F., Wechsung, F., Werner, P.C., 2003. Studie zur klimatischen Entwicklung im Land Brandenburg bis 2055 und deren Auswirkungen auf den Wasserhaushalt, die Forst- und Landwirtschaft sowie die Ableitung erster Perspektiven. Potsdam-Institut für Klimafolgenforschung, PIK Report 83, Potsdam.
- GLOWA ELBE, 2013. Auswirkungen des globalen Wandels auf Umwelt und Gesellschaft im Elbegebiet, <http://www.glowa-elbe.de/german/index-en.htm> (last access: 03.12.2013).
- Graham, L., Andreasson, J., Carlsson, B., 2007a. Assessing climate change impacts on hydrology from an ensemble of regional climate models, model scales and linking methods - a case study on the Lule River basin. *Climatic Change*, 81: 293-307.
- Graham, L., Hagemann, S., Jaun, S., Beniston, M., 2007b. On interpreting hydrological change from regional climate models. *Climatic Change*, 81: 97-122.
- Grossmann, M., Dietrich, O., 2012. Integrated economic-hydrologic assessment of water management options for regulated wetlands under conditions of climate change: A case study from the Spreewald (Germany). *Water Resources Management*, 26(7): 2081-2108.
- Grünewald, U., 2001a. Wasserwirtschaftliche Planungen. In: Lecher, K., Lühr, H.-P., Zanke, U. (Eds.), *Taschenbuch der Wasserwirtschaft*. Paul Rarey Verlag, Berlin, pp. 1123-1163.
- Grünewald, U., 2001b. Water resources management in river catchments influenced by lignite mining. *Ecological Engineering*, 17(2-3): 143-152.
- Grünewald, U., 2010. Wasserbilanzen der Region Berlin-Brandenburg. Material der Interdisziplinären Arbeitsgruppen IAG Globaler Wandel - Regionale Entwicklung, Diskussionspapier 7, Berlin-Brandenburgische Akademie der Wissenschaften, Berlin.
- Grünewald, U., 2012a. Landschaftswandel in der Lausitz: Bergbau(folgen) und Wasser - gestern, heute und morgen. In: Grünewald, U. et al. (Eds.), *Wasserbezogene Anpassungsmaßnahmen an den Landschafts- und Klimawandel*. Schweizerbart, Stuttgart, pp. 44-53.
- Grünewald, U., 2012b. Wasserbezogene Anpassungsmaßnahmen an den Landschafts- und Klimawandel in Deutschland - eine Einführung. In: Grünewald, U., Bens, O., Fischer, H., Hüttl, R.F., Knierim, A. (Eds.), *Wasserbezogene Anpassungsmaßnahmen an den Landschafts- und Klimawandel*. Schweizerbart, Stuttgart, pp. 2-12.
- Guerreiro, S.B., Kilsby, C.G., Serinaldi, F., 2014. Analysis of time variation of rainfall in transnational basins in Iberia: abrupt changes or trends? *International Journal of Climatology*, 34(1): 114-133.
- Gurtz, J., Zappa, M., Jasper, K., Lang, H., Verbunt, M., Badoux, A., Vitvar, T., 2003. A comparative study in modelling runoff and its components in two mountainous catchments. *Hydrological Processes*, 17(2): 297-311.

- Gustard, A., 1983. Regional variability of soil characteristics for flood and low flow estimation. *Agricultural Water Management*, 6(2–3): 255-268.
- Hamlet, A.F., Lettenmaier, D.P., 2000. Long-range climate forecasting and its use for water management in the Pacific Northwest region of North America. *Journal of Hydroinformatics*, 2: 163-182.
- Hattermann, F.F., Weiland, M., Huang, S., Krysanova, V., Kundzewicz, Z.W., 2011. Model-supported impact assessment for the water sector in Central Germany under climate change - A case study. *Water Resources Management*, 25(13): 3113-3134.
- Henderson-Sellers, A., 1993. An antipodean climate of uncertainty? *Climatic Change*, 25(3-4): 203-224.
- Hindley, D.R., 1973. The definition of dry weather flow in river flow measurement. *J. Inst. Wat. Eng. Sci.*, 27: 438-440.
- Hirsch, R.M., Slack, J.R., 1984. A nonparametric trend test for seasonal data with serial dependence. *Water Resources Research*, 20(6): 727-732.
- Hirsch, R.M., Slack, J.R., Smith, R.A., 1982. Techniques of trend analysis for monthly water quality data. *Water Resources Research*, 18: 107-121.
- Hölting, B., Coldewey, W., 2009. *Hydrogeologie: Einführung in die Allgemeine und Angewandte Hydrogeologie*, 7. Spektrum, 383 pp.
- Hölzel, H., 2011. Analyse und Parametrisierung von Landnutzungseigenschaften zur Modellierung von Abfluss, Bodenerosion und Sedimentation im Einzugsgebiet des Wahnbachs (Bergisches Land). E. Ferger Verlag, Bergisch Gladbach, 184 pp.
- Hölzel, H., Diekkrüger, B., 2011. Predicting the impact of linear landscape elements on surface runoff, soil erosion, and sedimentation in the Wahnbach catchment, Germany. *Hydrological Processes*, 26(11): 1642-1654.
- Hölzel, H., Diekkrüger, B., Biemelt, D., Gädeke, A., 2013. Impact of dumped sediment structures on hydrological modelling in the artificial Chicken Creek catchment, Germany. *Journal of Hydrology*, 477: 189-202.
- Hölzel, H., Rössler, O., Diekkrüger, B., 2011. Grope in the Dark – Hydrological modelling of the artificial Chicken Creek catchment without validation possibilities. *Physics and Chemistry of the Earth, Parts A/B/C*, 36(1–4): 113-122.
- Hörmann, G., Horn, A., Fohrer, N., 2005. The evaluation of land-use options in mesoscale catchments: Prospects and limitations of eco-hydrological models. *Ecological Modelling*, 187(1): 3-14.
- Huang, S., 2012. *Modelling of environmental change impacts on water resources and hydrological extremes in Germany*, Dissertation, Universität Potsdam, Potsdam, 206 pp.
- Huang, S., Hattermann, F., Krysanova, V., Bronstert, A., 2013a. Projections of climate change impacts on river flood conditions in Germany by combining three different RCMs with a regional eco-hydrological model. *Climatic Change*, 116(3-4): 631-663.

- Huang, S., Krysanova, V., Hattermann, F., 2013b. Projection of low flow conditions in Germany under climate change by combining three RCMs and a regional hydrological model. *Acta Geophysica*, 61(1): 151-193.
- Huang, S., Krysanova, V., Österle, H., Hattermann, F., 2010. Simulation of spatiotemporal dynamics of water fluxes in Germany under climate change. *Hydrological Processes*, 24(23): 3289-3306.
- HÜK 200, 2007. Hydrogeologische Übersichtskarte Deutschlands 1:200000. Sächsisches Landesamt für Umwelt, Landwirtschaft und Geologie (LFULG). Referat 105, Freiberg.
- Huxol, S., 2007. Trendanalyse von Zeitreihen der Komponenten des Wasserkreislaufes im Einzugsgebiet der Dreisam zur prozessorientierten Beurteilung hydrologischer Klimafolgen. Diplom Thesis, Diplomarbeit, Albert-Ludwigs-Universität Freiburg, Freiburg, 77 pp.
- IfWW, 1959. N-A-U Karte 1921-1940 über das Gebiet der Deutschen Demokratischen Republik 1:200 000. N: Niederschlagshöhen und -gleichen, A; Abflusshöhen und -gleichen, Unterschiedswerte und -gleichen, Abflüsse und Abflussspenden. Berlin, Institut für Wasserwirtschaft.
- INKA BB, 2009. Innovationsnetzwerk Klimaanpassung Berlin Brandenburg, <http://www.inka-bb.de/> (last access: 10.01.2012).
- IPCC, 2000. Special report on emission scenarios. Cambridge University Press, 570 pp.
- IPCC, 2007. Climate change 2007: The physical science basis. contribution of working group I to the fourth assessment report of the intergovernmental panel on climate change. In: Solomon, S. et al. (Eds.). Cambridge University Press, Cambridge, United Kingdom and New York, USA, pp. 996.
- Jacob, D., 2001. A note to the simulation of the annual and inter-annual variability of the water budget over the Baltic Sea drainage basin. *Meteorology and Atmospheric Physics*, 77(1): 61-73.
- Jacob, D., Van den Hurk, B.J.J.M., Andrae, U., Elgered, G., Fortelius, C., Graham, L.P., Jackson, S.D., Karstens, U., Köpken, C., Lindau, R., Podzun, R., Rockel, B., Rubel, F., Sass, B.H., Smith, R.N.B., Yang, X., 2001. A comprehensive model inter-comparison study investigating the water budget during the BALTEX-PIDCAP period. *Meteorology and Atmospheric Physics*, 77(1-4): 19-43.
- Jansson, P.E., Karlberg, L., 2001. Coupled heat and mass transfer model for soilplant-atmosphere system, ftp://www.lwr.kth.se/CoupModel/coupmanual_2004.pdf (last access: 03.02.2014).
- Jasper, K., 2005. Hydrological modelling of alpine river catchments using output variables from atmospheric models PhD Thesis, Dissertation, Eidgenössische Technische Hochschule, Zürich, 138 pp.
- Jasper, K., 2010. Personal Email contact.

- Jasper, K., Calanca, P., Fuhrer, J., 2006. Changes in summertime soil water patterns in complex terrain due to climatic change. *Journal of Hydrology*, 327(3-4): 550-563.
- Jasper, K., Gurtz, J., Lang, H., 2002. Advanced flood forecasting in Alpine watersheds by coupling meteorological observations and forecasts with a distributed hydrological model. *Journal of Hydrology*, 267(1-2): 40-52.
- Jiang, T., Chen, Y.D., Xu, C.-Y., Chen, X., Chen, X., Singh, V.P., 2007. Comparison of hydrological impacts of climate change simulated by six hydrological models in the Dongjiang Basin, South China. *Journal of Hydrology*, 336(3-4): 316-333.
- Jun, M., Knutti, R., Nychka, D.W., 2008. Spatial analysis to quantify numerical model bias and dependence. *Journal of the American Statistical Association*, 103(483): 934-947.
- Jung, I.W., Moradkhani, H., Chang, H., 2012. Uncertainty assessment of climate change impacts for hydrologically distinct river basins. *Journal of Hydrology*, 466-467: 73-87.
- Kallache, M., Rust, H.W., Kropp, J., 2005. Trend assessment: applications for hydrology and climate research. *Nonlinear Processes in Geophysics*, 12(2): 201-210.
- Kampata, J.M., Parida, B.P., Moalafhi, D.B., 2008. Trend analysis of rainfall in the headstreams of the Zambezi River Basin in Zambia. *Physics and Chemistry of the Earth, Parts A/B/C*, 33(8-13): 621-625.
- Kavetski, D., Kuczera, G., Franks, S.W., 2006. Calibration of conceptual hydrological models revisited: 1. Overcoming numerical artefacts. *Journal of Hydrology*, 320(1-2): 173-186.
- Kay, A.L., Davies, H., Bell, V., Jones, R., 2009. Comparison of uncertainty sources for climate change impacts: flood frequency in England. *Climatic Change*, 92(1): 41-63.
- Kelly, P.M., 1979. Towards the prediction of climate. *Endeavour*, 3(4): 176-182.
- Kemfert, C., 2003. The role of uncertainty in integrated assessment climate change modeling. In: Gottschalk-Mazouz, N., Mozouz, N. (Eds.), *Nachhaltigkeit und globaler Wandel. Integrative Forschung zwischen Normativität und Unsicherheit*. Campus, Frankfurt am Main, New York, pp. 121-140.
- Kendall, M.G., 1975. *Rank Correlation Methods*. Charles Griffin, London.
- Kinal, J., Stoneman, G.L., 2012. Disconnection of groundwater from surface water causes a fundamental change in hydrology in a forested catchment in south-western Australia. *Journal of Hydrology*, 472-473: 14-24.
- Klein, R.J.T., Schipper, E.L.F., Dessai, S., 2005. Integrating mitigation and adaptation into climate and development policy: three research questions. *Environmental Science & Policy*, 8(6): 579-588.
- Klemes, V., 1986. Operational testing of of hydrological simulation. *Hydrological Sciences*, 28: 2029-39.
- Knutti, R., 2008. Should we believe model predictions of future climate change? . *Philosophical Transactions of the Royal Society of London, Series A*, 366(1885): 4647-4664.

- Koch, H., Kaltofen, M., Grünewald, U., Messner, F., Karkuschke, M., Zwirner, O., Schramm, M., 2005. Scenarios of water resources management in the Lower Lusatian mining district, Germany. *Ecological Engineering*, 24(1-2): 49-57.
- Koch, H., Vögele, S., Kaltofen, M., Grünewald, U., 2012. Trends in water demand and water availability for power plants—scenario analyses for the German capital Berlin. *Climatic Change*, 110(3): 879-899.
- Köplin, N., Schädler, B., Viviroli, D., Weingartner, R., 2013. The importance of glacier and forest change in hydrological climate-impact studies. *Hydrology and Earth System Sciences*, 17(2): 619-635.
- Köplin, N., Viviroli, D., Schädler, B., Weingartner, R., 2010. How does climate change affect mesoscale catchments in Switzerland? - a framework for a comprehensive assessment. *Advances in Geosciences*, 27: 111-119.
- Koutsoyiannis, D., 2003. Climate change, the Hurst phenomenon, and hydrological statistics. *Hydrological Sciences Journal*, 48(1): 3-24.
- Koutsoyiannis, D., Montanari, A., 2007. Statistical analysis of hydroclimatic time series: Uncertainty and insights. *Water Resources Research*, 43(5): W05429.
- Krause, P., Boyle, D.P., Bäse, F., 2005. Comparison of different efficiency criteria for hydrological model assessment. *Advances in Geosciences*, 5: 89-97.
- Krause, S., Bronstert, A., 2007. The impact of groundwater–surface water interactions on the water balance of a mesoscale lowland river catchment in northeastern Germany. *Hydrological Processes*, 21(2): 169-184.
- Kreienkamp, F., Baumgart, S., Spekat, A., Enke, W., 2011. Climate signals on the regional scale derived with a statistical method: relevance of the driving model's resolution. *Atmosphere*, 2(2): 129-145.
- Krysanova, V., Dickens, C., Timmerman, J., Varela-Ortega, C., Schlüter, M., Roest, K., Huntjens, P., Jaspers, F., Buiteveld, H., Moreno, E., Pedraza Carrera, J., Slámová, R., Martínková, M., Blanco, I., Esteve, P., Pringle, K., Pahl-Wostl, C., Kabat, P., 2010. Cross-comparison of climate change adaptation strategies across large river basins in Europe, Africa and Asia. *Water Resources Management*, 24(14): 4121-4160.
- Krysanova, V., Müller-Wohlfeil, D.I., Becker, A., 1998. Development and test of a spatially distributed hydrological/water quality model for mesoscale watersheds. *Ecological Modelling*, 106(2-3): 261-289.
- Kundzewicz, Z.W., Mata, L.J., Arnell, N.W., Döll, P., Kabat, P., Jiménez, B., Miller, K.A., Oki, T., Sen, Z., Shiklomanov, I.A., 2007. Freshwater resources and their management. In: Parry, M.L., Canziani, O.F., Palutikof, J.P., van der Linden, P.J., Hanson, C.E. (Eds.), *Climate change 2007: Impacts, adaptation and vulnerability. Contribution of working group II to the fourth assessment report of the Intergovernmental Panel on Climate Change*. Cambridge University Press, Cambridge, UK, pp. 173-210.

- Kundzewicz, Z.W., Robson, A.J., 2004. Change detection in hydrological records - a review of the methodology. *Hydrological Sciences Journal*, 49(1): 7-19.
- Leander, R., Buishand, T.A., van den Hurk, B.J.J.M., de Wit, M.J.M., 2008. Estimated changes in flood quantiles of the river Meuse from resampling of regional climate model output. *Journal of Hydrology*, 351(3-4): 331-343.
- Legates, D.R., McCabe, G.J., 1999. Evaluating the use of "goodness-of-fit" Measures in hydrologic and hydroclimatic model validation. *Water Resources Research*, 35(1): 233-241.
- Lenderink, G., Buishand, A., van Deursen, W., 2007. Estimates of future discharges of the river Rhine using two scenario methodologies: direct versus delta approach. *Hydrology and Earth System Sciences*, 11(3): 1145-1159.
- Lettenmaier, D.P., 1976. Detection of trends in water quality data from records with dependent observations. *Water Resources Research*, 12(5): 1037-1046.
- Lettenmaier, D.P., Wood, E.F., Wallis, J.R., 1994. Hydro-climatological trends in the continental United States, 1948-88. *Journal of Climate*, 7(4): 586-607.
- LfULG, 2012. Wasserhaushaltsportal Sachsen - Analyse von Durchflussreihen 1951-2005, <http://141.30.240.113/lenya/kliwes/live/index/Wasserhaushalt/SaeuleA/Durchflussreihen.html> (last access: 01.10.2012).
- LfULG, 2013. Saxon State Agency of Environment Agriculture and Geology, GIS Data for Saxony, <http://www.umwelt.sachsen.de/umwelt/wasser/6021.htm> (last access: 11.12.2013).
- Li, Z.L., Xu, Z.X., Li, J.Y., Li, Z.J., 2008. Shift trend and step changes for runoff time series in the Shiyang River basin, northwest China. *Hydrological Processes*, 22(23): 4639-4646.
- Lischeid, G., 2013. Panta rhei - Wechselwirkungen zwischen Landnutzung, Klimawandel und Wasserhaushalt. *Bundesanstalt für Gewässerkunde, Koblenz*, pp. 83-88.
- Lischeid, G., Natkhin, M., 2011. The potential of land-use change to mitigate water scarcity in northeast Germany - a review. *Erde*, 142(1-2): 97-113.
- Lopez, A., Fung, F., New, M., Watts, G., Weston, A., Wilby, R.L., 2009. From climate model ensembles to climate change impacts and adaptation: A case study of water resource management in the southwest of England. *Water Resources Research*, 45(8): W08419.
- LUGV, 2013. Ministry of Environment, Health and Consumer Protection of the Federal State of Brandenburg, Luis BB - Geodata Brandenburg, <http://www.mugv.brandenburg.de/cms/detail.php/bb1.c.310481.de> (last access: 11.12.2013).
- Ma, Z., Kang, S., Zhang, L., Tong, L., Su, X., 2008. Analysis of impacts of climate variability and human activity on streamflow for a river basin in arid region of northwest China. *Journal of Hydrology*, 352(3-4): 239-249.

- Machlica, A., Horvat, O., Horacek, S., Oosterwijk, J., Van Loon, A.F., Fendekova, M., Van Lanen, H.A.J., 2012. Influence of model structure on base flow estimation using BILAN, FRIER and HBV-LIGHT model. *Journal of Hydrology and Hydromechanics*, 60(4): 242-251.
- Majewski, D., 1991. The Europa-Modell of the Deutscher Wetterdienst. ECMWF Seminar on numerical methods in atmospheric models, 2: 147-191.
- Mamun, A.A., Hashim, A., Daoud, J.I., 2010. Regionalisation of low flow frequency curves for the Peninsular Malaysia. *Journal of Hydrology*, 381(1–2): 174-180.
- Mann, H.B., 1945. Non-parametric test against trend. *Econometrica*, 13: 245–259.
- Mann, H.B., Whitney, D.R., 1947. On a test of whether one of two random variables is stochastically larger than the other. *Annals of Mathematical Statistics*, 18: 50-60.
- Manning, R., 1890. On the flow of water in open channels and pipes. *Trans. Inst. Civ. Eng. Irel.*, 20: 161-207.
- Marchetto, A., Rogora, M., Arisci, S., 2013. Trend analysis of atmospheric deposition data: A comparison of statistical approaches. *Atmospheric Environment*, 64(0): 95-102.
- Maurer, E., 2007. Uncertainty in hydrologic impacts of climate change in the Sierra Nevada, California, under two emissions scenarios. *Climatic Change*, 82(3): 309-325.
- Maurer, T., 1997. Physikalisch begründete, zeitkontinuierliche Modellierung des Wassertransports in kleinen ländlichen Einzugsgebieten, Dissertation, Universität Fridericiana zu Karlsruhe, 212 pp.
- McCabe, G.J., Wolock, D.M., 2002. A step increase in streamflow in the conterminous United States. *Geophysical Research Letters*, 29(24): 2185.
- McCarthy, J.J., Canziani, O.F., Leary, N.A., Dokken, D.J., White, K.S., 2001. Climate change 2001: impacts, adaptation and vulnerability. Contribution of Working Group II to the Third Assessment Report of the Intergovernmental Panel on Climate Change. In: McCarthy, J.J., Canziani, O.F., Leary, N.A., Dokken, D.J., White, K.S. (Eds.). Cambridge University Press, Cambridge, UK.
- Mein, R.G., Brown, B.M., 1978. Sensitivity of optimized parameters in watershed models. *Water Resources Research*, 14(2): 299-303.
- Merz, B., Maurer, T., Kaiser, K., 2012. Wie gut können wir vergangene und zukünftige Veränderungen des Wasserhaushalts quantifizieren? (How well can we quantify past and future changes of the water cycle?). *Hydrologie und Wasserbewirtschaftung*, 56(5): 244-256.
- Merz, C., Pekdeger, A., 2011. Anthropogenic changes in the landscape hydrology of the Berlin-Brandenburg region. *Erde*, 142(1-2): 21-39.
- Merz, R., Parajka, J., Blöschl, G., 2009. Scale effects in conceptual hydrological modeling. *Water Resources Research*, 45(9): W09405.
- Merz, R., Parajka, J., Blöschl, G., 2011. Time stability of catchment model parameters: Implications for climate impact analyses. *Water Resources Research*, 47(2): W02531.

- Milly, P.C.D., Betancourt, J., Falkenmark, M., 2008. Climate change: stationarity is dead: Whither water management? *Science*, 319(5863): 573-574.
- Montanari, A., Young, G., Savenije, H.H.G., Hughes, D., Wagener, T., Ren, L.L., Koutsoyiannis, D., Cudennec, C., Toth, E., Grimaldi, S., Blöschl, G., Sivapalan, M., Beven, K., Gupta, H., Hipsey, M., Schaefli, B., Arheimer, B., Boegh, E., Schymanski, S.J., Di Baldassarre, G., Yu, B., Hubert, P., Huang, Y., Schumann, A., Post, D.A., Srinivasan, V., Harman, C., Thompson, S., Rogger, M., Viglione, A., McMillan, H., Characklis, G., Pang, Z., Belyaev, V., 2013. "Panta Rhei—Everything Flows": Change in hydrology and society—The IAHS Scientific Decade 2013–2022. *Hydrological Sciences Journal*, 58(6): 1256-1275.
- Monteith, J.L., 1975. *Vegetation and the atmosphere, vol. 1: Principles*. Academic Press, London, 298 pp.
- Monteith, J.L., Unsworth, M.H., 1990. *Principles of Environmental Physics. Second Edition*. Edward Arnold, London, 422 pp.
- Moussa, R., Chahinian, N., Bocquillon, C., 2007. Distributed hydrological modelling of a Mediterranean mountainous catchment – Model construction and multi-site validation. *Journal of Hydrology*, 337(1–2): 35-51.
- Murphy, J.M., Sexton, D.M.H., Barnett, D.N., Jones, G.S., Webb, M.J., Collins, M.T., Stainforth, D.A., 2004. Quantification of modelling uncertainties in a large ensemble of climate change simulations. *Nature*, 430(7001): 768-772.
- Najafi, M.R., Moradkhani, H., Jung, I.W., 2011. Assessing the uncertainties of hydrologic model selection in climate change impact studies. *Hydrological Processes*, 25(18): 2814-2826.
- Nash, J.E., Sutcliffe, J.V., 1970. River flow forecasting through conceptual models part I — A discussion of principles. *Journal of Hydrology*, 10(3): 282-290.
- Nash, L.L., Gleick, P.H., 1991. Sensitivity of streamflow in the Colorado Basin to climatic changes. *Journal of Hydrology*, 125(3–4): 221-241.
- Natkin, M., Steidl, J., Dietrich, O., Dannowski, R., Lischeid, G., 2012. Differentiating between climate effects and forest growth dynamics effects on decreasing groundwater recharge in a lowland region in Northeast Germany. *Journal of Hydrology*, 448-449: 245-254.
- Němec, J., Schaake, J., 1982. Sensitivity of water resource systems to climate variation. *Hydrological Sciences Journal*, 27(3): 327-343.
- Nielsen, S.A., Hansen, E., 1973. Numerical simulation of the rainfall-runoff process on a daily basis. *Nordic Hydrology*, 4: 171-190.
- Oesterle, H., 2001. Reconstruction of daily global radiation for past years for use in agricultural models. *Physics and Chemistry of the Earth, Part B: Hydrology, Oceans and Atmosphere*, 26(3): 253-256.
- Oke, T.R., 1987. *Boundary Layer Climates*. Routledge London and New York, 435 pp.

- Orlowsky, B., Gerstengarbe, F.W., Werner, P.C., 2008. A resampling scheme for regional climate simulations and its performance compared to a dynamical RCM. *Theoretical and Applied Climatology*, 92(3): 209-223.
- Page, E.S., 1954. Continuous inspection scheme. *Biometrika*, 41(1/2): 100-115.
- Parkinson, C.L., Bindshadler, R.A., 1984. Response of Antarctic Sea ice to uniform atmospheric temperature increases. In: Hansen, J.E., Takahashi, T. (Eds.), *Climate Processes and Climate Sensitivity*. American Geophysical Union Monographie, Washington, D.C., pp. 265-264.
- Partal, T., Küçük, M., 2006. Long-term trend analysis using discrete wavelet components of annual precipitations measurements in Marmara region (Turkey). *Physics and Chemistry of the Earth, Parts A/B/C*, 31(18): 1189-1200.
- Patrinos, A., Bamzai, A., 2005. Policy needs robust climate science. *Nature*, 438(7066): 285-285.
- Pettitt, A.N., 1979. A non-parametric approach to the change-point problem. *Applied Statistics*, 28(2): 126-135.
- Pielke, R.A., 2005. Land use and climate change. *Science*, 310(5754): 1625-1626.
- Pielke, R.A., Prins, G., Rayner, S., Sarewitz, D., 2007. Climate change 2007: Lifting the taboo on adaptation. *Nature*, 445(7128): 597-598.
- Plate, E.J., Zehe, E., 2008. *Hydrologie und Stoffdynamik kleiner Einzugsgebiete - Prozesse und Modelle*. Schweizerbartsche Verlagsbuchhandlung, Altenburg, 366 pp.
- Plesca, I., Timbe, E., Exbrayat, J.F., Windhorst, D., Kraft, P., Crespo, P., Vache, K.B., Frede, H.G., Breuer, L., 2012. Model intercomparison to explore catchment functioning: Results from a remote montane tropical rainforest. *Ecological Modelling*, 239: 3-13.
- Press, W.H., Flannery, B.P., Teukolsky, S.A., Vetterling, W.T., 1992. *Numerical recipes in FORTRAN: The art of scientific computing*. Cambridge University Press, Cambridge, Great Britain, 963 pp.
- R, 2011. The R project for statistical computing. <http://www.r-project.org/> (last access: 12.03.2013).
- R MASS Package, 2013. <http://cran.r-project.org/web/packages/MASS/MASS.pdf> (last access: 05.02.2013).
- Raghavan, S.V., Vu, M.T., Liong, S.-Y., 2012. Assessment of future stream flow over the Sesan catchment of the Lower Mekong Basin in Vietnam. *Hydrological Processes*, 26(24): 3661-3668.
- Refsgaard, J.C., 1987. A methodology for distinguishing between the effects of human influence and climatic variability on the hydrologic cycle. *IAHS Publication*, 168: 557-570.
- Refsgaard, J.C., Storm, B., 1995. MIKE-SHE. In: Singh, V.P. (Ed.), *Computer models of watershed hydrology*. Water Resources Publications, Highlands Ranch, Colorado, USA, pp. 809-846.

- Reyer, C., Bachinger, J., Bloch, R., Hattermann, F., Ibisch, P., Kreft, S., Lasch, P., Lucht, W., Nowicki, C., Spathelf, P., Stock, M., Welp, M., 2011. Climate change adaptation and sustainable regional development: a case study for the Federal State of Brandenburg, Germany. *Regional Environmental Change*, 12(3): 523-542.
- Rieger, W., Disse, M., 2013. Physikalisch basierter Modellansatz zur Beurteilung der Wirksamkeit einzelner und kombinierter dezentraler Hochwasserschutzmaßnahmen (A physically-based model approach to assess the effectiveness of single and combined measures of decentralized flood protection). *Hydrologie und Wasserbewirtschaftung*, 57(1): 14 – 25.
- Rockel, B., Will, A., Hense, A., 2008. The regional climate model COSMO-CLM (CCLM). *Meteorologische Zeitschrift*, 17: 347-348.
- Roeckner, E., Bauml, G., Bonaventura, L., Brokopf, R., Esch, M., Giorgetta, M., Hagemann, S., Kirchner, Kornblueh, L., Manzini, E., Rhodin, A., Schlese, U., Schulzweida, U., Tompkins, A., 2003. The atmospheric general circulation model ECHAM 5. PART I: model description, http://www.mpimet.mpg.de/fileadmin/publikationen/Reports/max_scirep_349.pdf (last access: 03.02.2014).
- Rosbjerg, D., Madsen, H., 2005. Concepts of hydrologic modeling. In: Anderson, M.G., McDonnell, J. (Eds.), *Encyclopaedia of Hydrological Sciences*. John Willey & Sons Lds., Chichester, pp. 155-163.
- Rosenberg, N.J., 1982. The increasing CO₂ concentration in the atmosphere and its implication on agricultural productivity II. Effects through CO₂-induced climatic change. *Climatic Change*, 4(3): 239-254.
- Rössler, O., 2011. A Climate Change Impact Assessment Study on Mountain Soil Moisture with Emphasis on Epistemic Uncertainties Dissertation, Universität Bonn, Bonn, 105 pp.
- Rössler, O., Diekkrüger, B., Löffler, J., 2012. Potential drought stress in a Swiss mountain catchment - Ensemble forecasting of high mountain soil moisture reveals a drastic decrease, despite major uncertainties. *Water Resources Research*, 48(4): W04521.
- Rougé, C., Ge, Y., Cai, X., 2013. Detecting gradual and abrupt changes in hydrological records. *Advances in Water Resources*, 53: 33-44.
- Rounsevell, M.D.A., Ewert, F., Reginster, I., Leemans, R., Carter, T.R., 2005. Future scenarios of European agricultural land use: II. Projecting changes in cropland and grassland. *Agriculture, Ecosystems & Environment*, 107(2–3): 117-135.
- Rousseeuw, P.J., Leroy, A.M., 1987. *Robust Regression and Outlier Detection*. Wiley, New York, USA, 335 pp.
- Ruhrverband, 2014. <http://www.ruhrverband.de/en/home/> (last access: 01.03.2014).
- Rybski, D., Neumann, J., 2011. A review on the Pettitt test In: Kropp, J., Schellnhuber, H.-J. (Eds.), *In Extremis*. Springer Berlin Heidelberg, pp. 202-213.

- Santoso, H., Idinoba, M., Imbach, P., 2008. Climate scenarios: What we need to know and how to generate them. Center for International Forestry Research (CIFOR), CIFOR Working Paper No.45, Bogor, Indonesia, 27 pp.
- Scherzer, J., Pöhler, H., Jasper, K., Sames, D., 2006. KliWEP - Abschätzung der Auswirkungen der für Sachsen prognostizierten Klimaveränderungen auf den Wasser- und Stoffhaushalt im Einzugsgebiet der Parthe Teil 2: Weiterentwicklung von WaSiM-ETH sowie Durchführung von Testsimulationen. Sächsisches Staatsministerium für Umwelt und Landwirtschaft, Leipzig.
- Schneider, S.H., 1983. CO₂, climate and society: A brief overview. In: Chen, R.S., Boulding, E., Schneider, S.H. (Eds.), Social science research and climate change. Springer Netherlands, pp. 9-15.
- Schneider, S.H., Chen, R.S., 1980. Carbon dioxide warming and coastline flooding: Physical factors and climatic impact. *Annual Review of Energy*, 5(1): 107-140.
- Schoenheinz, D., Grünewald, U., Koch, H., 2011. Aspects of Integrated Water Resources Management in River Basins Influenced by Mining Activities in Lower Lusatia. *Erde*, 142(1-2): 163-186.
- Schulla, J., 1997. Hydrologische Modellierung von Flussgebieten zur Abschätzung von Folgen von Klimaänderungen, Dissertation, Eidgenössische Technische Hochschule Zürich, 163 pp.
- Schulla, J., 2010. Personal Email contact.
- Schulla, J., Jasper, K., 2007. Model description WaSiM-ETH, http://www.wasim.ch/downloads/doku/wasim/wasim_2007_en.pdf (last access: 03.02.2014).
- Schulla, J., Jasper, K., 2012. Model description WaSiM-ETH, www.wasim.ch/downloads/doku/wasim/wasim_2012_ed2_en.pdf (last access: 03.02.2014).
- Schwarze, R., 1991. Rechnergestützte Analyse von Abflusskomponenten und Verweilzeiten in kleinen Einzugsgebieten. *Acta Hydrophysica*, 35(2): 143-184.
- Schwarze, R., Grünewald, U., Becker, A., Fröhlich, W., 1989. Computer-aided analyses of flow recessions and coupled basin water balance investigations. *IAHS Publication*, 187(78-83).
- Seibert, J., 1997. Estimation of parameter uncertainty in the HBV model. *Nordic Hydrology*, 28: 247-262.
- Seibert, J., 1999. Regionalisation of parameters for a conceptual rainfall-runoff model. *Agricultural and Forest Meteorology*, 98-99: 279-293.
- Seibert, J., 2000. Multi-criteria calibration of a conceptual runoff model using a genetic algorithm. *Hydrology and Earth System Sciences*, 4(2): 215-224.
- Seibert, J., 2003. Reliability of model predictions outside calibration conditions. *Nordic Hydrology*, 34: 477-492.

- Seibert, J., 2005. HBV-light. User's manual.
http://people.su.se/~jseib/HBV/HBV_manual_2005.pdf (last access: 05.12.2013).
- Seibert, J., Vis, M.J.P., 2012. Teaching hydrological modeling with a user-friendly catchment-runoff-model software package. *Hydrol. Earth Syst. Sci. Discuss.*, 9(5): 5905-5930.
- Sen, P.K., 1968. Estimates of the regression coefficient based on Kendall's tau. *Journal of the American Statistical Association*, 63(324): 1379–1389.
- Senatore, A., Mendicino, G., Smiatek, G., Kunstmann, H., 2011. Regional climate change projections and hydrological impact analysis for a Mediterranean basin in Southern Italy. *Journal of Hydrology*, 399(1-2): 70-92.
- Sennikovs, J., Bethers, U., 2009. Statistical downscaling method of regional climate model results for hydrological modelling. In: Anderssen, R.S., Braddock, R.D., Newham, L.T.H. (Eds.), 18th World IMACS Congress and MODSIM09 International Congress on Modelling and Simulation. Modelling and Simulation Society of Australia and New Zealand and International Association for Mathematics and Computers in Simulation, Cairns, Australia, pp. 3962-3968.
- Sevruk, B., 1986. Correction of precipitation measurements. *Geographische Schriften*, 23: Zürich.
- Shadmani, M., Marofi, S., Roknian, M., 2012. Trend analysis in reference evapotranspiration using Mann-Kendall and Spearman's Rho tests in arid regions of Iran. *Water Resources Management*, 26(1): 211-224.
- Sicard, P., Dalstein-Richier, L., Vas, N., 2011. Annual and seasonal trends of ambient ozone concentration and its impact on forest vegetation in Mercantour National Park (South-eastern France) over the 2000–2008 period. *Environmental Pollution*, 159(2): 351-362.
- Simon, M., Bekele, V., Kulasová, B., Maul, C., Oppermann, R., Řehák, P., 2005. Die Elbe und ihr Einzugsgebiet - Ein geographisch-hydrologischer und wasserwirtschaftlicher Überblick, <http://www.ikse-mkol.org/index.php?id=210> (last access: 03.02.2014).
- Singh, V.P., 1995. *Computer Models of Watershed Hydrology* Water Resources Publications, Highlands Ranch, Colorado, USA, 1130 pp.
- Skjelkvåle, B.L., Mannio, J., Wilander, A., Andersen, T., 1999. Recovery from acidification of lakes in Finland, Norway and Sweden 1990–1999. *Hydrology and Earth System Sciences*, 5(3): 327-338.
- SLFS, 2012. Statistisches Landesamt des Freistaates Sachsen, Regionaldata Kreisstatistik Sachsen, Landwirtschaft,
<http://www.statistik.sachsen.de/apps1/Kreistabelle/jsp/KREISAGS.jsp?Jahr=2012&Ags=14625000#zur%C3%BCck272> (last access: 01.03.2013).
- Smakhtin, V.U., 2001. Low flow hydrology: a review. *Journal of Hydrology*, 240(3-4): 147-186.
- Spekat, A., Kreienkamp, F., Enke, W., 2010. An impact-oriented classification method for atmospheric patterns. *Physics and Chemistry of the Earth, Parts A/B/C*, 35(9-12): 352-359.

- Stahl, K., Hisdal, H., Hannaford, J., Tallaksen, L.M., van Lanen, H.A.J., Sauquet, E., Demuth, S., Fendekova, M., Jódar, J., 2010. Streamflow trends in Europe: evidence from a dataset of near-natural catchments. *Hydrology and Earth System Sciences*, 14(12): 2367-2382.
- Steele-Dunne, S., Lynch, P., McGrath, R., Semmler, T., Wang, S., Hanafin, J., Nolan, P., 2008. The impacts of climate change on hydrology in Ireland. *Journal of Hydrology*, 356(1-2): 28-45.
- Strickler, A., 1923. Beiträge zur Frage der Geschwindigkeitsformel und der Rauigkeitszahl für Ströme, Kanäle und geschlossene Leitungen, 16. Mitteilungen des Eidgenössischen Amtes für Wasserwirtschaft, Bern, 357 pp.
- Surfleet, C.G., Tullos, D., 2013. Uncertainty in hydrologic modelling for estimating hydrologic response due to climate change (Santiam River, Oregon). *Hydrological Processes*, 27(25): 3560-3576.
- Svensson, C., Kundzewicz, Z.W., Maurer, T., 2005. Trend detection in river flow series: 2. Flood and low-flow index series *Hydrological Sciences Journal*, 50(5): 811-824.
- SWOT, 2014. 3. SWOT Analyse, INKA BB, TP 21. Internal document.
- Tabari, H., Somee, B.S., Zadeh, M.R., 2011. Testing for long-term trends in climatic variables in Iran. *Atmospheric Research*, 100(1): 132-140.
- Telisca, M., 2013. Study on global dimming generated by atmospheric aerosols. *Environmental Engineering and Management Journal*, 12(4): 747-750.
- Tetzlaff, D., Soulsby, C., Buttle, J., Capell, R., Carey, S.K., Laudon, H., McDonnell, J., McGuire, K., Seibert, J., Shanley, J., 2013. Catchments on the cusp? Structural and functional change in northern ecohydrology. *Hydrological Processes*, 27(5): 766-774.
- Teutschbein, C., Seibert, J., 2010. Regional climate models for hydrological impact studies at the catchment scale: A review of recent modeling strategies. *Geography Compass*, 4(7): 834-860.
- Teutschbein, C., Seibert, J., 2012a. Bias correction of regional climate model simulations for hydrological climate-change impact studies: Review and evaluation of different methods. *Journal of Hydrology*, 456-457: 12-29.
- Teutschbein, C., Seibert, J., 2012b. Is bias correction of Regional Climate Model (RCM) simulations possible for non-stationary conditions? *Hydrol. Earth Syst. Sci. Discuss.*, 9(11): 12765-12795.
- Teutschbein, C., Wetterhall, F., Seibert, J., 2011. Evaluation of different downscaling techniques for hydrological climate-change impact studies at the catchment scale. *Climate Dynamics*: 1-19.
- Thomas, B., Lischeid, G., Steidl, J., Dannowski, R., 2012. Regional catchment classification with respect to low flow risk in a Pleistocene landscape. *Journal of Hydrology*, 475: 392-402.

- Thomas, R.H., 1984. Ice sheet margins and ice shelves. In: Hansen, J.E., Takahashi, T. (Eds.), *Climate Processes and Climate Sensitivity American Geophysical Union Monographie*, Washington, D.C.
- Thompson, N., Barrie, J.A., Ayles, M., 1981. The Meteorological Office rainfall and evaporation calculation system: MORECS. Meteorological Office, Great Britain, 69 pp.
- Troch, P.A., Martinez, G.F., Pauwels, V.R.N., Durcik, M., Sivapalan, M., Harman, C.J., Brooks, P.D., Gupta, H.V., Huxman, T., 2009. Climate and vegetation water use efficiency at catchment scales. *Hydrological Processes*, 23(16): 2409-2414.
- Uhlenbrook, S., 1999. Untersuchung und Modellierung der Abflussbildung in einem mesoskaligen Einzugsgebiet Band 10. Institut für Hydrologie, Freiburg, 201 pp.
- Uhlmann, W., Theiss, S., Nestler, W., Zimmermann, K., Claus, T., 2012. Weiterführende Untersuchungen zu den hydrochemischen und ökologischen Auswirkungen der Exfiltration von eisenhaltigen, saurem Grundwasser in die Kleine Spree und in die Spree, Projektphase 2: Präzisierung der Ursachen und Quellstärken für die hohe Eisenbelastung des Grundwassers, Teil 1: Erkundung. LMBV Studie.
- Van der Linden, P., Mitchell, J.F.B., 2009. ENSEMBLES: Climate change and its impacts: Summary of research and results from the ENSEMBLES project. Met Office Hadley Centre, Exeter, 160 pp.
- van der Perk, M., Bierkens, M.F.P., 1997. The identifiability of parameters in a water quality model of the Biebrza River, Poland. *Journal of Hydrology*, 200(1-4): 307-322.
- van Genuchten, M.T., 1980. A closed-form equation for predicting the hydraulic conductivity of unsaturated soils. *Soil Science Society of America Journal*, 44(5): 892-898.
- Varis, O., Kajander, T., Lemmelä, R., 2004. Climate and water: From climate models to water resources management and vice versa. *Climatic Change*, 66(3): 321-344.
- Velázquez, J.A., Schmid, J., Ricard, S., Muerth, M.J., Gauvin St-Denis, B., Minville, M., Chaumont, D., Caya, D., Ludwig, R., Turcotte, R., 2013. An ensemble approach to assess hydrological models' contribution to uncertainties in the analysis of climate change impact on water resources. *Hydrology and Earth System Sciences*, 17(2): 565-578.
- Venables, W.N., Ripley, B.D., 2002. *Modern Applied Statistics with S. Statistics and Computing*. Springer, New York, 497 pp.
- Verbunt, M., Zwaafink, M.G., Gurtz, J., 2005. The hydrologic impact of land cover changes and hydropower stations in the Alpine Rhine basin. *Ecological Modelling*, 187(1): 71-84.
- Villarini, G., Serinaldi, F., Smith, J.A., Krajewski, W.F., 2009. On the stationarity of annual flood peaks in the continental United States during the 20th century. *Water Resources Research*, 45(8): W08417.
- Villarini, G., Smith, J.A., 2010. Flood peak distributions for the eastern United States. *Water Resources Research*, 46(6): W06504.

- Villarini, G., Smith, J.A., Baeck, M.L., Vitolo, R., Stephenson, D.B., Krajewski, W.F., 2011. On the frequency of heavy rainfall for the Midwest of the United States. *Journal of Hydrology*, 400(1–2): 103-120.
- von Storch, H., 1995. Misuses of statistical analysis in climate research. In: Storch, V.H., Navarra, A. (Eds.), *Analysis of Climate Variability: Applications of Statistical Techniques*. Springer, Berlin, pp. 11–26.
- von Storch, H., 2009. On adaptation – a secondary concern? *The European Physical Journal Special Topics*, 176(1): 13-20.
- Vrochidou, A.E.K., Tsanis, I.K., Grillakis, M.G., Koutroulis, A.G., 2013. The impact of climate change on hydrometeorological droughts at a basin scale. *Journal of Hydrology*, 476: 290-301.
- Warrick, R.A., 1984. The possible impacts on wheat production of a recurrence of the 1930s drought in the U.S. Great Plains. *Climatic Change*, 6(1): 5-26.
- Wattenbach, M., Zebisch, M., Hattermann, F., Gottschalk, P., Goemann, H., Kreins, P., Badeck, F., Lasch, P., Suckow, F., Wechsung, F., 2007. Hydrological impact assessment of afforestation and change in tree-species composition – A regional case study for the Federal State of Brandenburg (Germany). *Journal of Hydrology*, 346(1–2): 1-17.
- Webb, A.A., Kathuria, A., Turner, L., 2012. Longer-term changes in streamflow following logging and mixed species eucalypt forest regeneration: The Karuah experiment. *Journal of Hydrology*, 464–465: 412-422.
- Wechsung, F., 2013. *Das Stadt-Land-Flussgebiet der Elbe projiziert in eine Plus-zwei-Grad-Welt*. Glowa Elbe Buch - unpublished.
- Wechsung, F., Lüttger, A., Hattermann, F.F., 2008. Projektionen zur klimabedingten Änderung der Erträge von einjährigen Sommer- und Winterkulturen des Ackerlandes am Beispiel von Silomais und Winterweizen. Die Ertragsfähigkeit ostdeutscher Ackerflächen unter Klimawandel., PIK-Report 112. Potsdam-Institut für Klimafolgenforschung, 18-22 pp.
- Wendling, U., Schellin, H.-G., Thomä, M., 1991. Bereitstellung von täglichen Informationen zum Wasserhaushalt des Bodens für die Zwecke der agrarmeteorologischen Beratung. *Zeitschrift für Meteorologie*, 41(6): 468-475.
- Wilby, R.L., Dawson, C.W., Barrow, E.M., 2002. SDSM - a decision support tool for the assessment of regional climate change impacts. *Environmental Modelling & Software*, 17(2): 145-157.
- Wilby, R.L., Dessai, S., 2010. Robust adaptation to climate change. *Weather*, 65(7): 180-185.
- Wilby, R.L., Harris, I., 2006. A framework for assessing uncertainties in climate change impacts: Low-flow scenarios for the River Thames, UK. *Water Resources Research*, 42(2): W02419.

- Wilby, R.L., Whitehead, P.G., Wade, A.J., Butterfield, D., Davis, R.J., Watts, G., 2006. Integrated modelling of climate change impacts on water resources and quality in a lowland catchment: River Kennet, UK. *Journal of Hydrology*, 330(1–2): 204-220.
- Wilcoxon, F., 1945. Individual Comparisons by Ranking Methods. *Biometrics Bulletin*, 1(6): 80-83.
- Wild, M., 2009. Global dimming and brightening: A review. *Journal of Geophysical Research: Atmospheres*, 114(D10): D00D16.
- Wilks, D.S., 2006. On “Field Significance” and the False Discovery Rate. *Journal of Applied Meteorology and Climatology*, 45(9): 1181-1189.
- WMO, 1974. *International Glossary of Hydrology*. World Meteorological Organization, Geneva.
http://www.wmo.int/pages/prog/hwrrp/publications/international_glossary/385_IGH_2012.pdf (last access: 15.05.2014).
- WMO, 2008. *Manual on Low-Flow Estimation and Prediction*. Operational hydrology report No 50, World Meteorological Organisation, Geneva. No. 1029, World Meteorological Organisation. http://www.wmo.int/pages/prog/hwrrp/publications/low-flow_estimation_prediction/WMO%201029%20en.pdf (last access: 15.05.2014).
- Wolfe, D.A., 2012. Nonparametrics: Statistical Methods Based on Ranks and Its Impact on the Field of Nonparametric Statistics. In: Rojo, J. (Ed.), *Selected Works of E. L. Lehmann*. *Selected Works in Probability and Statistics*. Springer US, pp. 1101-1110.
- Wood, E.F., 1978. Analyzing hydrologic uncertainty and its impact upon decision making in water resources. *Advances in Water Resources*, 1(5): 299-305.
- Xiong, L., Guo, S., 2004. Trend test and change-point detection for the annual discharge series of the Yangtze River at the Yichang hydrological station. *Hydrological Sciences Journal*, 49(1): 99-112.
- Xu, C.-Y., 1999a. Climate change and hydrologic models: A review of existing gaps and recent research developments. *Water Resources Management*, 13(5): 369-382.
- Xu, C.-Y., 1999b. From GCMs to river flow: a review of downscaling methods and hydrologic modelling approaches. *Progress in Physical Geography*, 23(2): 229-249.
- Xu, C.-Y., Widén, E., Halldin, S., 2005. Modelling hydrological consequences of climate change—Progress and challenges. *Advances in Atmospheric Sciences*, 22(6): 789-797.
- Yates, D.N., 1996. WatBal: An integrated water balance model for climate impact assessment of river basin runoff. *International Journal of Water Resources Development*, 12(2): 121-140.
- Yue, S., Pilon, P., Cavadias, G., 2002a. Power of the Mann–Kendall and Spearman's rho tests for detecting monotonic trends in hydrological series. *Journal of Hydrology*, 259(1–4): 254-271.

- Yue, S., Pilon, P., Phinney, B.O.B., 2003. Canadian streamflow trend detection: impacts of serial and cross-correlation. *Hydrological Sciences Journal*, 48(1): 51-63.
- Yue, S., Pilon, P., Phinney, B.O.B., Cavadias, G., 2002b. The influence of autocorrelation on the ability to detect trend in hydrological series. *Hydrological Processes*, 16(9): 1807-1829.
- Zehe, E., Maurer, T., Ihringer, J., Plate, E., 2001. Modeling water flow and mass transport in a loess catchment. *Physics and Chemistry of the Earth, Part B: Hydrology, Oceans and Atmosphere*, 26(7-8): 487-507.
- Zhang, S., Lu, X.X., Higgitt, D.L., Chen, C.-T.A., Han, J., Sun, H., 2008. Recent changes of water discharge and sediment load in the Zhujiang (Pearl River) Basin, China. *Global and Planetary Change*, 60(3-4): 365-380.

Acknowledgements

This thesis was integrated into the framework of the KLIMZUG project “Innovation Network Climate Change Adaption Brandenburg Berlin” (INKA BB, FZK: 01LR0803A) which was funded by the Federal Ministry of Education and Research (BMBF). I acknowledge the Potsdam Institute for Climate Impact Research, especially Ylva Hauf and Tobias Vetter, the Ministry of Environment, Health and Consumer Protection of the Federal State of Brandenburg (LUGV) and Saxon State Agency of Environment, Agriculture and Geology (LfULG) for data provision.

I would like to especially thank my supervisor Prof. Uwe Grünewald for his support, trust and encouragement. Thank you for giving me the freedom to try out different things. By that, I have had the valuable chance to create passion for my work and to get to know myself better.

I am very thankful to Prof. Markus Disse for being the second reviewer of this thesis and his interest in my work. Your suggestions really helped to improve the final thesis!

I would also like to thank all my actual and former colleagues at the department of Hydrology and Water Resources Research of the Brandenburg University of Technology. It has been great working with you! I would like to thank especially Dr. Dagmar Schoenheinz for being such an inspirational woman during my studies and so supportive as a colleague. I really appreciate your effort and guidance during the last year of this thesis!

I would like to thank Dr. Hagen Koch for supporting this work from the Potsdam Institute of Climate Impact Research. Thank you for always taking time to read and comment on my work as well as to share your experience.

I also acknowledge my former colleague Dr. Herwig Hölzel for teaching and introducing me to the world of hydrological modelling and supporting me even after leaving the university.

I would like to thank Dr. Jörg Schulla for his helpful support on the great hydrological model WaSiM-ETH which I hope to continue using in the future.

Ina Pohle, as a friend and colleague, I thank you for the many great and fun moments, talks and conference travels.

The biggest thank you I owe to my family. Thanks for always believing in and supporting me, but also reminding me of the really important things in life!

There are many more people who have contributed to this work in one way or the other. I will thank you personally!

Appendix

Content of appendix

Appendix A Data basis, data preparation and climate downscaling approaches

Appendix B Study areas

Appendix C Trend analysis for change detection

Appendix D Hydrological modelling

Appendix E Hydrological climate change impact assessments

Appendix F Land use change analysis

List of figures appendix

Figure B-1: Spatial distribution of land use (left) and soil type (right) in the Spree river catchment	B-1
Figure B-2: Spatial distribution of land use (left) and soil type (right) in the Schwarze Elster river catchment	B-1
Figure B-3: Long term (1963-2006) monthly sums of precipitation, potential evapotranspiration, average temperature and the climatic water balance in the study catchments	B-2
Figure B-4: Location of groundwater gauges and measured groundwater levels in the Dahme river catchment.....	B-3
Figure C-1: Maximum (top) and minimum (bottom) temperature (interpolated annual values) in the Spree and Schwarze Elster river catchments and trend interpretation (1951-2006).....	C-7
Figure C-2: Global radiation (interpolated annual values) in the Spree and Schwarze Elster river catchments and trend interpretation (1951-2006)	C-7
Figure C-3: Spatial distribution of mean temperature change points (1951-2006). The months were trends are above field significance are denoted with *	C-8
Figure C-4: Spatial distribution of mean temperature gradual trends (1951-2006). The months were trends are above field significance are denoted with *	C-9
Figure C-5: Maximum temperature (1951-2006): number of stations with significant and non-significant (a) positive and (b) negative trends, (c) number of significant trends and field significance for change points and gradual trends in the Spree (left) and Schwarze Elster (right) river catchments.....	C-10
Figure C-6: Minimum temperature (1951-2006): number of stations with significant and non-significant (a) positive and (b) negative trends, (c) number of significant trends and field significance for change points and gradual trends in the Spree (left) and Schwarze Elster (right) river catchments.....	C-11
Figure C-7: Spatial distribution of maximum temperature change points (1951-2006). The months were trends are above field significance are denoted with * (April only Spree)	C-12
Figure C-8: Spatial distribution of maximum temperature gradual trends (1951-2006). The months were trends are above field significance are denoted with *	C-13
Figure C-9: Spatial distribution of minimum temperature change points (1951-2006). The months were trends are above field significance are denoted with * (April and July only Schwarze Elster).....	C-14

Figure C-10: Spatial distribution of minimum temperature gradual trends (1951-2006). The months were trends are above field significance are denoted with * (July only Schwarze Elster).....	C-15
Figure C-11: Spatial distribution of potential evapotranspiration change points (1951-2006). Significant above field significance months are displayed in Figure 5-12.....	C-16
Figure C-12: Spatial distribution of potential evapotranspiration gradual trends (1951-2006). Significant above field significance months are displayed in Figure 5-10.....	C-17
Figure C-13: Spatial distribution of precipitation change points (1951-2006). In no month, field significance is reached	C-18
Figure C-14: Spatial distribution of precipitation gradual trends (1951-2006). In no month, field significance is reached	C-19
Figure C-15: Global radiation (1951-2006): number of stations with significant and non-significant (a) positive and (b) negative trends, (c) number of significant trends and field significance for change points and gradual trends in the Spree (left) and Schwarze Elster (right) river catchments.....	C-20
Figure C-16: Temperature (T), potential evapotranspiration (ETP), precipitation (P), runoff (R): interpolated annual sums and trend interpretation	C-21
Figure C-17: Mean temperature: Comparison of trend magnitude between measured and simulated temperature for the period 1961-2006 (top) and between simulations for the period 2015-2061 (bottom) for the subcatchments	C-23
Figure C-18: Precipitation: Comparison of trend magnitude between measured and simulated precipitation for the period 1961-2006 (top) and between simulations for the period 2015-2061 (bottom) for the subcatchments.....	C-24
Figure D-1: Model calibration for the Pulsnitz river catchment using WaSiM-ETH and HBV-light.....	D-9
Figure D-2: Model validation for the Pulsnitz river catchment using WaSiM-ETH and HBV-light.....	D-10
Figure D-3: Model calibration for the Weißer Schöps river catchment using WaSiM-ETH and HBV-light.....	D-11
Figure D-4: Model validation for the Weißer Schöps river catchment using WaSiM-ETH and HBV-light.....	D-12
Figure D-5: Model calibration for the Dahme river catchment using WaSiM-ETH and HBV-light.....	D-13

Figure D-6: Model validation for the Dahme river catchment using WaSiM-ETH and HBV-light.....	D-14
Figure E-1: Flow Duration Curve based on WaSiM-ETH and HBV-light driven by the DAs in the reference (1963-1991) and the scenario period (2032-2060) for the Pulsnitz and Dahme river catchments.....	E-6
Figure E-2: Change in the return period of the 50-year AM(7) between the reference and scenario for the the Pulsnitz and Dahme river catchments. The arrows in the Figure display the change in occurrence of the return period of the reference 50 year low-flow in the scenario period.....	E-7
Figure E-3: Difference in actual evapotranspiration (ETA) based on REMO (top left), CCLM (top right), STAR (bottom left) and WettReg (bottom right) between the scenario and reference period for the Weißer Schöps river catchment.....	E-9
Figure E-4: Difference in actual evapotranspiration (ETA) based on REMO (top left), CCLM (top right), STAR (bottom left) and WettReg (bottom right) between the scenario and reference period for the Dahme river catchment.....	E-10
Figure E-5: Difference in groundwater recharge (GWR) based on REMO (top left), CCLM (top right), STAR (bottom left) and WettReg (bottom right) between the scenario and reference period for the Weißer Schöps river catchment.....	E-11
Figure E-6: Difference in groundwater recharge (GWR) based on REMO (top left), CCLM (top right), STAR (bottom left) and WettReg (bottom right) between the scenario and reference period for the Dahme river catchment.....	E-12
Figure F-1: Potential (ETP), actual evapotranspiration (ETA) and discharge (Q) for current land use and changed agricultural parameterisation under current climate conditions (1963-1992) as well as the dry, moderate and wet climate realisation of STAR 2 K (2031-2060) in the Pulsnitz river catchment.....	F-5
Figure F-2: Potential (ETP), actual evapotranspiration (ETA) and discharge (Q) for current land use and changed agricultural parameterisation under current climate conditions (1963-1992) as well as the dry, moderate and wet climate realisation of STAR 2 K (2031-2060) in the Weißer Schöps river catchment	F-6
Figure F-3: Potential (ETP), actual evapotranspiration (ETA) and discharge (Q) for current land use and the combined effect of changed agricultural	

parameterisation and forest change under current climate conditions (1963-1992) as well as the dry, moderate and wet climate realisation of STAR 2 K (2031-2060) in the Dahme river catchment..... F-8

Figure F-4: Potential (ETP), actual evapotranspiration (ETA) and discharge (Q) for current land use and the combined effect of changed agricultural parameterisation and forest change under current climate conditions (1963-1992) as well as the dry, moderate and wet climate realisation of STAR 2 K (2031-2060) in the Pulsnitz river catchment..... F-9

List of tables appendix

Table A-1:	Data bases	A-1
Table A-2:	Site descriptions and locations of meteorological stations in the Schwarze Elster river catchment for the period 1951-2006	A-2
Table A-3:	Site descriptions and locations of meteorological stations in the Spree river catchment for the period 1951-2006	A-3
Table C-1:	Temperature (T), potential evapotranspiration (ETP), precipitation (P), runoff R: seasonal trend and significance (Mann-Kendall and Pettitt) analysis. Values highlighted in dark grey are significant at a level of 0.01, values in light grey at a level of 0.05	C-22
Table D-1:	Comparison of WaSiM-ETH and HBV-light as applied in this study	D-1
Table D-2:	Statistical performance indicators used for calibration and validation of runoff simulations	D-4
Table D-3:	Meteorological input variables for WaSiM-ETH.....	D-4
Table D-4:	Soil and land use model parameters defined for each grid cell.....	D-5
Table D-5:	Calibrated effective model parameters for WaSiM-ETH in the study catchments	D-6
Table D-6:	Calibrated effective model parameters for the different HBV-light model configurations in the study catchments.....	D-7
Table D-7:	Statistical performance indicators of discharge calibration and validation for *daily and ** long term mean monthly time step for the gauging stations located within the study catchments	D-8
Table E-1:	Comparison of measured and simulated precipitation [mm] and temperature [°C] on a daily, monthly and annual basis during the reference period (1963-1992)	E-1
Table E-2:	Long term water balance components [mm/a] for the Pulsnitz river catchment for the reference and scenario period as well as the difference between both.....	E-2
Table E-3:	Long term water balance components [mm/a] for the Weißer Schöps river catchment for the reference and scenario period as well as the difference between both.....	E-3
Table E-4:	Long term water balance components [mm/a] for the Dahme river catchment for the reference and scenario period as well as the difference between both.....	E-4
Table E-5:	MAM(7) and Q95 simulated by WaSiM-ETH and HBV-light driven by the different DAs for the reference and scenario period.....	E-5

Table E-6: P-value of Wilcoxon-Mann-Whitney test comparing the simulated discharge of the hydrological models during reference (ref) and scenario (scen) period concerning different hydrological indicators. Values highlighted in dark grey are significant at a level of 0.01 and light grey at a level of 0.05	E-8
Table F-1: Land use parameterisation in WaSiM-ETH.....	F-1
Table F-2: Water balance components [mm/a] for the extreme scenarios where the entire catchment areas are parameterised as coniferous forest and uncultivated land compared to the current land use under current climate conditions (1963-1992).....	F-4
Table F-3: Water balance components [mm/a] for current land use and change in agricultural cultivation under current climate conditions (1963-1992) and climate scenarios (2031-2060) in the Pulsnitz, Weißer Schöps and Dahme river catchments.....	F-7
Table F-4: Water balance components [mm/a] for current land use and the combined effect of changed agricultural parameterisation and forest change under current climate conditions (1963-1992) and climate scenarios (2031-2060) in the Pulsnitz and Dahme river catchments.....	F-10

Appendix A. Data basis, data preparation and climate downscaling approaches

Table A-1: Data bases

Data	Origin	Spatial resolution	Temporal resolution/Time span
Climate			
Meteorological measurements (wind speed [m/s], temperature [°C], global radiation [W/m ²], sunshine duration [-], relative humidity [%])	PIK (based on DWD data)	station based	daily (1951-2006)
Meteorological output from DAs	PIK	station and raster	daily values
Hydrology			
Hydrological measurements	LFULG, LUGV	station based	<u>Discharge:</u> <i>Weißer Schöps</i> 1) Initially: Gauges Särichen, Königshain, Holtendorf: 1999-2006 2) Later during the project: Gauge Särichen: 1963-2009 <i>Dahme</i> Gauges: Prierow 1961-2009; Dahme Stadt: 1974-2009 <i>Pulsnitz</i> Gauges: Ortrand: 1989-2009; Königsbrück: 1927-2009
Spatial Data Sets (DGM, soil, land use, hydrogeology)			
Digital Elevation Model	LFULG, ASTER ¹	100 m	2009
Soil Map (BK50, BÜK200, BÜK300, BÜK1000)	LFULG, LUGV	BK 50 1:5000 BÜK 200 1:200000 BÜK 300 1:300000 BÜK 1000 1:1000000	BK50: 2009 BÜK200: 2007 BÜK300: 2001 BÜK1000: 1998
Land Use data (CORINE Land Cover)	LFULG, Commission of the European Communities	100 m	2006 (used for hydrological modelling), 1990 (used for comparison)
Hydrogeological map (HÜK200)	LFULG, BGR		2007

¹ <http://asterweb.jpl.nasa.gov/gdem.asp>

Table A-2: Site descriptions and locations of meteorological stations in the Schwarze Elster river catchment (at all stations, the following daily meteorological input parameters were available: precipitation [mm], temperature (min, mean, max) [C°], global radiation [J/cm²], sunshine duration [h], wind speed [m/s], air humidity [%] , air pressure [hPa], cloudage [1/8]) for the period 1951-2006, (data provided by PIK)

Station ID	Site Name	PIK ID	Latitude	Longitude	Elevation
1	Annaburg	22128	51.73	13.05	75
2	Belgern	22114	51.48	13.12	120
3	Bethau	22129	51.67	13.00	78
4	Bischofswerda	23106	51.13	14.2	300
5	Coswig	22108	51.12	13.58	110
6	Dahme	22182	51.87	13.43	86
7	Danna-Eckmannsdorf	22184	52.00	12.90	113
8	Doberlug-Kirchhain	22002	51.65	13.58	100
9	Drebkau	23117	51.65	14.23	87
10	Dresden	22003	51.13	13.78	222
11	Elsterwerda	22124	51.47	13.53	91
12	Fürstlich Drehna	22180	51.75	13.80	77
13	Gröditz	22122	51.42	13.45	93
14	Herzberg (Elster)	22125	51.70	13.23	81
15	Hirschfeld *	22120	51.38	13.62	105
16	Hohenbuckow	22126	51.77	13.47	131
17	Hoyerswerda	23108	51.43	14.25	118
18	Jüterbog	22185	52.00	13.10	75.00
19	Kemnitz	22181	51.85	13.53	108
20	Kozsdorf	22115	51.50	13.23	87
21	Langebrück	22103	51.13	13.85	213
22	Lohsa	23111	51.38	14.42	125
23	Luga	23107	51.25	14.37	155
24	Oppach	23110	51.05	14.50	320
25	Peickwitz	22118	51.47	13.98	102
26	Petkus	22183	51.98	13.37	145
27	Pulsnitz *	23109	51.18	14.00	280
28	Radeburg *	22121	51.22	13.73	153
29	Riesa (West)	22113	51.30	13.25	142
30	Ruhland *	22119	51.45	13.87	98
31	Schönnewalde	22127	51.82	13.23	79
32	Skassa	22104	51.28	13.47	125
33	Sollschwitz	23105	51.35	14.22	132
34	Spremberg (Kläranlage)	23116	51.58	14.38	99
35	Torgau	22010	51.59	13.00	80
36	Übigau	22123	51.60	13.30	84
37	Zahna	22130	51.92	12.78	94

* stations used for analysis of the Pulsnitz river catchment (e.g. trend analysis, input for the hydrological models)

Table A-3: Site descriptions and locations of meteorological stations in the Spree river catchment (at all stations, the following daily meteorological input parameters were available: precipitation [mm], temperature (min, mean, max) [C°], global radiation [J/cm²], sunshine duration [h], wind speed [m/s], air humidity [%] , air pressure [hPa], cloudage [1/8]) for the period 1951-2006, (data provided by PIK)

Station ID	Site Name	PIK ID	Latitude	Longitude	Elevation
1	Bad Muskau	23102	51.55	14.72	125
2	Beeskow	18106	52.17	14.25	43
3	Berlin Dahlem	17001	52.47	13.30	51
4	Berlin Schönefeld	17003	52.38	13.53	46
5	Berlin Tempelhof	17002	52.46	13.40	48
6	Berlin Lichterfelde-Ost	17117	52.42	13.33	45
7	Bischofswerda	23106	51.13	14.20	300
8	Burg (Spreevald)	23118	51.83	14.15	55
9	Cottbus	23001	51.78	14.32	70
10	Dahme **	22182	51.87	13.43	86
11	Drebkau	23117	51.65	14.23	87
12	Frankfurt Oder	18110	52.37	14.53	48
13	Fürstenwalde (Spree)	18109	52.35	14.07	38
14	Fürstlich Drehna	22180	51.75	13.80	77
15	Görlitz *	23002	51.17	14.95	238
16	Guben	23103	51.93	14.70	46
17	Hähnichen *	23115	51.37	14.87	155
18	Hartmannsdorf	17115	52.35	13.83	37
19	Haselberg	18102	52.72	14.03	107
20	Hohenbuckow	22126	51.77	13.47	131
21	Hohendubrau *	23113	51.23	14.67	196
22	Hoyerswerda	23108	51.43	14.25	118
23	Kemnitz **	22181	51.85	13.53	108
24	Klitten	23114	51.35	14.60	132
25	Lieberose	23119	51.98	14.32	58
26	Lindenberg	18002	52.22	14.12	98
27	Löbau *	23112	51.10	14.68	249
28	Lohsa	23111	51.38	14.42	125
29	Luckenwalde	17120	52.07	13.18	50
30	Luga	23107	51.25	14.37	155
31	Märkisch-Buchholz	17118	52.12	13.77	42
32	Müncheberg	18004	52.51	14.12	62
33	Oppach	23110	51.05	14.50	320
34	Peickwitz	22118	51.47	13.98	102
35	Petkus **	22183	51.98	13.37	145
36	Rüdnitz	17155	52.73	13.63	65
37	Schöneiche (bei Berlin)	17116	52.47	13.68	40
38	Seelow	18101	52.53	14.38	55
39	Spremberg (Kläranlage)	23116	51.58	14.38	99
40	Storkow	17119	52.25	13.95	39
41	Velten	17114	52.68	13.17	36

* stations used for analysis of the Weißer Schöps (*) and Dahme (**) catchment (e.g. trend analysis, input for the hydrological models)

Appendix B. Study areas

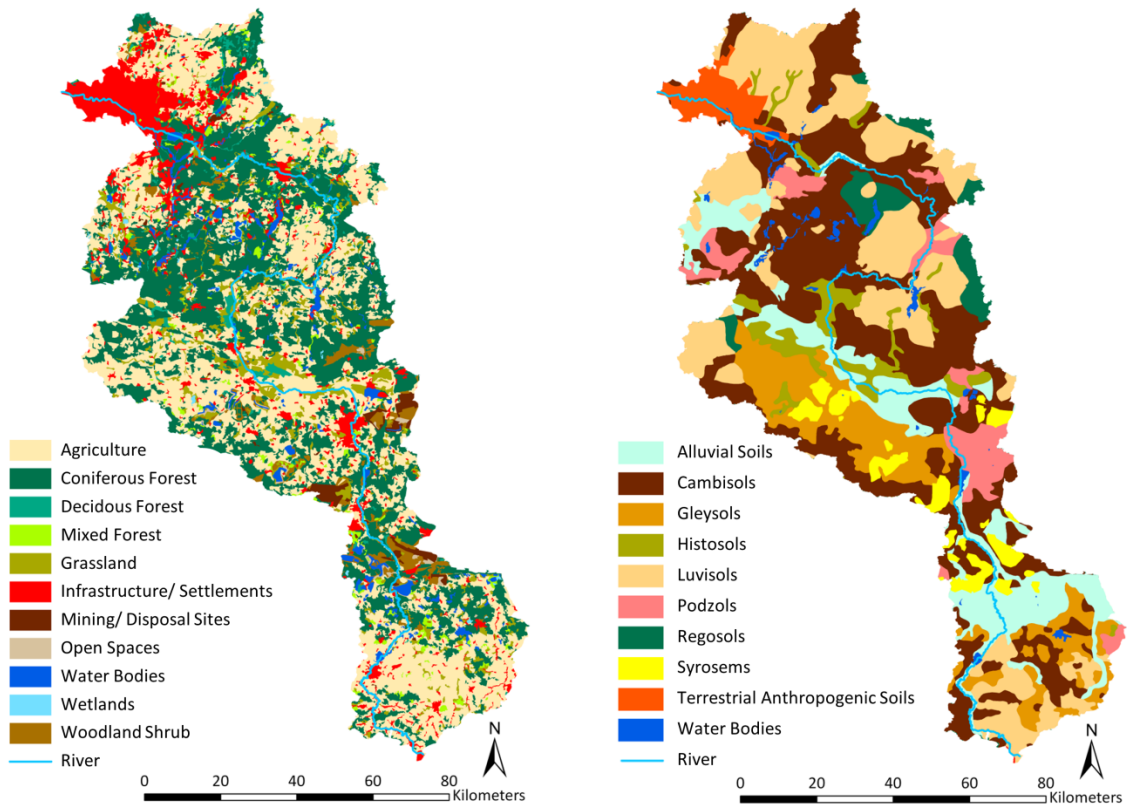


Figure B-1: Spatial distribution of land use (left, data basis: (CLC, 2006)) and soil type (right, databasis: (BÜK 1000, 1998)) in the Spree river catchment

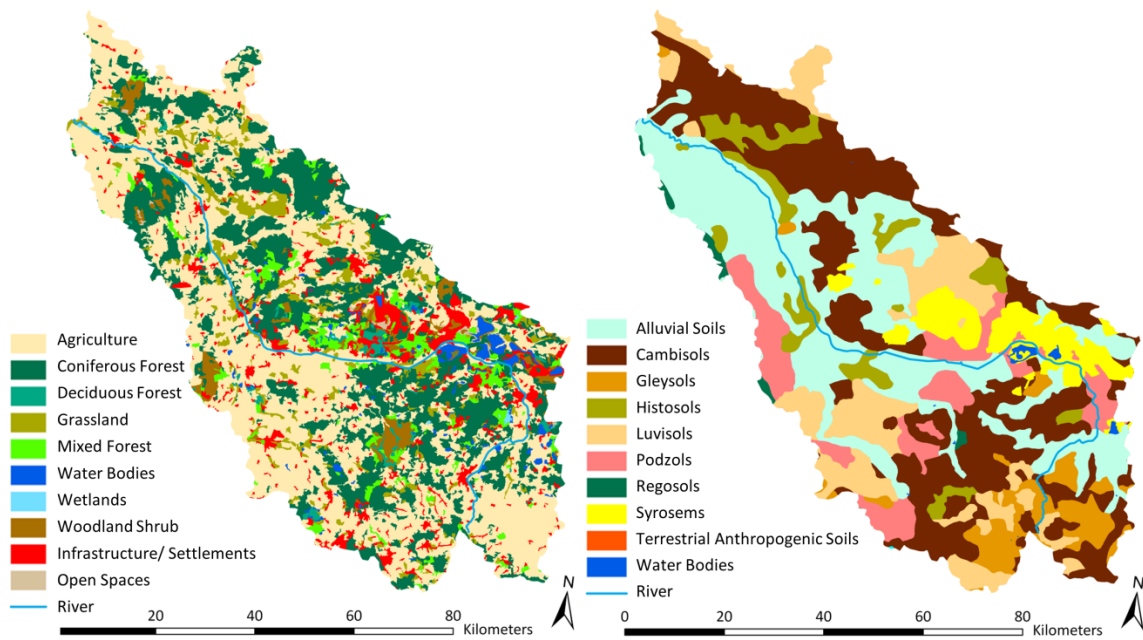


Figure B-2: Spatial distribution of land use (left, data basis: (CLC, 2006)) and soil type (right, databasis: (BÜK 1000, 1998)) in the Schwarze Elster river catchment

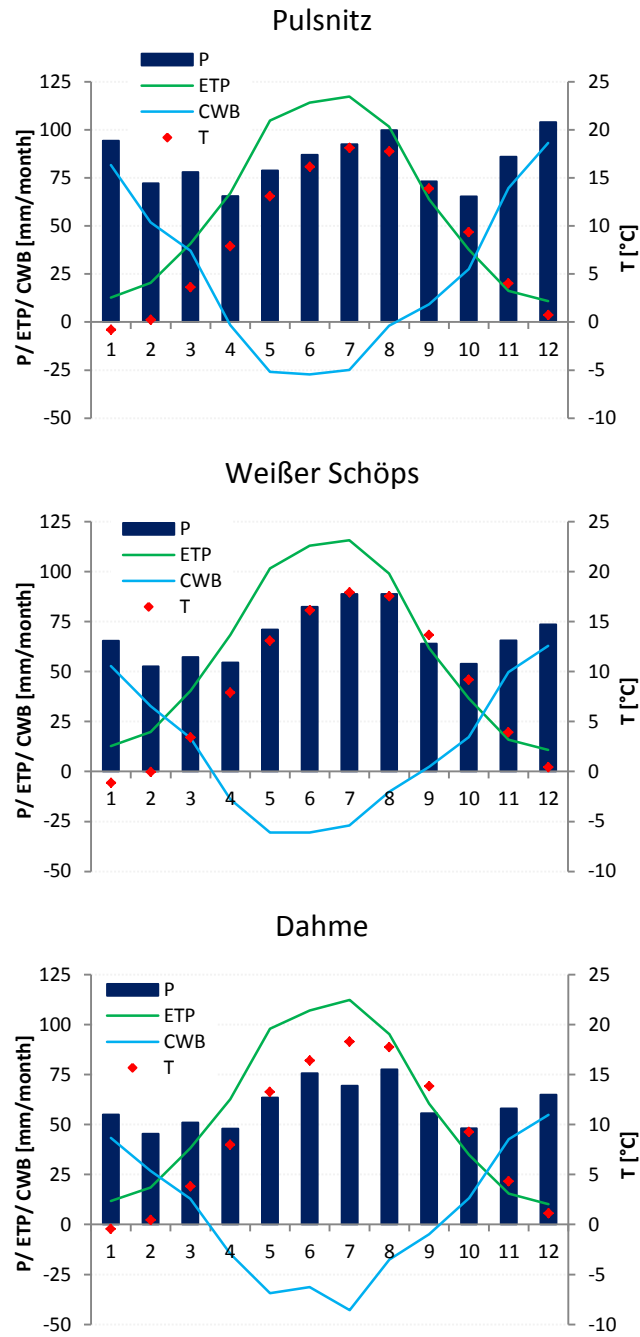


Figure B-3: Long term (1963-2006) monthly sums of precipitation, potential evapotranspiration, average temperature and the climatic water balance in the study catchments

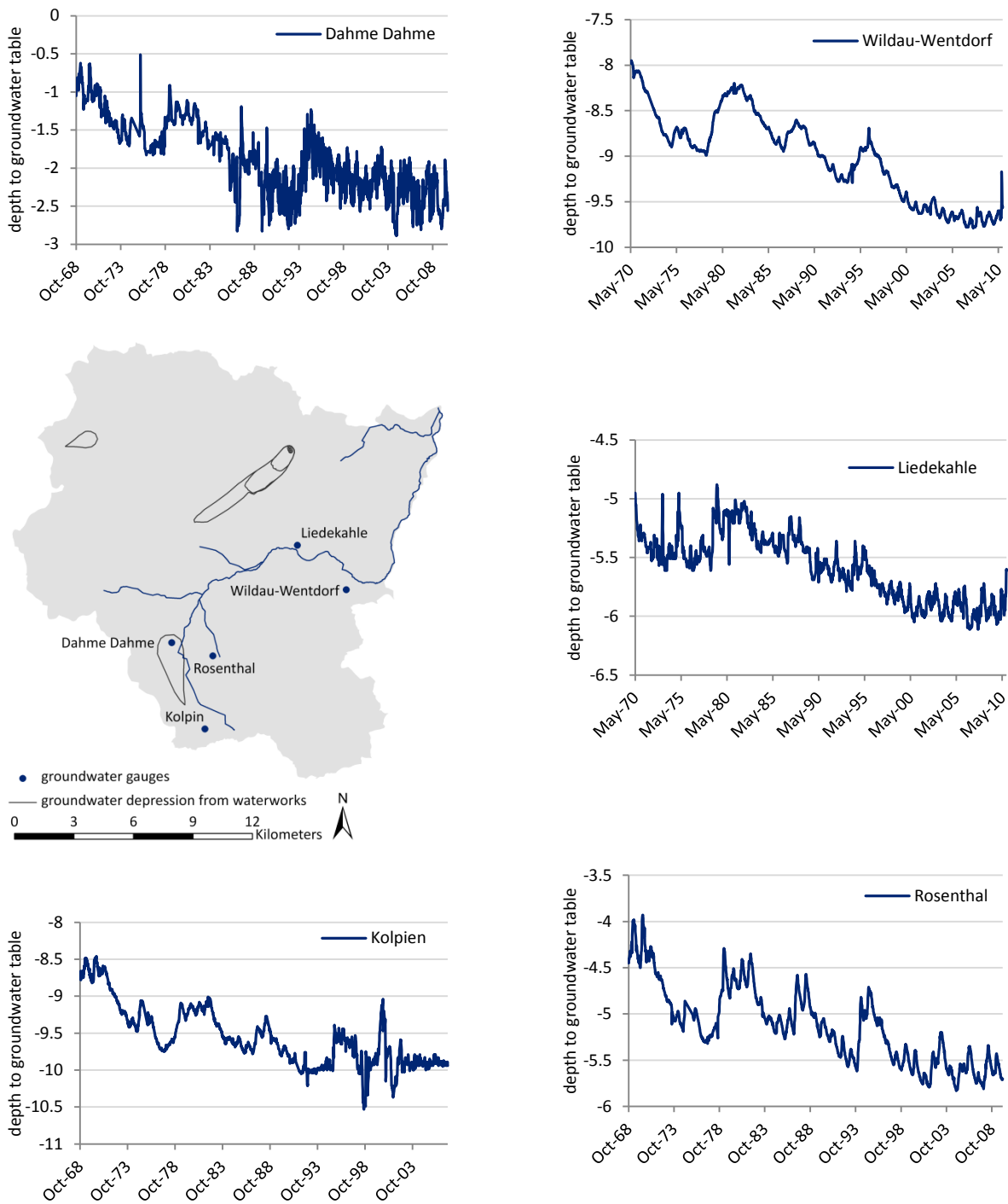


Figure B-4: Location of groundwater gauges and measured groundwater levels in the Dahme river catchment

Appendix C. Trend analysis for change detection

Linear regression:

Linear regression is a commonly used method to model a relationship between two variables, one explanatory and one dependent, by fitting a linear equation (Equation C-1) to observed data. The goal of the fitting is the minimization of the sum of the squared residuals which is known as the least-square approach. Linear regression is based on the following assumptions:

- i) Linearity of the relationship between explanatory and dependent variables
- ii) Independence of the errors which means that the time series should not be autocorrelated (see Equation C-10 in Appendix C)
- iii) Homoscedasticity which means constant variance of the errors
- iv) Normality of the error distribution.

In case of violation of the assumptions, the predictions made by linear regression can be biased.

$$Y = a + bX$$

Equation C-1

with

X	explanatory variable (or independent variable)
Y	dependent variable
b	slope of the line
a	intercept (the value of y when x = 0)

The Pettitt Test

The Pettitt test considers a sequence of random variables X_1, X_2, \dots, X_T which have a change point at τ . This implies that X_t for $t=1, 2, \dots, \tau$ have a common distribution function $F_1(x)$ and X_t for $t=\tau+1, \dots, T$ have a common distribution $F_2(x)$; $F_1(x) \neq F_2(x)$. The Pettitt test is based on the non-parametric Mann-Whitney two-sample test (Equation C-2, Equation C-3) where the statistics $U_{t,T}$, tests if two samples X_1, \dots, X_t and X_{t+1}, \dots, X_T come from the same population.

$$U_{t,T} = \sum_{i=1}^t \sum_{j=i+1}^T \text{Sgn}(X_i - X_j) \quad \text{Equation C-2}$$

$$\text{Sgn}(x) = \begin{cases} 1, & \text{if } x > 0 \\ 0, & \text{if } x = 0 \\ -1, & \text{if } x < 0 \end{cases} \quad \text{Equation C-3}$$

with	$\text{sgn}()$	sign function
	X_1, X_2, \dots, X_T	sequence of random variables
	τ	location of change point

Using the Pettitt test, the null hypothesis H_0 : no change or $\tau=T$ is tested against the alternative hypothesis H_1 : change for $1 \leq \tau < T$ using the statistics in Equation C-4 and for changes in one direction Equation C-5 and Equation C-6 for downward and upward shifts, respectively.

$$K_t = \max_{1 \leq t \leq T} |U_{t,T}| = \max(K_T^+, K_T^-) \quad \text{Equation C-4}$$

$$K_T^+ = \max_{1 \leq t \leq T} U_{t,T} \quad \text{Equation C-5}$$

$$K_T^- = -\min_{1 \leq t \leq T} U_{t,T} \quad \text{Equation C-6}$$

The significance level associated with K_T^+ and K_T^- are determined by Equation C-7.

$$p = \exp\left(\frac{-6K_T^2}{T^3 + T^2}\right) \quad \text{Equation C-7}$$

When p is below a chosen significance level, the null hypothesis is rejected. The time t when K_T occurs is the change point time with T being the total number of observations.

The Mann-Kendall test using prewhitening approach

- 1) The slope b of the trend is calculated using nonparametric approach of Sen (SEN, 1968) (Equation C-8). The Sen slope, which is quite robust again outliers, computes a linear trend as the median of all possible pairwise slopes.

$$Q_i = \left(\frac{x_j - x_k}{j - k} \right), i = 1, 2, \dots, N, j > k (j = 2, \dots, n; k = 1, \dots, n-1) \quad \text{Equation C-8}$$

For n values of the time series x , $N = n(n-1)/2$ values of Q are obtained. The Sen slope b is then calculated as the median of $Q_i, i = 1, 2, \dots, N$.

If the slope is close to zero, it is not necessary to continue the trend analysis. If the slope differs from zero, the linear trend is eliminated from the time series X_t (Equation C-9).

$$X'_t = X_t - T_t = X_t - bt \quad \text{Equation C-9}$$

With

- X'_t trend free time series
- X_t time series (containing trend)
- T_t trend component
- b sen slope
- t time index

- 2) Determination of the first order autocorrelation coefficient r_k (Equation C-10) of the trend free time series.

Autocorrelation describes the correlation between different data points against their temporal distance (lag) (Equation C-10).

$$r_k = \frac{\sum_{i=1}^{n-k} (x_i - \bar{x})(x_{i+k} - \bar{x})}{\sum_{i=1}^n (x_i - \bar{x})^2} \quad \text{Equation C-10}$$

With

- x_i variable at time i
- \bar{x} mean of the n total number of observations
- k time interval (1)
- r_k autocorrelation coefficient

In this study, only the first order autocorrelation was considered as many authors agree that it has the largest impact on the results of the outcome of the statistical tests (HUXOL, 2007; VON STORCH, 1995).

Subsequently, “trend free pre-whitening” (Equation C-11) is carried out, as developed by YUE et al. (2002b).

$$Y_t = X_t - r_1 X_{t-1} \quad \text{Equation C-11}$$

with Y_t pre-whitened time series
 X_t original time series
 r_1 first order autocorrelation coefficient
 t time index

3) Merge of the two time series and the trend from step 1 (Equation C-12)

$$Y'_t = Y_t + T_t \quad \text{Equation C-12}$$

with Y_t pre-whitened time series
 T_t trend component
 Y'_t trend free pre-whitened time series

4) Calculation of the Mann-Kendall trend test in order to assess the significance of the test.

The null hypothesis H_0 of the trend test states that a time series is independent and identically distributed implying that there is not trend (Equation C-13). The alternative hypothesis H_1 assumes that a monotonic trend exists (Equation C-14).

$$H_0 : P(x_j > x_i) = 0.5; j > i \quad \text{Equation C-13}$$

$$H_1 : P(x_j > x_i) \neq 0.5 \text{ (two-sided test)} \quad \text{Equation C-14}$$

The Mann-Kendall score S is calculated after Equation C-15.

$$S = \sum_{k=1}^{n-1} \sum_{j=k-1}^n \text{sgn}(x_j - x_k) \quad \text{Equation C-15}$$

$$\text{sgn}(x_j - x_k) = \begin{cases} 1, & \text{if } x_j - x_k > 0 \\ 0, & \text{if } x_j - x_k = 0 \\ -1, & \text{if } x_j - x_k < 0 \end{cases}$$

with S Mann-Kendall test statistic
 Y'_t, x_i time series at time step j and k (j>k)
 $\text{sgn}()$ sign function

According to MANN (1945) and KENDALL (1975), the statistic S is approximately normally distributed when $n \geq 8$. The mean and the variance can be estimated according to Equation C-16 and Equation C-17.

$$\mu_S = 0 \tag{Equation C-16}$$

$$\sigma_S^2 = \left[n(n-1)(2n+5) - \sum_{i=1}^m t_i(t_i-1)(2t_i+5) \right] / 18 \tag{Equation C-17}$$

with μ_S mean
 σ_S^2 variance
 m number of tied groups
 t_i number of ties of extent I (a tied group is a set of sample data having the same value)

The standardised test statistic Z, being the standard normal variant, is calculated and used for hypothesis testing (Equation C-18).

$$Z = \begin{cases} \frac{S-1}{\sigma_S} & \text{if } S > 0 \\ 0 & \text{if } S = 0 \\ \frac{S+1}{\sigma_S} & \text{if } S < 0 \end{cases} \tag{Equation C-18}$$

Considering a two-tailed test, the null hypothesis is rejected at significance level α (0.05) if, $|Z| > Z_{\alpha/2}$ where $Z_{\alpha/2}$ is the value of the standard normal distribution with an exceedance probability of $\alpha/2$.

Locally Weighted Scatterplot Smoothering (LOWESS**):**

Using LOWESS a polynomial is fitted to a subset of the data using weighted least squares. In that way, more weight is given to points near the point whose response is being estimated and less weight to points further away. How many neighbouring data points influence the local fitting is determined by smoothing parameter (0.45 in this study) which can flexibly be defined by the user. By evaluating the local (linear) polynomial, the value of the regression function for the point is obtained. The LOWESS fit is complete when the regression function values for each of the n data points have been computed.

The following steps are carried out:

- 1) Compute the regression weights for each data point in the span. The weights are given by Equation C-19.

$$w_i = \left(1 - \left| \frac{x - x_i}{d(x)} \right|^3 \right)^3 \quad \text{Equation C-19}$$

with

- x predictor value
- x_i nearest neighbours of x as defined by the span
- d(x) distance along the abscissa from x to the most distant predictor value within the span

The weights have the following characteristics:

- The data point to be smoothed has the largest weight and the biggest influence on the fit
 - Data points outside the span have zero weights and no influence on the fit
- 2) A weighted linear least squares regression is performed using a first degree polynomial.
 - 3) The smoothed value is given by the weighted regression at the predictor value of interest.

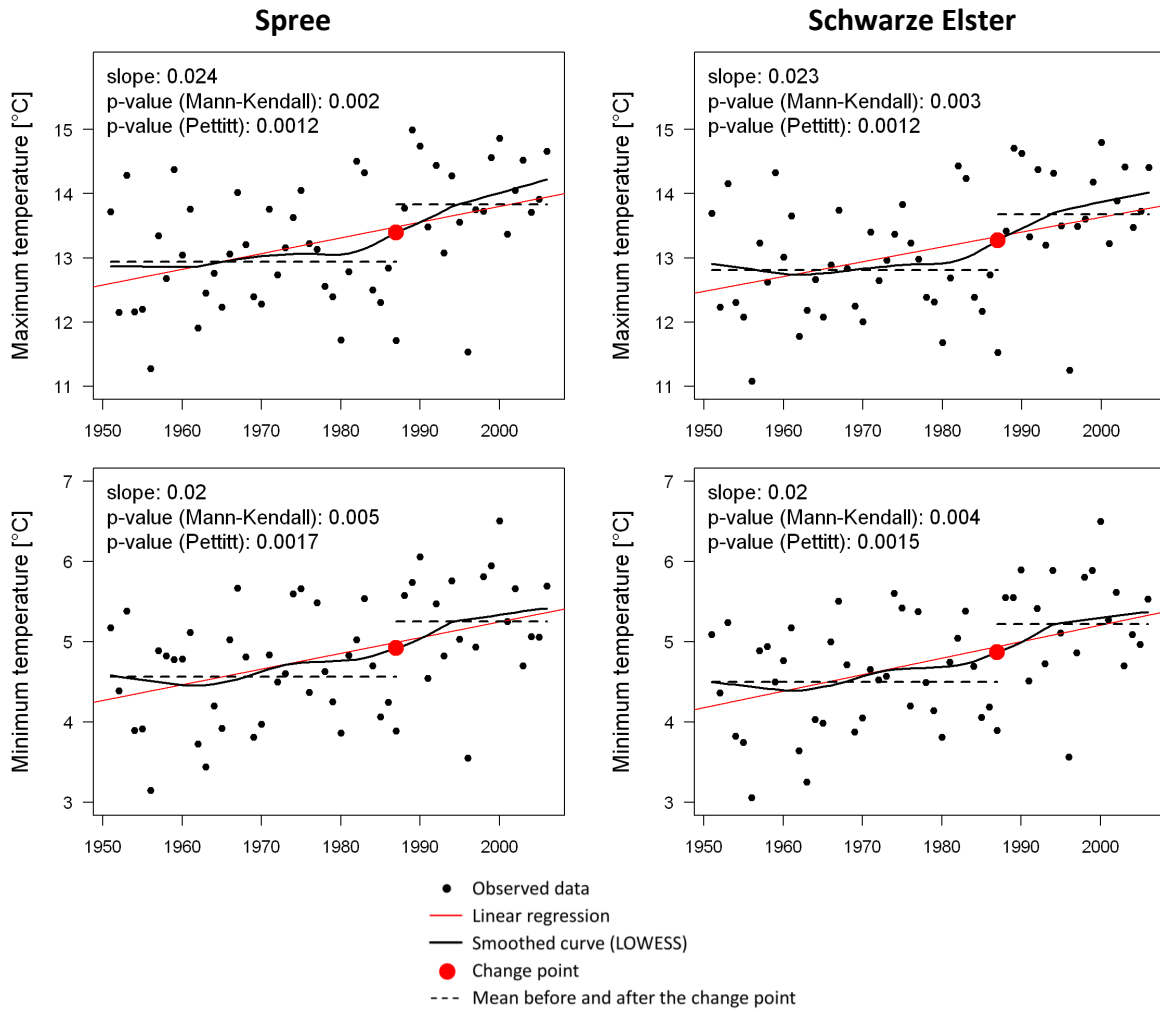


Figure C-1: Maximum (top) and minimum (bottom) temperature (interpolated annual values) in the Spree and Schwarze Elster river catchments and trend interpretation (1951-2006)

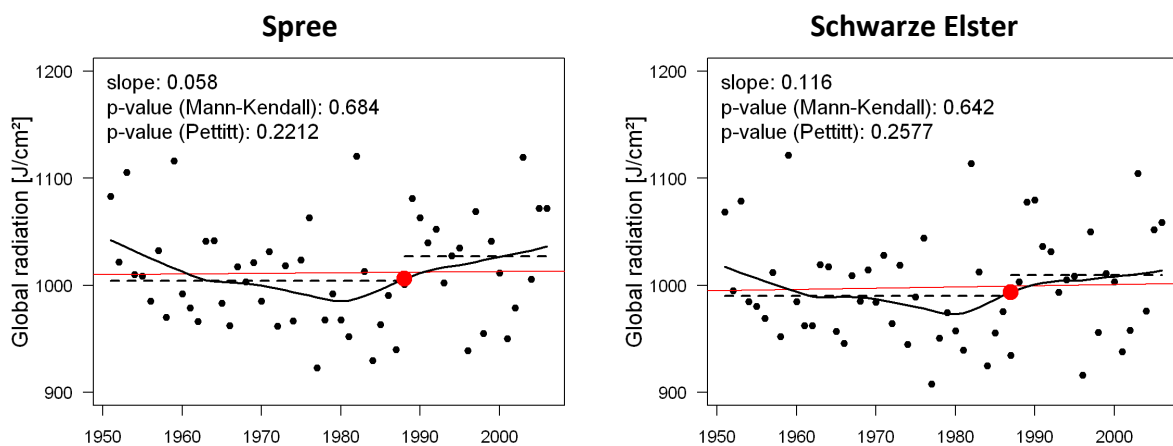


Figure C-2: Global radiation (interpolated annual values) in the Spree and Schwarze Elster river catchments and trend interpretation (1951-2006)

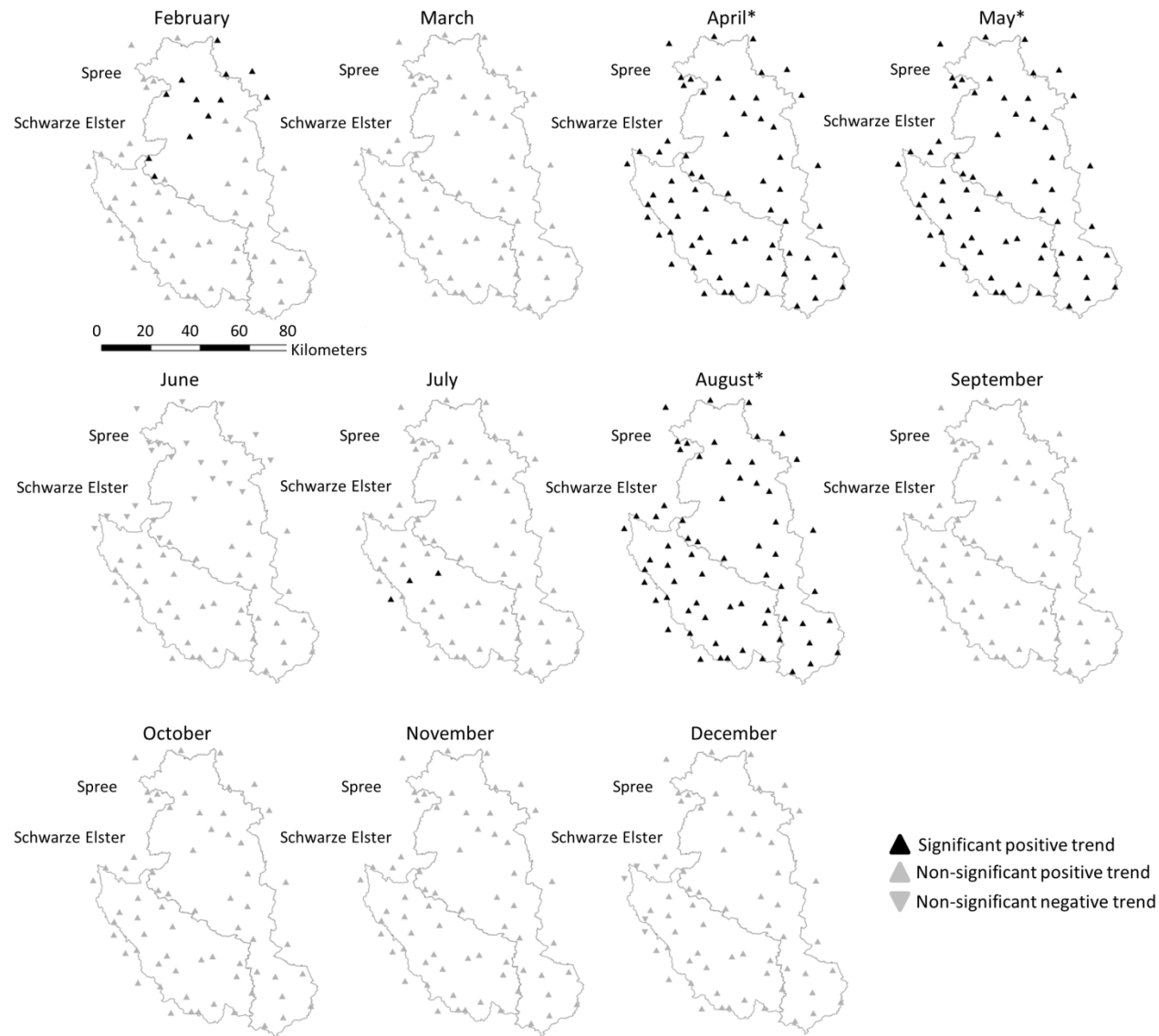


Figure C-3: Spatial distribution of mean temperature change points (1951-2006). The months where trends are above field significance are denoted with *

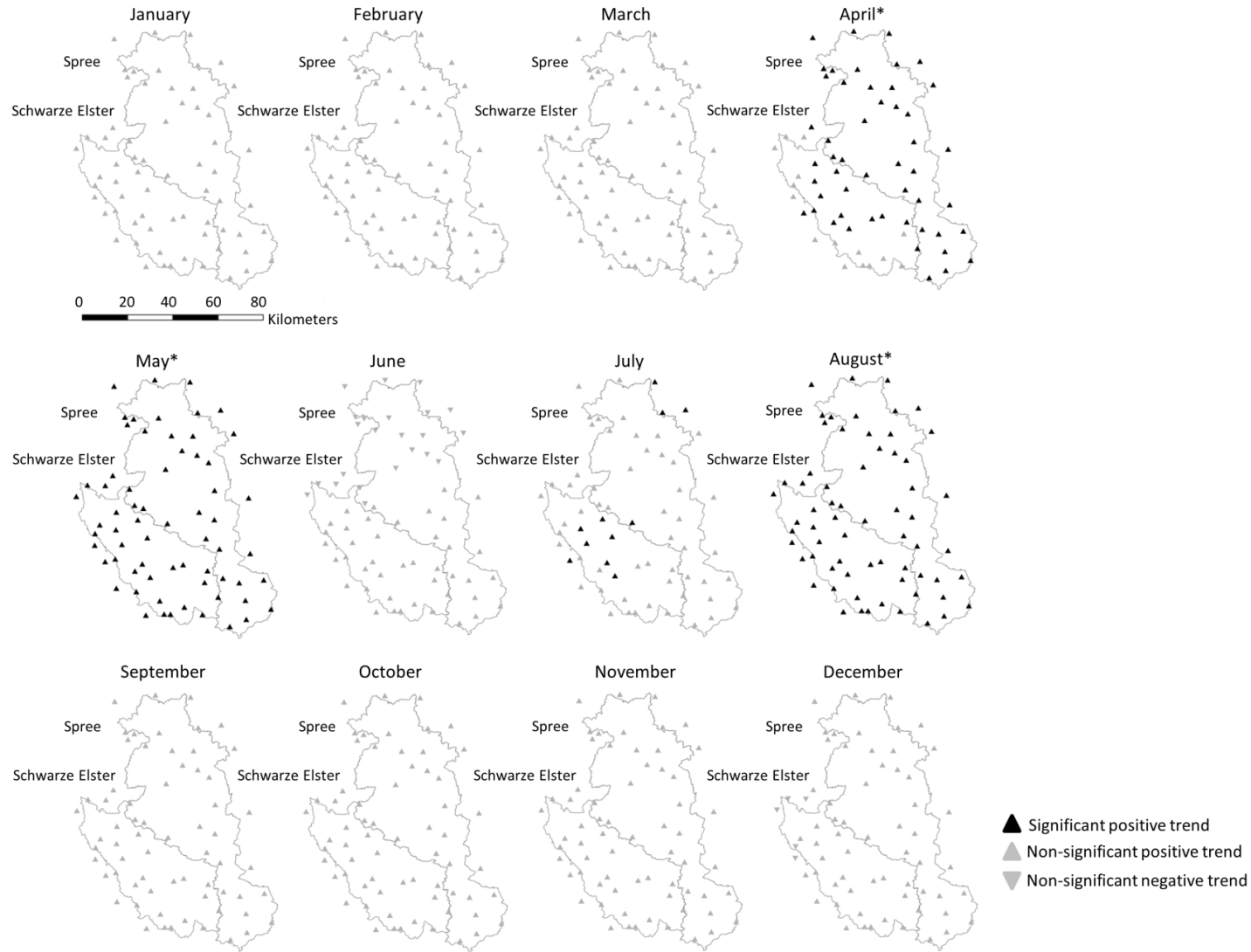


Figure C-4: Spatial distribution of mean temperature gradual trends (1951-2006). The months where trends are above field significance are denoted with *

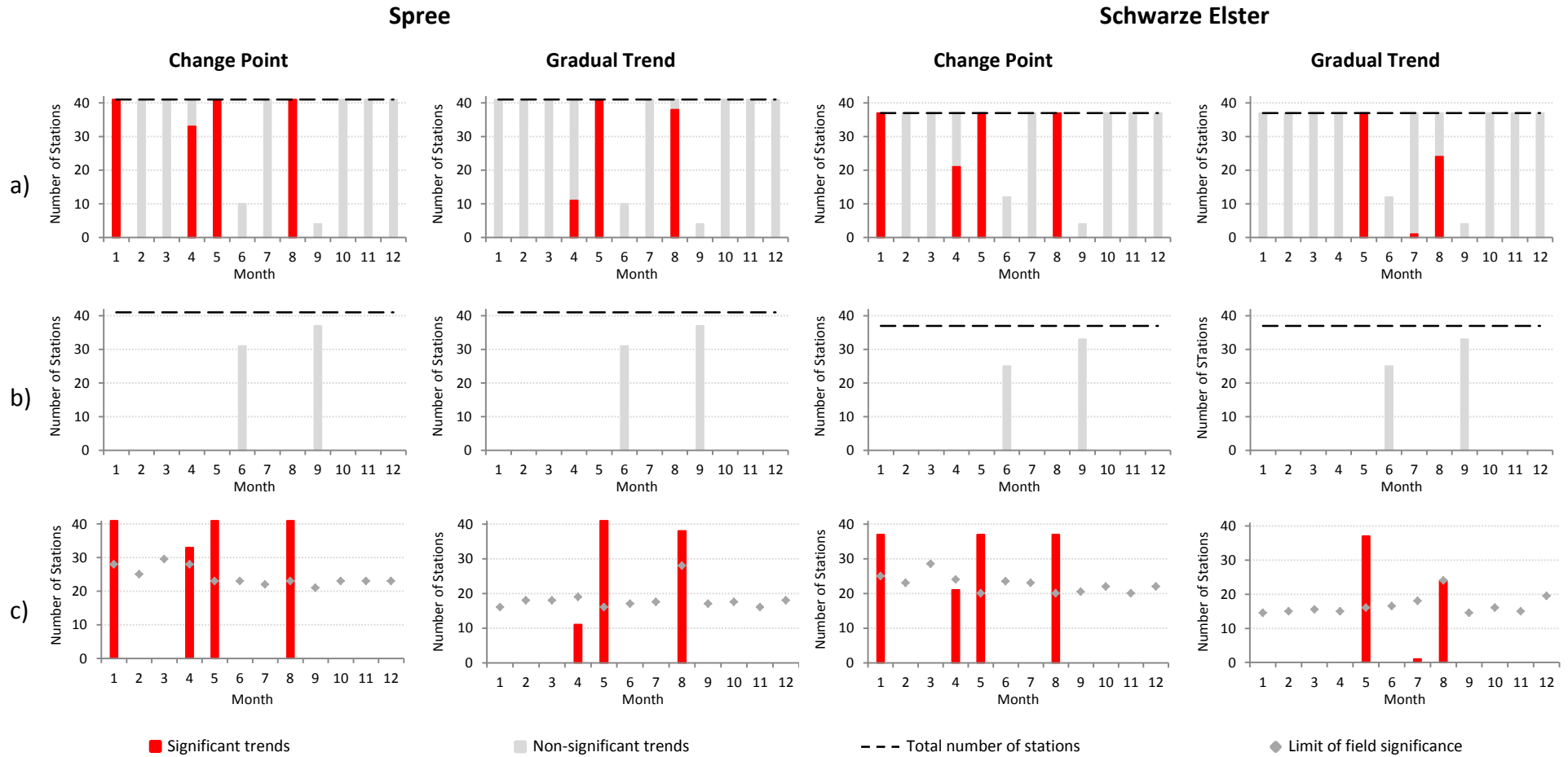


Figure C-5: Maximum temperature (1951-2006): number of stations with significant and non-significant (a) positive and (b) negative trends, (c) number of significant trends and field significance for change points and gradual trends in the Spree (left) and Schwarze Elster (right) river catchments

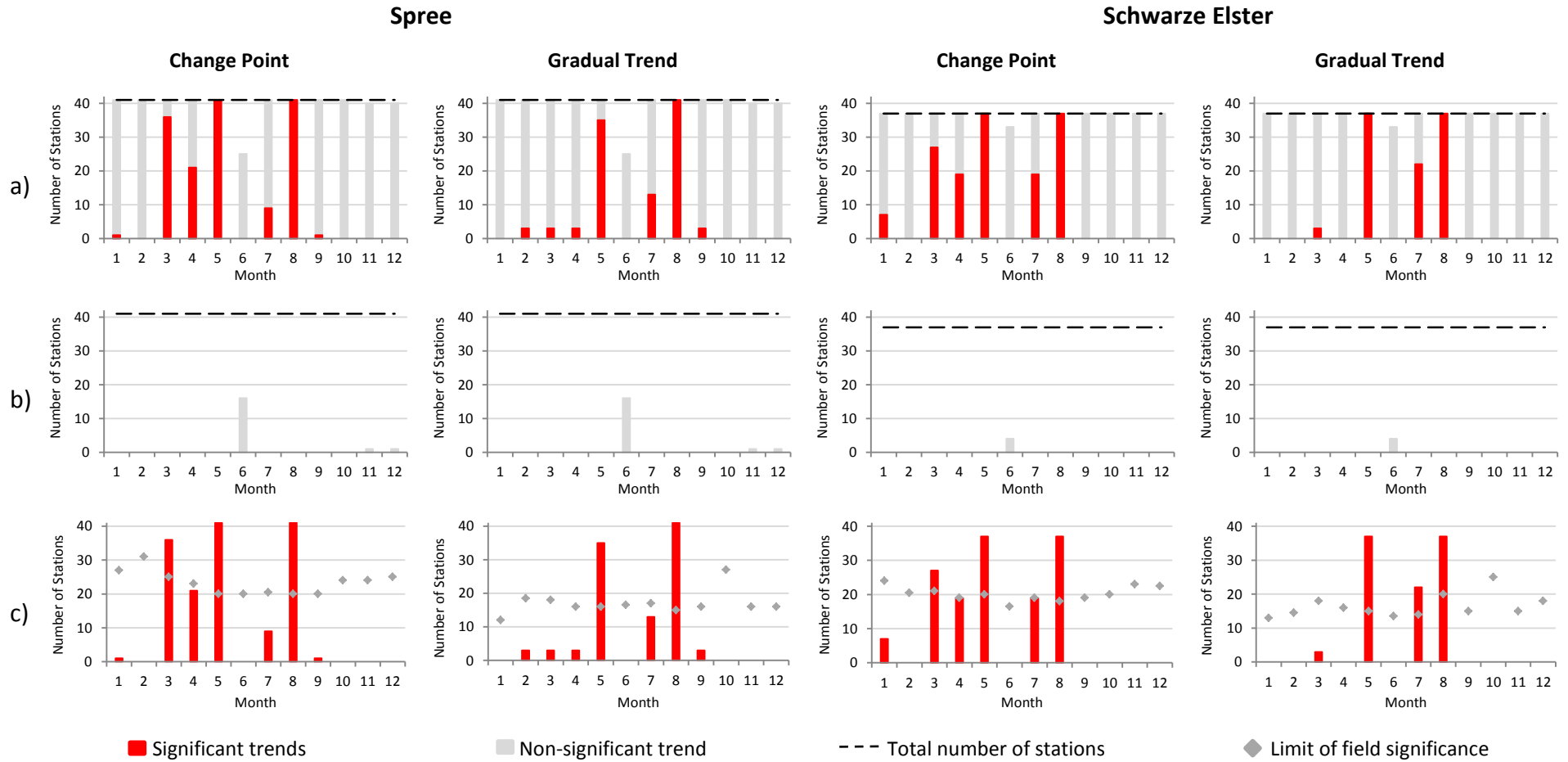


Figure C-6: Minimum temperature (1951-2006): number of stations with significant and non-significant (a) positive and (b) negative trends, (c) number of significant trends and field significance for change points and gradual trends in the Spree (left) and Schwarze Elster (right) river catchments

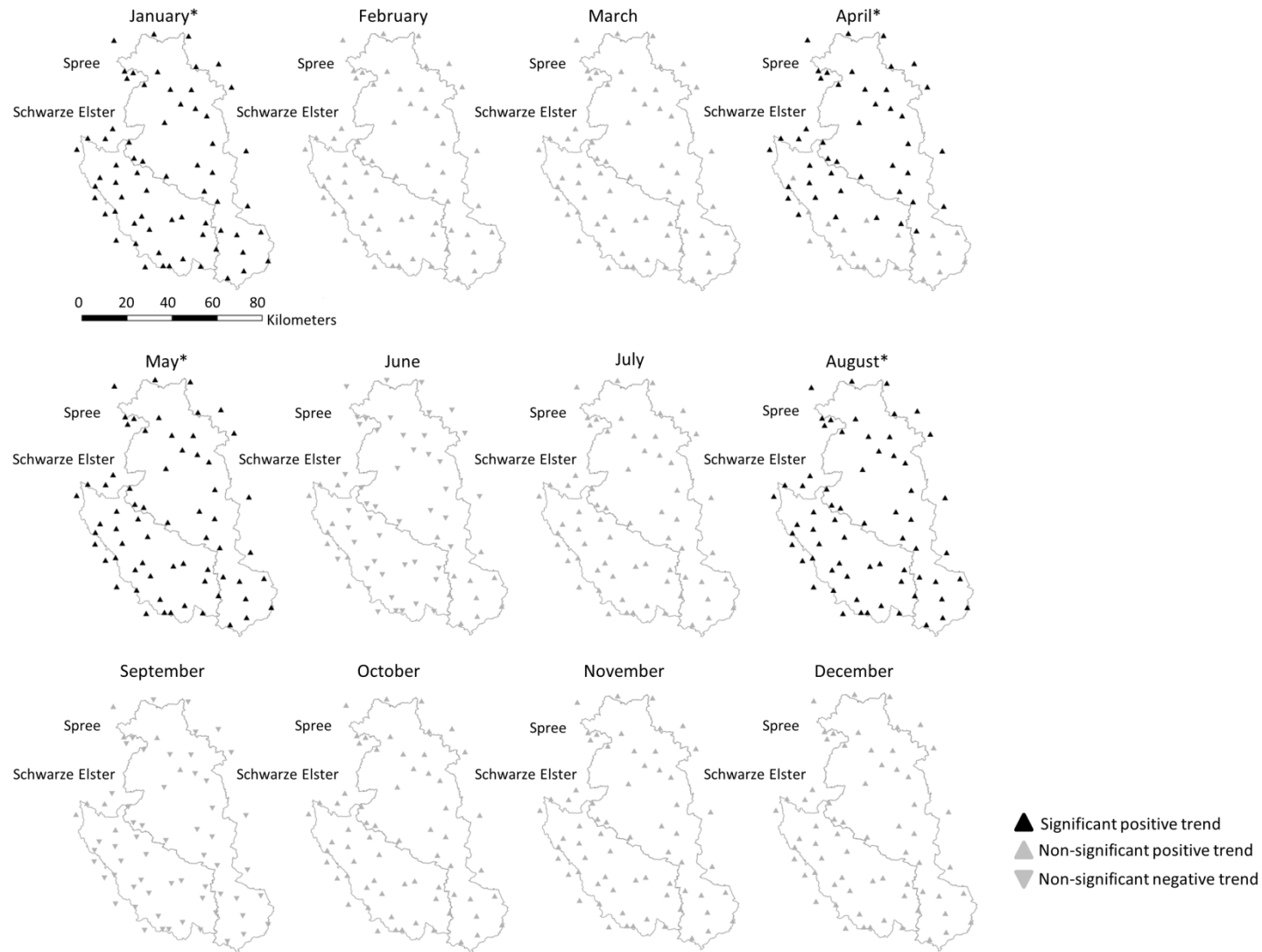


Figure C-7: Spatial distribution of maximum temperature change points (1951-2006). The months where trends are above field significance are denoted with * (April only Spree)

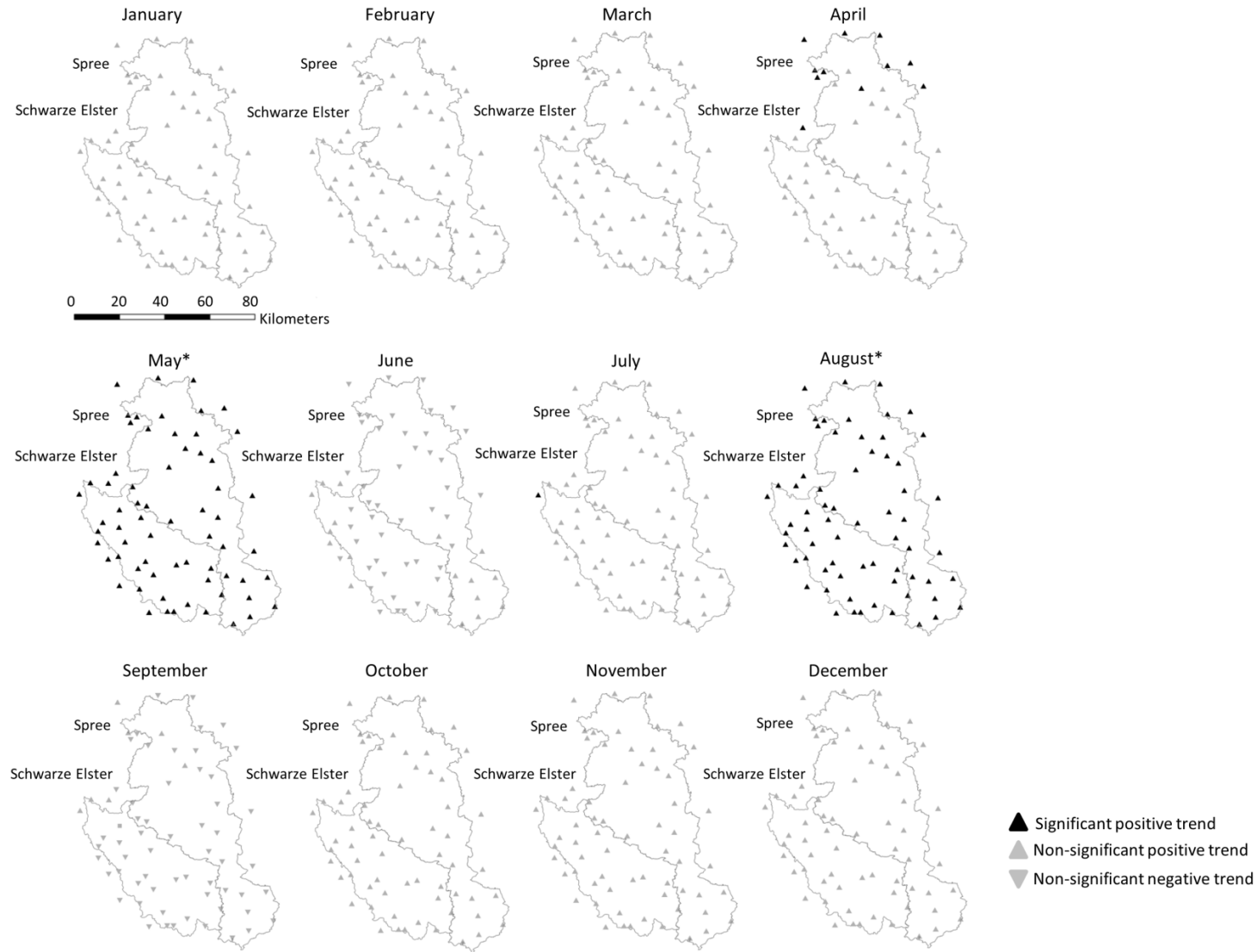


Figure C-8: Spatial distribution of maximum temperature gradual trends (1951-2006). The months where trends are above field significance are denoted with *

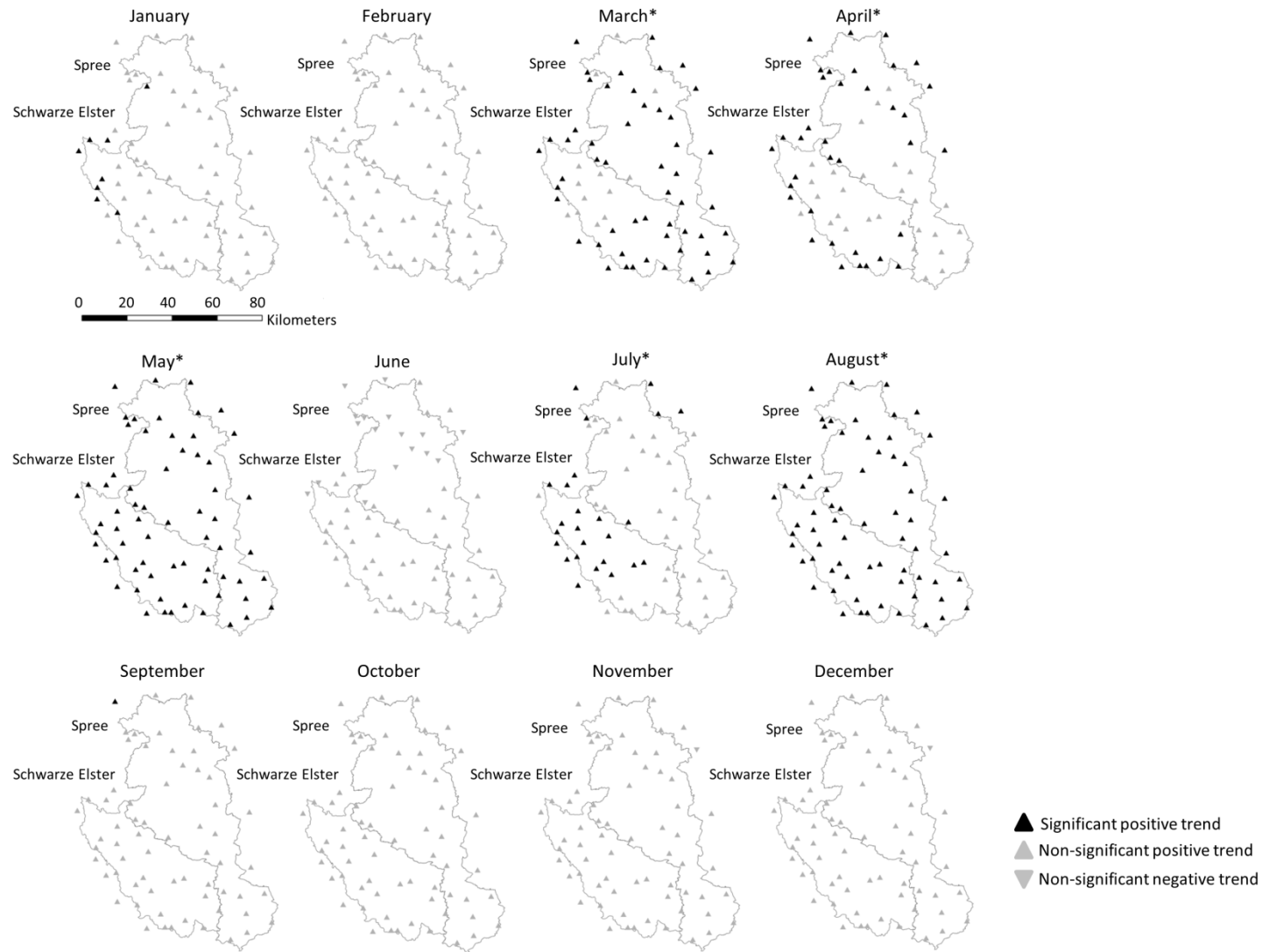


Figure C-9: Spatial distribution of minimum temperature change points (1951-2006). The months where trends are above field significance are denoted with * (April and July only Schwarze Elster)

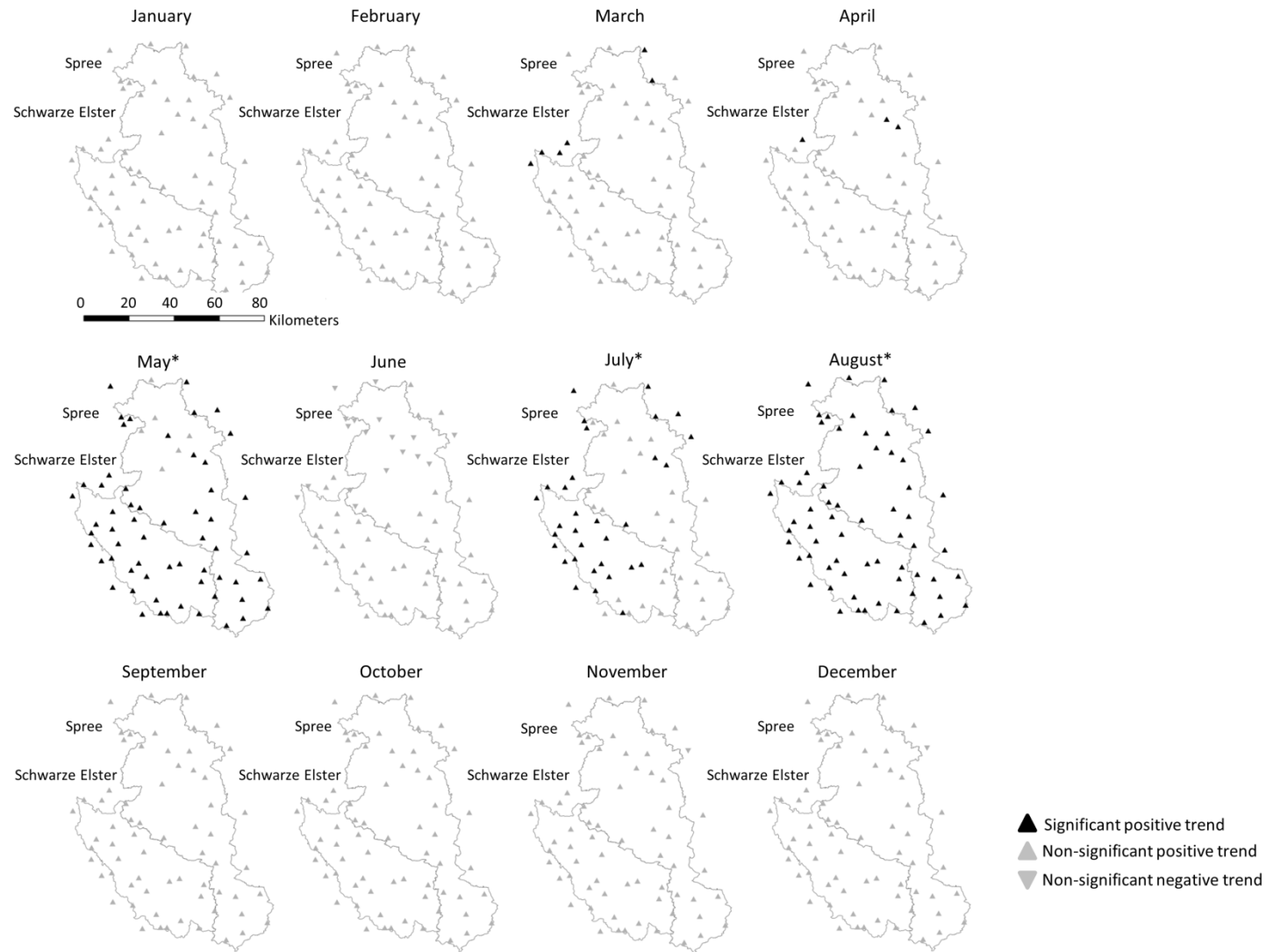


Figure C-10: Spatial distribution of minimum temperature gradual trends (1951-2006). The months where trends are above field significance are denoted with * (July only Schwarze Elster)

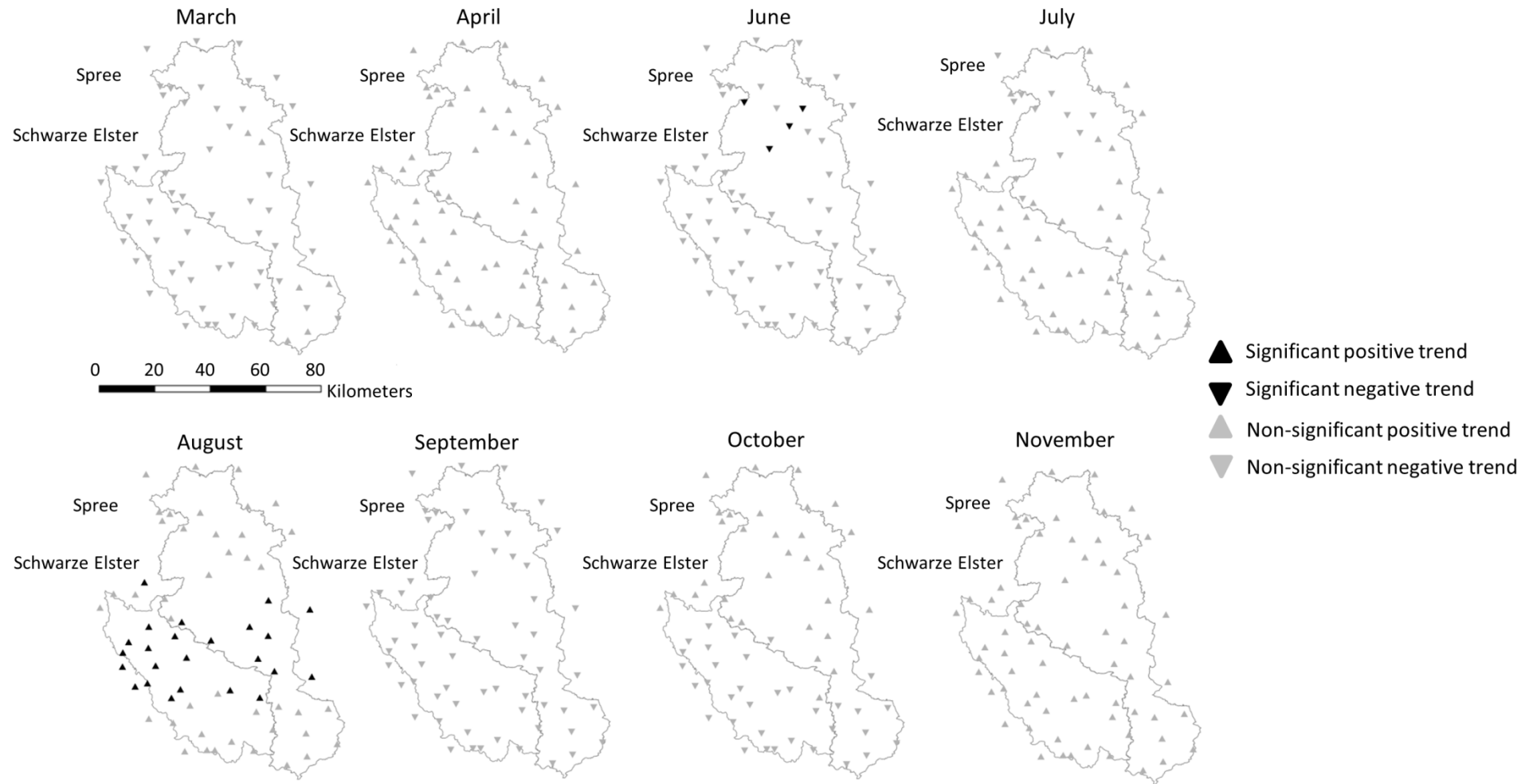


Figure C-11: Spatial distribution of potential evapotranspiration change points (1951-2006). Significant above field significance months are displayed in Figure 5-12

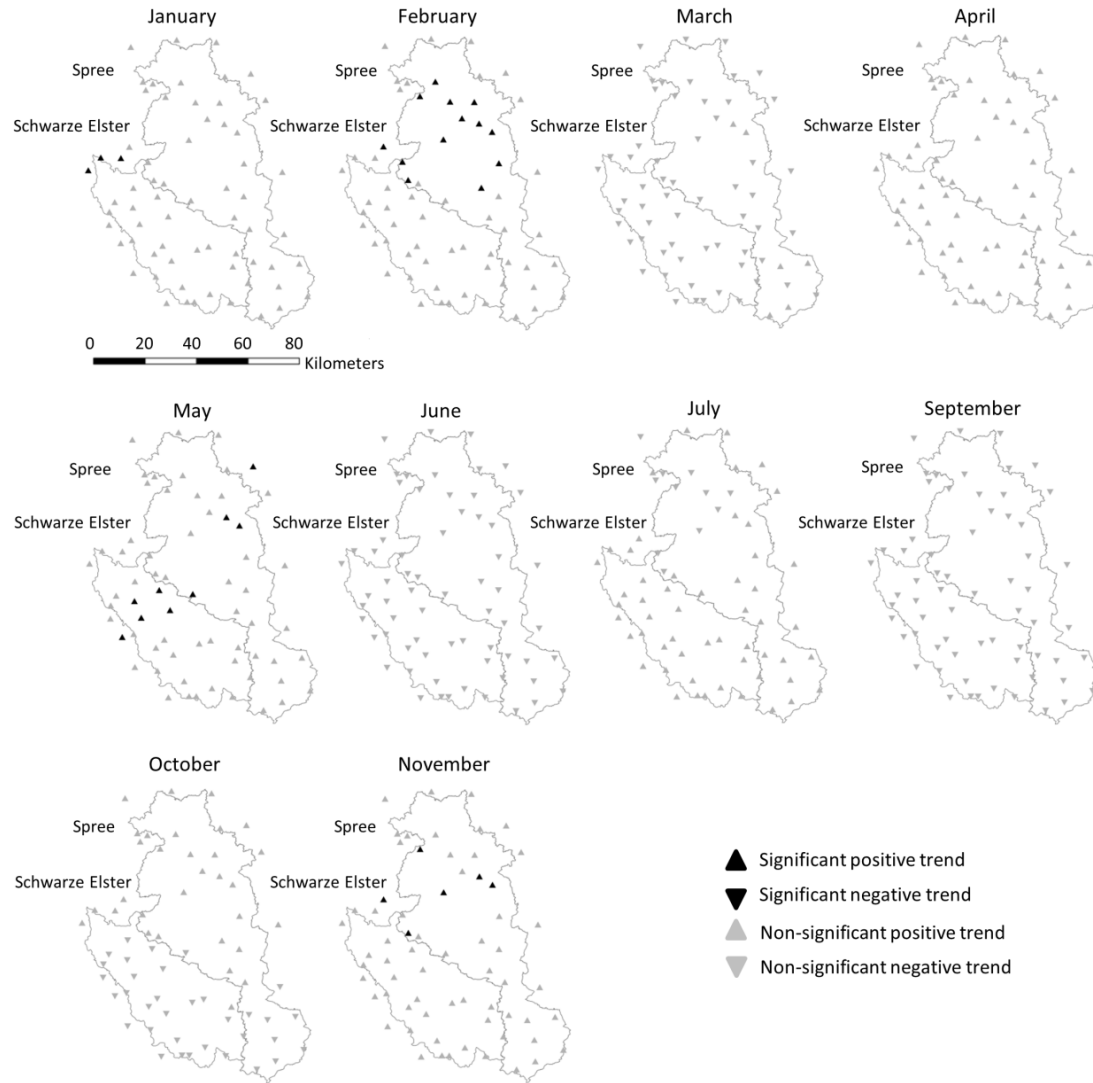


Figure C-12: Spatial distribution of potential evapotranspiration gradual trends (1951-2006). Significant above field significance months are displayed in Figure 5-10

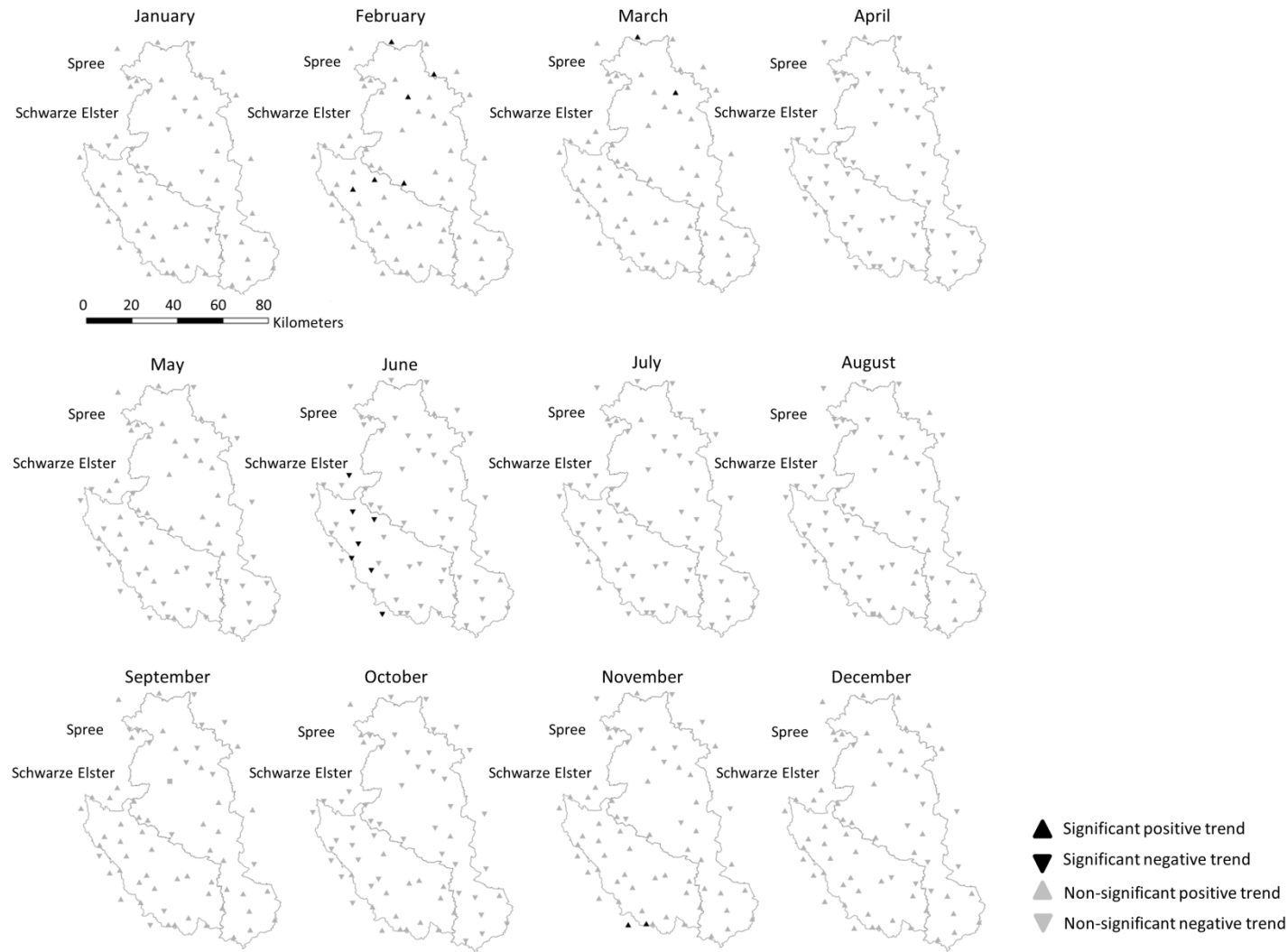


Figure C-13: Spatial distribution of precipitation change points (1951-2006). In no month, field significance is reached

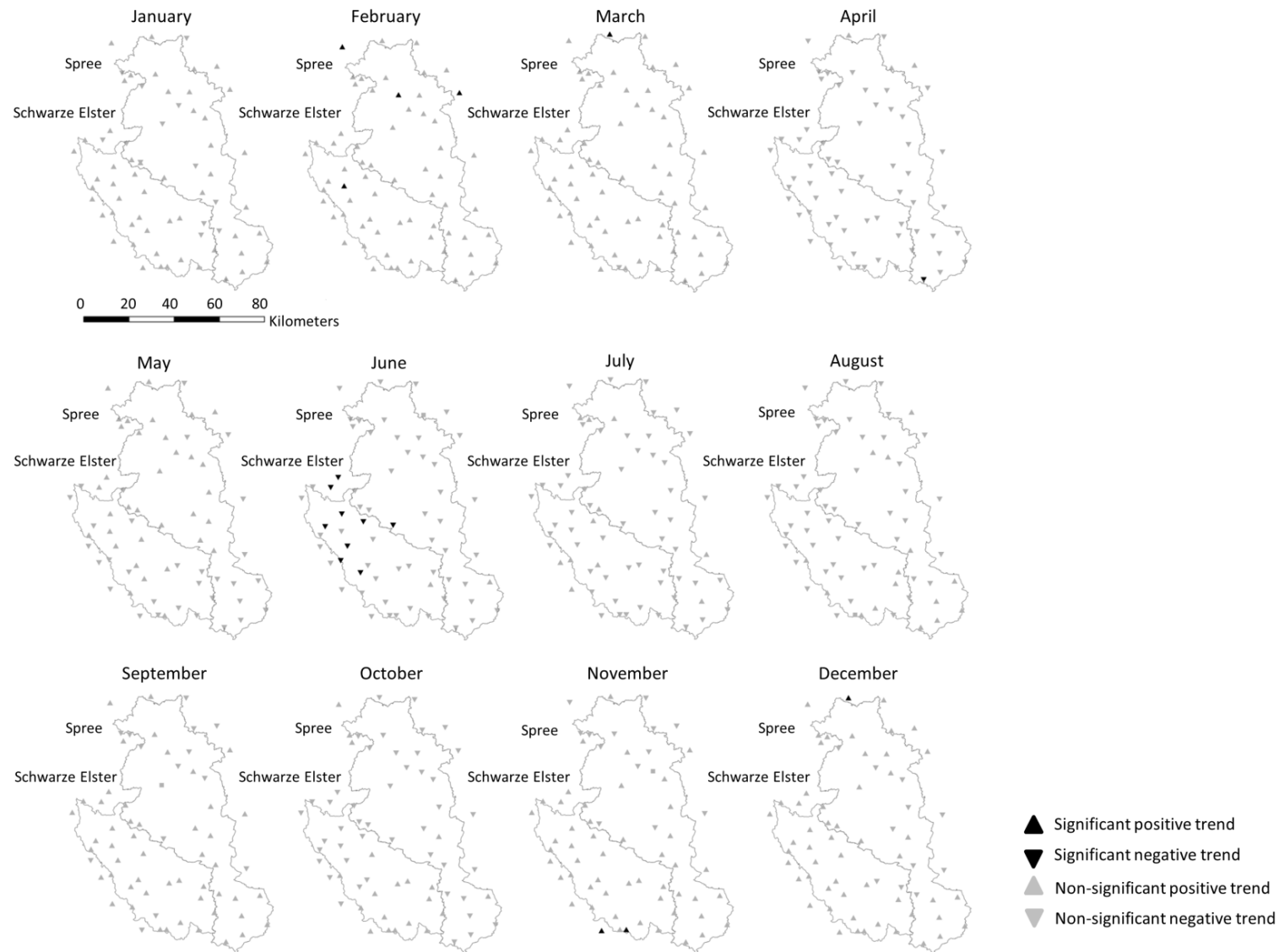


Figure C-14: Spatial distribution of precipitation gradual trends (1951-2006). In no month, field significance is reached

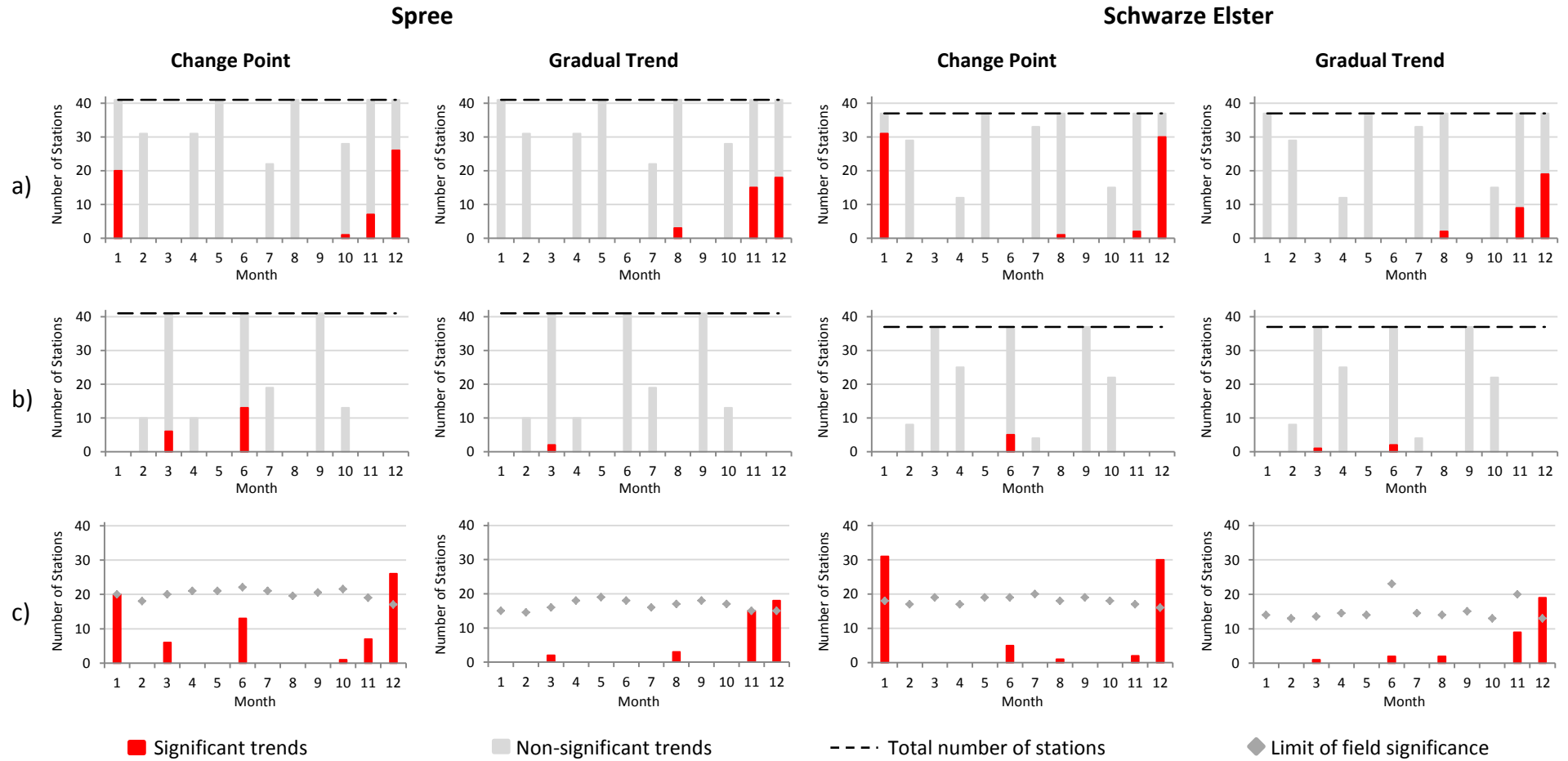


Figure C-15: Global radiation (1951-2006): number of stations with significant and non-significant (a) positive and (b) negative trends, (c) number of significant trends and field significance for change points and gradual trends in the Spree (left) and Schwarze Elster (right) river catchments

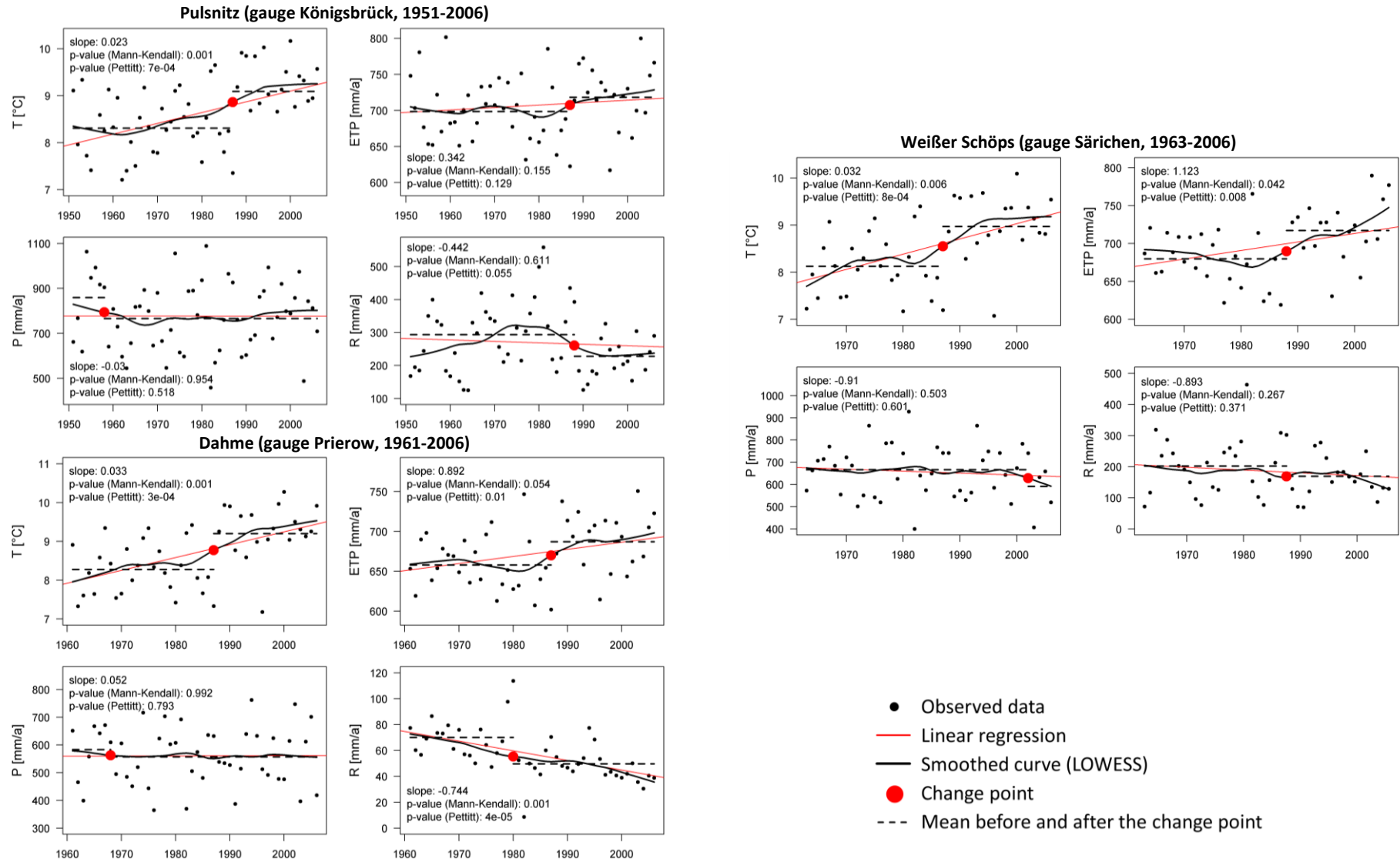


Figure C-16: Temperature (T), potential evapotranspiration (ETP), precipitation (P), runoff (R): interpolated annual sums and trend interpretation

Appendix C

Table C-1: Temperature (T), potential evapotranspiration (ETP), precipitation (P), runoff R: seasonal trend and significance (Mann-Kendall and Pettitt) analysis. Values highlighted in dark grey are significant at a level of 0.01, values in light grey at a level of 0.05

	DJF				MAM				JJA				SON			
	T	ETP	P	R	T	ETP	P	R	T	ETP	P	R	T	ETP	P	R
Pulsnitz (1951-2006)*																
Slope	0.030	0.105	0.488	0.112	0.030	0.139	-0.128	-0.057	0.023	0.138	-0.825	-0.380	0.009	-0.040	0.434	-0.118
p-value (Mann-Kendall)	0.098	0.074	0.408	0.989	0.003	0.338	0.532	0.850	0.012	0.477	0.523	0.172	0.283	0.642	0.309	0.368
p-value (Pettitt)	0.021	0.004	0.414	0.056	0.003	0.147	0.494	0.154	0.023	0.537	0.131	0.032	0.268	0.362	0.562	0.098
Weißer Schöps (1963-2006)																
Slope	0.043	0.125	-0.283	-0.308	0.040	0.613	-0.283	-0.362	0.034	0.295	0.437	-0.218	0.012	0.091	-0.542	-0.005
p-value (Mann-Kendall)	0.503	0.295	0.258	0.233	0.007	0.006	0.258	0.601	0.006	0.267	0.572	0.167	0.233	0.645	0.451	0.851
p-value (Pettitt)	0.021	0.013	0.195	0.275	0.005	0.003	0.195	0.435	0.003	0.217	0.488	0.488	0.137	0.269	0.110	0.615
Dahme (1961-2006)**																
Slope	0.050	0.162	0.431	-0.299	0.038	0.479	-0.280	-0.208	0.033	0.114	0.147	-0.100	0.013	0.137	-0.245	-0.191
p-value (Mann-Kendall)	0.140	0.003	0.278	0.003	0.002	0.035	0.792	0.003	0.015	0.717	0.807	0.063	0.145	0.207	0.747	0.007
p-value (Pettitt)	0.004	2e-04	0.333	7e-05	0.001	0.010	0.413	0.006	0.014	0.495	0.660	0.011	0.168	0.182	0.333	0.004

* gauging station Königsbrück

** for runoff 1981 and 1982 are missing

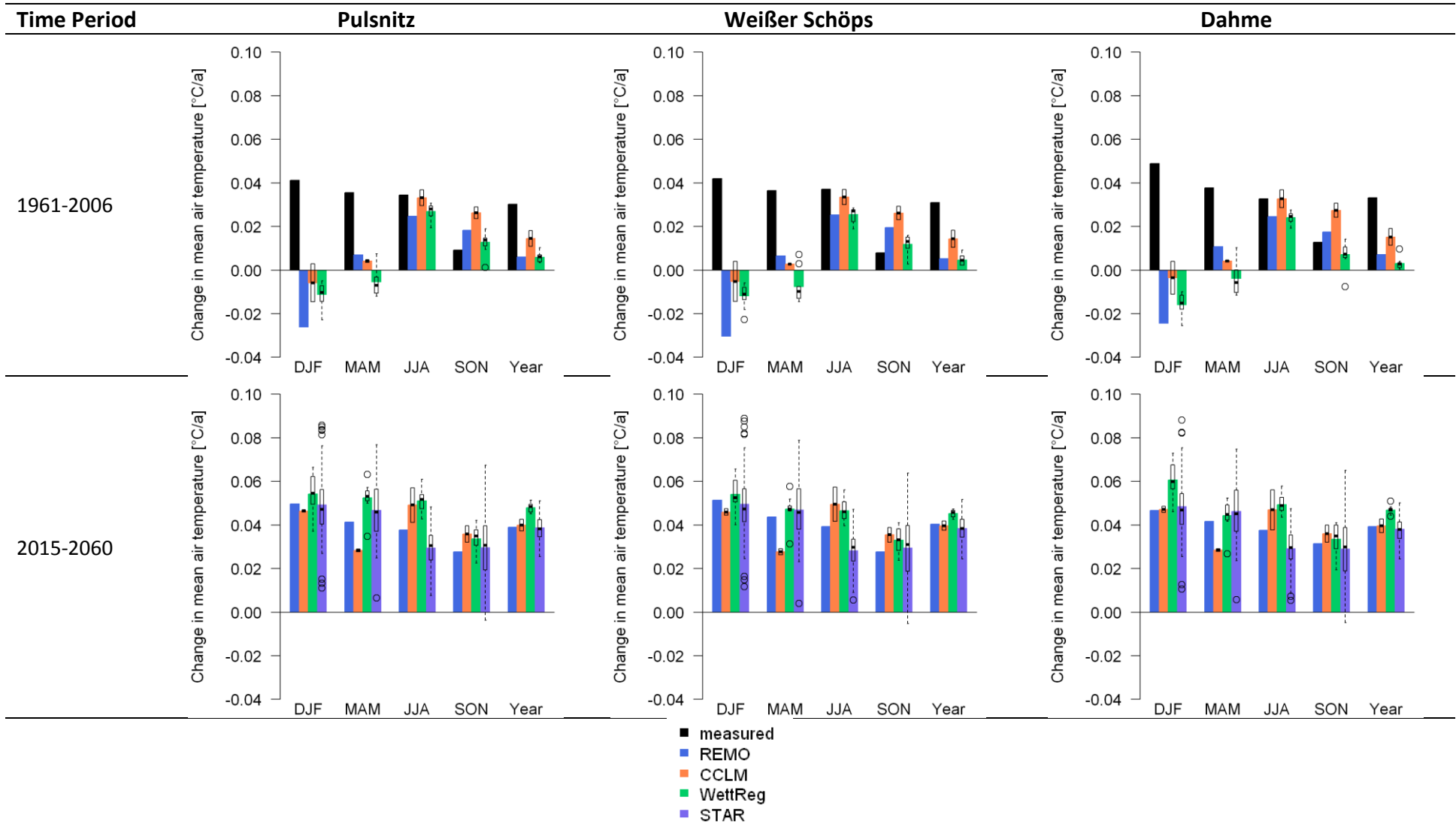


Figure C-17: Mean temperature: Comparison of trend magnitude between measured and simulated temperature for the period 1961-2006 (top) and between simulations for the period 2015-2061 (bottom) for the subcatchments

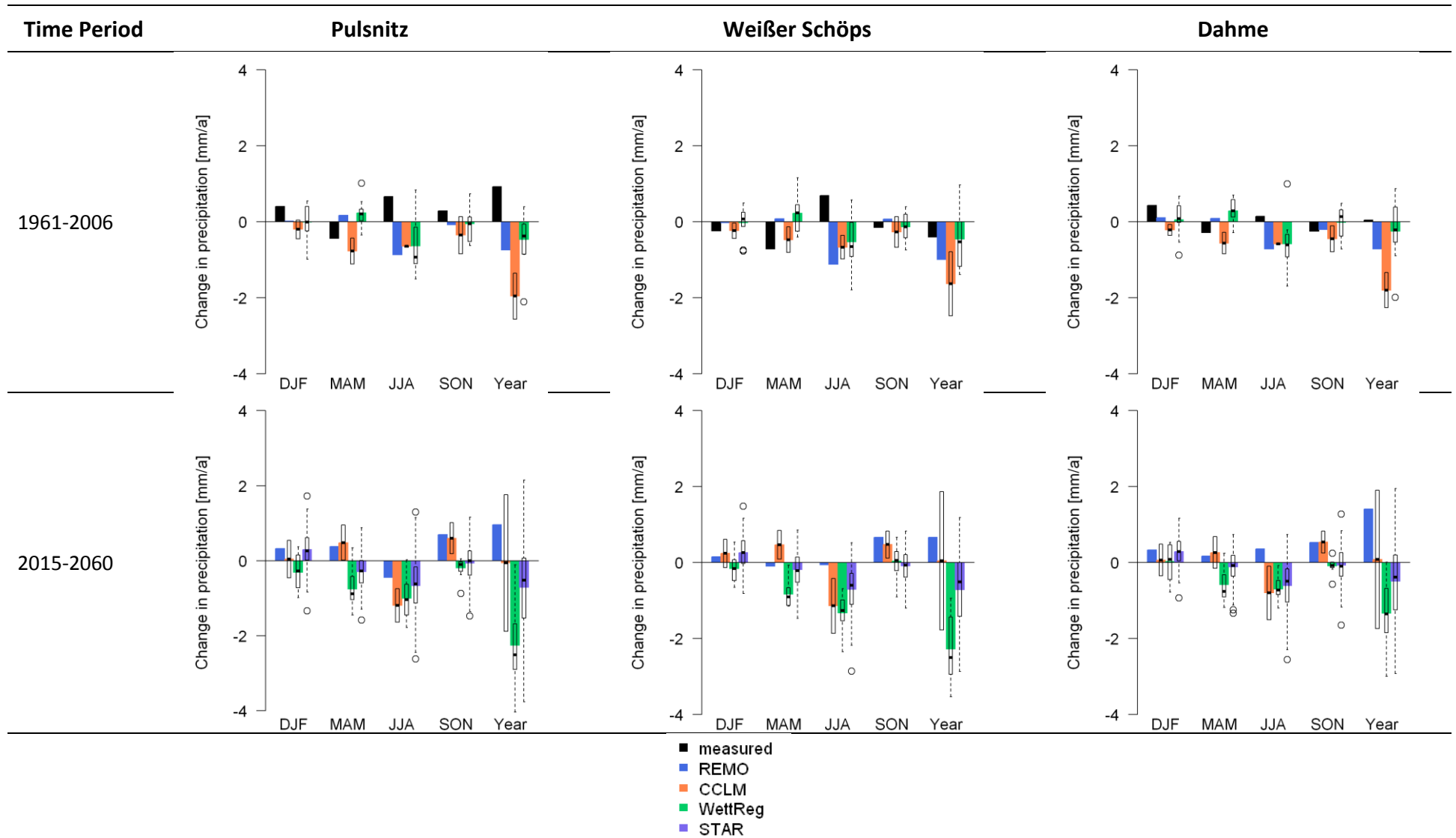


Figure C-18: Precipitation: Comparison of trend magnitude between measured and simulated precipitation for the period 1961-2006 (top) and between simulations for the period 2015-2061 (bottom) for the subcatchments

Appendix D. Hydrological modelling

Table D-1: Comparison of WaSiM-ETH and HBV-light as applied in this study

Characteristic	WaSiM-ETH	HBV-light
Spatial reference	fully distributed	lumped
Temporal resolution	daily	daily
Meteorological input data	P, T, HUM, W, Rad and/or SD	R, T, ETP
Spatial input data requirement	Uniform rasters for: land use, soil, elevation (minimum requirement)	not required
Calibration/Objective Function	automated, local gradient-based approach plus manual tuning on NSE, LNSE, volume error	automated, global approach (3 different objective functions: NSE, LNSE, MARE) without manual tuning
Soil Horizons	12-30 layers being 9-13 m thick (soil horizon has to include the groundwater table elevation)	1 (no real soil depth approach)
Precipitation Correction	separately for rain and snow depending on temperature (SEVRUK, 1986)	not included
Interpolation of meteorological input data	<u>I</u> nverse <u>D</u> istance <u>W</u> eighting (IDW) method	not included
ETP/ETA	Penman-Monteith approach, reduction to ETA depending on soil moisture	Calculation of ETP is not included in the model, ETA is calculated based on soil water storage
Snow melt	Degree-day method	Degree-day method
Interception	LAI dependent bucket approach	not included
Infiltration	Richards equation	not included
Unsaturated flow	Richards equation parameterized based on VAN GENUCHTEN (1980)	based on a linear storage approach
Saturated flow	integrated 2D groundwater model	linear storage approach
Routing	kinematic wave approach/flow velocity after Manning-Strickler (MANNING, 1890; STRICKLER, 1923)	runoff transformation by triangular weighting function

Selected model equations of WaSiM-ETH

$$\lambda E = \frac{3.6 * \frac{\Delta}{\gamma_p} * (R_N - G) + \frac{\rho * c_p}{\gamma * r_a} (e_s - e) * t_i}{\frac{\Delta}{\gamma_p} + 1 + \frac{r_s}{r_a}} \quad \text{Equation D-1}$$

- with λ latent vaporization heat $\lambda=(2500.8 - 2.372*T)$ [kJ/kg]
 E latent heat flux [mm/m²]
 Δ tangent of the saturated vapour pressure curve [hPa/K]
 R_N net radiation
 G soil heat flux, here $0.1 * R_N$
 ρ density of dry air [kg/m³]
 c_p specific heat capacity of dry air at constant pressure, $c_p = 1.005$ kJ/(kg*K)
 e_s saturation vapour pressure at temperature T [hPa]
 e observed actual vapour pressure [hPa]
 t_i number of seconds within a time step
 γ_p psychrometric constant [hPa/K]
 r_s bulk-surface resistance [s/m]
 r_a bulk-aerodynamic resistance [s/m]

$$ETA_i = \begin{cases} 0 & \theta(\Psi) > \theta_{pwp} \\ ETP_i * \frac{(\theta(\Psi_i) - \theta_{pwp})}{(\theta_{\Psi_g} - \theta_{pwp})} & \theta_{pwp} \leq \theta(\Psi) \leq \theta_{\Psi_g} \\ ETP_i & \theta_{\Psi_g} \leq \eta * \theta_{sat} \\ ETP_i * \frac{(\theta_{sat} - \theta(\Psi_i))}{(\theta_{sat} - \eta * \theta_{sat})} & \eta * \theta_{sat} < \theta(\Psi) \leq \theta_{sat} \end{cases} \quad \text{Equation D-2}$$

- with i index of the soil layer
 ETA actual evapotranspiration [mm]
 ETP potential evapotranspiration [mm]
 $\theta(\Psi)$ actual relative soil water content at suction [-]
 Ψ actual suction (capillary pressure) [m]
 η maximum relative water content without partly or total anaerobe conditions ($\approx 0.9-0.95$)
 θ_{sat} saturation water content of the soil [-]
 θ_{Ψ_g} soil water content at a given suction
 θ_{pwp} water content of the soil at permanent wilting point ($=1.5$ MPa ≈ 150 m)

$$q_{ifl} = k_{sat}(\theta_m) * \Delta z * d_r * \tan\beta \quad \text{Equation D-3}$$

with k_{sat} saturated hydraulic conductivity [m/s]

θ_m water content in the actual layer m [-]

d_r drainage density for interflow [m^{-1}]

β local slope angle (important: if $\beta > 45^\circ$, β is limited to 45°)

Δz layer thickness [m]

$$q_i = q_{i-1} * e^{\frac{-\Delta t}{k_D}} + \hat{q} * (1 - e^{\frac{-\Delta t}{k_D}}) \quad \text{Equation D-4}$$

with q_i transformed (by a single linear storage) surface runoff/interflow in the time step i [mm]

q_{i-1} transformed (by a single linear storage) surface runoff/interflow in the time step i-1 [mm]

\hat{q} surface runoff/interflow in the time step I within the lowest flow time zone [mm]

Δt time step [h]

k_D recession constant for surface runoff/interflow single linear storage [h]

$$k_{sat,z} = k_{sat,z=0} * (k_{rec})^z \quad \text{Equation D-5}$$

with t depth

k_{sat} saturated hydraulic conductivity [m/s]

k_{rec} recession of the hydraulic conductivity with depth

z depth

Table D-2: Statistical performance indicators used for calibration and validation of runoff simulations (t: time index, Q_{mes} : measured discharge, Q_{sim} simulated discharge)

Performance indicators	Range	Value for “perfect” fit	Definition
NSE	$-\infty - 1$	1	$NSE = 1 - \frac{\sum(Q_{sim}(t) - Q_{mes}(t))^2}{\sum(Q_{mes}(t) - \bar{Q}_{mes})^2}$
LNSE	$-\infty - 1$	1	$LNSE = 1 - \frac{\sum(\ln Q_{sim}(t) - \ln Q_{mes}(t))^2}{\sum(\ln Q_{mes}(t) - \ln \bar{Q}_{mes})^2}$
r^2	0 – 1	1	$r^2 = \frac{(\sum(Q_{mes}(t) - \bar{Q}_{mes}) * (Q_{sim}(t) - \bar{Q}_{sim}))^2}{\sum(Q_{mes}(t) - \bar{Q}_{mes})^2 * \sum(Q_{sim}(t) - \bar{Q}_{sim})^2}$
MARE	$-\infty + \infty$	1	$MARE = 1 - \frac{1}{n} \sum \frac{ Q_{mes}(t) - Q_{sim}(t) }{Q_{mes}(t)}$
MBE [%]	$-\infty + \infty$	0	$MBE = - \frac{\sum(Q_{mes}(t) - Q_{sim}(t)) * 100}{\sum Q_{mes}(t)}$

NSE: Nash-Sutcliffe Efficiency, LNSE: Nash-Sutcliffe Efficiency using logarithmic discharges, r^2 : Coefficient of determination, MARE: mean absolute relative error, MBE: Mass balance error

Table D-3: Meteorological input variables for WaSiM-ETH

Meteorological input variables	Unit
precipitation	mm
temperature	°C
air humidity	1/1
global radiation	W/m ²
relative sunshine duration	1/1
wind speed	m/s

Table D-4: Soil and land use model parameters defined for each grid cell

Parameter	Unit
macropores (integrated into soil model)	
maximum depth of the macropores	m
maximum capacity of the macropores	mm/h
precipitation capacity thresholding macropore runoff	mm/h
reduction of the macropore capacity with depth	1/1
soil	
saturated water content (=fillable porosity) (Θ_s)	m^3/m^3
residual water content (water content which cannot be poured by transpiration, only by evaporation) (Θ_r)	m^3/m^3
saturated hydraulic conductivity (k_{sat})	m/s
layer-based recession constant of k_{sat} with depth (k_{rec})	-
van Genuchten parameter α	1/hPa
van Genuchten parameter n	-
land use	
leaf area index	m^2/m^2
vegetation covered fraction	m^2/m^2
albedo	-
root depth	m
roughness length	m
leaf/interception/soil surface resistance	s/m
specific thickness of the water layer on the leaves	mm
hydraulic head (suction) for beginning of stress of the vegetation due to dryness or water stress	hPa
root density distribution	-

Table D-5: Calibrated effective model parameters for WaSiM-ETH in the study catchments (parameter k_{rec} was set uniform for whole catchment)

Parameter	Unit	Without Calibration	Pulsnitz		Weißer Schöps			Dahme
Gauge			Ortrand	Königsbrück	Särichen	Königshain	Holtendorf	Prierow, Dahme Stadt
$q_{d_{rec}}$	h	24.0	118.0	62.3	49.5	19.0	24.0	200.0
$q_{i_{rec}}$	h	120.0	148.0	93.4	92.6	35.6	36.0	350.0
d_r	m^{-1}	35.0	15.0	20.0	10.1	16.9	10.1	25.0
k_{rec}	-	0.4	0.74		0.9			0.9

Table D-6: Calibrated effective model parameters for the different HBV-light model configurations (NSE: Nash-Sutcliffe efficiency; LNSE: Nash-Sutcliffe efficiency using logarithmic discharge; MARE: mean absolute relative error) in the study catchments

Parameter	Without Calibration	Pulsnitz			Weißer Schöps			Dahme		
		HBV-light _{NSE}	HBV-light _{LNSE}	HBV-light _{MARE}	HBV-light _{NSE}	HBV-light _{LNSE}	HBV-light _{MARE}	HBV-light _{NSE}	HBV-light _{LNSE}	HBV-light _{MARE}
<i>Snow Routine</i>										
TT [°C]	-2	-0.15	-1.95	-1.98	-0.3323	-0.23	-0.33	-1.79	-2.00	-1.78
CFMAX [mm °C ⁻¹ d ⁻¹]	3	2.35	3.18	3.27	2.76	3.52	3.50	1.18	4.00	1.11
SFCF [-]	1	0.73	0.90	0.83	0.64	0.90	0.90	0.90	0.88	0.67
<i>Soil Moisture Routine</i>										
FC [mm]	200	427.19	341.78	339.10	269.27	293.85	324.81	464.08	429.36	391.96
LP [-]	0.5	0.30	0.30	0.30	0.58	0.43	0.52	0.43	0.30	0.46
BETA [-]	5	1.11	1.26	1.18	3.45	2.49	3.43	2.25	1.74	2.57
<i>Runoff Response Routine</i>										
K0 [d ⁻¹]	0.5	0.12	0.10	0.50	0.28	0.15	0.26	0.10	0.10	0.26
K1 [d ⁻¹]	0.2	0.10	0.04	0.08	0.10	0.19	0.11	9.38	0.05	0.06
K2 [d ⁻¹]	0.005	0.038	0.002	0.023	0.0016	0.0016	0.0007	0.1	0.0011	0.00025
PERC [mm d ⁻¹]	4	1.72	0.38	0.75	0.25	0.43	0.32	1.03	0.10	0.09
UZL [mm]	10	25.02	29.07	23.17	7.03	4.42	8.69	9.38	21.48	25.70
<i>Routing Routine</i>										
MAXBAS [d]	1	2.50	2.26	2.50	2.29	2.45	2.50	1.50	1.28	1.22

Table D-7: Statistical performance indicators of discharge calibration and validation for *daily (1999-2006) and ** long term mean monthly time step (Weißer Schöps und Pulsnitz: 1963-1992 (Weißer Schöps gauge Königshain (1979-1992); Dahme: 1974-1992)) for the gauging stations located within the study catchments

Performance indicators	Calibration*(1999-2001)		Validation*(2001-2006)		Validation **	
	Without Calibration	Calibrated	Without Calibration	Calibrated	Without Calibration	Calibrated
Pulsnitz (gauge Königsbrück)						
r^2	0.68	0.71	0.58	0.54	0.77	0.77
NSE	0.07	0.37	0.51	0.50	0.47	0.47
LNSE	0.53	0.57	-0.07	-0.03	-0.32	-0.28
MBE	17.67	10.03	-7.87	-12.54	-31.76	-33.31
Weißer Schöps (gauge Königshain)						
r^2	0.40	0.60	0.51	0.58	0.64	0.80
NSE	0.38	0.51	0.45	0.54	0.54	0.71
LNSE	0.79	0.87	0.56	0.56	0.43	0.72
MBE	-6.97	-14.26	-26.14	-28.98	-21.99	-19.58
Weißer Schöps (gauge Holtendorf)						
r^2	0.75	0.80	0.65	0.73	0.69	0.86
NSE	0.74	0.80	0.59	0.68	0.64	0.70
LNSE	0.78	0.84	0.78	0.81	0.75	0.78
MBE	0.86	-5.09	-9.80	-12.28	1.22	-26.07
Dahme (gauge Dahme Stadt)						
r^2	0.69	0.68	0.46	0.26	0.01	0.00

Coefficient of determination (r^2), Coefficient of model efficiency (NSE), Coefficient of model efficiency using logarithmic runoff (LNSE), Mass balance error (MBE) [%]

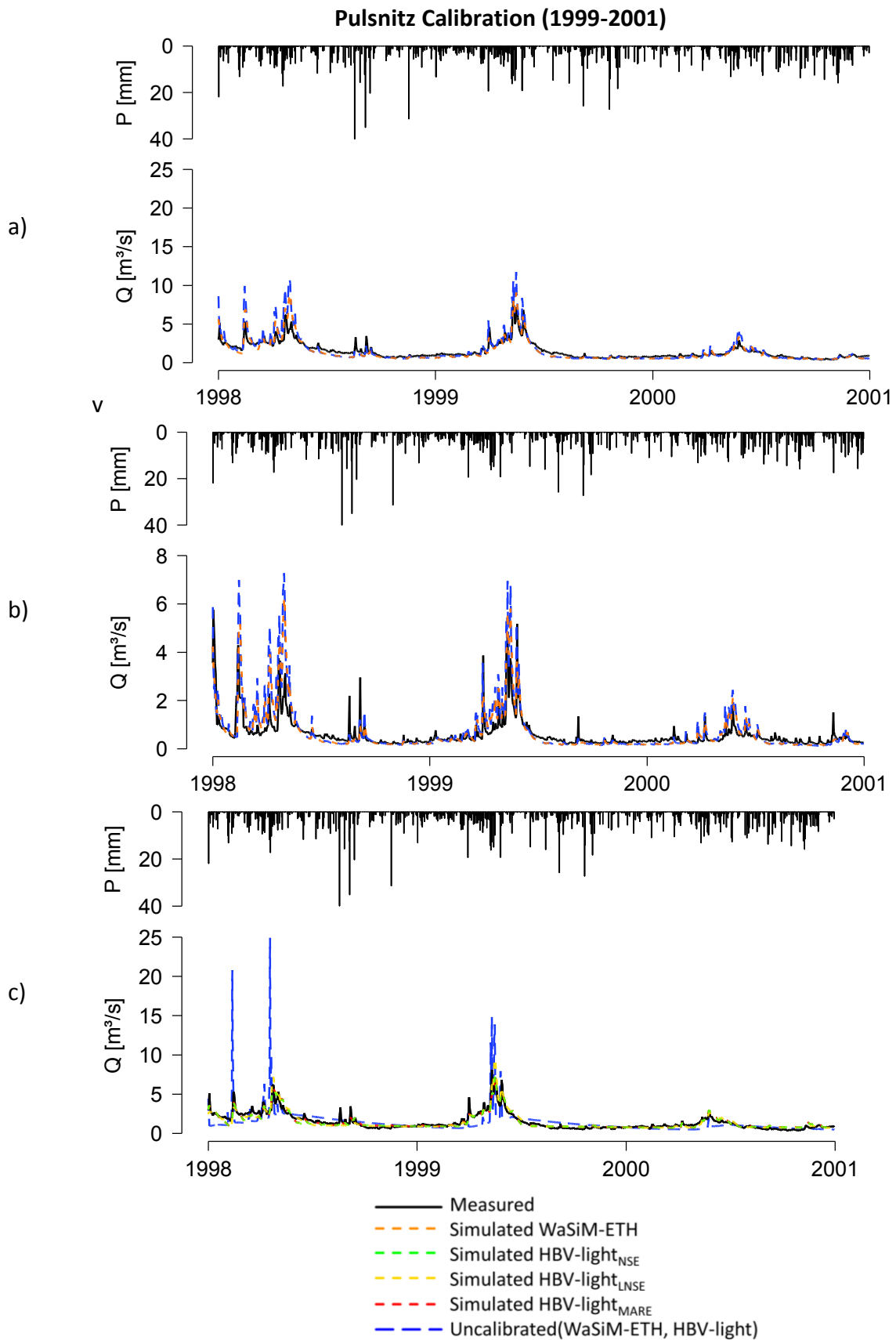


Figure D-1: Model calibration for the Pulsnitz river catchment using WaSiM-ETH (a: gauge Ortrand, b: gauge Königsbrück) and HBV-light (c: gauge Ortrand). Efficiency criteria can be found in Table 6-5 and Table D-7 in Appendix D (P = precipitation, Q = discharge)

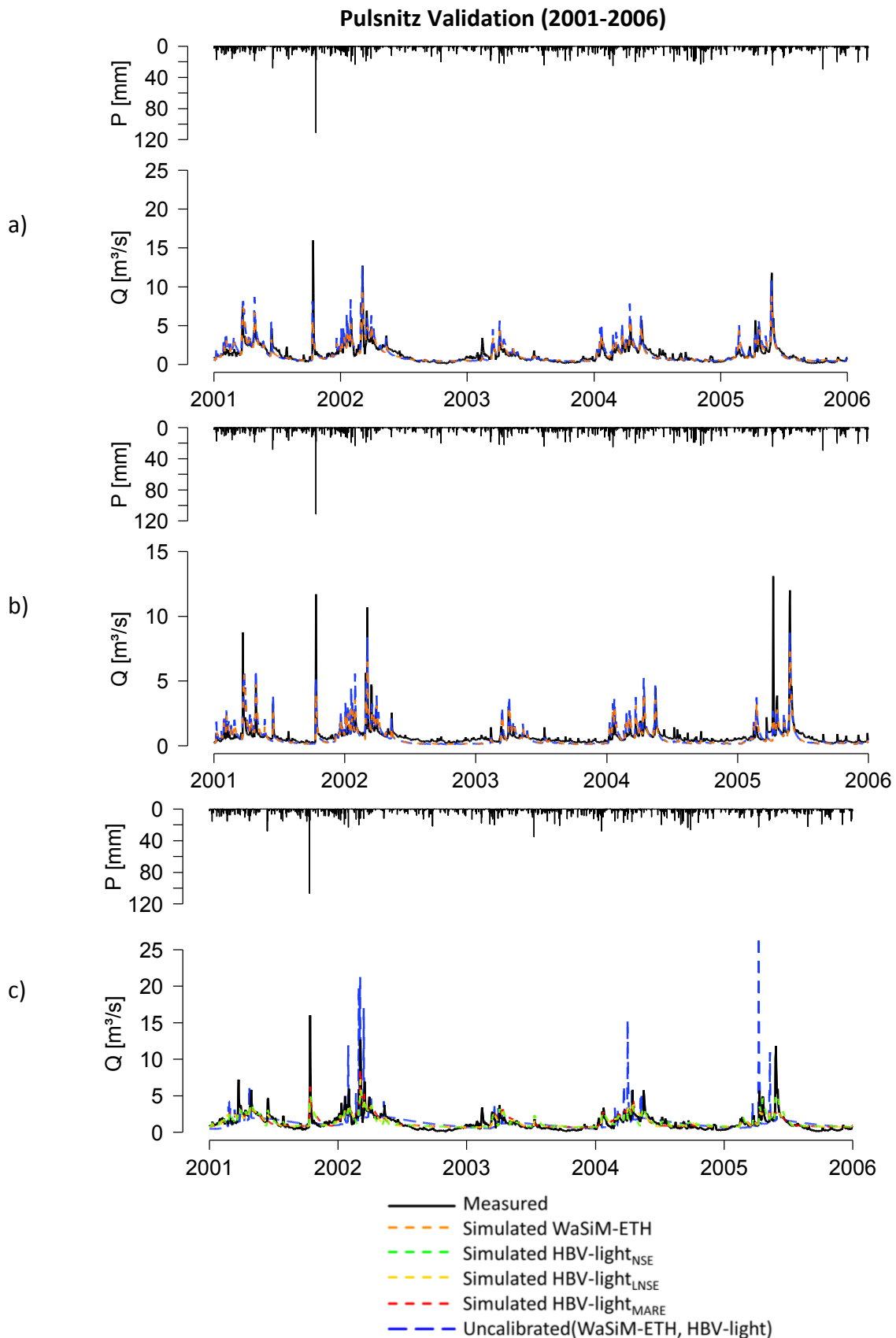


Figure D-2: Model validation for the Pulsnitz river catchment using WaSiM-ETH (a: gauge Ortrand, b: gauge Königsbrück) and HBV-light (c: gauge Ortrand). Efficiency criteria can be found in Table 6-5 and Table D-7 in Appendix D (P = precipitation, Q = discharge)

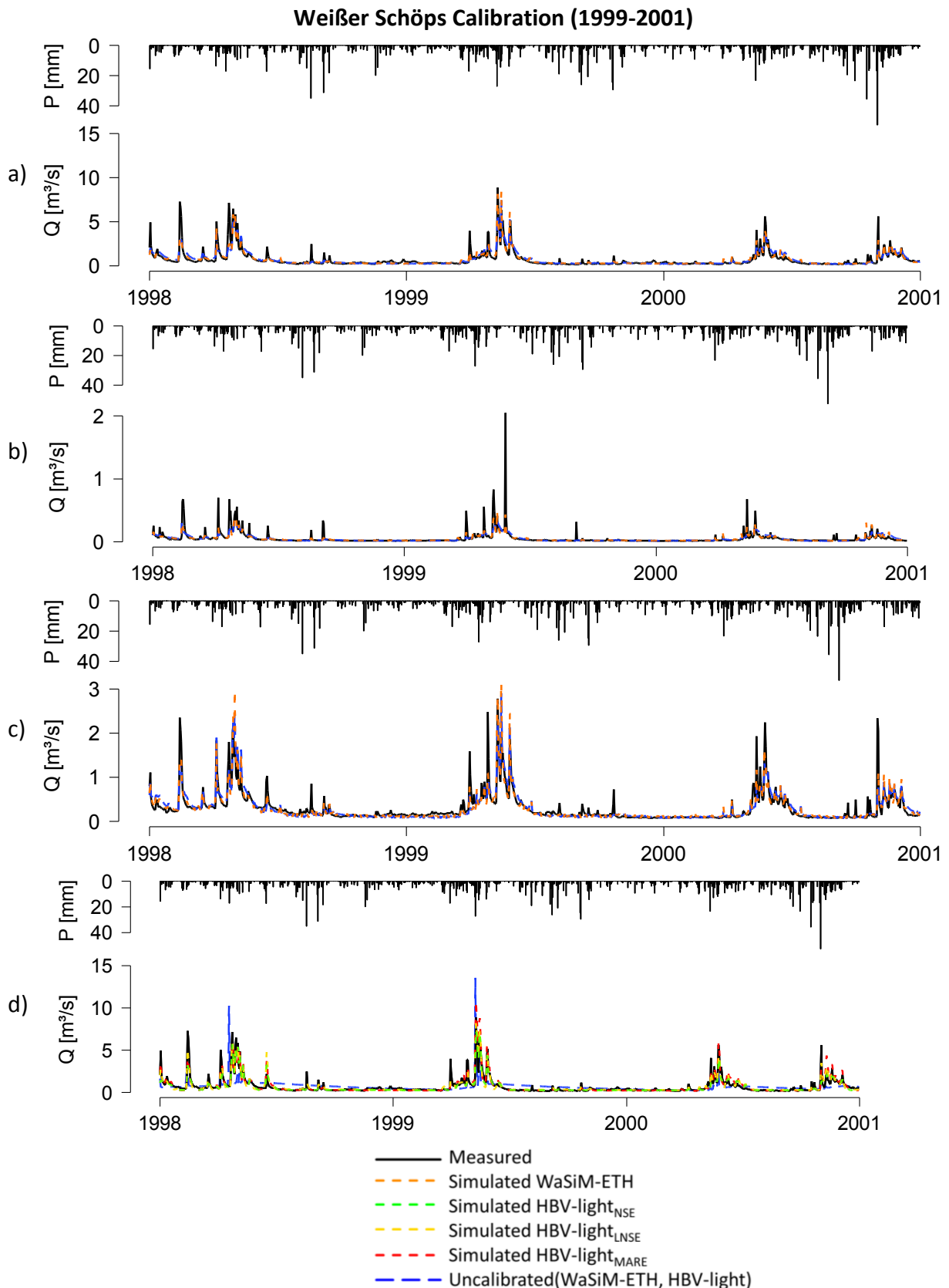


Figure D-3: Model calibration for the Weißer Schöps river catchment using WaSiM-ETH (a: gauge Särichen, b: gauge Königsbrück, c: gauge Holtendorf) and HBV-light (c: gauge Särichen). Efficiency criteria can be found in Table 6-5 and Table D-7 in Appendix D (P = precipitation, Q = discharge)

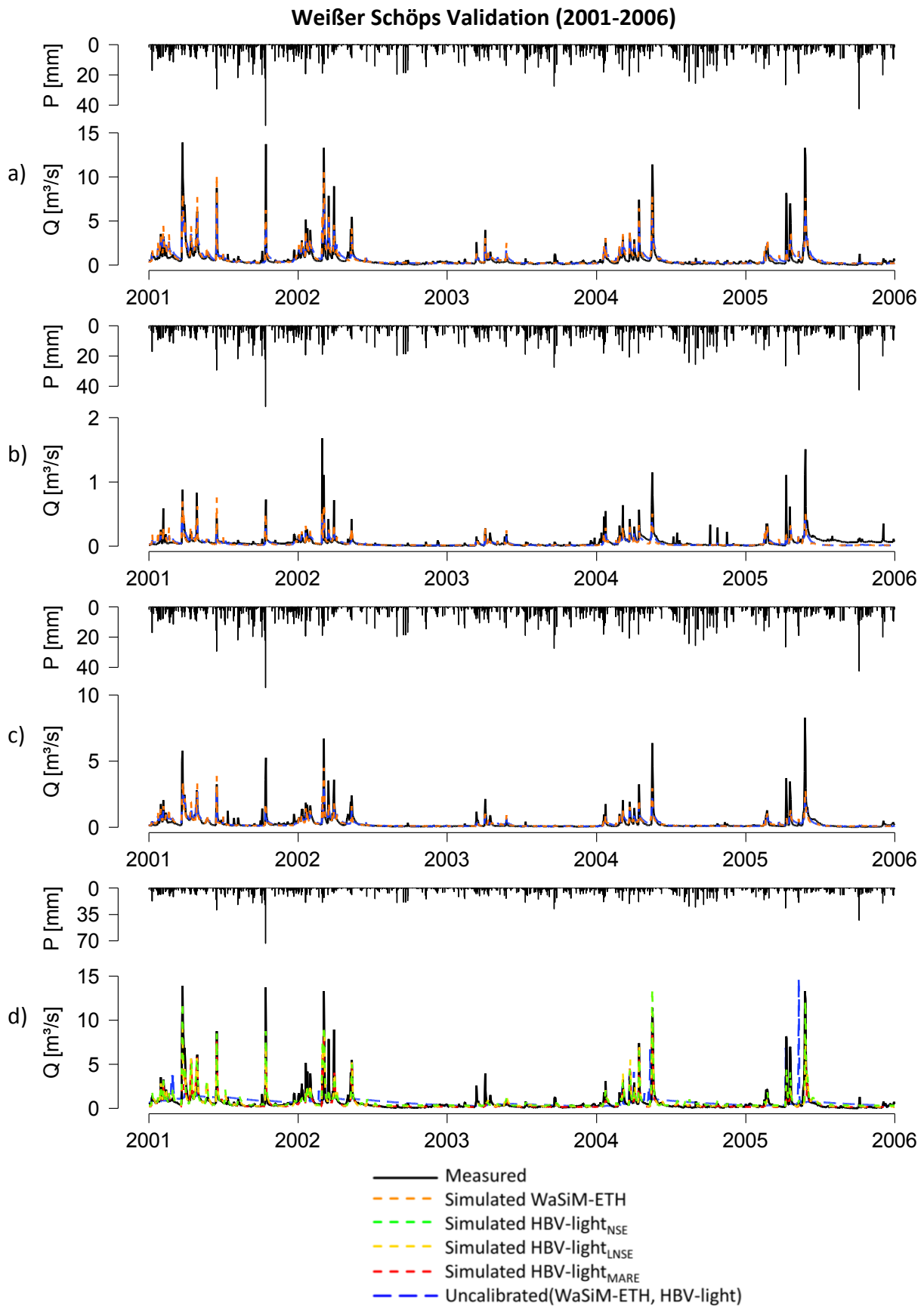


Figure D-4: Model validation for the Weißer Schöps river catchment using WaSiM-ETH (a: gauge Särichen, b: gauge Königsbrück, c: gauge Holtendorf) and HBV-light (c: gauge Särichen). Efficiency criteria can be found in Table 6-5 and Table D-7 in Appendix D (P = precipitation, Q = discharge)

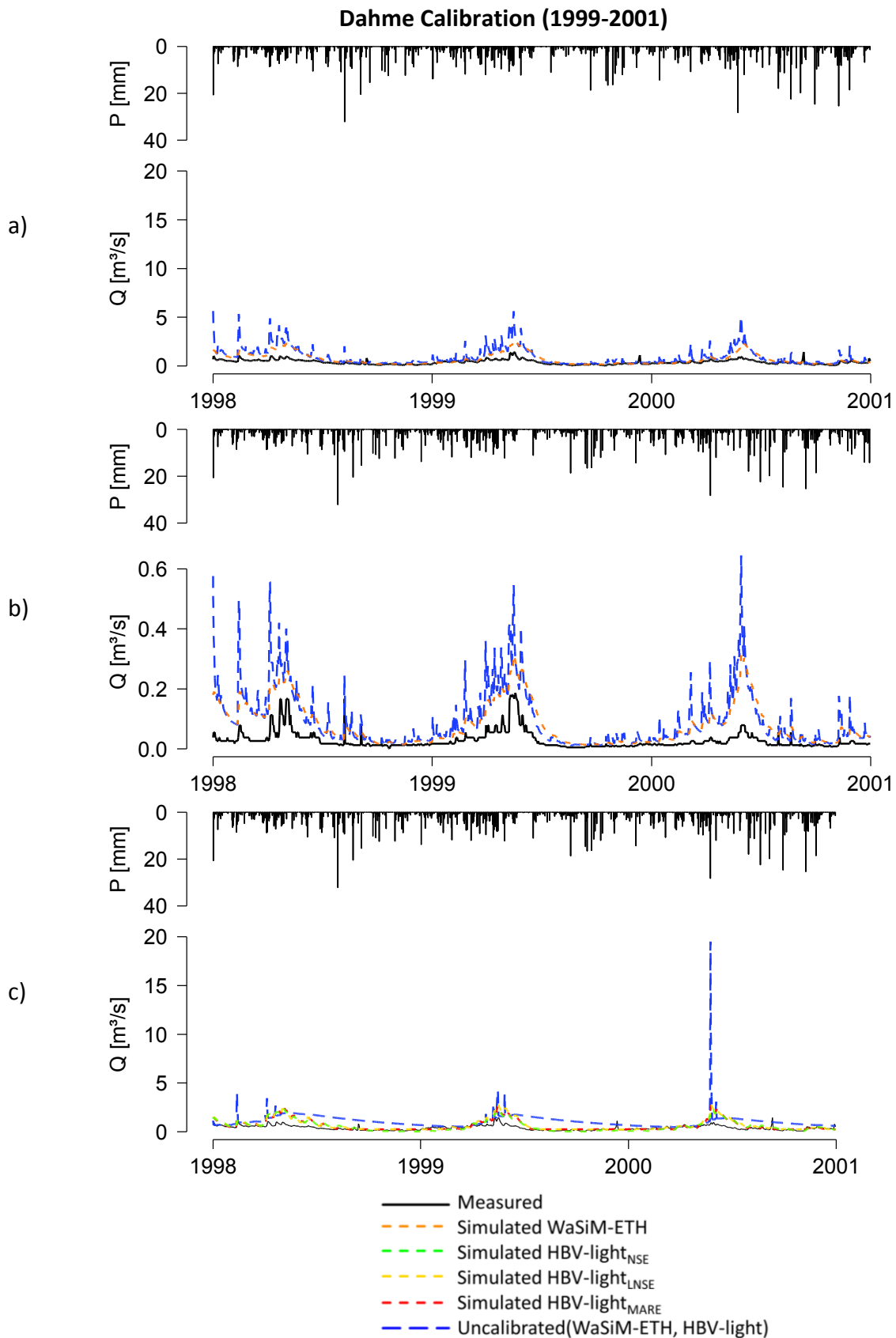


Figure D-5: Model calibration for the Dahme river catchment using WaSiM-ETH (a: gauge Prierow, b: gauge Dahme Stadt) and HBV-light (c: gauge Prierow). Efficiency criteria can be found in Table 6-5 and Table D-7 in Appendix D (P = precipitation, Q = discharge)

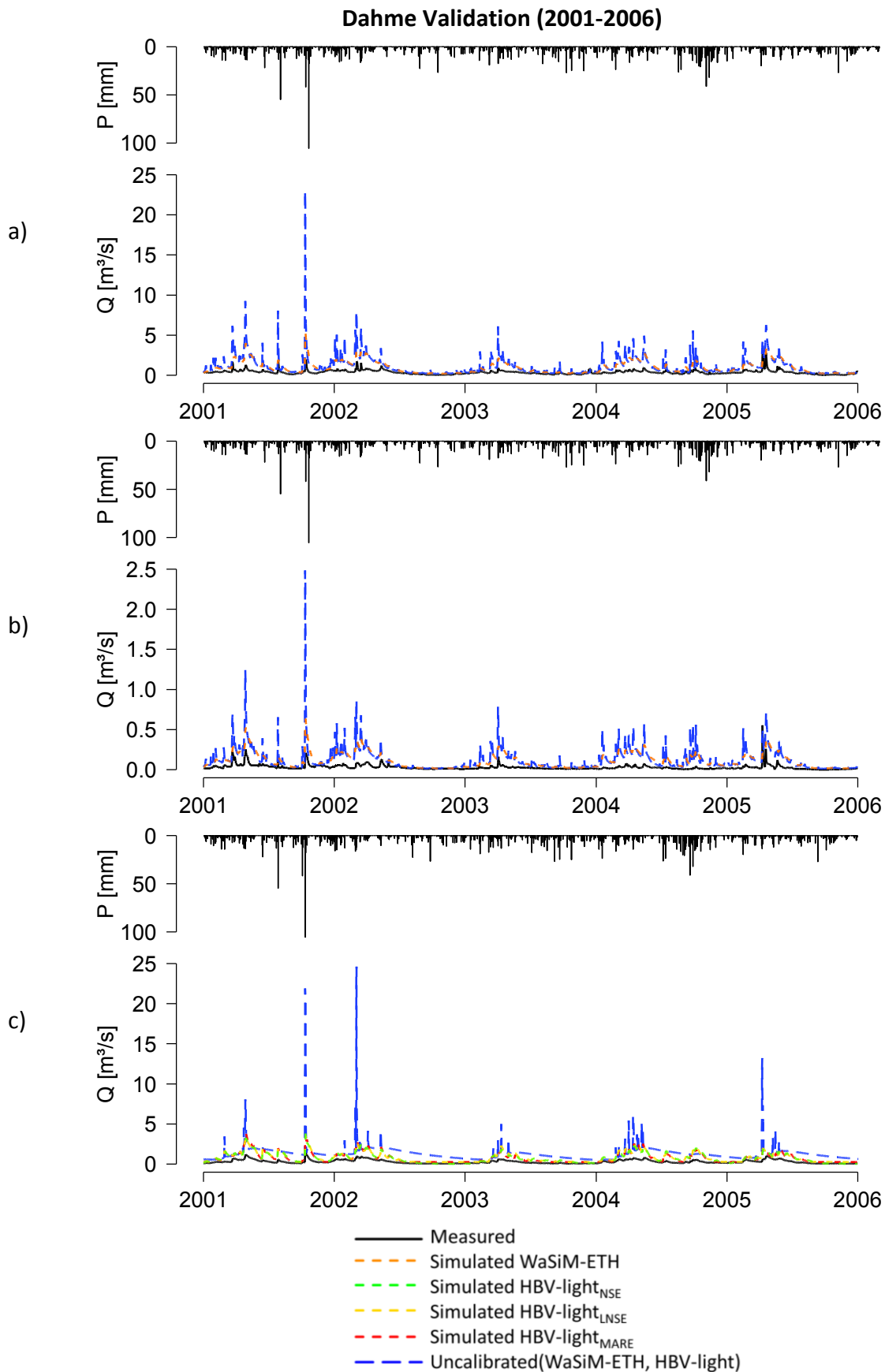


Figure D-6: Model validation for the Dahme river catchment using WaSiM-ETH (a: gauge Prierow, b: gauge Dahme Stadt) and HBV-light (c: gauge Prierow). Efficiency criteria can be found in Table 6-5 and Table D-7 in Appendix D (P = precipitation, Q = discharge)

Appendix E. Hydrological climate change impact assessments**Table E-1: Comparison of measured and simulated precipitation [mm] and temperature [°C] on a daily, monthly and annual basis during the reference period (1963-1992)**

		Precipitation				Temperature			
		Measured	REMO	CCLM	WettReg	Measured	REMO	CCLM	WettReg
Pulsnitz									
Day	Max	103.5	61.6	66.1	136.4	29.5	30.1	32.4	30.6
	Mean	1.91	1.89	1.87	2.0	8.9	9.2	9.0	9.1
	Median	0.13	0.34	0.58	0.55	9.1	9.6	9.2	9.2
	Min	0	0	0	0	-21.4	-23.5	-17.1	-20.6
	Standard Deviation	4.1	3.6	3.2	4.1	7.9	7.5	7.5	7.5
Month	Max	199	154	218	249	21.5	23.3	22.0	22.0
	Mean	58.1	57.6	56.9	62	8.8	9.2	8.9	9.1
	Median	51.6	53.4	54	58	8.6	9.7	9.1	8.8
	Min	4.4	1.6	3.9	4.0	-8.6	-4.6	-5.8	-7.1
	Standard Deviation	32.3	30.3	26.9	29.2	7.0	6.8	6.8	6.6
Year	Max	936	995	869	1071	10.3	11.0	10.6	10.0
	Mean	698	691	682	743	8.9	9.2	9	9.1
	Median	682	686	683	739	8.9	9	8.9	9.1
	Min	508	501	475	477	7.3	7.8	7.6	8.0
	Standard Deviation	126	107	92	100	0.8	0.7	0.6	0.4
Weißer Schöps									
Day	Max	77	58	110	98	29.0	29.1	31.9	29.3
	Mean	1.99	1.97	1.96	2.00	8.3	8.7	8.5	8.5
	Median	0.1	0.4	0.6	0.2	8.6	9.1	8.7	8.6
	Min	0	0	0	0	-22.7	-23.3	-18.0	-21.8
	Standard Deviation	4.4	3.7	3.4	4.5	7.9	7.6	7.6	7.5
Month	Max	298	218	230	307	21	22.7	21.6	21.1
	Mean	61	60	60	61	8.2	8.7	8.4	8.5
	Median	54	56	55	55	8.3	9.3	8.8	8.3
	Min	4	1	6	2	-9.1	-5.4	-6.4	-7.7
	Standard Deviation	36	32	30	32	7.1	6.8	6.9	6.7
Year	Max	1020	950	910	1148	9.7	10.4	10.2	9.4
	Mean	727	718	714	728	8.3	8.7	8.5	8.5
	Median	711	712	703	723	8.4	8.6	8.4	8.5
	Min	537	526	479	477	6.8	7.3	7.1	7.5
	Standard Deviation	114	96	100	113	0.8	0.7	0.6	0.4
Dahme									
Day	Max	162	102	68	203.2	28.9	29.2	31.7	29.0
	Mean	1.78	1.87	1.79	1.94	8.5	8.9	8.7	8.9
	Median	0.05	0.26	0.47	0.40	8.6	9.2	8.8	9.0
	Min	0	0	0	0	-20.1	-24.1	-17.6	-19.8
	Standard Deviation	4.2	4.1	3.2	4.2	7.9	7.5	7.6	7.3
Month	Max	239	209	144	288	20.8	22.9	21.7	21.4
	Mean	54.1	56.9	54	59	8.43	8.9	8.6	8.9
	Median	51	52	52	54	8.22	9.2	8.6	8.6
	Min	2.3	2.7	2.7	2.8	-8.56	-5.6	-6.6	-7.5
	Standard Deviation	30.1	32.6	25.7	29.7	7.2	6.9	6.9	6.5
Year	Max	826	929	808	1042	10	10.7	10.1	10.0
	Mean	650	683	653	707	8.47	8.9	8.6	8.9
	Median	643	681	658	696	8.46	8.8	8.6	9.0
	Min	438	447	481	468	7	7.5	7.2	7.9
	Standard Deviation	110	108	87	99	0.83	0.74	0.62	0.38

Table E-2: Long term water balance components [mm/a] for the Pulsnitz river catchment for the reference and scenario period as well as the difference between both (coloured arrows mark the magnitude of change)

DA	Hydrological Model	P _{cor}		ETP		ETA		R		ΔS	
		Reference	Scenario	Reference	Scenario	Reference	Scenario	Reference	Scenario	Reference	Scenario
REMO	WaSiM-ETH	691	724 →	901	916 →	598	612 →	102	113 ↗	-9	-1
	HBV-light _{NSE}					517	543 ↗	142	168 ↗	32	13
	HBV-light _{LNSE}					536	555 →	146	168 ↗	9	1
	HBV-light _{MARE}					527	546 →	153	177 ↗	11	1
CCLM	WaSiM-ETH	682	691 →	849	899 ↗	585	588 →	114	115 →	-17	-12
	HBV-light _{NSE}					510	521 →	156	163 →	16	7
	HBV-light _{LNSE}					525	528 →	157	162 →	0	1
	HBV-light _{MARE}					515	519 →	164	171 →	3	1
STAR	WaSiM-ETH	698*	670 →	866*	1031 ↗	581	590 →	126	95 ↘	-9	-15
	HBV-light _{NSE}					513	522 →	166	138 ↘	19	10
	HBV-light _{LNSE}					526	531 →	170	137 ↘	2	2
	HBV-light _{MARE}					516	522 →	176	145 ↘	6	3
WettReg	WaSiM-ETH	743	652 ↘	880	1090 ↗	623	605 →	137	76 ↓	-17	-29
	HBV-light _{NSE}					546	524 →	176	118 ↓	21	10
	HBV-light _{LNSE}					562	537 →	178	115 ↓	3	0
	HBV-light _{MARE}					552	528 →	186	122 ↓	5	2

↓ < -25% ↘ -5 to -25% → -5 to 5% ↗ +5 to +25% ↑ > 25%

*based on meteorological measurements during the reference period

P_{cor}: corrected precipitation, ETP: potential evapotranspiration, ETA: actual evapotranspiration, R: runoff, ΔS: change in storage

Table E-3: Long term water balance components [mm/a] for the Weißer Schöps river catchment for the reference and scenario period as well as the difference between both (coloured arrows mark the magnitude of change)

DA	Hydrological Model	P _{cor}		ETP		ETA		R		ΔS	
		Reference	Scenario	Reference	Scenario	Reference	Scenario	Reference	Scenario	Reference	Scenario
REMO	WaSiM-ETH	718	756 →	757	769 →	587	594 →	147	179 ↗	-16	-17
	HBV-light _{NSE}					561	579 →	131	169 ↑	26	8
	HBV-light _{LNSE}					576	591 →	147	175 ↗	-5	-10
	HBV-light _{MARE}					593	608 →	132	158 ↗	-7	-10
CCLM	WaSiM-ETH	714	715 →	715	722 →	568	572 →	165	162 →	-19	-19
	HBV-light _{NSE}					541	552 →	158	161 →	15	2
	HBV-light _{LNSE}					555	562 →	168	163 →	-9	-10
	HBV-light _{MARE}					570	580 →	153	144 ↘	-9	-9
STAR	WaSiM-ETH	727*	607 ↘	730*	865 ↗	557	545 →	195	83 ↓	-25	-21
	HBV-light _{NSE}					537	520 →	173	86 ↓	17	1
	HBV-light _{LNSE}					550	526 →	183	91 ↓	-6	-10
	HBV-light _{MARE}					567	545 →	167	72 ↓	-7	-10
WettReg	WaSiM-ETH	728	623 ↘	736	907 ↗	569	565 →	177	81 ↓	-18	-23
	HBV-light _{NSE}					538	536 →	171	85 ↓	19	2
	HBV-light _{LNSE}					554	543 →	181	91 ↓	-7	-11
	HBV-light _{MARE}					571	561 →	165	71 ↓	-8	-9

↓ < -25% ↘ -5 to -25% → -5 to 5% ↗ +5 to +25% ↑ > 25%

*based on meteorological measurements during the reference period

P_{cor}: corrected precipitation, ETP: potential evapotranspiration, ETA: actual evapotranspiration, R: runoff, Δ S: change in storage

Table E-4: Long term water balance components [mm/a] for the Dahme river catchment for the reference and scenario period as well as the difference between both (coloured arrows mark the magnitude of change)

DA	Hydrological Model	P _{cor}		ETP		ETA		R		ΔS	
		Reference	Scenario	Reference	Scenario	Reference	Scenario	Reference	Scenario	Reference	Scenario
REMO	WaSiM-ETH	683	709 →	889	909 →	598	610 →	114	121 ↗	-29	-22
	HBV-light _{NSE}					559	578 →	75	89 ↗	49	42
	HBV-light _{LNSE}					553	570 →	81	86 ↗	49	53
	HBV-light _{MARE}					554	573 →	70	85 ↗	59	51
CCLM	WaSiM-ETH	653	658 →	863	905 →	577	580 →	107	105 →	-31	-27
	HBV-light _{NSE}					541	546 →	73	73 →	39	39
	HBV-light _{LNSE}					533	536 →	80	83 →	40	39
	HBV-light _{MARE}					536	542 →	69	71 →	48	45
STAR	WaSiM-ETH	652*	625 →	883*	1043 ↗	569	570 →	109	81 ↓	-26	-26
	HBV-light _{NSE}					536	533 →	76	53 ↓	40	39
	HBV-light _{LNSE}					528	523 →	83	63 ↓	41	39
	HBV-light _{MARE}					530	530 →	69	50 ↓	53	45
WettReg	WaSiM-ETH	707	641 →	880	1049 ↗	615	602 →	119	68 ↓	-27	-29
	HBV-light _{NSE}					582	555 →	81	48 ↓	44	38
	HBV-light _{LNSE}					574	545 ↘	88	57 ↓	45	39
	HBV-light _{MARE}					577	553 →	77	44 ↓	53	44

↓ < -25% ↘ -5 to -25% → -5 to 5% ↗ +5 to +25% ↑ > 25%

*based on meteorological measurements during the reference period

P_{cor}: corrected precipitation, ETP: potential evapotranspiration, ETA: actual evapotranspiration, R: runoff, ΔS: change in storage

Table E-5: MAM(7) and Q95 simulated by WaSiM-ETH and HBV-light driven by the different DAs for the reference and scenario period (unit: 1000 m³/day)

	DA	Hydrological Model	Reference (01.04.1963 - 31.03.1991)		Scenario (01.04.2032 - 31.03.2060)	
			MAM(7)	Q95	MAM(7)	Q95
Pulsnitz						
	measured		*	*	-	-
	REMO	WaSiM-ETH	36.8	29.9	38.7	34.3
		HBV-light	56.5	46.9	59.7	51.1
	CCLM	WaSiM-ETH	40.1	33.5	38.9	34.2
		HBV-light	63.2	56.2	61.7	55.0
	STAR**	WaSiM-ETH	41.3	36.0	34.4	30.1
		HBV-light	60.8	53.7	53.1	45.7
	WettReg	WaSiM-ETH	44.1	39.2	29.3	25.8
		HBV-light	67.4	63.6	52.9	45.4
Weißer Schöps						
	measured		11.2	7.8	-	-
	REMO	WaSiM-ETH	16.9	13.0	19.1	16.0
		HBV-light	22.9	17.1	26.2	21.7
	CCLM	WaSiM-ETH	18.7	15.0	18.4	15.1
		HBV-light	27.1	22.5	27.0	22.4
	STAR**	WaSiM-ETH	20.2	17.2	13.6	10.8
		HBV-light	25.6	21.4	17.0	12.8
	WettReg	WaSiM-ETH	19.4	16.1	13.4	10.6
		HBV-light	26.5	22.8	17.8	14.2
Dahme						
	measured		18.2	16.4	-	-
	REMO	WaSiM-ETH	23.8	16.2	24.0	18.2
		HBV-light	21.9	18.5	21.9	18.8
	CCLM	WaSiM-ETH	23.8	17.1	21.0	15.4
		HBV-light	23.5	21.5	22.3	20.0
	STAR**	WaSiM-ETH	22.2	18.3	16.4	13.5
		HBV-light	21.9	20.6	18.8	17.0
	WettReg	WaSiM-ETH	25.6	21.7	15.4	12.5
		HBV-light	24.0	23.0	20.0	18.5

* no measurements at gauge Ortrand available for reference period (1964-1992)

** during the reference based on meteorological measurements

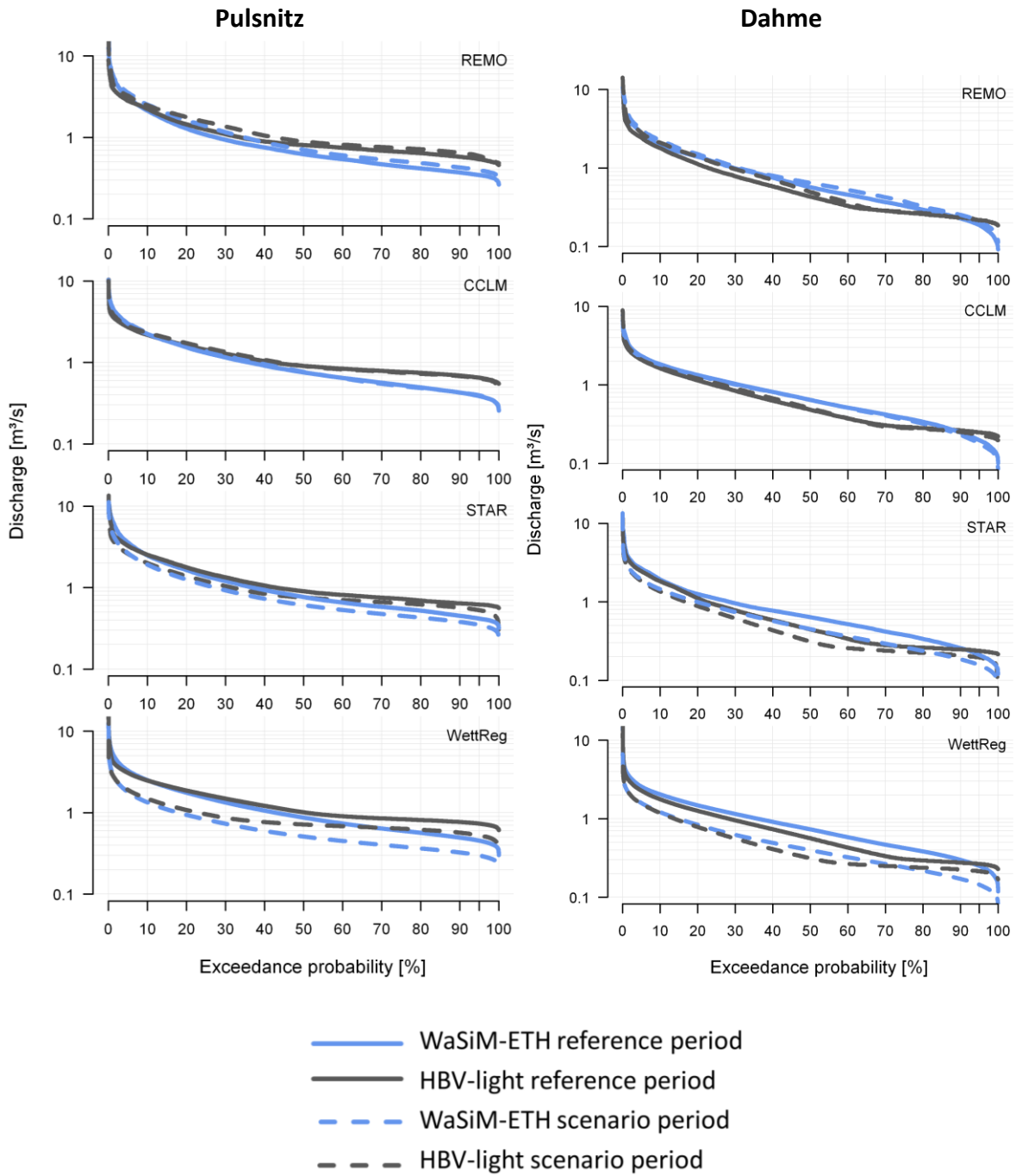
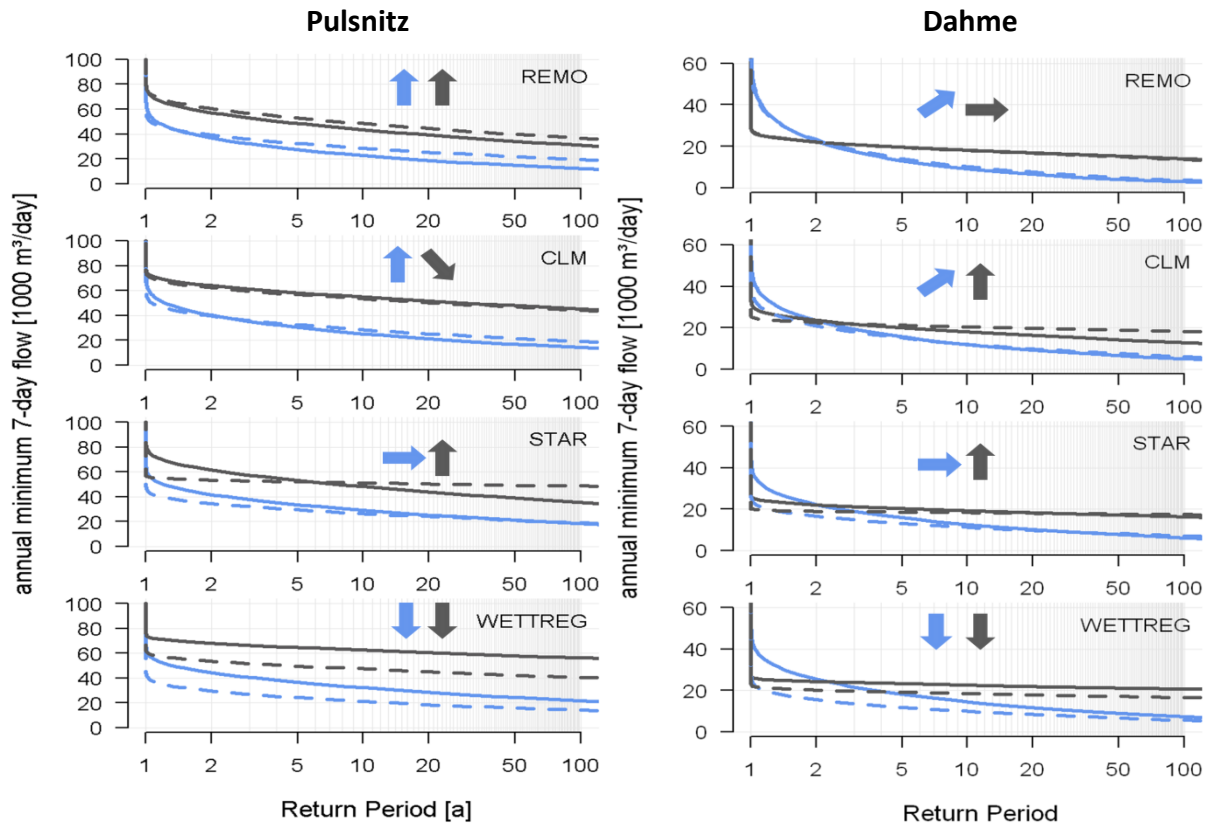







Figure E-1: Flow Duration Curve based on WaSiM-ETH and HBV-light driven by the DAs in the reference (1963-1991) and the scenario period (2032-2060) for the Pulsnitz and Dahme river catchments



Change in return period of the reference 50 year low-flow in the scenario period (unit: years) – arrow colours: blue = WaSiM-ETH, grey = HBV-light:

-  < 25
-  45-25
-  45-55
-  55-100
-  > 100





-  WaSiM-ETH reference period
-  HBV-light reference period
-  WaSiM-ETH scenario period
-  HBV-light scenario period

Figure E-2: Change in the return period of the 50-year AM(7) between the reference and scenario for the the Pulsnitz and Dahme river catchments. The arrows in the Figure display the change in occurrence of the return period of the reference 50 year low-flow in the scenario period (blue arrows: WaSiM-ETH; grey arrows: HBV-light)

Table E-6: P-value of Wilcoxon-Mann-Whitney test comparing the simulated discharge of the hydrological models during reference (ref) and scenario (scen) period concerning different hydrological indicators. Values highlighted in dark grey are significant at a level of 0.01 and light grey at a level of 0.05

Parameter			Pulsnitz	Weißer Schöps	Dahme
Mean annual discharge					
	REMO	ref	0.33	0.83	0.24
		scen	0.19	0.99	0.32
	CCLM	ref	0.10	0.55	0.13
		scen	0.01	0.58	0.08
	STAR	ref	0.68	0.91	0.10
		scen	< 0.01	< 0.01	0.01
	WettReg	ref	0.02	0.24	< 0.01
		scen	< 0.01	0.31	0.66
Minimum annual discharge					
	REMO	ref	< 0.01	< 0.01	0.07
		scen	< 0.01	< 0.01	0.09
	CCLM	ref	< 0.01	< 0.01	0.01
		scen	< 0.01	< 0.01	< 0.01
	STAR	ref	< 0.01	< 0.01	0.03
		scen	< 0.01	< 0.01	< 0.01
	WettReg	ref	< 0.01	< 0.01	0.16
		scen	< 0.01	< 0.01	< 0.01
AM(7)					
	REMO	ref	< 0.01	< 0.01	0.63
		scen	< 0.01	< 0.01	0.42
	CCLM	ref	< 0.01	< 0.01	0.37
		scen	< 0.01	< 0.01	0.23
	STAR	ref	< 0.01	< 0.01	0.54
		scen	< 0.01	< 0.01	< 0.01
	WettReg	ref	< 0.01	< 0.01	0.95
		scen	< 0.01	< 0.01	< 0.01

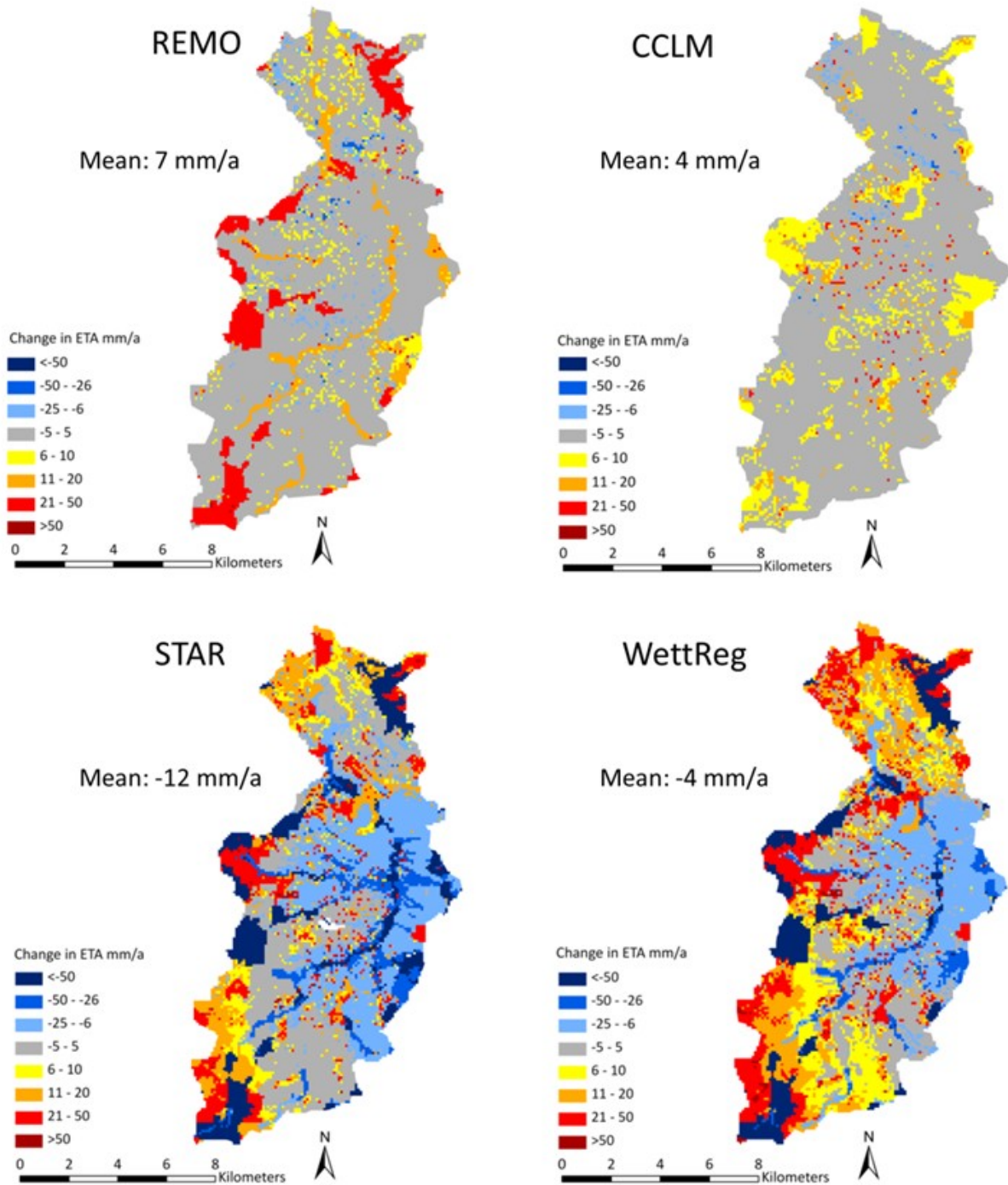


Figure E-3: Difference in actual evapotranspiration (ETA) based on REMO (top left), CCLM (top right), STAR (bottom left) and WettReg (bottom right) between the scenario and reference period for the Weißer Schöps river catchment. The average change is displayed in each figure

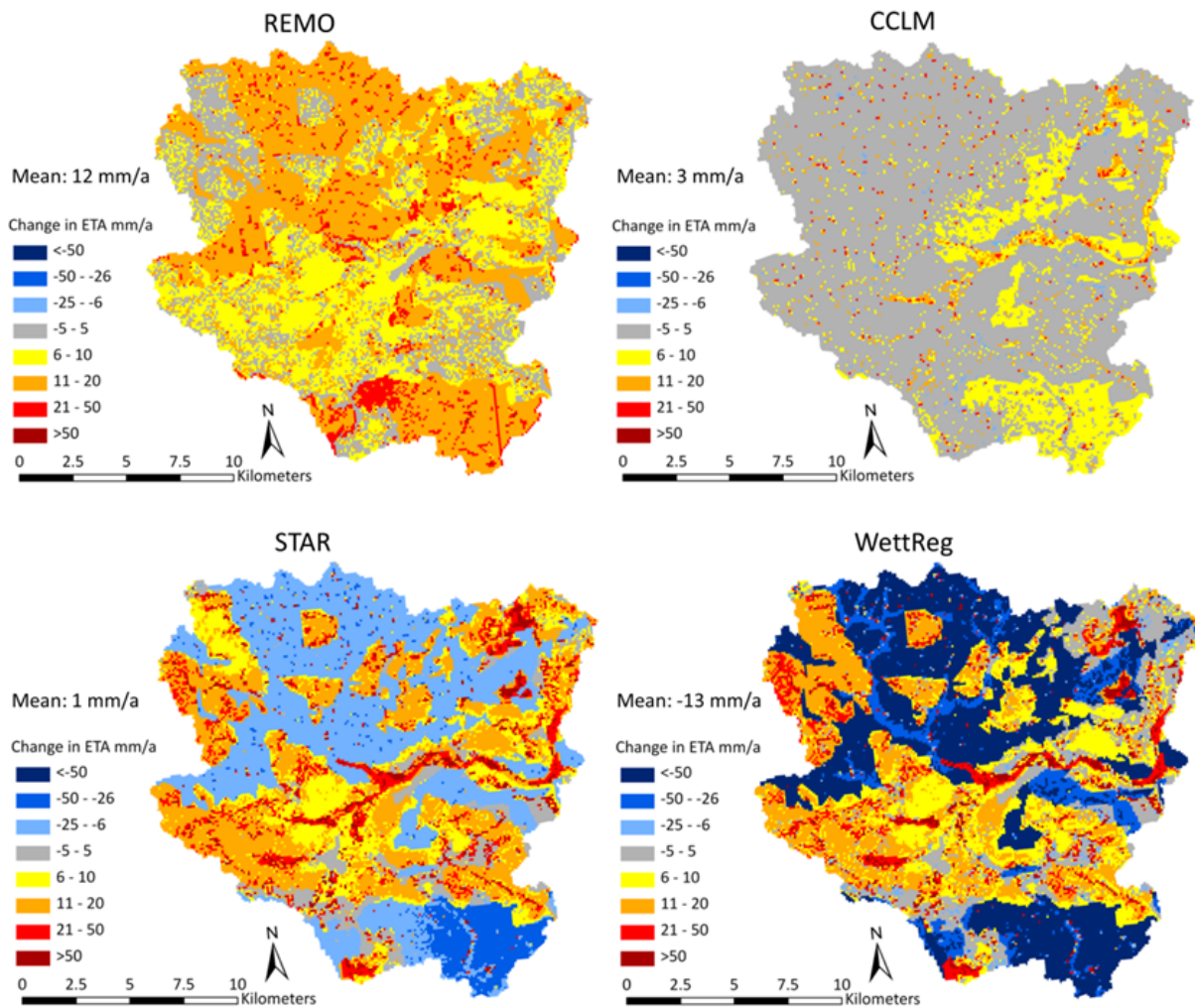


Figure E-4: Difference in actual evapotranspiration (ETA) based on REMO (top left), CCLM (top right), STAR (bottom left) and WettReg (bottom right) between the scenario and reference period for the Dahme river catchment. The average change is displayed in each figure

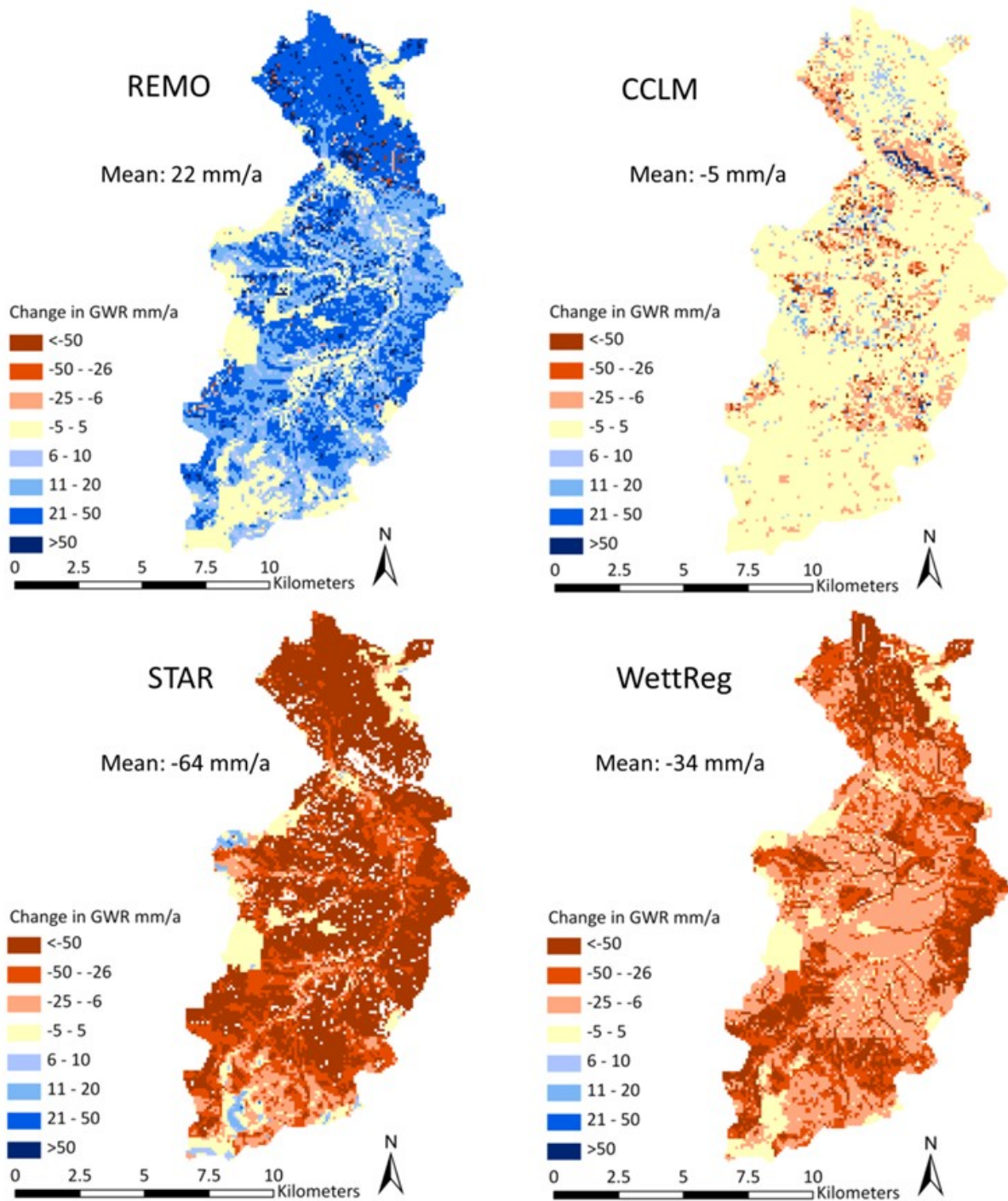


Figure E-5: Difference in groundwater recharge (GWR) based on REMO (top left), CCLM (top right), STAR (bottom left) and WettReg (bottom right) between the scenario and reference period for the Weißer Schöps river catchment. The average change is displayed in each figure.

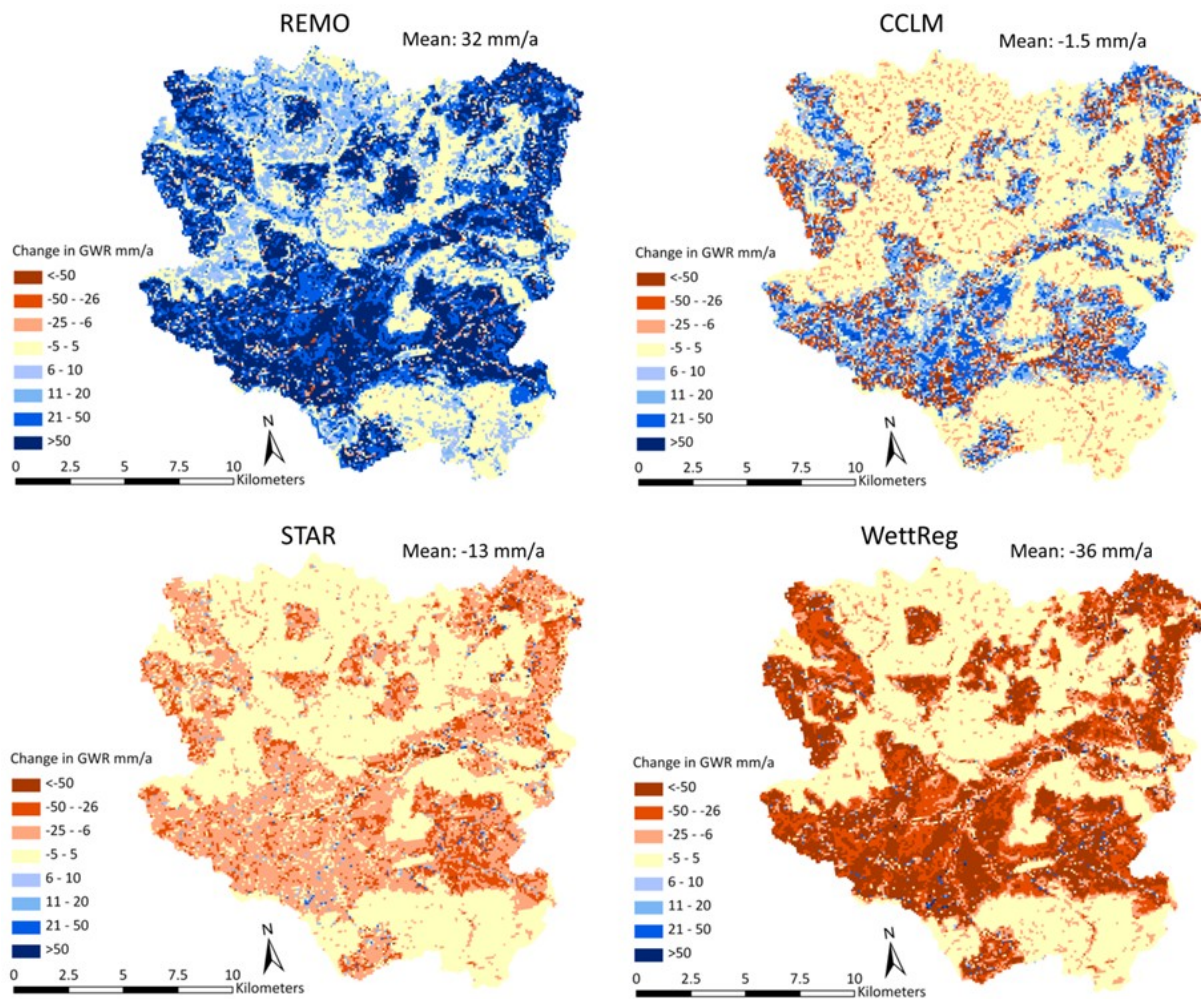


Figure E-6: Difference in groundwater recharge (GWR) based on REMO (top left), CCLM (top right), STAR (bottom left) and WettReg (bottom right) between the scenario and reference period for the Dahme river catchment. The average change is displayed in each figure.

Appendix F. Land use change analysis

Table F-1: Land use parameterisation in WaSiM-ETH (RootDistr: root distribution; TRW: threshold for anaerobic conditions in the root zone; LRW: reduction factor of anaerobic conditions in the root zone; HRD: hydraulic head for beginning dryness stress [m]; IntC: specific thickness of water layer on leaves [mm]; rsc: leaf surface resistance [s/m]; $rS_{interception}$: interception surface resistance [s/m]; $rS_{evaporation}$: LAI: Leaf Area Index; Z0: roughness length[m]; VCF: Vegetation Covered Fraction; Root Depth [m])

Agriculture												
RootDistr	1	TRW	0.95	LRW	0.5	HRD	3.5	IntC	0.4			
JulDays	15	46	74	105	135	166	196	227	258	288	319	349
Albedo	0.25	0.25	0.25	0.25	0.25	0.25	0.25	0.25	0.25	0.25	0.25	0.25
rsc	80	80	75	75	65	55	55	55	65	75	90	90
$rS_{interception}$	0.5	0.5	0.5	0.5	0.5	0.5	0.5	0.5	0.5	0.5	0.5	0.5
$rS_{evaporation}$	200	200	200	200	200	200	200	200	200	200	200	200
LAI	1	1	2	3	4	5	5	4	3	2	1	1
Z0	0.03	0.03	0.03	0.04	0.05	0.05	0.05	0.05	0.04	0.03	0.03	0.03
VCF	0.3	0.3	0.3	0.7	0.8	0.95	0.95	0.8	0.7	0.3	0.3	0.3
Root Depth	0.15	0.15	0.2	0.4	0.5	0.5	0.5	0.5	0.4	0.2	0.15	0.15
Changed agricultural parameterisation												
RootDistr	1	TRW	0.95	LRW	0.5	HRD	3.45	IntC	0.4			
JulDays	15	46	74	105	135	166	196	227	258	288	319	349
Albedo	0.25	0.25	0.25	0.25	0.25	0.25	0.25	0.25	0.25	0.25	0.25	0.25
rsc	40	20	20	20	20	20	20	20	20	20	40	40
$rS_{interception}$	0.5	0.5	0.5	0.5	0.5	0.5	0.5	0.5	0.5	0.5	0.5	0.5
$rS_{evaporation}$	200	200	200	200	200	200	200	200	200	200	200	200
LAI	1	2	3	3	3	3	1	2	2	2	1	1
Z0	0.01	0.02	0.05	0.05	0.07	0.08	0.08	0.01	0.01	0.01	0.01	0.01
VCF	0.1	0.3	0.8	0.9	0.9	0.9	0.1	0.3	0.5	0.5	0.1	0.1
Root Depth	0.2	0.5	0.6	0.6	0.6	0.6	0.1	0.3	0.3	0.3	0.2	0.2

Appendix F

Deciduous forest

RootDistr	1	TRW	0.95	LRW	0.5	HRD	3.5	IntC	0.6			
JulDays	15	46	74	105	135	166	196	227	258	288	319	349
Albedo	0.15	0.15	0.15	0.15	0.15	0.15	0.15	0.15	0.15	0.15	0.15	0.15
rsc	100	100	95	75	65	65	65	65	65	85	100	100
rS _{interception}	0.5	0.5	0.5	0.5	0.5	0.5	0.5	0.5	0.5	0.5	0.5	0.5
rS _{evaporation}	1500	1500	1500	1500	1500	1500	1500	1500	1500	1500	1500	1500
LAI	1	1	4	4	6	7	7	6	5	4	1	1
Z0	2	2	2	2	2	2	2	2	2	2	2	2
VCF	0.7	0.7	0.7	0.8	0.95	0.95	0.95	0.95	0.9	0.8	0.7	0.7
Root Depth	1.4	1.4	1.4	1.4	1.4	1.4	1.4	1.4	1.4	1.4	1.4	1.4

Coniferous forest

RootDistr	1	TRW	0.95	LRW	0.5	HRD	3.5	IntC	0.6			
JulDays	15	46	74	105	135	166	196	227	258	288	319	349
Albedo	0.12	0.12	0.12	0.12	0.12	0.12	0.12	0.12	0.12	0.12	0.12	0.12
rsc	80	80	75	65	55	55	55	55	55	75	80	80
rS _{interception}	0.5	0.5	0.5	0.5	0.5	0.5	0.5	0.5	0.5	0.5	0.5	0.5
rS _{evaporation}	1000	1000	1000	1000	1000	1000	1000	1000	1000	1000	1000	1000
LAI	6	6	8	8	10	10	10	10	8	8	6	6
Z0	3	3	3	3	3	3	3	3	3	3	3	3
VCF	0.9	0.9	0.9	0.9	0.95	0.95	0.95	0.95	0.95	0.9	0.9	0.9
Root Depth	1.2	1.2	1.2	1.2	1.2	1.2	1.2	1.2	1.2	1.2	1.2	1.2

Forest grass

RootDistr	1	TRW	0.95	LRW	0.5	HRD	3.5	IntC	0.4			
JulDays	15	46	74	105	135	166	196	227	258	288	319	349
Albedo	0.25	0.25	0.25	0.25	0.25	0.25	0.25	0.25	0.25	0.25	0.25	0.25
rsc	90	90	80	75	70	65	60	65	70	80	90	90
rS _{interception}	0.5	0.5	0.5	0.5	0.5	0.5	0.5	0.5	0.5	0.5	0.5	0.5
rS _{evaporation}	1000	1000	1000	1000	1000	1000	1000	1000	1000	1000	1000	1000
LAI	2	2	2	2	2	2	2	2	2	2	2	2
Z0	0.03	0.03	0.03	0.04	0.04	0.04	0.04	0.04	0.04	0.03	0.03	0.03
VCF	0.7	0.7	0.7	0.8	0.8	0.8	0.8	0.8	0.8	0.7	0.7	0.7
Root Depth	0.4	0.4	0.4	0.4	0.4	0.4	0.4	0.4	0.4	0.4	0.4	0.4

Uncultivated area

RootDistr	1	TRW	0.95	LRW	0.5	HRD	3.45	IntC	0.2
JulDays	1-365								
Albedo	0.35								
rsc	0.01								
rS _{interception}	150								
rS _{evaporation}	150								
LAI	0.01								
Z0	0.01								
VCF	0.01								
Root Depth	0.01								

Table F-2: Water balance components [mm/a] for the extreme scenarios where the entire catchment areas are parameterised as coniferous forest and uncultivated land compared to the current land use under current climate conditions (1963-1992)

Scenario	P _{cor}	ETA	R
Pulsnitz			
current land use	698	581	126
coniferous forest		683	50
uncultivated land		383	313
Weißer Schöps			
current land use	727	557	195
coniferous forest		713	39
uncultivated land		400	339
Dahme			
current land use	652	569	109
coniferous forest		655	34
uncultivated land		372	298

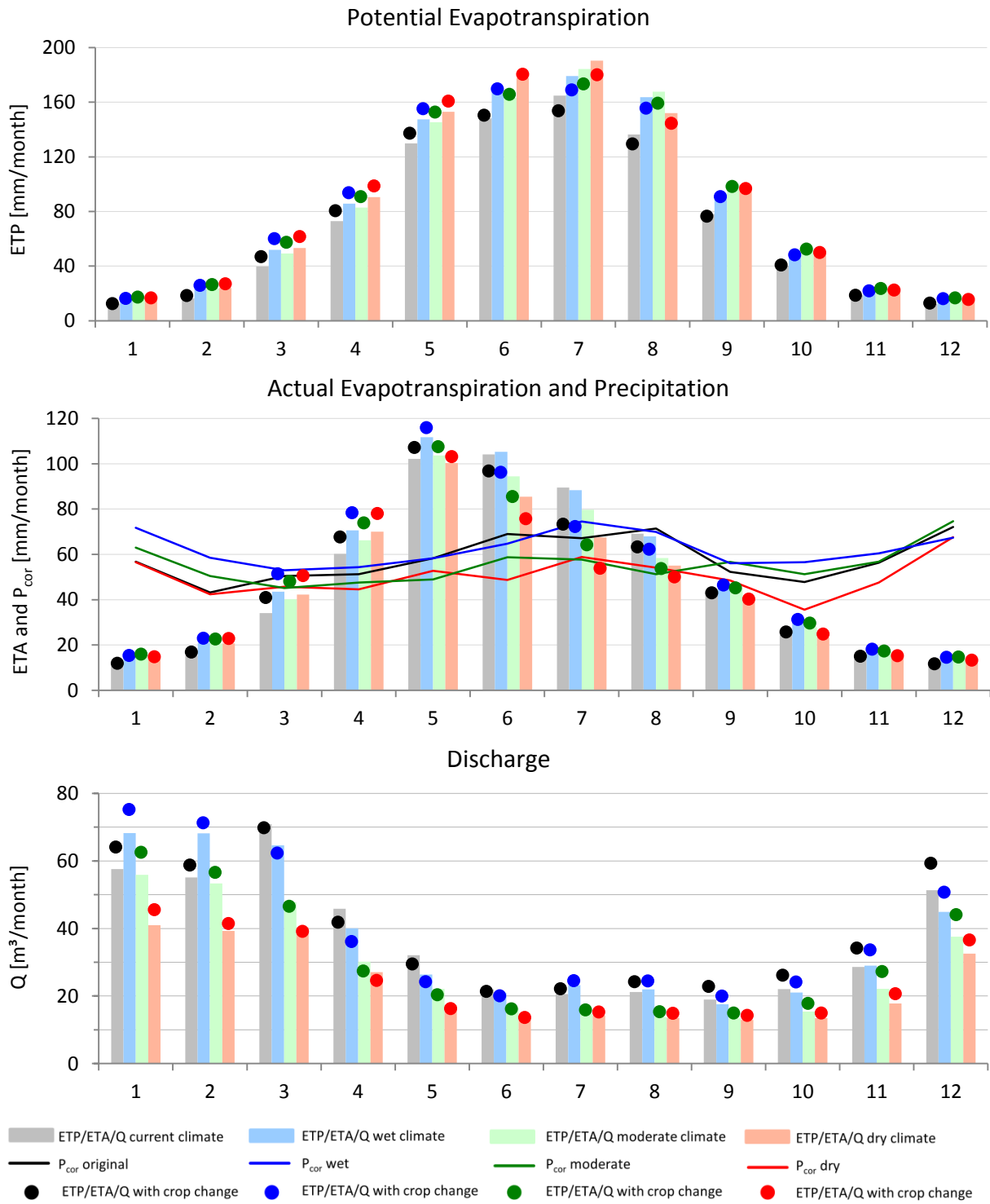


Figure F-1: Potential (ETP), actual evapotranspiration (ETA) and discharge (Q) for current land use and changed agricultural parameterisation under current climate conditions (1963-1992) as well as the dry, moderate and wet climate realisation of STAR 2 K (2031-2060) in the Pulsnitz river catchment

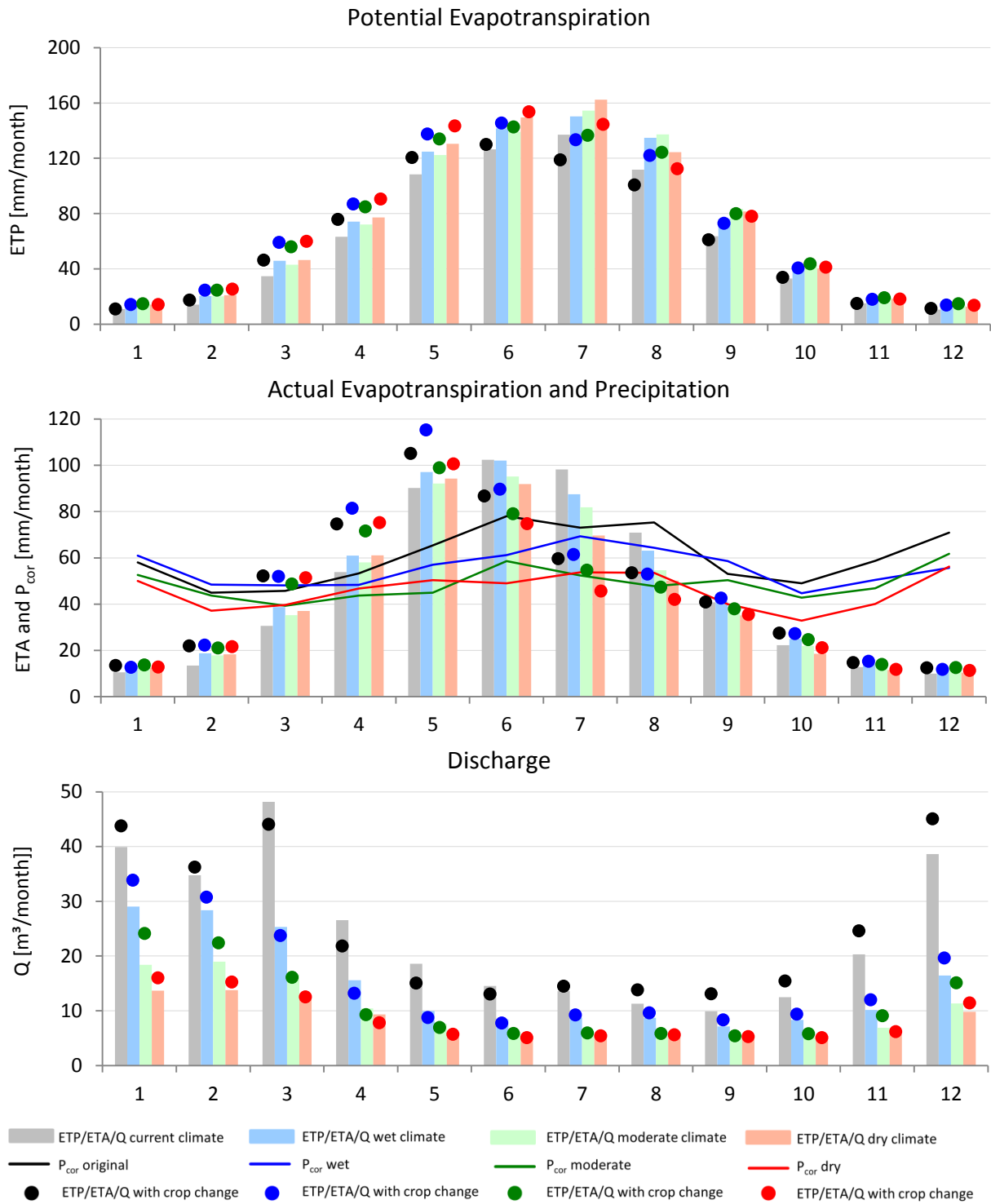


Figure F-2: Potential (ETP), actual evapotranspiration (ETA) and discharge (Q) for current land use and changed agricultural parameterisation under current climate conditions (1963-1992) as well as the dry, moderate and wet climate realisation of STAR 2 K (2031-2060) in the Weißer Schöps river catchment

Table F-3: Water balance components [mm/a] for current land use and change in agricultural cultivation under current climate conditions (1963-1992) and climate scenarios (2031-2060) in the Pulsnitz, Weißer Schöps and Dahme river catchments

Scenario	P	ETA	R
Pulsnitz			
original		581	126
original with crop change	698	573	134
<i>difference due to crop change (original)</i>		-8	+8
dry climate scenario		547	78
dry climate scenario with crop change	603	543	83
<i>difference due to crop change (dry scenario)</i>		-4	+5
moderate climate scenario		582	94
moderate climate scenario with crop change	662	578	100
<i>difference due to crop change (moderate scenario)</i>		-4	+6
wet climate scenario		630	125
wet climate scenario with crop change	745	625	131
<i>difference due to crop change (wet scenario)</i>		-5	6
Weißer Schöps			
original		557	195
original with crop change	727	543	200
<i>difference due to crop change (original)</i>		-14	+5
dry climate scenario		511	62
dry climate scenario with crop change	549	503	64
<i>difference due to crop change (dry scenario)</i>		-8	+2
moderate climate scenario		533	75
moderate climate scenario with crop change	585	523	85
<i>difference due to crop change (moderate scenario)</i>		-10	+10
wet climate scenario		574	114
wet climate scenario with crop change	667	562	121
<i>difference due to crop change (wet scenario)</i>		-12	+7
Dahme			
original		569	109
original with crop change	652	555	124
<i>difference due to crop change (original)</i>		-14	+15
dry climate scenario		525	56
dry climate scenario with crop change	551	518	65
<i>difference due to crop change (dry scenario)</i>		-7	+9
moderate climate scenario		569	85
moderate climate scenario with crop change	630	561	98
<i>difference due to crop change (moderate scenario)</i>		-8	+13
wet climate scenario		594	97
wet climate scenario with crop change	664	584	109
<i>difference due to crop change (wet scenario)</i>		-10	+12

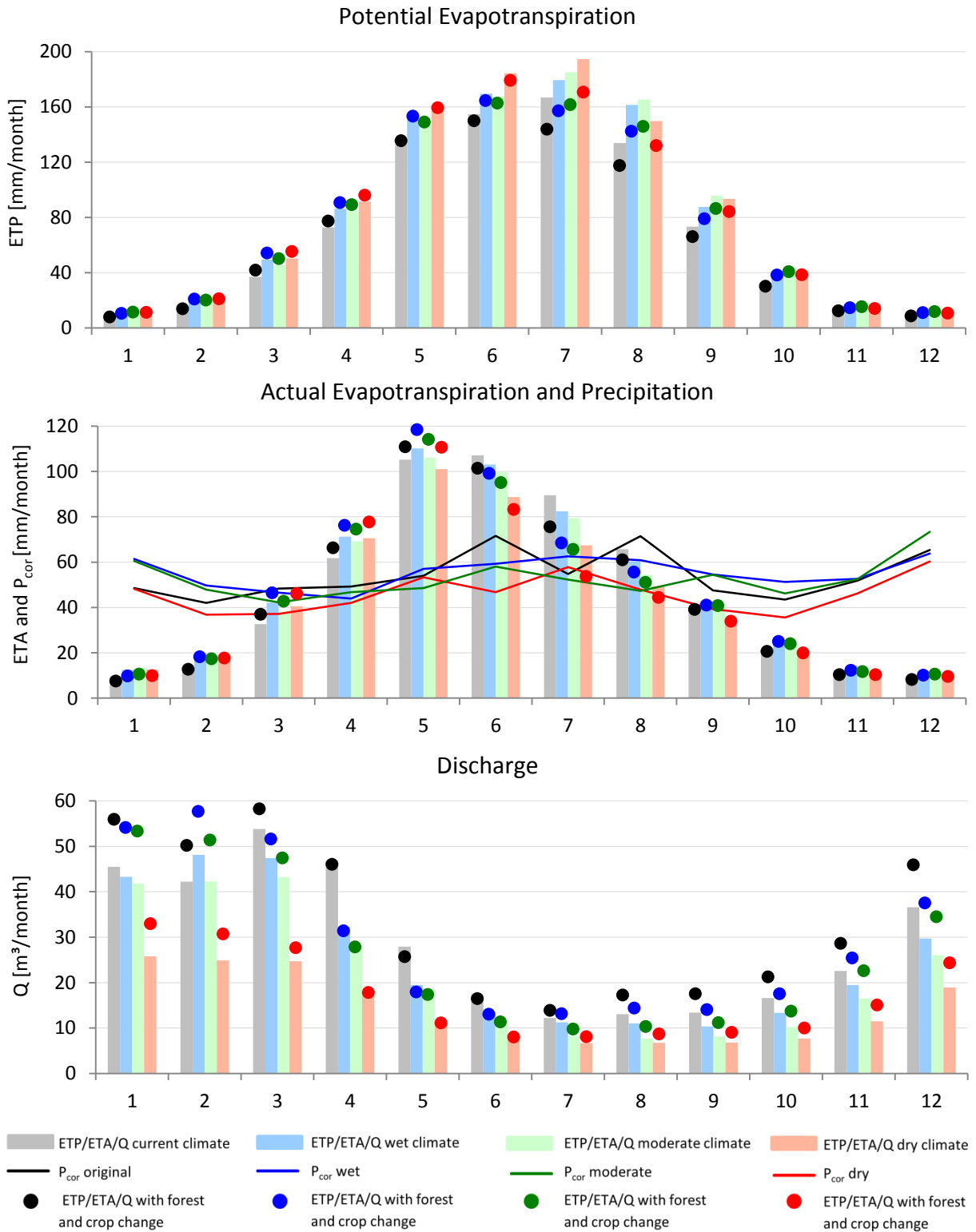


Figure F-3: Potential (ETP), actual evapotranspiration (ETA) and discharge (Q) for current land use and the combined effect of changed agricultural parameterisation and forest change under current climate conditions (1963-1992) as well as the dry, moderate and wet climate realisation of STAR 2 K (2031-2060) in the Dahme river catchment

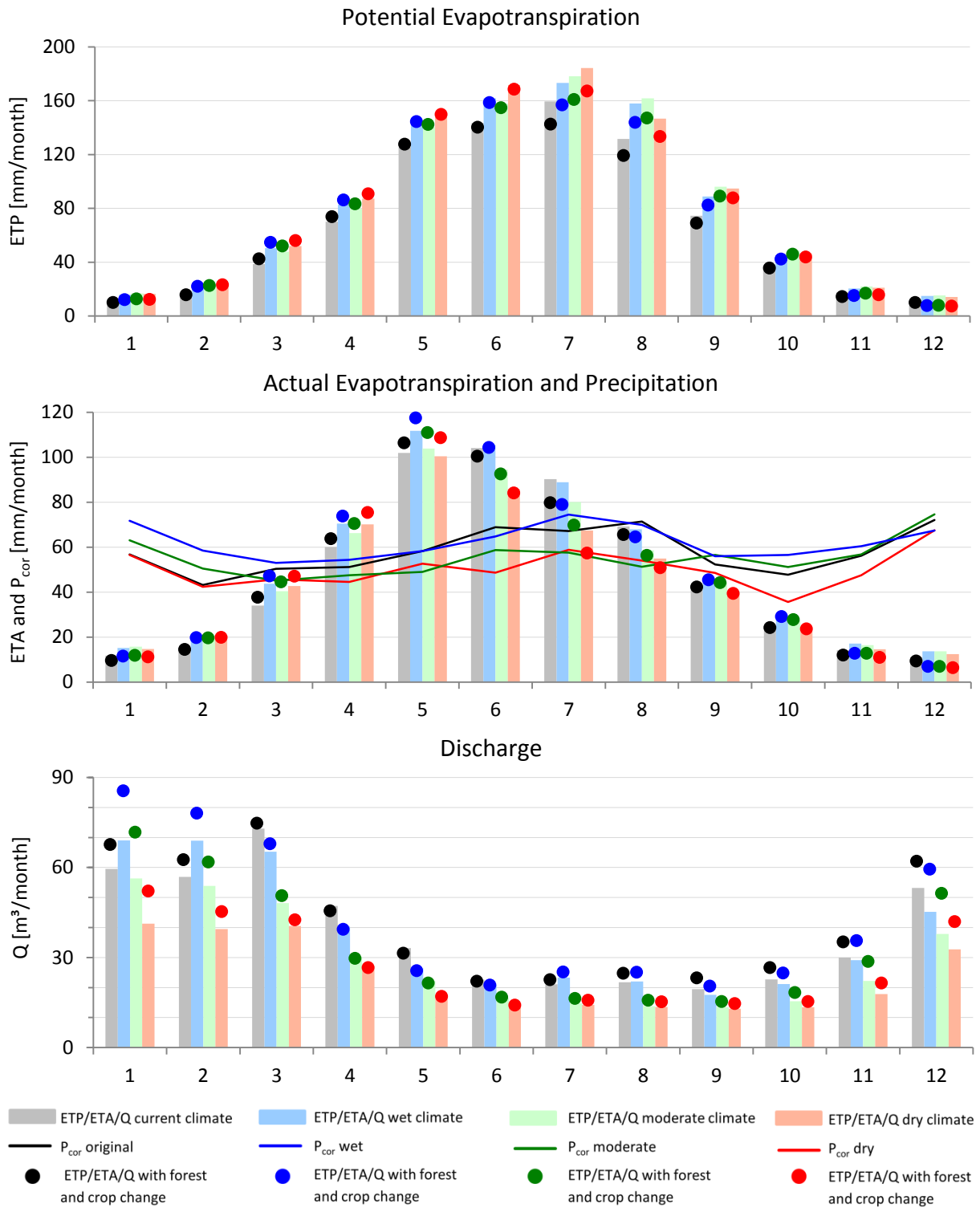


Figure F-4: Potential (ETP), actual evapotranspiration (ETA) and discharge (Q) for current land use and the combined effect of changed agricultural parameterisation and forest change under current climate conditions (1963-1992) as well as the dry, moderate and wet climate realisation of STAR 2 K (2031-2060) in the Pulsnitz river catchment

Table F-4: Water balance components [mm/a] for current land use and the combined effect of changed agricultural parameterisation and forest change under current climate conditions (1963-1992) and climate scenarios (2031-2060) in the Pulsnitz and Dahme river catchments

Scenario	P _{cor}	ETA	R
Pulsnitz			
original	698	581	126
original with crop change		565	139
<i>difference due to crop change (original)</i>		-16	+13
dry climate scenario	603	547	78
dry climate scenario with crop change		534	88
<i>difference due to crop change (dry scenario)</i>		-13	+10
moderate climate scenario	662	582	94
moderate climate scenario with crop change		567	108
<i>difference due to crop change (moderate scenario)</i>		-15	+14
wet climate scenario	745	630	125
wet climate scenario with crop change		611	141
<i>difference due to crop change (wet scenario)</i>		-19	+16
Dahme			
original	652	569	109
original with crop change		551	128
<i>difference due to crop change (original)</i>		-18	+19
dry climate scenario	551	525	56
dry climate scenario with crop change		518	66
<i>difference due to crop change (dry scenario)</i>		-7	+10
moderate climate scenario	630	569	85
moderate climate scenario with crop change		559	100
<i>difference due to crop change (moderate scenario)</i>		-10	+15
wet climate scenario	664	594	97
wet climate scenario with crop change		581	112
<i>difference due to crop change (wet scenario)</i>		-13	+15